The Activation of Small Molecules using Frustrated Lewis Pairs

by

Hasna Zaher

A thesis submitted in part fulfilment of the requirements for the degree of Doctor of Philosophy at the University of Oxford

New College

Oxford

August 2012

The work described in this thesis was carried out in the Chemistry Research Laboratory, Mansfield Road, Oxford from October 2008 to August 2012 under the supervision of Professor Dermot O'Hare. All the work is my own unless stated to the contrary and has not been previously submitted for any degree at this or any other university.

Hasna Zaher
New College
August 2012

ABSTRACT

The Activation of Small Molecules using Frustrated Lewis Pairs

Hasna Zaher **D. Phil Thesis**

New College **Trinity Term 2012**

This thesis describes the activation of small molecules using frustrated Lewis pairs, in particular investigating their use to reduce CO_2 to methanol, thus producing a new route towards a renewable fuel.

Chapter One summarises the requirement for a renewable fuel source, the alternative methods currently available and previous research conducted into converting CO_2 to methanol using FLPs and other reducing agents.

Chapter Two describes the synthesis of a new family of electron-deficient *tris*(aryl)boranes, $B(C_6F_5)_{3-x}(C_6Cl_5)_x$ (x = 1-3), allowing the electronic effects, resulting from the gradual replacement of C_6F_5 with C_6Cl_5 ligands, to be studied. The novel Lewis acids have been fully characterised and their Lewis acidities have been determined using NMR spectroscopy, electrochemistry and DFT studies.

Chapter Three discusses the synthesis of nine novel FLPs and their use to successfully split H_2. Each borohydride salt has been spectroscopically fully characterised and five of the salts have been characterised using single crystal X-ray diffraction. To determine the exact positions of the H atoms, single crystal neutron diffraction and DFT experiments were carried out on [**1**-H][H-TMP].

Chapter Four details attempts to use the borohydride salts, synthesised in Chapter Three, to reduce CO_2 to methanol. Each experiment was been fully investigated and their catalytic viability was determined. The X-ray crystal structure of [**1**-OCHO][H-TMP] is described and each formatoborate and methoxyborate salt were fully characterised.

Chapter Five describes experimental procedures and characterisation data. Crystallographic data in the form of CIF files may be found in the **Electronic Appendix**, found on the compact disc at the back of this thesis.

ACKNOWLEDGEMENTS

Firstly my thanks must go to my supervisor, Prof. Dermot O'Hare for his guidance, help and support over the last four years. I would also like to thank Dr. Andrew Ashley for his guidance and supervision in the lab and for initiating this project, especially all the advice you provided, it was invaluable. Thank you to the two Part II's who also worked on this project; Thomas Herrington and Samantha Binding, your contributions will never be forgotten.

Many thanks must go to everyone who assisted me during this research project. Dr. Amber Thompson and Mark Irwin helped me with crystal structure determinations and in collaboration with Dr. Matthias Gutmann successfully collected a single crystal neutron diffraction structure. Dr. Nick Rees was incredibly patient, always available to help and trained me to use the NMR spectrometers. Dr Gregory Wildgoose ran every electrochemistry experiment. Mr. Colin Sparrow and Mr. James Wickens ran all my mass spectrometry samples. Dr Tobias Krämer provided me with extremely efficient DFT studies, thank you so much for putting up with my emails.

During my D.Phil. I had many obstacles to overcome (including surgery) and I would not have survived if it was not for the support from my friends both in the lab and outside. Thank you to Dr. Chengle 'Sexy Joyce' Wang and Anchalee Wongariyakawee for the close friendships we had. A huge thanks to my D.Phil. lab mates, Dr. Charles 'Sporcle' Markland, Tom Arnold, Samantha Binding, Henry Fisher, Saul Moorhouse and Hannah Buckley. Thank you to the post docs that have helped me; Dr. J-C Buffet, Dr. Ian Casely and Dr. Zoe Turner, the guidance and support you provided was priceless. Thanks to Dr. Qiang Wang, Dr. Gareth Williams and Dr. Andrew Jupe. Part II's are a special, memorable group of people and thank you to Aran, Rosie, Tom, Bully, Chio, Emily, Ali, George, Jamie and Dan for all the entertainment you provided. To some older lab members, Dr. Paul Ransom and Dr. Paulina Aguirre, thank you for the advice and support you provided in the short time we spent together, I really should have listened to you Paulina.

I have made many friends in the CRL, in particular Rob 'Relissa' Tubervill, Mike 'Kellykins' Kelly, Gabby Quintero, Dr. Josh Bates, Vicky Chislett and the Mountford Group, especially the weekend dream team, Matt Blake and my little sister Guun. Thank you being my weekend buddies and for the fun times we had.

Now for those outside the lab. I have had a fantastic time in Oxford over the last four years and made so many wonderful friends. I loved my time at New college, especially all the guest nights I attended.

Thank you to Bonolo ‘Danolo’ Mathibela, Malebogo Ngoepe, Evgenia Ivanova, Laura Schaposnik, Kate Greasley, Tom Adcock, Nicole Milligan and Isabelle Ouwehand. You have all been amazing and I hope to stay close to all of you. I have had many friends come and go and you will all be remembered. A huge thanks to my London and Edinburgh friends, you have all been an important part of my life.

My family have supported me throughout my academic career and without their encouragement to finish my D.Phil. I might not have made it this far. I would especially like to thank my mum, she is an amazing woman and her strength has been my inspiration.

Last but by no means least, I would like to thank Mark Irwin. I am glad I continued with my D.Phil. otherwise I would never have met you. Thank you for your support and keeping me going.

Finally, thank you to everyone who kindly proof read my thesis.

TABLE OF CONTENTS

CHAPTER ONE – Introduction **1**

1.1 Overview 1

1.2 The Battle for Renewable Fuels 1

1.3 Methanol Economy 4

1.4 Reduction of CO_2 7

1.5 Frustrated Lewis Pairs 8

1.6 Activation of H_2 using FLPs 10

1.7 Theoretical Studies of H_2 Activation using FLPs 13

1.8 Proposed Mechanism for the Heterolytic Splitting of H_2 using FLPs 16

1.9 CO_2 Reactions with FLP Systems 23

1.10 Reduction of CO_2 to Methanol using an FLP System 25

1.11 Proposed Mechanism for the Reduction of CO_2 to Methanol using $[(C_6F_5)_3B\text{-}H][H\text{-}TMP]$ 28

1.12 Structure Function Relationship of the Lewis Acid 31

1.13 Aims of Research 35

1.14 References 35

CHAPTER TWO - Synthesis and Characterisation of Three Novel *Tris*(aryl)boranes **41**

2.1 Introduction 41

2.2 Synthesis of Novel Lewis Acids 43

2.2.1 Synthesis of C_6Cl_5Li 43

2.2.2 Synthesis of $B(C_6F_5)_2(C_6Cl_5)$; **1** 44

2.2.3 Synthesis of $B(C_6F_5)(C_6Cl_5)_2$; **2** 47

2.2.4 Synthesis of $B(C_6Cl_5)_3$; **3** 48

2.3 NMR Spectroscopy 49

2.4 Structural Characterisation 52

2.5 Lewis Acidity Measurements 58

2.6 Electrochemical Studies 62

2.7 Electronic Structure Analysis 68

2.8 Kinetics of H_2O Dissociation from H_2O.[1] 68

2.9 Conclusions 72

2.10 References 73

CHAPTER THREE - Synthesis and Reactions of Novel Frustrated Lewis Pairs with H_2 78

3.1 Introduction 78

3.2 Synthesis of Novel Frustrated Lewis Pairs and Reactions with H_2 79

3.3 NMR Spectroscopy 83

3.4 Monitoring H_2 Reactions using $B(C_6F_5)_2(C_6Cl_5)$ FLP Systems 85

3.4.1 H_2 Activation using [**1**][DABCO] 85

3.4.2 H_2 Activation using [**1**][TMP] 91

3.4.3 H_2 Activation using [**1**][Lut] 95

3.5 Side Reactions Observed using the DABCO FLP Systems 99

3.5.1 Single X-ray Crystal Structures of the DABCO Side Products 101

3.6 Structural Characterisation of the Borohydride Salts 105

3.6.1 Structural Characterisation of the [B-H][H-DABCO] Systems 105

3.6.2 Structural Characterisation of the [B-H][H-TMP] Systems 111

3.7 Mechanism of H_2 Activation 116

3.7.1 Single Crystal Neutron Diffraction of [**1**-H][H-TMP] 117

3.7.2 Electronic Structure Analysis of [**1**-H][H-TMP] 122

3.7.3 NMR Studies of [**1**-H][H-TMP] 122

3.8 FT-IR Spectroscopy 124

3.9 Conclusions 125

3.10 References 127

CHAPTER FOUR – Conversion of CO_2 to Methanol using the [B-H][H-N] Salts ..129

4.1 Introduction 129

4.2 Reducing CO_2 to Methanol 131

4.3 Reduction of $^{13}CO_2$ using $[(C_6F_5)_3B\text{-}H][H\text{-}DABCO]$ 133

4.4 Attempts to Reduce $^{13}CO_2$ to Methanol using [**1**-H][H-N] 137

4.4.1 [**1**-H][H-DABCO] 139

4.4.2 [**1**-H][H-Lut] 139

4.4.3 [**1**-H][H-TMP] 144

4.4.3.1 Single X-ray Crystal Structure of [**1**-OCHO][H-TMP] 147

4.5 Attempts to Reduce $^{13}CO_2$ to Methanol using [**2**-H][H-N] 150

4.5.1 [**2**-H][H-DABCO] 151

4.5.2 [**2**-H][H-Lut] 153

4.5.3 [**2**-H][H-TMP] 154

4.6 Attempts to Reduce $^{13}CO_2$ to Methanol using [**3**-H][H-N] 155
4.6.1 [**3**-H][H-DABCO] 155
4.6.2 [**3**-H][H-Lut] 157
4.6.3 [**3**-H][H-TMP] 158
4.7 Conclusions 160
4.8 References 163

CHAPTER FIVE – Experimental Details and Characterising Data 165
5.1 General Procedures and Physical Measurements 165
5.1.1 General Procedures 165
5.1.2 Elemental Analysis 166
5.1.3 Mass Spectrometry 166
5.1.4 NMR Spectroscopy 166
5.1.5 Infrared Spectroscopy 166
5.1.6 Electrochemistry 166
5.1.7 Crystal Structure Determinations 166
5.1.8 Determination of Lewis Acidities 168
5.1.9 Computational Details 169
5.2 Source of Starting Materials 169
5.2.1 Commercially Available Starting Material 169
5.2.2 Literature Preparations 170
5.3 Experimental Details for Chapter Two 171
5.3.1 Synthesis of C_6Cl_5Br (2.1) 171
5.3.2 Synthesis of C_6Cl_5Li 171
5.3.3 Synthesis of $Zn(C_6Cl_5)_2$ (2.2) 172
5.3.4 Synthesis of $B(C_6Cl_5)Br2$ (2.3) 172
5.3.5 Synthesis of **1**; $B(C_6Cl_5)(C_6F_5)_2$ (2.4) 174
5.3.6 Synthesis of $B(C_6Cl_5)_2Cl$ (2.5) 175
5.3.7 Synthesis of **2**; $B(C_6Cl_5)_2(C_6F_5)$ (2.6) 176
5.3.8 Synthesis of **3**; $B(C_6Cl_5)_3$ (2.7) 177
5.4 Experimental Details for Chapter Three 178
5.4.1 Synthesis of $[(C_6F_5)_3B$-H][H-DABCO] (3.1) 178
5.4.2 Synthesis of $(C_6F_5)_2BH$.DABCO (3.2) 179
5.4.3 Synthesis of [**1**-H][H-DABCO] (3.3) 180
5.4.4 Synthesis of [**2**-H][H-DABCO] (3.4) 181
5.4.5 Synthesis of $(C_6F_5)(C_6Cl_5)BH$.DABCO (3.5) 182

5.4.6 Synthesis of [**3**-H][H-DABCO] (3.6)....183
5.4.7 Synthesis of [**1**-H][H-TMP] (3.7)....183
5.4.8 Synthesis of [**2**-H][H-TMP] (3.8)....184
5.4.9 Synthesis of [**3**-H][H-TMP] (3.9)....185
5.4.10 Synthesis of [**1**-H][H-Lut] (3.10)....186
5.4.11 Synthesis of [**2**-H][H-Lut] (3.11)....187
5.4.12 Synthesis of [**3**-H][H-Lut] (3.12)....188
5.5 Experimental Details for Chapter Four....189
5.5.1 Synthesis of the Formatoborates using Route A1....189
5.5.2 Synthesis of the Formatoborates using Route B1....190
5.5.2.1 Synthesis of [HCO_2][H-DABCO] (4.1)....190
5.5.2.2 Synthesis of [$(C_6F_5)_3$B-OCHO][H-DABCO] (4.2)....190
5.5.2.3 Synthesis of [**1**-OCHO][H-DABCO] (4.3)....191
5.5.2.4 Synthesis of [**2**-OCHO][H-DABCO] (4.4)....192
5.5.2.5 Synthesis of [**3**-OCHO][H-DABCO] (4.5)....193
5.5.2.6 Synthesis of [$H^{13}CO_2$][H-TMP] (4.6)....194
5.5.2.7 Synthesis of [**1**-O^{13}CHO][H-TMP] (4.7)....194
5.5.2.8 Synthesis of [**2**- O^{13}CHO][H-TMP] (4.8)....195
5.5.2.9 Synthesis of [$H^{13}CO_2$][H-Lut] (4.9)....196
5.5.2.10 Synthesis of [**1**- O^{13}CHO][H-Lut] (4.10)....197
5.5.2.11 Synthesis of [**2**- O^{13}CHO][H-Lut] (4.11)....198
5.5.3 Synthesis of the Methoxyborates using Route A2....199
5.5.4 Synthesis of the Methoxyborates using Route B2....199
5.5.4.1 Synthesis of [$(C_6F_5)_3$B-OMe][H-DABCO] (4.12)....199
5.5.4.2 Synthesis of [**1**-OMe][H-DABCO] (4.13)....200
5.5.4.3 Synthesis of [**1**-OMe][H-TMP] (4.14)....201
5.6 References....202

ABBREVIATIONS

AN	Acceptor Number
Ar	Aryl
^{n}Bu	*n*-Butyl
^{t}Bu	*tert*-Butyl
CV	Cyclic Voltammetry
DABCO	1,4-diazobicyclo[2.2.2]octane
DCM	Dichloromethane
esu	Estimated Standard Uncertainties
Et	Ethyl
FLP	Frustrated Lewis Pair
h	Hours
HSAB	Hard Soft Acid Base
LA	Lewis Acid
LB	Lewis base
Lut	2,6-lutidine
Me	Methyl
Mes	2,4,6-trimethylphenyl
min	Minutes
MS	Mass Spectrometry
MS(EI)	Mass Spectrometry (Electron Ionisation)
MS(ESI)	Mass Spectrometry (Electrospray Ionisation)
NMR	Nuclear Magnetic Resonance
Ph	Phenyl
^{i}Pr	*iso*-Propyl
ppm	Parts Per Million
SCE	Saturated Calomel Electrode
TBAF	*tert*-Butyl Ammonium Flouride
THF	Tetrahydrofuran
TMP	2,2,6,6-tetramethylpiperidine
VT	Variable Temperature

CHAPTER ONE

Introduction

1.1 Overview

This thesis investigates the activation of small molecules using frustrated Lewis pairs (FLPs), in particular the possibility of using them to catalytically reduce CO_2 to methanol, thus producing a new route towards a renewable fuel. The chapter summarises the requirement for a renewable fuel source, the alternative methods currently available and previous research conducted into converting CO_2 to methanol using FLPs and other reducing agents.

1.2 The Battle for Renewable Fuels

Ever since the industrial revolution, the combustion of coal, oil and natural gas has been the world's major source of fuel, as well as having many other applications including the synthesis of plastics and in the pharmaceuticals industry. However, these fossil fuels are a finite resource and current estimates predict they will be exhausted in 40-200 years.[1] Consumption of fossil fuels has had a major impact on the environment, in particular the release of CO_2, nitrogen oxides and heavy metals into the atmosphere upon combustion. With the global concern for the long-term availability of non-renewable fuels and their contribution to global warming, research is taking place into finding a renewable fuel.

Novel processes and reactions that will positively impact the global carbon balance are required, however converting CO_2 to a chemically useful feedstock presents a variety of challenges, essentially because the molecule is so kinetically and

thermodynamically stable ($\Delta_f G° = –396$ kJ mol^{-1}). This will first be accomplished by utilising the high concentrations (when compared to atmospheric concentrations of 380 ppm) of CO_2-rich flue gases produced from fossil fuel burning power plants and other industrial plants. Capture of CO_2 can also be achieved using the CO_2 produced with geothermal hot water and natural gas.[2] However, in the future, technological advancements will hopefully allow for low concentrations of CO_2 (e.g. atmospheric CO_2) to be captured and employed as a fuel. Current techniques for capturing CO_2 primarily focus on membrane separation technology or selective absorption methods using a series of high surface area macro and microporous materials.[3-6] In the near future it might be possible to chemically recycle CO_2 on the human time scale. In comparison, nature needs to first produce new plant life via photosynthesis and then undergo transformation over millions of years to produce fossil fuels.[7]

Another alternative to the current fossil fuel economy is to use agricultural and natural product based biofuels. This requires relocating valuable food resources to fuel production, which has already resulted in rapidly increasing food prices and an increase in pollution.[8,9] Renewable power sources (e.g. biofuel, hydrogen, solar, tidal, wave, and wind)[10-12] are increasingly being harnessed, however, they have yet to be developed on a scale that could replace fossil fuels.[13] Nuclear power is another viable alternative to fossil fuels, however, due to the recent Fukushima incident in Japan, nuclear power has lowered in popularity.[14]

Conversion of CO_2 into useful chemicals for both energy production and as chemical feedstocks, preferably at low temperature and pressure, is the most desirable method of producing a renewable fuel. As a result catalytically reducing CO_2 using H_2 to selectively produce a fuel is of high interest. Currently H_2 can successfully be produced from the electrolytic splitting of water to give H_2 and O_2; and as long as the

cell current is generated from a renewable fuel source the process is carbon neutral. Unfortunately once H_2 is formed, it is not a convenient energy store for use as a fuel, as it is both highly volatile (boiling point –253 °C) and a potentially explosive gas demanding special storage and handling. As a replacement for petroleum, a completely new and different infrastructure would need to be built for commercial transportation. This process is further disadvantaged, as H_2 has a third of the volumetric power density of petroleum (Table 1.1) and its compression is highly energy intensive.[15] In comparison methanol production is the ideal alternative to fossil fuels, especially as it can easily be incorporated into the current infrastructure.[2]

Table 1.1 Energy densities of various fuels by mass and volume.[15]

	Energy density by mass ($MJ\ kg^{-1}$)	Energy density by volume ($MJ\ L^{-1}$)
$H_{2(g)}$	143	0.01079
$H_{2(l)}$	143	10.1
CH_3OH	19.7	15.6
Petroleum	46.4	34.2

The Nobel Prize winner George Olah has campaigned for a methanol economy since the early 1990s as a solution to our dependence on fossil fuels.[16-18] Methanol is a more attractive alternative to fossil fuels as it is relatively easy to store and transport, can be converted to gasoline and be used as a precursor in the chemical industry.

1.3 Methanol Economy

Methanol was first produced industrially in the 19th century as a minor by-product from forming charcoal via the destructive distillation of wood and was therefore referred to as 'wood alcohol' and then subsequently used for cooking, heating and lighting until cheaper fuels were produced.[2] At the time this was the only method of manufacturing methanol, until BASF developed a method of producing it from syngas (a mixture of CO/H_2) on an industrial scale in the 1920s.[19-21] Since World War II, syngas has been manufactured using natural gas, which is a finite resource and gives off CO_2 as a by-product. Today syngas is the primary raw material for the chemical industry.[21] Methanol is manufactured on a huge scale (approximately 40 million tonnes in 2007) and is used as an intermediate for the production of other chemicals such as acetic acid, formaldehyde and methyl *tert*-butyl ether. These are subsequently used to produce many everyday items, e.g. adhesives, paints and plastics.[21] Despite the huge number of advantages that methanol brings, there are also some disadvantages. Methanol is highly toxic when consumed in large amounts (30 – 100 mL), causing blindness and ultimately death.[22] However, just like gasoline and diesel fuel, methanol is not designed to be consumed internally and has been used in a large variety of consumer products for many years. Therefore, no major safety problems are expected if methanol was to be used and dispensed as a fuel. Similarly to gasoline, methanol has outstanding combustion qualities as seen by its use in the internal combustion engine where it has been used in race cars since the 1960s.[23]

The current method of manufacturing methanol using syngas is not a long term solution to the shortage of renewable fuels, as it is produced from methane (sourced from CO) and the technique releases CO_2. However, if the CO_2 could be recycled and

used to synthesise methanol, an economy could be generated which does not rely on a limited resource and reduces the greenhouse gas effect (Figure 1.1).[2]

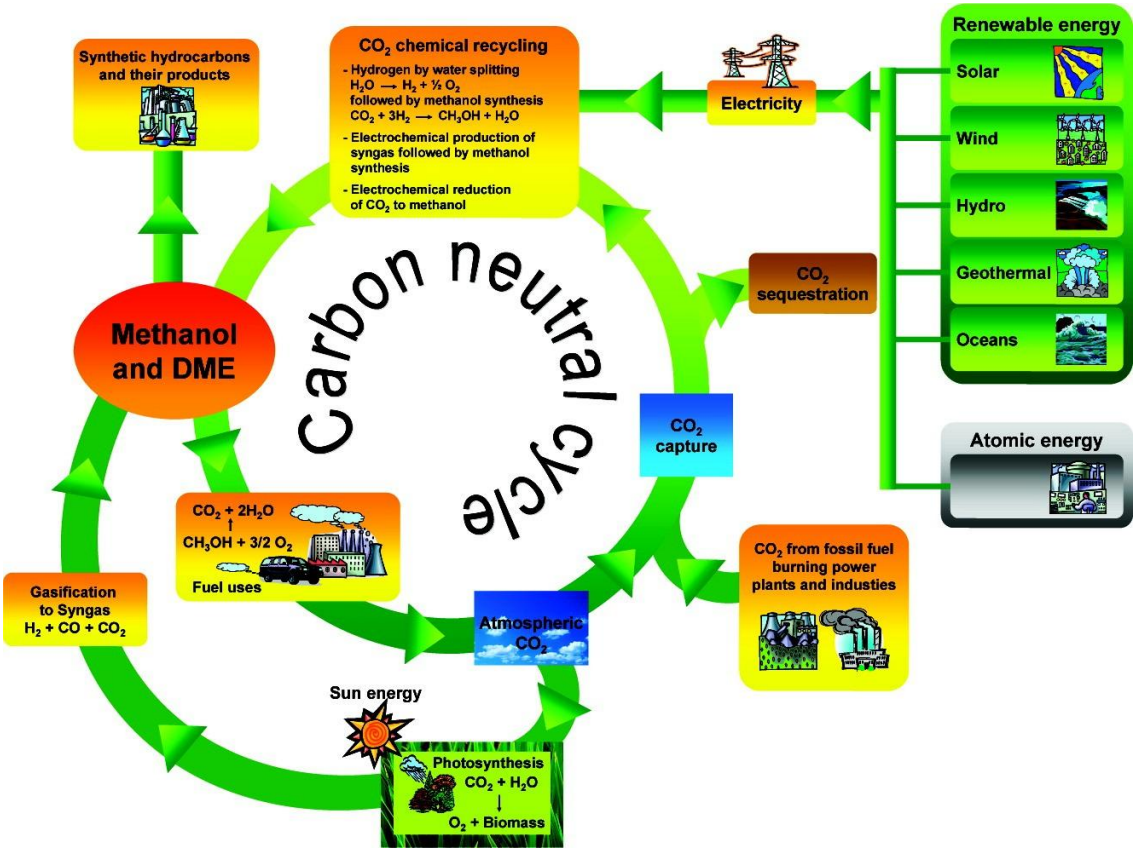


Figure 1.1 Carbon neutral reduction of CO_2 to methanol. Image taken from Olah *et al.*, reference 2.

Figure 1.1 displays a hypothetical route that could be taken to produce a carbon neutral fuel. This begins with the capturing of CO_2, which is reduced either electrochemically or with H_2 (produced from renewable sources) to give methanol, which is utilised in various industrial processes. Combustion of methanol releases CO_2, which is released back into the atmosphere, after which there are various routes it can take, namely recapture or photosynthesis.

Although CO_2 is kinetically and thermodynamically inert, the reduction of CO_2 is possible.[24,25] Thermodynamically, methane is the most favourable product from the

reduction of CO_2 using H_2 (Scheme 1.1), however, methanol is the more desirable product as it is easier to manage.[26]

$$CO_2(aq) + H_2(aq) \rightarrow CO(aq) + H_2O(l)$$

$$\Delta G^{\ominus} = 11\ kJ\ mol^{-1};\ \Delta H^{\ominus} = 11\ kJ\ mol^{-1};\ \Delta S^{\ominus} = -0.8\ J\ mol^{-1}\ K^{-1}$$

$$CO_2(aq) + 3H_2(aq) \rightarrow CH_3OH(l) + H_2O(l)$$

$$\Delta G^{\ominus} = -79\ kJ\ mol^{-1};\ \Delta H^{\ominus} = -106\ kJ\ mol^{-1};\ \Delta S^{\ominus} = -88\ J\ mol^{-1}\ K^{-1}$$

$$CO_2(aq) + 4H_2(aq) \rightarrow CH_4(l) + 2H_2O(l)$$

$$\Delta G^{\ominus} = -193\ kJ\ mol^{-1};\ \Delta H^{\ominus} = -230\ kJ\ mol^{-1};\ \Delta S^{\ominus} = -125\ J\ mol^{-1}\ K^{-1}$$

Scheme 1.1 Thermodynamics of carbon dioxide reduction.[27]

The reduction of CO_2 using homogeneous catalysts has been studied for over 40 years but these methods usually produce formate and not methanol,[28] and until recently, required metal ions as electrocatalytic reagents.[29] The use of heterogeneous catalysts (Ru and Pd catalysts) results in the reduction of CO_2 and formate to methanol with considerable activity and selectivity.[30,31] However, these methods require the use of rare and expensive metals which in many cases are highly toxic.

1.4 Reduction of CO_2

Reduction of CO_2 can be achieved both electrochemically and chemically, and further progress has been made over the last 20 years with interests growing in Japan, China, Australia, the European Union, and other countries to recycle their CO_2 output.[2]

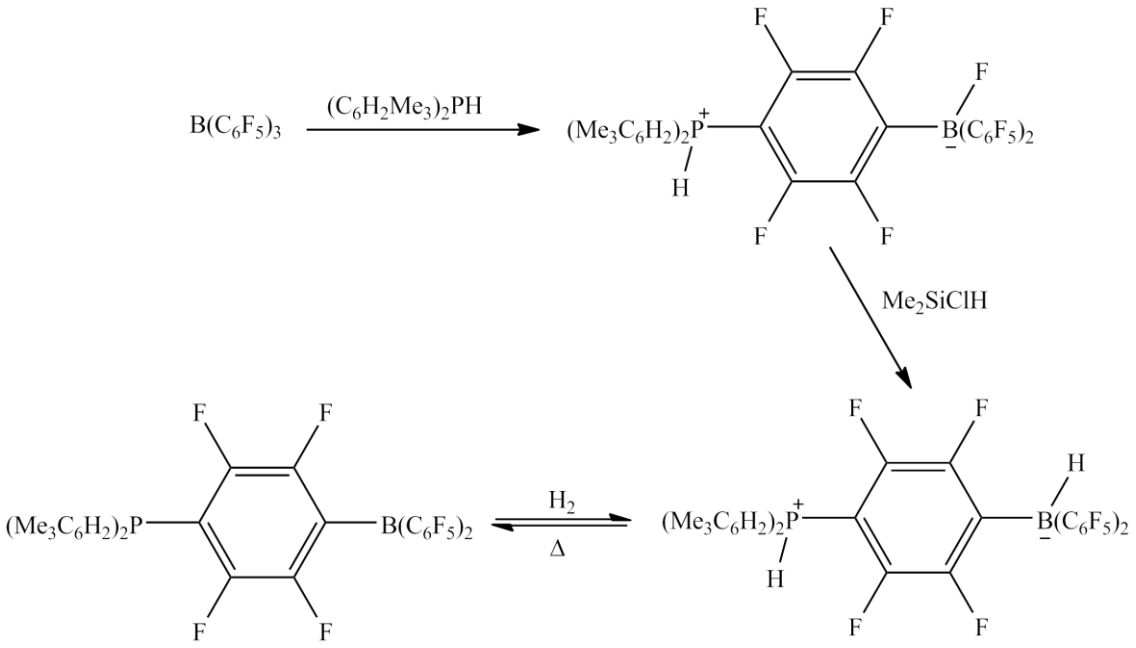
Electrochemical reduction can be administered catalytically and non-catalytically, with the majority of the methods producing carbon monoxide, formaldehyde, formic acid, hydrogen, methane, methanol and oxygen as the main products, but without selectively forming methanol.[33] Advances have been made in developing various metal catalysts to successfully reduce CO_2 to methanol that could rival the current method using the syngas catalyst Cu/ZnO. Reduction of CO_2 to methanol, even though not the most favourable process, is thermodynamically possible (Scheme 1.1) and is driven by the production of H_2O. The hydrogenation of CO_2 to methanol was reported by Tominaga *et al.* using the homogeneous catalyst $Ru_3(CO)_{12}$ with halide salts which aided in the stabilisation of the Ru catalyst. However, as well as producing methanol this process also gave carbon monoxide and methane.[34] Investigations have also been made into determining the active site in the syngas process and the role Cu/ZnO plays as a catalyst, as well as attempts to improve the catalyst by the addition of other components e.g. Al_2O_3, Ga_2O_3 and SiO_2.[35-37] However, all of these methods require the use of highly expensive and in some cases toxic metals which are in limited supply.

Studies into the use of metal-free catalysts as reducing agents for the production of methanol from CO_2 have seen a considerable amount of interest in the last 10 years. Recently Ashley *et al.* have shown that CO_2 can be reduced using a metal-free species known as a frustrated Lewis Pair.[32]

1.5 Frustrated Lewis Pairs

In 2006 the Stephan group uncovered the first metal-free system that reversibly splits H_2.[38] They succeeded in activating H_2 using a frustrated Lewis pair (FLP). An FLP is defined as when a Lewis acid and a Lewis base are unable to form a 'classical' Lewis adduct due to steric hindrance on the acid and base.[39] The now universally accepted molecular orbital-based principle for acid/base reactions that describes the dative donor-acceptor adducts was first proposed by Lewis in 1923.[40] Since then Lewis acids and Lewis bases have played a major role in chemistry. Lewis acidic boranes are widely used in olefin polymerisation studies[41-43] as well as a variety of organic reactions using Lewis acid catalysis.[44-47] Lewis basic phosphine ligands are widely seen in transition metal chemistry and catalysis.

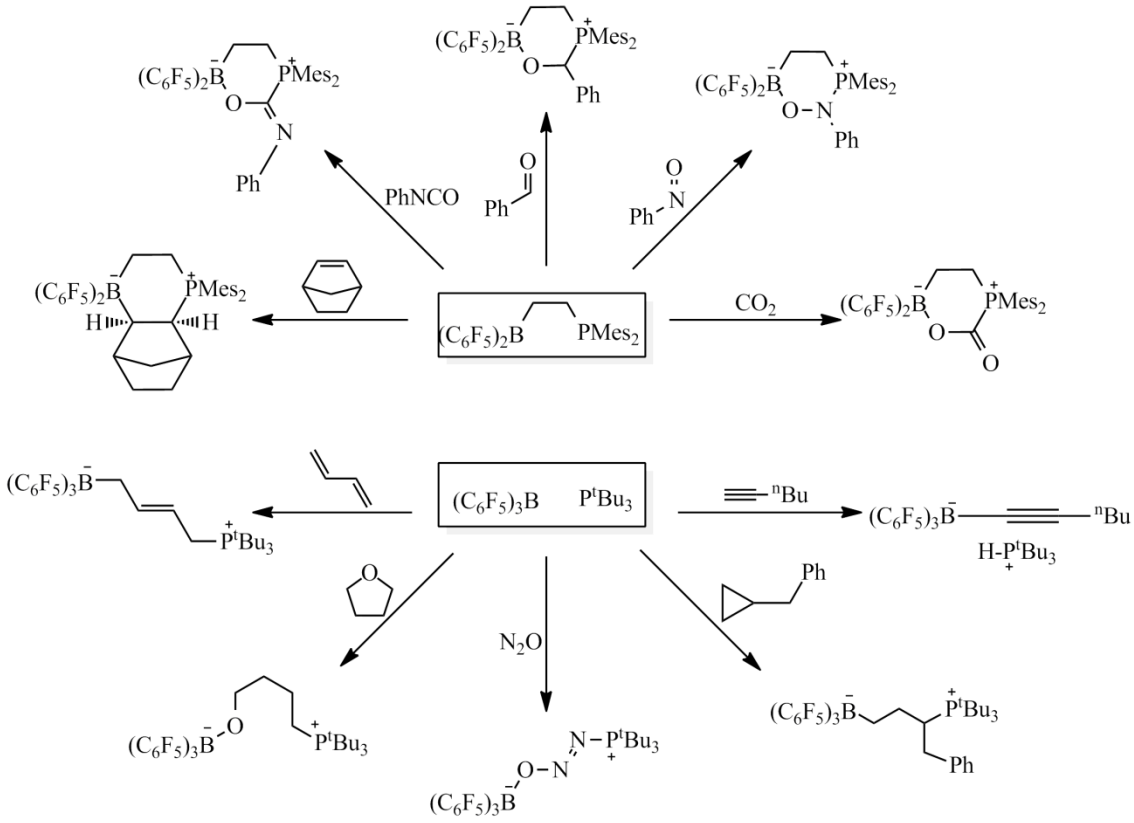
The ability of a Lewis acid to behave as an activator in olefin polymerisation has led to the investigation of simple donor-acceptor adducts and the impact of steric bulk on such activators. Stephan *et al.* found that $B(C_6F_5)_3$ reacts with sterically hindered secondary phosphines R_2PH (R = ^{t}Bu, Mes) *via* nucleophilic aromatic substitution at the carbon *para* to B to provide air and moisture stable zwitterions of the formula $R_2PH(C_6F_4)BF(C_6F_5)_2$ as shown in Scheme 1.2.[48]



Scheme 1.2 First example of the reversible activation of H_2 using a metal-free system.[38]

Addition of Me_2SiClH to $R_2PH(C_6F_4)BF(C_6F_5)_2$ resulted in B-F metathesis to the hydride to generate $R_2PH(C_6F_4)BH(C_6F_5)_2$. Thermolysis of $R_2PH(C_6F_4)BH(C_6F_5)_2$ at 150 °C led to the release of H_2 and the production of a unimolecular phosphino-borane, $(Mes)_2P(C_6F_4)B(C_6F_5)_2$. Intermolecular coordination of P to B is not witnessed in either solution or solid state. The loss of H_2 could be easily monitored by a colour change from colourless to an intense orange-red solution. Exposure of $(Mes)_2P(C_6F_4)B(C_6F_5)_2$ to H_2 at 25 °C resulted in rapid and facile regeneration of the zwitterionic salt and thus the system was determined to be reversible.

Subsequent studies have shown FLPs can activate other molecules such as CO_2,[49-52] nitrous oxide,[53] and unsaturated systems,[54-56] they can effect the ring opening of cyclopropanes[57] and heterocycles,[58] and the cleavage of disulfide bonds.[59] A summary of some of these FLP reactions are shown in Scheme 1.3.



Scheme 1.3 Small molecule activation using $^{t}Bu_3P/B(C_6F_5)_3$ and $(C_6F_5)_2BC_2H_4PMes_2$ FLP system.

The examples provided in Scheme 1.3 have only taken into account the use of phosphine bases combined with boranes to form FLP systems. However, there are many examples of Al/P FLP systems which are also capable of activating alkynes,[60] fixate CO_2,[61] reduce CO_2 to CO,[62] and even reduce CO_2 to methanol.[63]

1.6 Activation of H_2 using FLPs

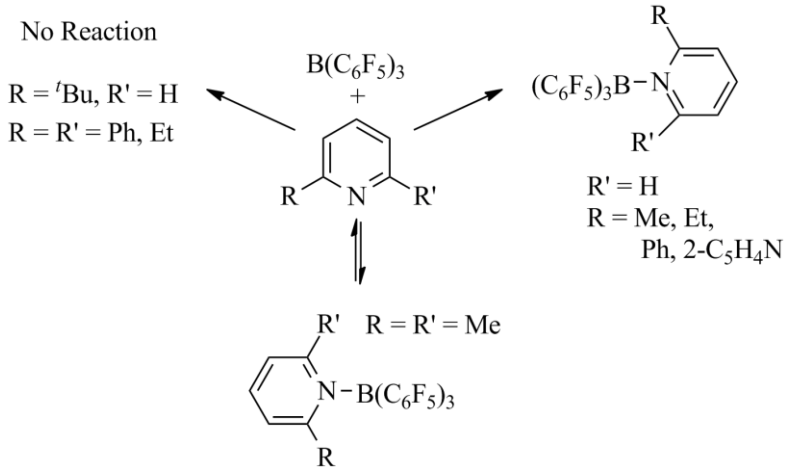
The Stephan group followed up their original findings with further research and discovered that the combination of the simple borane, $B(C_6F_5)_3$, and phosphines, R_3P (R = ^{t}Bu, Mes), do not exhibit the classical adduct formation and are able to heterolytically split H_2 (1 atm at 25 °C) to produce phosphonium hydridoborate salts

$[R_3PH][HB(C_6F_5)_3]$.[64] However, when these salts are heated above 100 ^oC, H_2 is not liberated unlike $(Mes)_2PH(C_6F_4)BH(C_6F_5)_2$.

Similarly, $^tBu_3P$ and BPh_3 activate H_2 to furnish $[^tBu_3PH][HBPh_3]$ albeit in only 33% yield.[64] The resulting H^+/H^- pairs are able to hydrogenate imines, enamines and enol ethers. In comparison, combinations of $PMes_3$ and BPh_3, $P(C_6F_5)_3$ and $B(C_6F_5)_3$ or $^tBu_3P$ and $BMes_3$ resulted in no reaction under identical conditions, which could be due to the change in Lewis acidity/basicity. FLPs have shown to be extremely useful synthetic reagents due to their ability to catalyse hydrogenation reactions under mild conditions. One of the most useful examples is the addition of H_2 to bulky imines,[65-68] which has recently been carried out enantioselectively.[69] FLPs can act as hydrogenation catalysts for nitriles[65] (reduction of imines and nitriles being particularly important in the pharmaceutical industry as a route to primary and secondary amines), aziridines[65] and enamines.[70] There are many examples of FLPs containing boron or aluminium Lewis acids used in combination with either nitrogen or phosphine bases.[38,64-66,71-77] $B(C_6F_5)_3$, as part of an FLP system, has over 200 known H_2 activation reactions and is one of the most widely used Lewis acids due to its ease of handling.[75]

There has also been some research conducted into the use of N bases in FLP systems, in particular the use of substituted pyridines with $B(C_6F_5)_3$. Monosubstituted pyridines were mostly found to form classic adducts whereas 2,6-disubstituted pyridines were found to be sterically hindered enough to behave as FLPs.[78] Using a 1:1 mixture of 2,6-lutidine (R=R'=Me, Lut) with $B(C_6F_5)_3$ (Scheme 1.4) gave rise to broad ^1H and ^{19}F NMR resonances at room temperature, suggesting that in solution there is an equilibrium between free Lut/$B(C_6F_5)_3$ and the dative adduct. Formation of both the 'classical' adduct and the FLP proved these reaction pathways are not mutually exclusive, as long as a thermodynamic equilibrium between the two species is

established. Addition of H_2 (1 atm) to this solution led to the pyrdinium salt [Lut-H][H-$B(C_6F_5)_3$]. [79]



Scheme 1.4 Effect of steric bulk on the formation of the adduct for pyridine-based FLP systems.[78]

In looking to broaden the range of N bases, work by Sumerin *et al.* has included various inexpensive amines.[80] Solutions of $B(C_6F_5)_3$ with $^{i}Pr_2NEt$ and $^{i}Pr_2NH$ gave 1:1 mixtures of the corresponding ammonium salts and zwitterionic products produced from amine H^- abstraction.[81] In comparison, no dehydrogenation was observed when 2,2,6,6-tetramethylpiperidine (TMP), a bulky secondary amine lacking an α-NH(CH) moiety, was used. Addition of H_2 (1 atm) at 20 °C to the $B(C_6F_5)_3$/TMP system resulted in the formation of the ammonium-borate salt in 95% yield.[80] However, replacing $B(C_6F_5)_3$ with BPh_3 resulted in no product formation, even at 110 ^{o}C. This is most likely due to the difference in Lewis acidities between $B(C_6F_5)_3$ and BPh_3. There are a few examples of TMP and Lut being used in an FLP system, however 1,4-diazabicyclo[2.2.2]octane (DABCO) has experienced limited use in FLP systems[82] and when added to $B(C_6F_5)_3$ forms a classical Lewis adduct.[83] Comparison of these Lewis bases shows that DABCO is less sterically hindered than TMP and Lut as it is able to form a classical Lewis adduct with $B(C_6F_5)_3$, whereas with Lut the system is in

equilibrium[79] and TMP forms an FLP.[84] However, $[TMP\text{-}H]^+$ is more basic than $[Lut\text{-}H]^+$ and $[DABCO\text{-}H]^+$ (pKa = 11.07,[85] 6.75[86] and 8.82,[87] respectively). When considering both the sterics and the basicity of the Lewis bases, it can be concluded that upon combination of a Lewis acid with Lut a weaker FLP system is formed than when combined with TMP or DABCO. However, even though TMP is an extremely bulky base, its strong basicity allows its FLP system to successfully activate H_2 in high yields.[80]

1.7 Theoretical Studies of H_2 Activation using FLPs

The requirements for H_2 activation exist not only with steric preclusion but also electronically i.e. the cumulative Lewis acidity and basicity must exceed a threshold. Calculations have been conducted on various intermolecular and intramolecular donor-acceptor components, and the calculated free energies for H_2 activation correlate with the cumulative acid-base strengths displayed in Figures 1.2 and 1.3.[88]

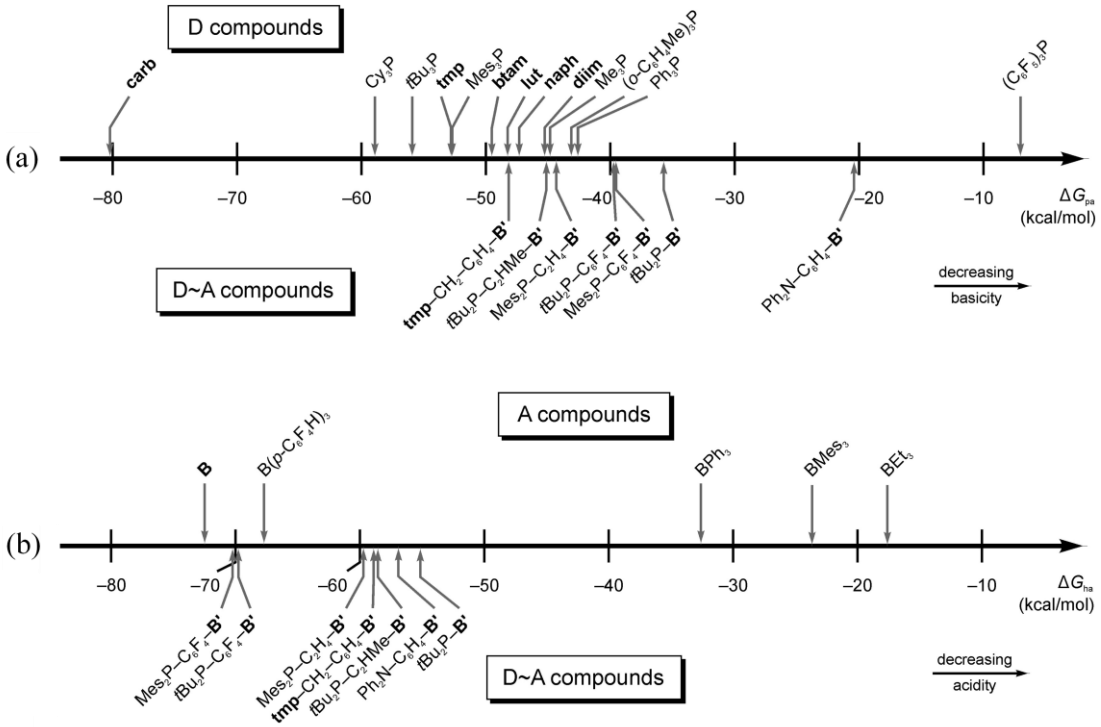


Figure 1.2 Calculated Gibbs free energies of (a) the proton attachment of the Lewis donors, and (b) of the hydride attachment to the Lewis acceptors, where B = $B(C_6F_5)_3$. D/A are unlinked FLPs and D~A are linked FLPs. Images taken from Rokob *et al.*, reference 87.

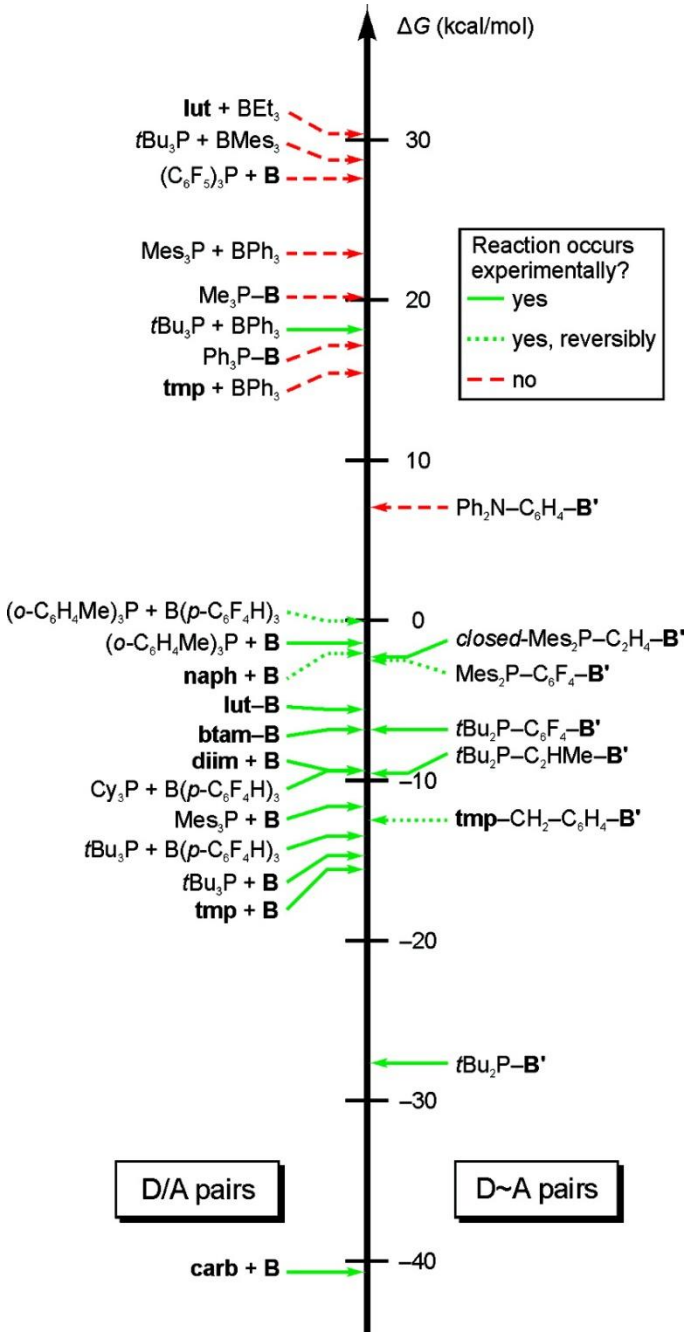


Figure 1.3 Calculated Gibbs free energies for the hydrogen splitting reaction of Lewis pairs, where B = $B(C_6F_5)_3$ and B' = $B(C_6F_5)_2$, D/A are unlinked FLPs and D~A are linked FLPs. Image taken from Rokob *et al.*, reference 87.

Rokob *et al.* showed that among the systems they studied; the inability for the systems to split H_2 is consistent with the unfavourable thermodynamics of the reaction. The calculations also showed that non-linked Lewis acid/base pairs (unable to form a 'classical' Lewis adduct) exhibit good correlation between the increasing acid/base

strength and the overall reaction free energy. The acidity, basicity and the stability of the final product also contribute to the ability of the FLP system to split H_2 and in particular when cleaving the acceptor-donor bond these factors should be considered when trying to overcome the energetic cost of splitting the H-H bond.[88] A decrease in the loss of entropy is observed with linked systems when compared to non-linked systems. As a result, for linked systems, a lower acid-base strength may be enough to produce a reactive system.

1.8 Proposed Mechanism for the Heterolytic Splitting of H_2 using FLPs

The definitive mechanism by which intermolecular FLPs activate H_2 is still under investigation. Knowledge of the mechanistic and structural details of these FLP systems are highly important in helping to improve future systems.

Following on from their success in discovering an intramolecular FLP that reversibly activates H_2, Stephan *et al.* hypothesised a mechanism based on the initial signs of first-order kinetics upon the loss of H_2.[75] However, trying to confirm this experimentally only lead to misleading kinetic data. Attempts to experimentally monitor the uptake of H_2 using borane/phosphine FLP systems proved challenging, in particular it was difficult to control the concentration of H_2 in solution, which led to diffusion controlled reactions. It was theorised that, based on early computational studies, the activation of H_2 is initiated by the Lewis acid followed by the protonation of the Lewis base.[75]

Papai *et al.* carried out computational experiments on the use of borane/phosphine FLPs to activate H_2. They presented a comprehensive molecular orbital diagram

(Figure 1.4) of the reaction and found that the means to breaking the strong H-H bond is the simultaneous interaction of H_2 with a filled and a vacant orbital in the FLP system.[89]

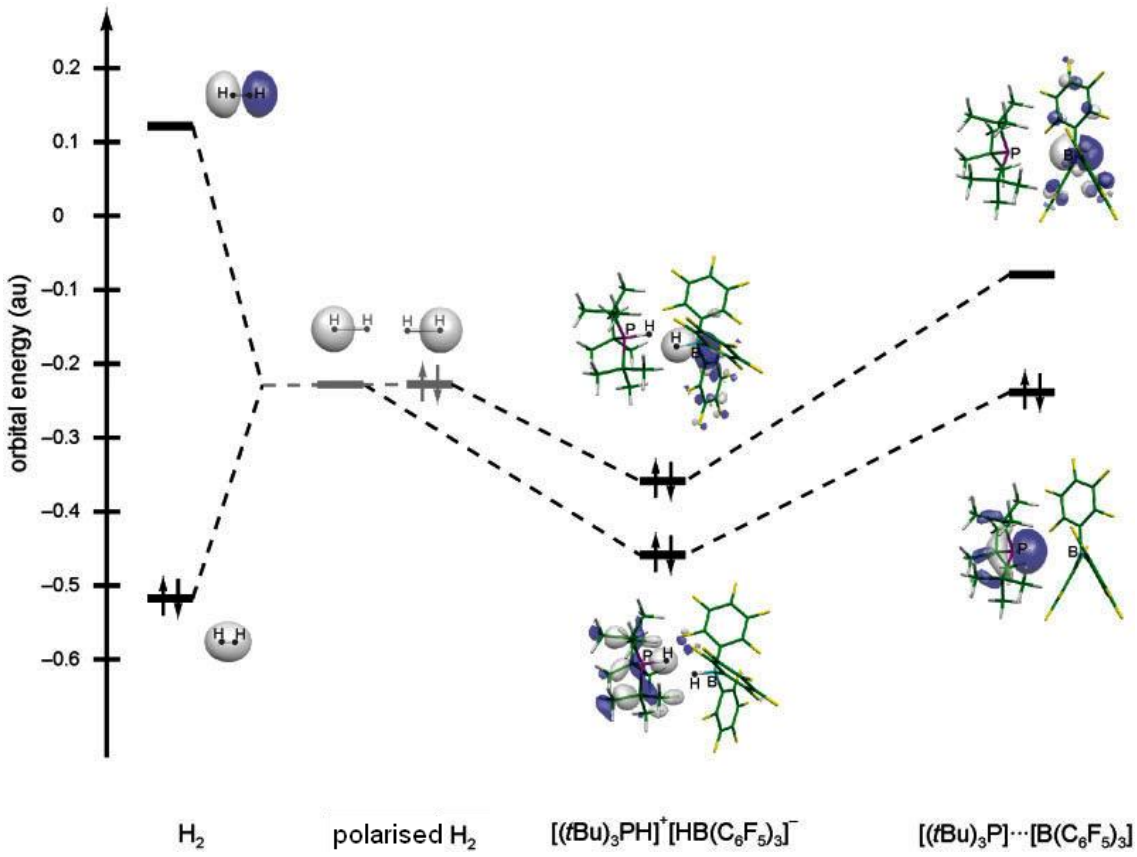


Figure 1.4 Molecular orbital diagram displaying the formation of the two dative bonds of the product. Image taken from Hamza *et al.* reference 88.

They proposed that due to the orbital symmetry, H_2 becomes polarised in the transition state, thus maximising the favourable interactions with the orbitals. Hamza *et al.* went on to say that the cleavage of the H-H bond and formation of the new B-H and P-H bonds occur at the same time and that the reactive intermediate is stabilised by the secondary interactions in the frustrated complex.[89]

Further calculations by Tamm *et al.* studied the activation of H_2 using a carbene and borane which produced a carbene-borane "encounter complex" and showed that a transition state, similar to Papai *et al.*, existed.[90]

However, the theory that the breaking of the H-H bond is mediated by a linear [LA]-H···H-[LB] transition state has recently been discredited because the theory did not allow for the interaction between large substituents.[91] Grimme and Erker proposed a bimolecular process, demonstrated for the FLP $^{t}Bu_3P$ and $B(C_6F_5)_3$, whereby the reaction is thought to be asymmetric-concerted with the LA-H bond forming a little earlier than that of H-LB, similar to the idea proposed by Stephan. This suggests that using the electric field created by the donor/acceptor atoms in the FLP, activation of H_2 occurs *via* polarisation of the molecule (Figure 1.5).[92]

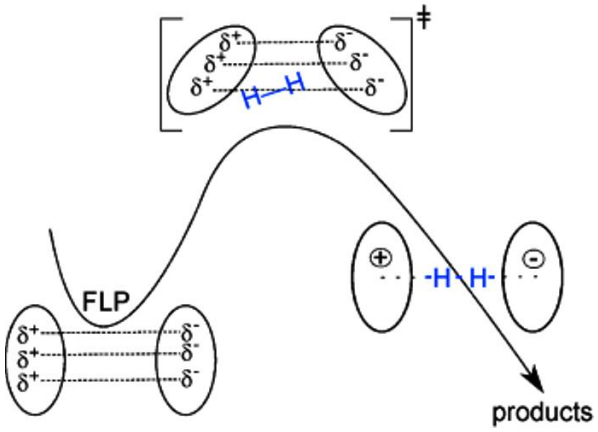


Figure 1.5 Postulated electric field polarisation of the H_2 molecule involving FLPs. Image taken from Grimme *et al.* reference 91.

Stephan *et al.* have concluded that a certain cumulative Lewis acid and base strength is necessary for successful activation of H_2 and thermodynamic considerations suggest that $\Delta G^{\ddagger}$ of activation needs to be lower than +41.8 kJ mol^{-1}.[39] To better understand the hydrogen splitting reaction, it has been split into five hypothetical steps (Figures 1.6 and 1.7).[88]

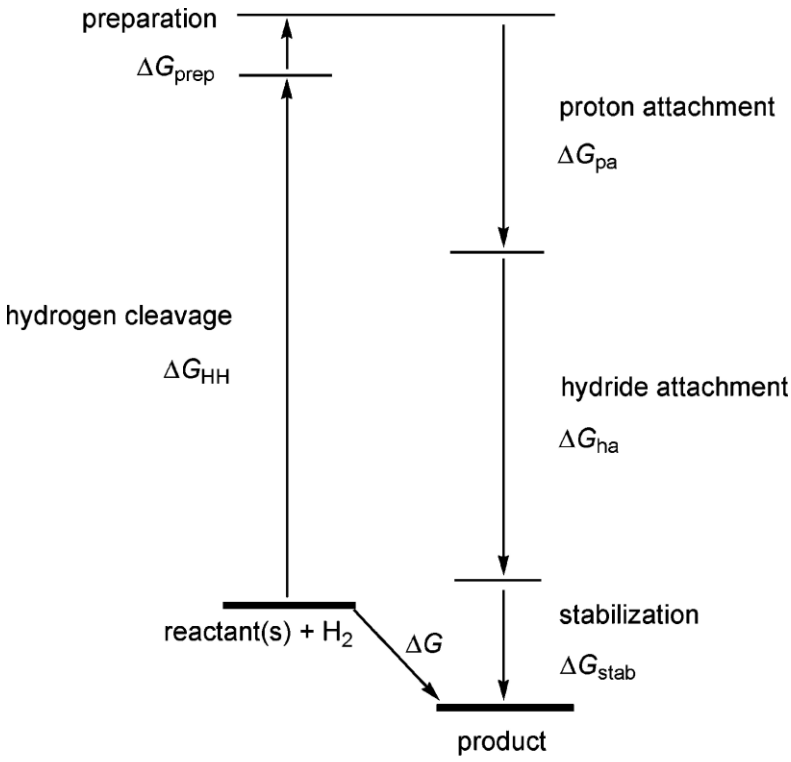


Figure 1.6 Division of the free energy of the H_2 splitting reaction of FLPs. Image taken from Rokob *et al.* reference 87.

$$\Delta \mathbf{G} = \Delta \mathbf{G_{HH}} + \Delta \mathbf{G_{prep}} + \Delta \mathbf{G_{pa}} + \Delta \mathbf{G_{ha}} + \Delta \mathbf{G_{stab}}$$

H_2	$\longrightarrow$	H^+	+	H^-	ΔG_{HH}	**Hydrogen cleavage**
LB—LA	$\longrightarrow$	LB	+	LA	ΔG_{prep}	**Preparation**
LB + H^+	$\longrightarrow$	$[LB\text{-}H]^+$			ΔG_{pa}	**Proton attachment**
LA + H^-	$\longrightarrow$	$[LA\text{-}H]^-$			ΔG_{ha}	**Hydride attachment**
$[LB\text{-}H]^+$ + $[H\text{-}LA]^-$	$\longrightarrow$	$[LB\text{-}H]^+$		$[H\text{-}LA]^-$	ΔG_{stab}	**Stabilisation**

Figure 1.7 A breakdown of the reaction steps involved for splitting H_2 using intermolecular FLP systems.[88]

According to the breakdown of energy processes proposed in Figures 1.6 and 1.7, the first step of the thermodynamic cycle is the heterolytic splitting of H_2 into H^+ and H^- ions (in a toluene solution). This process is rather endergonic with a calculated free energy of ΔG_{HH} = +538.9 kJ mol^{-1}, which is higher than the dissociation energy of H_2 (432 kJ mol^{-1})[93] and is not dependent on the FLP.[94] For most of the systems examined, which contained no dative bond between the Lewis centres, this is the only uphill step in free energy. Nevertheless, if the active sites are quenched, i.e. a dative bond is present in the system, an additional amount of free energy (ΔG_{prep}) is required to break the dative bonds, so that the acceptor and donor centres are prepared to accept the H^+ and H^- ions. With the non-linked systems, they adopted the Gibbs free energies of the attachment of a hydride (ΔG_{ha}) and a proton (ΔG_{pa}) ion to the acceptor or donor species, respectively. The final step (stabilisation of the product), a consequence of a non-linked system, is the formation of the product ion pair from the separated $[DH]^+$ and $[HA]^-$ ions. The free energy, ΔG_{stab}, which is related to this step is simply the free binding energy of the ion pair. Whereas, for the linked FLPs, which are both electrophilic and nucleophilic molecules, the strengths of the acid and base sites are defined as the free energies of proton and hydride attachments to the D~A compounds (ΔG_{pa} and ΔG_{ha}). Therefore, in the last step of the reaction is the ionic $[HD\sim A]^+$ and $[D\sim AH]^-$ species of the thermodynamic cycle which yields the zwitterionic $[^+HD\sim AH^-]$ product and a neutral D~A molecule. The free energy of the final step (ΔG_{stab}) is a measure of stabilising effects arising from the acid−base active centres cooperating together.[88]

It is essential to overcome the free energy cost of heterolytic H-H bond splitting by favourable free energy contributions for the proton attachment and hydride attachment. These favourable free energy contributions correlate with the cumulative acid-base

strength of the Lewis pairs. FLP systems capable of reversibly splitting H_2 have been found to have slightly favourable free energies of attachment (ΔG_{pa} and ΔG_{ha}) in favour of H_2 uptake at standard conditions, showing overall $\Delta_r G$ values typically within the region 0 and –41.8 kJ mol^{-1}; a value of –65.2 kJ mol^{-1} has been determined for the FLP system $B(C_6F_5)_3$ and TMP, which exhibits irreversible activation.[95]

These theoretical studies so far have made great strides in trying to gain an understanding of the mechanism of these reactions. The computational studies have also revealed the importance of secondary interactions in the preorganisation of the reacting partners. The sterically hindered Lewis acid and base, which are incapable of forming a dative bond, may combine to a "frustrated complex" through non-covalent interactions. This reactive intermediate needs to be well prepared for a cooperative interaction with the incoming H_2 molecule (see Figure 1.8a),[96] which assists in the process of splitting the molecule. The participation of a frustrated complex was also suggested for intramolecular FLPs where the link between the acidic and basic centres does not allow for intramolecular assistance (Figure 1.8b).[96,97] On the other hand, if the reactive centres were able to arrange themselves appropriately, the linked FLPs may also be able to cleave H_2 intramolecularly (Figure 1.8c).[88]

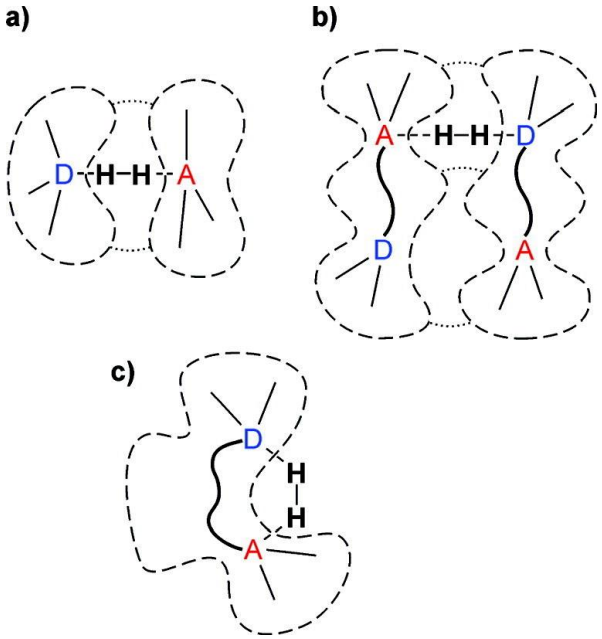
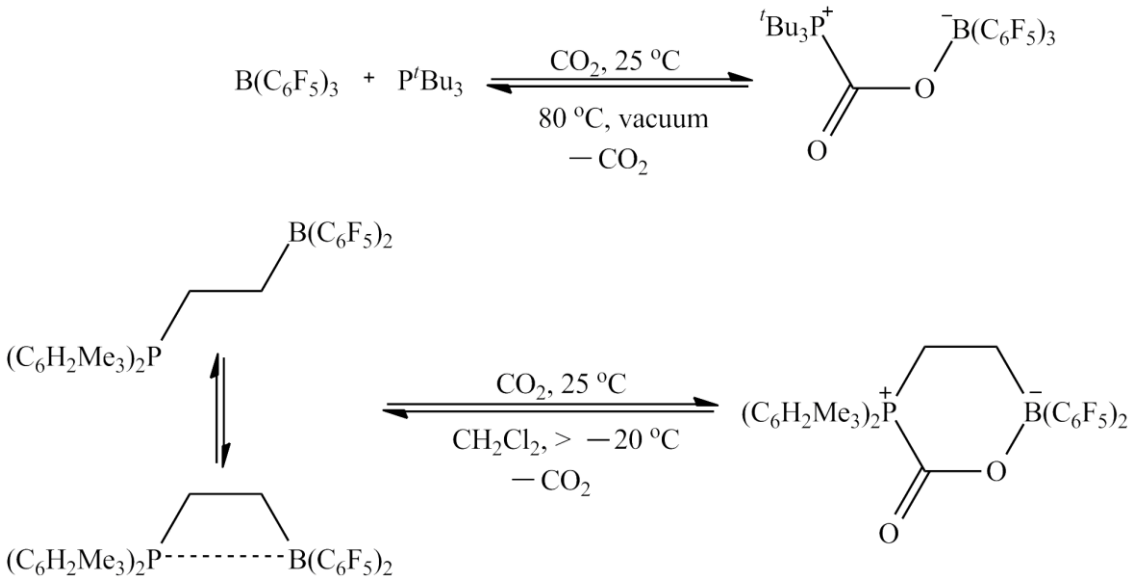


Figure 1.8 H_2 activation using (a) a non-linked acceptor/donor (A/D) pairs, (b) a disorganised linked pair, and (c) an organised linked pair. Image taken from Rokob *et al.* reference 85.

Schulz *et al.* demonstrated using single crystal neutron diffraction and NMR spectroscopy that the distance between the split H_2 molecule for an intramolecular FLP system (ansa-aminoborane; 1-N-TMPH-CH_2-2-[$HB(C_6F_5)_2$]C_6H_4) was 1.67 Å.[98] These findings have helped improve the understanding of the mechanism of H_2 splitting using intramolecular FLPs. On the other hand, H_2 activation using intermolecular systems (e.g. $B(C_6F_5)_3$/TMP) are still under investigation, as upon crystallisation there is possibility for the rearrangement of the salt thus extending the distance between the H atoms (N-H···H-B) to 2.97 Å.[80]

1.9 CO_2 Reactions with FLP Systems

FLPs can be used to activate a vast number of small molecules, in particular CO_2. Following on from the success the splitting of H_2 using $R_2P(C_6F_4)B(C_6F_5)_2$, Mömming *et al.* were able to show the reversible binding of CO_2 under mild conditions using a range of B-P FLPs.[99]

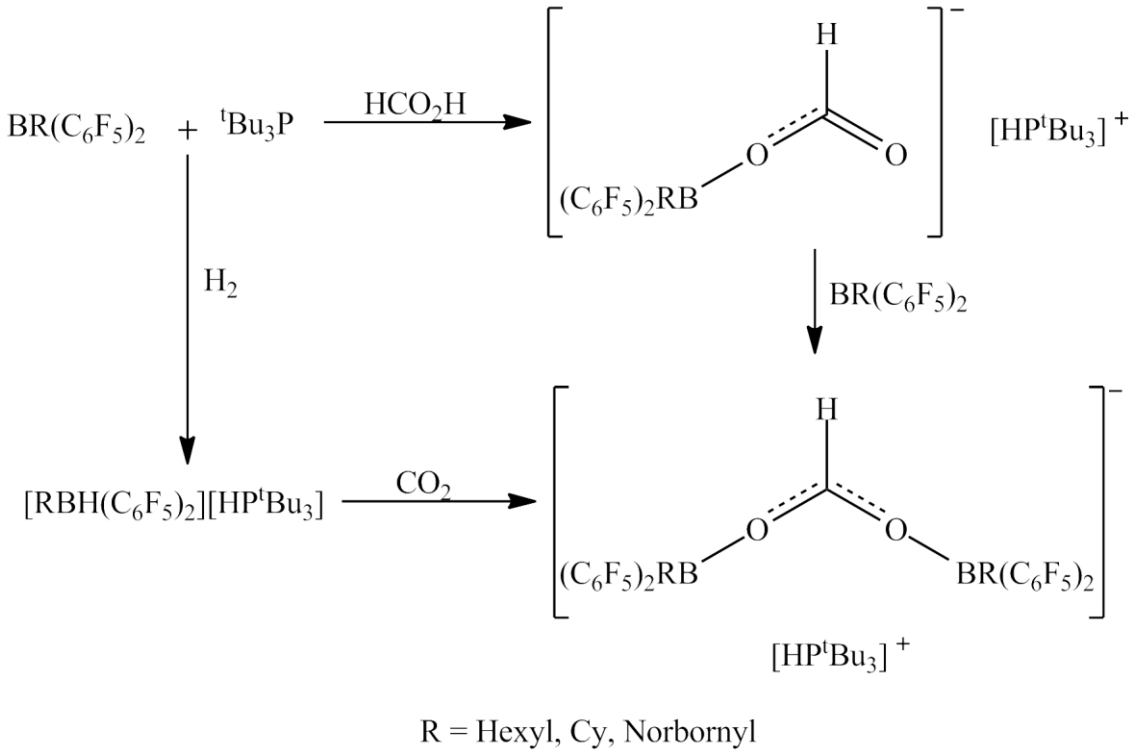


Scheme 1.5 Reversible activation of CO_2 using an FLP.[99]

Mömming *et al.* were the first to successfully synthesise and characterise the carboxylic acid derivatives displayed in Scheme 1.5. They were also able to show that the CO_2 activation was reversible by either heating under vacuum or by altering the solvent of the reaction.[99] In 2011 the Stephan group followed with another publication by Zhao reporting the use of bis-boranes to activate CO_2. In this instance, they were able to successfully provide an effective method of producing a six-membered heterocycle via the chelate binding of CO_2 using a frustrated borane-phosphine Lewis pair.[51]

In 2011, the Stephan group took the research one step further with a publication by Peuser *et al.* where they investigated computationally and experimentally the binding of

CO_2 using a range of frustrated borane-phosphine Lewis pairs.[100] They found the borohydride species; [^{t}Bu$_3$PH][RBH(C$_6$F$_5$)$_2$] (R = hexyl, Cy, norbornyl), successfully inserted CO_2 to give [((C$_6$F$_5$)$_2$BR)$_2$(μ-HCO$_2$)][*t*Bu$_3$PH] as shown in Scheme 1.6.

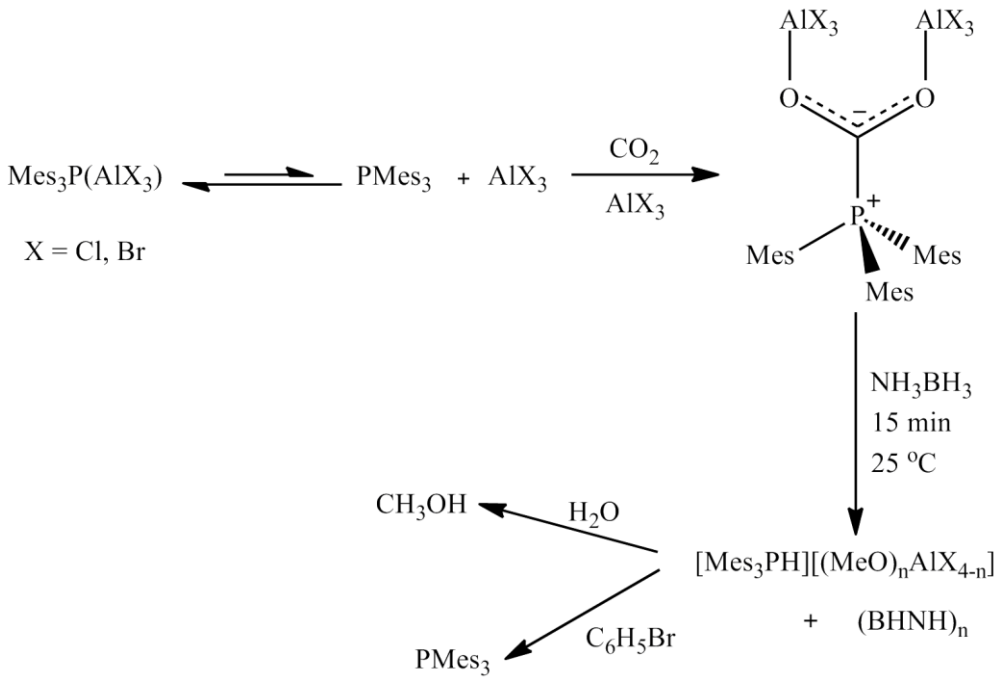


Scheme 1.6 Activation of CO_2 using a bis-borane FLP. Scheme adapted from Peuser *et al.* Reference 100.

As Scheme 1.6 shows, the CO_2 molecule inserts into the B-H bond, then coordinates a second acid molecule to give a bis-borane species, which can be synthesised using the FLP and formic acid. They determined that even though hydride salts of FLPs can capture CO_2 and formate fragments, the thermal instability of the CO_2 adducts prevents the complete reduction, concluding that the FLP system required a stronger Lewis acid.[100] Further work by the Stephan group has explored the use of aluminium/phosphorus based FLPs and their ability to fixate or reduce CO_2 to carbon monoxide.[61,62]

1.10 Reduction of CO_2 to Methanol using an FLP System

In 2010, Ménard and Stephan were able to successfully show the reduction of CO_2 to methanol using an Al/P FLP and ammonia borane as the hydrogen source (Scheme 1.7).[63]

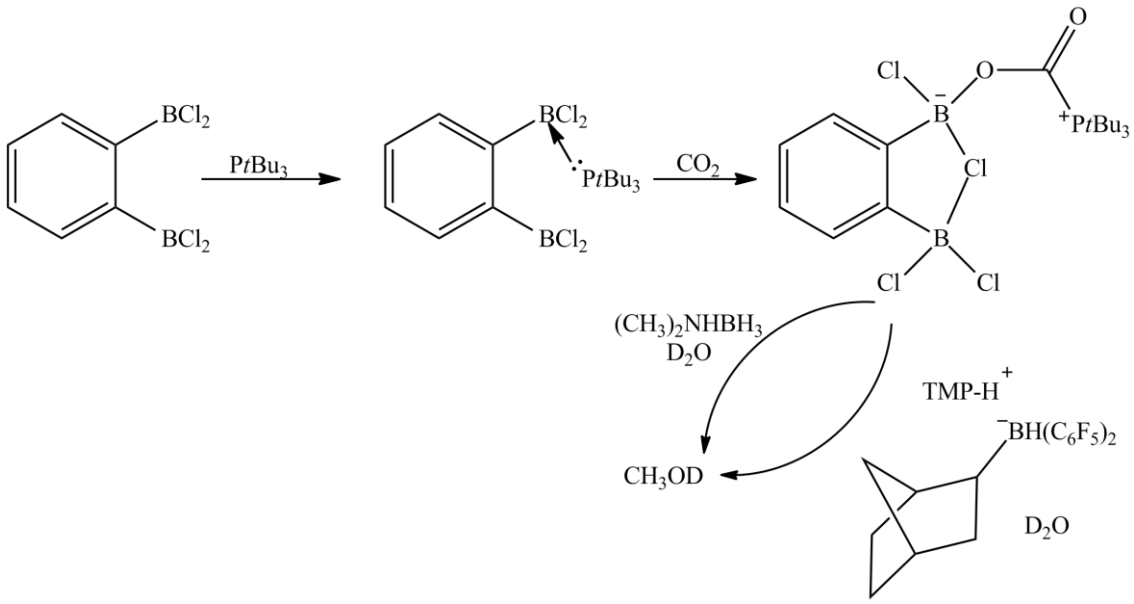


Scheme 1.7 Reduction of CO_2 to CH_3OH using ammonia borane as a hydrogen source.[63]

The weak Lewis adducts, $AlX_3/PMes_3$ (X = Cl, Br), were shown to doubly activate CO_2, which is a rare occurrence, with 2 Al-O bonds observed. Upon quenching the reaction with H_2O, 'free' methanol was observed in yields of 37-51%. However, since the fate of the Al species is unknown, they could not determine the catalytic viability of the system.[63]

Sgro *et al.* showed the use of a bis-borane-based frustrated Lewis pair to stoichiometrically reduce CO_2 to methanol.[101] They demonstrated that using the bis-borane 1,2-$C_6H_4(BCl_2)_2$ in conjunction with P^tBu_3, formed an FLP that can

asymmetrically bind CO_2. This allowed further stoichiometric reactions to take place using reducing agents as exhibited in Scheme 1.8.[101]

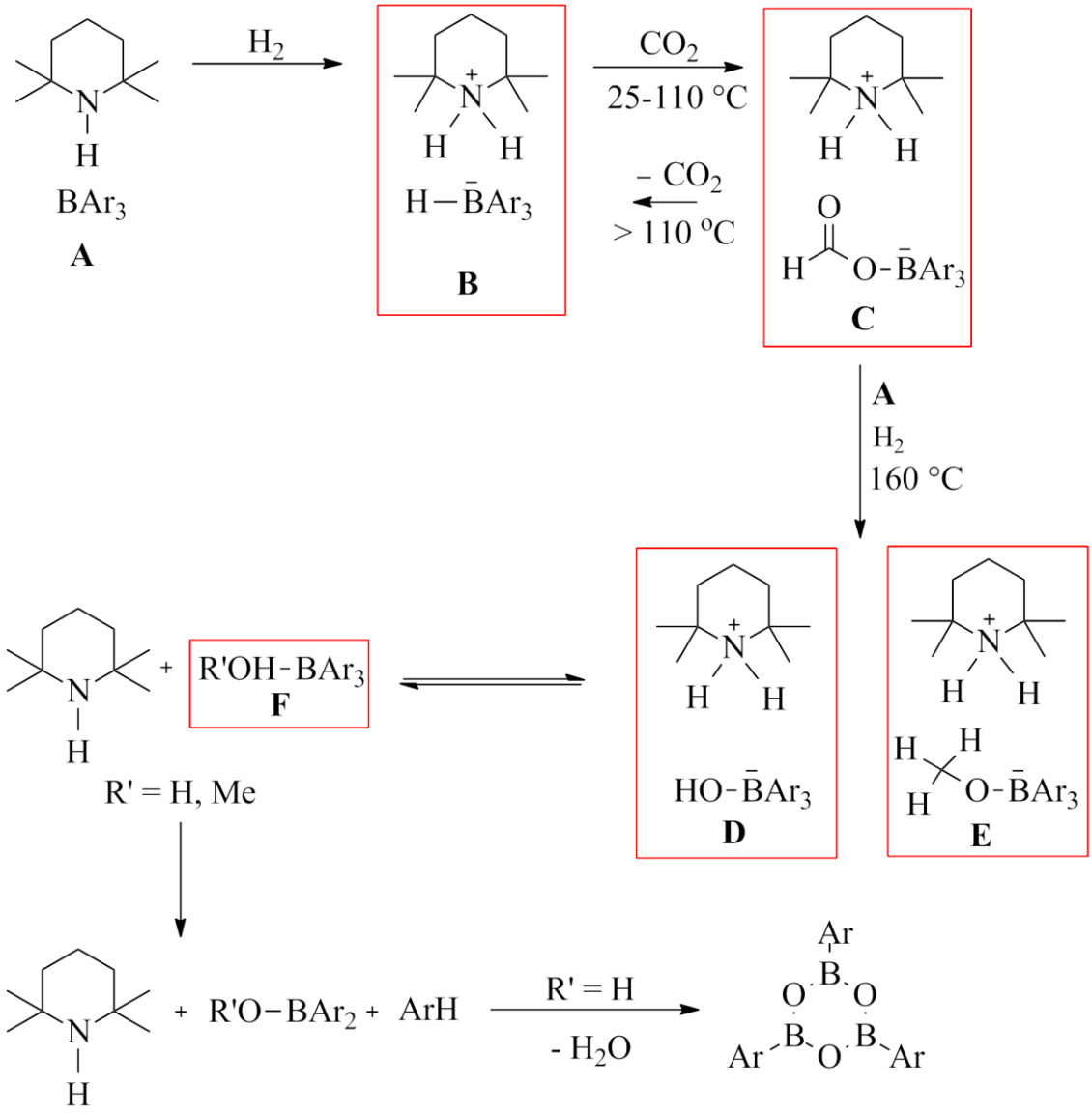


Scheme 1.8 Reduction of CO_2 to methanol using a bis-borane/phosphorus FLP.[101]

Scheme 1.8 shows after treatment of the formatoborate with a borohydride salt and then D_2O, methanol was successfully isolated in yields of 15-57%. They found that the enhanced thermal stability provided by the bridging chlorine atom between the boron atoms enhances the Lewis acidity of the boron atom bonded to the oxygen atom of the CO_2. This could explain the increased stability that was observed for the formatoborate after CO_2 activation. Unfortunately they do not indicate the fate of the FLP system in their publication.[101] However, this is not the first example of a non-metal mediated reduction of CO_2 to methanol.

In 2009, three years prior to Sgro *et al.*'s publication, Ashley *et al.* demonstrated the first selective homogeneous process for the reduction of CO_2 to CH_3OH, mediated by a non-metal system using the $[(C_6F_5)_3B\text{-}H][H\text{-}TMP]$ system as displayed in Scheme

1.9. The reaction could be conveniently monitored using ^{1}H, ^{19}F, ^{11}B and ^{13}C NMR spectroscopy.[32,80]



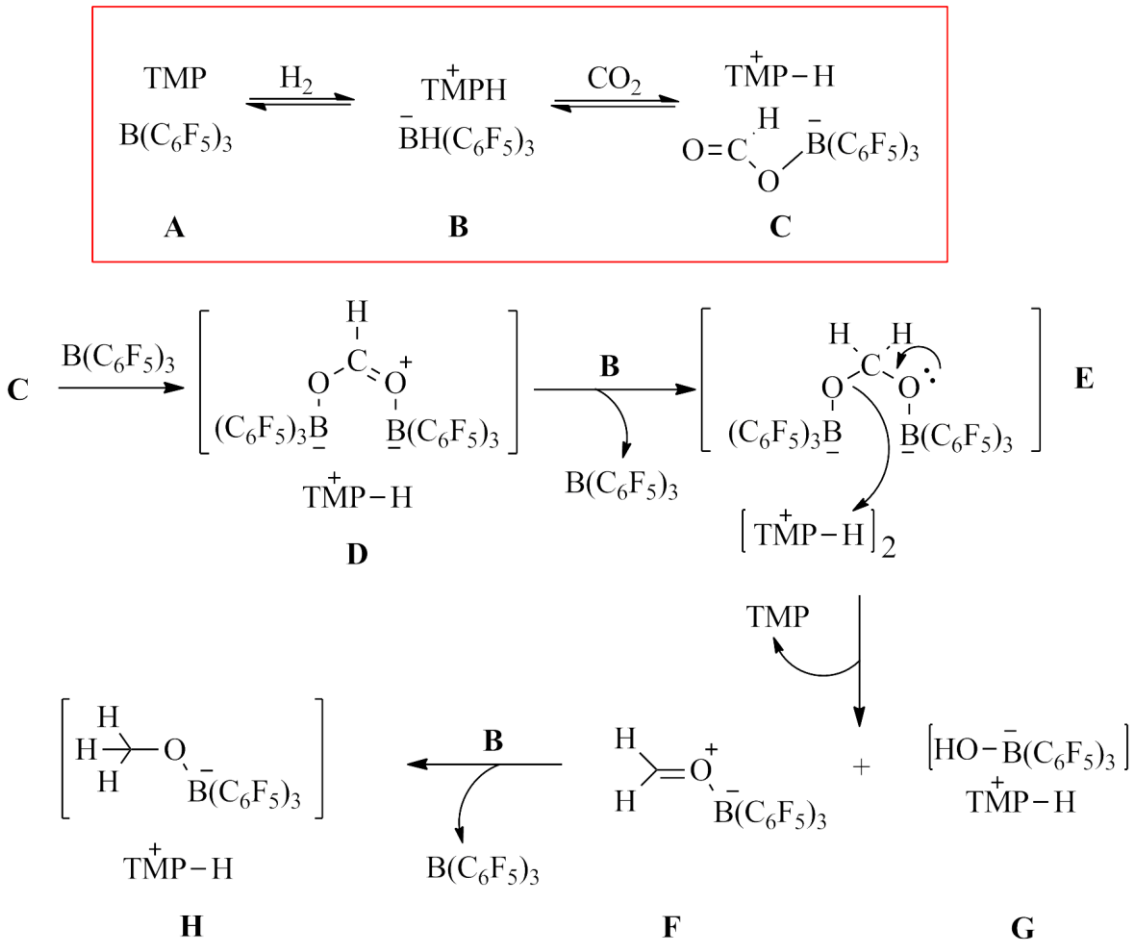
Scheme 1.9 $B(C_6F_5)_3$/TMP FLP-mediated hydrogenation of CO_2; Ar = C_6F_5.[32]

As shown in Scheme 1.9, the reaction begins by splitting H_2, using an FLP, **A**, to give salt **B**. Addition of CO_2 (1 atm) to a solution of **B** in toluene produced the formatoborate complex $[(C_6F_5)_3B\text{-}OCHO][H\text{-}TMP]$ **C**, even at room temperature (15% conversion is observed). Alternatively, **C** can be synthesised in high yield by the reaction of TMP and formic acid (HCO_2H) to give $[TMP\text{-}H][HCO_2]$, followed by the

addition of $B(C_6F_5)_3$. The alternative method has the additional advantage of permitting regiospecific isotopic labelling of the formate group using $H^{13}CO_2H$. Heating a solution of **C** (^{13}C labelled) above 110 °C revealed an equilibrium between the formate complex, **B** and free $^{13}CO_2$. The temperature was increased to 160 °C for 5-6 days which led to a mixture containing C_6F_5H, the cyclic boroxin $[OB(C_6F_5)]_3$, while the only ^{13}C-labelled products were $^{13}CH_3O\text{-}B(C_6F_5)_2$ and $^{13}CO_2$. Thus this reaction represents the disproportionation of HCO_2^- to CH_3O^- and CO_2; complete consumption of CO_2 can be achieved using a H_2/CO_2 mixture (> 3:1) in the presence of the FLP at 160 °C to form $CH_3O\text{-}B(C_6F_5)_2$ in 100% C_1 selectivity. Vacuum distillation of the solvent led to the isolation of methanol (17-25% yield), presumably *via* decomposition of the methoxyborate.[32]

1.11 Proposed Mechanism for the Reduction of CO_2 to Methanol using $[(C_6F_5)_3B\text{-}H][H\text{-}TMP]$

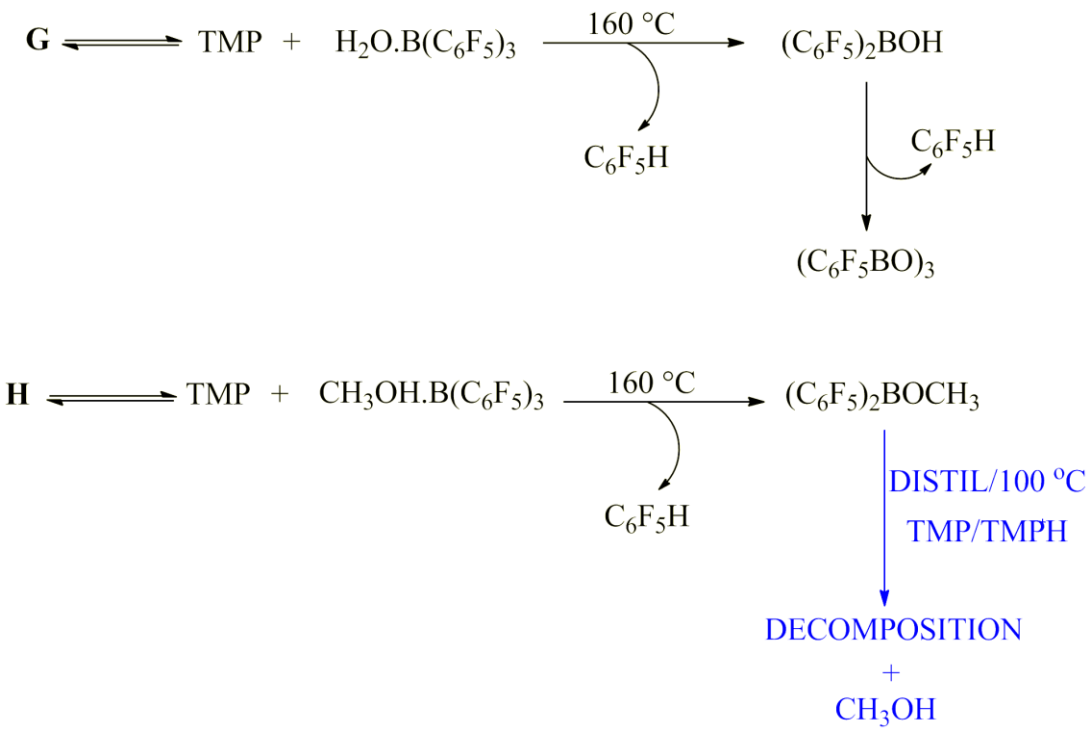
After observing the reduction of CO_2 to methanol using $[(C_6F_5)_3BH][HTMP]$ and the decomposition of the system, Ashley *et al.* proposed a possible mechanism for the disproportionation of the formatoborate to the methoxyborate. The mechanism proposed takes into consideration the experimental findings, where each reduction step depends on an equilibrium between the FLP, borohydride**,** formatoborate**,** H_2, and CO_2, as shown in Scheme 1.10.[32]



Scheme 1.10 Proposed mechanism for the disproportionation of the formatoborate, **C**, into methoxyborate, **H**, and CO_2.[32]

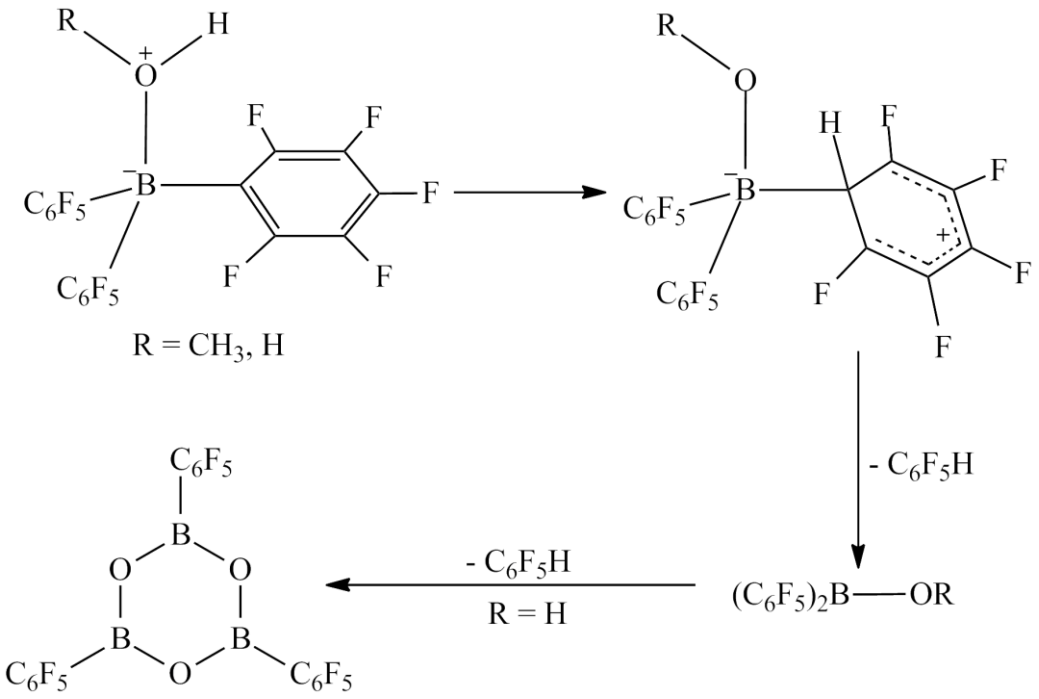
Scheme 1.10 shows the attack of a free $B(C_6F_5)_3$ upon the acyl oxygen atom of **C** which produces the bis-borane intermediate **D,** an activated formate which was observed as a broad doublet at 174.5 ppm in the ^{13}C NMR spectrum. Following hydride reduction of **D** with one equivalent of **B** leads to the formaldehyde acetal, **E**, and $B(C_6F_5)_3$. The instability of acetals in protic media is well established and the $[TMPH]^+$ counterion acts as a source of H^+ for the cleavage step, forming the formaldehyde intermediate **F,** TMP and **G**.[46] The final hydride reduction of **F** using **B** liberates the methoxyborate salt **H**. Due to the absence of any reduction products between the formate and methoxide steps this indicated that the conversion of **D** to **E** is the rate determining step. This could be a consequence of the steric hindrance caused by the

three bulky $B(C_6F_5)_3$ molecules around a single formate in such a transition state. To definitely determine that **G** and **H** are formed, each of the species were synthesised independently by adding one equivalent of H_2O or CH_3OH, respectively, to a 1:1 mixture of $B(C_6F_5)_3$ and TMP. When solutions of these salts were heated in toluene at 160 °C, a product distribution matching that of the FLP reductive system was observed (Scheme 1.11).[32]



Scheme 1.11 Thermolysis of [TMP-H][HO-$B(C_6F_5)_3$] (**G**) and [TMP-H][CH_3O-$B(C_6F_5)_3$] (**H**), producing CH_3OH.[32]

As $[TMPH]^+$ is the only source of labile protons within the system, then recombination of the ions to produce TMP and $ROH{\cdot}B(C_6F_5)_3$ (R= CH_3, H) must take place. If this was an ideal system, dissociation of H_2O and CH_3OH (isolated by distillation) would regenerate the FLP, making the system catalytic. Unfortunately, at these elevated temperatures, H^+ attack on the *ipso*-C on the C_6F_5 ring is faster, thus causing the Lewis acid to decompose (Scheme 1.12).[32]



Scheme 1.12 Decomposition of $ROH{\cdot}B(C_6F_5)_3$ adduct *via* H^+ attack on *ipso*-C_6F_5.[32]

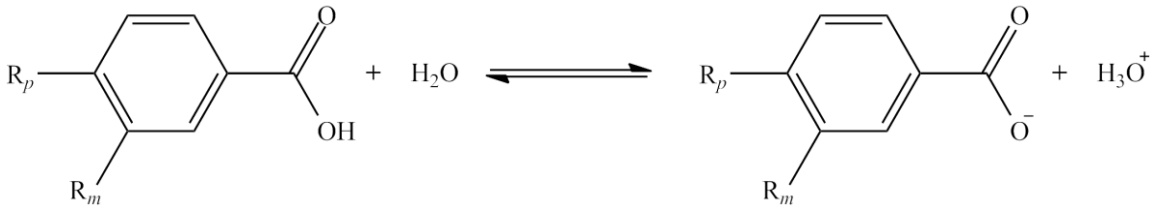
1.12 Structure Function Relationships of the Lewis Acid

It is well established that perfluoroaryl groups (C_6F_5) are powerfully electron-withdrawing groups *via* inductive electron withdrawal due to the high electronegativity of fluorine atom [χ(Pauling) = 3.98],[102] making the boron centre very Lewis acidic. Nevertheless, the π-system within the ring is activated towards electrophiles caused by mesomeric donation from the *ortho*- and *para*-F lone pairs. The 2p-2p overlap is particularly effective and makes the aromatic centre electron rich. This property is most likely the reason why protonation of the *ipso*-C_6F_5 occurs efficiently at elevated temperatures in $H_2O{\cdot}B(C_6F_5)_3$ and other similar hydroxylic adducts. Ultimately protonolysis leads to decomposition of the Lewis acid.

Replacing the C_6F_5 groups with perchloroaryl groups (C_6Cl_5) [χ(Pauling) = 2.55, Cl][102] may increase the hydrolytic stability of the Lewis acid while maintaining the electron withdrawing properties necessary for the activation of H_2.

Studies have shown that the methyl groups in mesityl (mes, 2,4,6-tri(methyl)phenyl) substituents have been able to block the binding of water to the boron in mesitylboranes. Chlorine subsituents are considered to be sterically equivalent to methyl groups and in theory should be able to shield the boron centre from reacting with H_2O.[103] Despite the fact that Cl is less electronegative then F, the weaker (3p-2p) overlap should decrease mesomeric back-donation into the aromatic system, thus reducing the electron density of the C_6Cl_5 aromatic ring.[104]

Using the Hammett relationship, the degree of activation of the aryl ring can be determined. The Hammett equation obtains a free energy relationship between reaction rates and equilibrium constants for various *meta*- and *para*- substituted aromatic compounds.[105]



Scheme 1.13 Ionisation of *meta*- and *para*-substituted benzoic acids.

Scheme 1.13 displays the ionization of benzoic acid, which can be used as a reaction standard. The relationship for a series of reactions with substituted benzene derivatives is defined in Equation 1.1.

$$\log \frac{k}{k_0} = \rho\sigma$$

k = rate (or equilibrium) constant for a *meta*- or *para*-substituted aromatic compound

k_0 = rate (or equilibrium) constant for $PhCO_2H$

ρ = reaction constant (taken as unity for the ionization of $PhCO_2H$)

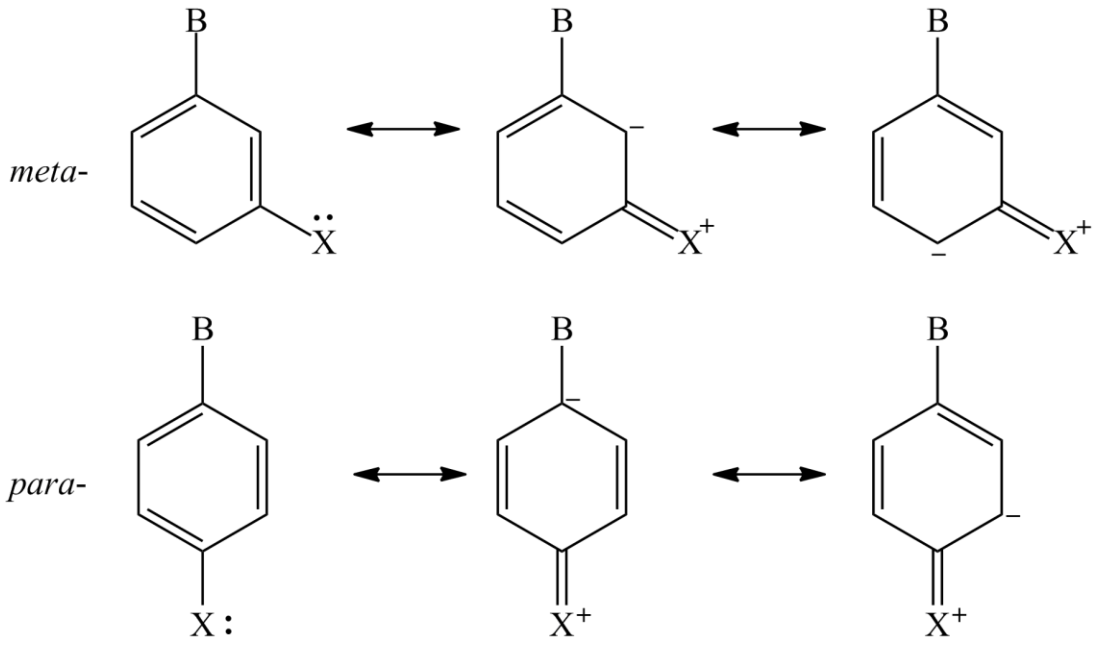
σ = constant for a given substituent (taken as unity for $PhCO_2H$)

Equation 1.1 The Hammett Relationship.

The reaction constant, ρ, defines the relative susceptibility of a reaction to the substituents. When $\rho > 1$, the reaction builds up a negative charge which indicates the reaction is more sensitive to substituents when compared to benzoic acid. A negative charge is also built up $0 < \rho < 1$, but the reaction is less sensitive to substituents. However, when $\rho < 0$, the reaction builds up a positive charge as it proceeds, facilitating the protonation upon the C_6F_5 π-system. To counteract this affect, incorporation of substituents more electron withdrawing than F would be ideal, i.e. substituents with highly positive σ values that deactivate the aromatic ring e.g. Cl.

The ionization of benzoic acid shows (ρ = 1) that the rate for the forward reaction increases with R_p or R_m substituents which assist in the stabilisation of the carboxylate anion i.e. electron withdrawing (σ = positive) instead of electron donating (σ = negative). Halogen substituents remove electron density inductively, however, mesomeric donation can go towards partial cancellation. This is significant for F substituents which can form short C-F bonds and thus facilitate mesomeric donation. Therefore a difference in σ values is seen for *para*-F and *para*-Cl (0.062 and 0.227 respectively). This means Cl substituents are considerably more electron withdrawing

in the *para* position.[106] On the other hand, *meta*-F and *meta*-Cl substituents have similar σ values (0.337 and 0.373). This is due to the inability to establish a negative charge on the *ipso*-C by mesomeric donation in the canonical form (Scheme 1.14).



Scheme 1.14 Canonical forms for *meta* and *para*-substituted aryl boranes with π-donors.

Due to steric effects, σ values cannot be calculated reliably for *ortho*-substituents. The inclination to form a resonance canonical on the *ipso*-C *via* mesomeric donation also indicates that the *ortho*-Cl substituents are more deactivating, thus increasing the Lewis acidity.

Therefore, hypothetically, the synthesis of Lewis acids containing C_6Cl_5 moieties should produce a more Lewis acidic borane, which may suppress decomposition through protonolysis and at the same time promote dissociation of H_2O and methanol. Consequently producing a catalytic method of reducing CO_2 to methanol using a metal-free FLP system.

1.13 Aims of Research

The aims of the research are to synthesise and fully characterise a systematic series of novel *tris*(aryl)borane Lewis acids containing C_6Cl_5 groups: $B(C_6F_5)_{3-n}(C_6Cl_5)_n$ (n = 1-3). The trends in the Lewis acidity of these new boranes will be determined using established donor-acceptor methods and electrochemical studies. New FLPs will then be synthesised using these Lewis acids and three Lewis bases (2,2,6,6-tetramethylpiperidine (TMP), 2,6-lutidine (Lut) and 1,4-diazobicyclo[2.2.2]octane (DABCO)). The activation of H_2 and reduction of CO_2 will be investigated using these FLPs, as well as the $B(C_6F_5)_3$/DABCO adduct to complete the series.

1.14 References

(1) Shafiee, S. T., E. *Energy Policy* **2009**, 181.

(2) Olah, G. A.; Goeppert, A.; Prakash, G. K. S. *J. Org. Chem.* **2008**, *74*, 487-498.

(3) Lee, K. B.; Beaver, M. G.; Caram, H. S.; Sircar, S. *Ind. Eng. Chem. Res.* **2008**, *47*, 8048-8062.

(4) Demessence, A.; D'Alessandro, D. M.; Foo, M. L.; Long, J. R. *J. Am. Chem. Soc.* **2009**, *131*, 8784-8786.

(5) Fletcher, A. J.; Cussen, E. J.; Prior, T. J.; Rosseinsky, M. J.; Kepert, C. J.; Thomas, K. M. *J. Am. Chem. Soc.* **2001**, *123*, 10001-10011.

(6) Surble, S.; Millange, F.; Serre, C.; Duren, T.; Latroche, M.; Bourrelly, S.; Llewellyn, P. L.; Ferey, G. *J. Am. Chem. Soc.* **2006**, *128*, 14889-14896.

(7) Campbell, C. J. *The Coming Oil Crisis* Multi-science Publishing: Brentwood, England, 1988.

(8) Searchinger, T.; Heimlich, R.; Houghton, R. A.; Dong, F.; Elobeid, A.; Fabiosa, J.; Tokgoz, S.; Hayes, D.; Yu, T.-H. *Science* **2008**, *319*, 1238-1240.

(9) Fargione, J.; Hill, J.; Tilman, D.; Polasky, S.; Hawthorne, P. *Science* **2008**, *319*, 1235-1238.

(10) Patzek, T.; Anti, S. M.; Campos, R.; Ha, K.; Lee, J.; Li, B.; Padnick, J.; Yee, S. A. *Environ. Dev, Sustain.* **2005**, *7*, 319-336.

(11) Leung, D. *Water, Air, & Soil Pollution* **2001**, *130*, 277-282.

(12) Chum, H. L.; Overend, R. P. *Fuel Processing Technology* **2001**, *71*, 187-195.

(13) Thiel, C.; Perujo, A.; Mercier, A. *Energy Policy* **2010**, *38*, 7142-7151.

(14) Wang, Q.; Chen, X. *Renew. Sust. Energ. Rev.* **2012**, *16*, 2610-2617.

(15) Coontz, R. *Science* **2004**, *305*.

(16) Bossel, U.; Eliasson, B.; Taylor, G. *The Future of the Hydrogen Economy: Bright or Bleak?; European Fuel Cell Forum Lucerne, Switzerland* **2002**.

(17) Pickett, J.; Anderson, D.; Bowles, D.; Bridgwater, T.; Jarvis, P.; Mortimer, N.; Pliakoff, M.; Woods, J. *The Royal Society, London, UK* **2008**.

(18) Olah, G. A. *Angew. Chem., Int. Ed.* **2005**, *44*, 2636-2639.

(19) Marsden, S. S. *Annual Review of Energy* **1983**, *8*, 333-354.

(20) Stiles, A. B. *AIChE J.* **1977**, *23*, 362-375.

(21) Weissermel, K.; Arpe, H.-J. *Industrial Organic Chemistry*; Wiley-VCH Verlag GmbH, 2008.

(22) *Methanol in Fuel Cell Vehicles: Human Toxicity and Risk Evaluation (Revised)* Statoil: Norway, 2001.

(23) Methanol Fuels and Fire Safety, F. S. O., EPA 400-F-92-010; US Environmental Protection Agency (EPA), Ed. Washington, DC, 1994.

(24) Collin, J. P.; Sauvage, J. P. *Coord. Chem. Rev.* **1989**, *93*, 245-268.

(25) Fujita, E.; Brunschwig, B. S.; Cabelli, D.; Rentier, M. W.; Furenlid, L. R.; Ogata, T.; Wada, Y.; Yanagida, S. In *Stud. Surf. Sci. Catal.*; Elsevier: 1998; Vol. Volume 114, p 97-106.

(26) *DOE Hydrogen Program 2000 Annual Review, May 9-11, 2000, San Ramon, California*.

(27) Jessop, P. G.; Ikariya, T.; Noyori, R. *Chem. Rev.* **1995**, *95*, 259-272.

(28) Jessop, P. G.; Joó, F.; Tai, C.-C. *Coord. Chem. Rev.* **2004**, *248*, 2425-2442.

(29) Benson, E. E.; Kubiak, C. P.; Sathrum, A. J.; Smieja, J. M. *Chem. Soc. Rev.* **2009**, *38*, 89-99.

(30) Aresta, M.; Dibenedetto, A. *Dalton Trans.* **2007**, 2975-2992.

(31) Brown, H. C.; Schlesinger, H. I.; Cardon, S. Z. *J. Am. Chem. Soc.* **1942**, *64*, 325-329.

(32) Ashley, A. E.; Thompson, A. L.; O'Hare, D. *Angew. Chem., Int. Ed.* **2009**, *48*, 9839-9843.

(33) Leitner, W. *Angew. Chem.* **1994**, *106*, 950-951.

(34) Tominaga, K.-i.; Sasaki, Y.; Kawai, M.; Watanabe, T.; Saito, M. *J. Chem. Soc., Chem. Commun.* **1993**, 629-631.

(35) Saito, M.; Fujitani, T.; Takeuchi, M.; Watanabe, T. *Appl. Catal. A-Gen.* **1996**, *138*, 311-318.

(36) Saito, M.; Takeuchi, M.; Fujitani, T.; Toyir, J.; Luo, S.; Wu, J.; Mabuse, H.; Ushikoshi, K.; Mori, K.; Watanabe, T. *Appl. Organomet. Chem.* **2000**, *14*, 763-772.

(37) Nakamura, J.; Choi, Y.; Fujitani, T. *Top. Catal.* **2003**, *22*, 277-285.

(38) Welch, G. C.; Juan, R. R. S.; Masuda, J. D.; Stephan, D. W. *Science* **2006**, *314*, 1124-1126.

(39) Welch, G. C.; Cabrera, L.; Chase, P. A.; Hollink, E.; Masuda, J. D.; Wei, P. R.; Stephan, D. W. *Dalton Trans.* **2007**, 3407-3414.

(40) Lewis, G. N.; Chemical Catalogue Company: New York, 1923.

(41) Bochmann, M.; Lancaster, S. J.; Hannant, M. D.; Rodriguez, A.; Schormann, M.; Walker, D. A.; Woodman, T. J. *Pure Appl. Chem.* **2003**, *75*, 1183-1195.

(42) Chen, E. Y. X.; Marks, T. J. *Chem. Rev.* **2000**, *100*, 1391-1434.

(43) Conifer, C. M.; Law, D. J.; Sunley, G. J.; White, A. J. P.; Britovsek, G. J. P. *Organometallics* **2011**, *30*, 4060-4066.

(44) Piers, W. E.; Chivers, T. *Chem. Soc. Rev.* **1997**, *26*, 345-354.

(45) Erker, G. *Dalton Trans.* **2005**, 1883-1890.

(46) Smith, M. B.; March, J. *March's Advanced Organic Chemistry: Reactions, Mechanisms, and Structure*; 5th ed.; Wiley-Interscience, 2001.

(47) Tang, C. Y.; Thompson, A. L.; Aldridge, S. *J. Am. Chem. Soc.* **2010**, *132*, 10578-10591.

(48) Cabrera, L.; Welch, G. C.; Masuda, J. D.; Wei, P. R.; Stephan, D. W. *Inorg. Chim. Acta* **2006**, *359*, 3066-3071.

(49) Mömming, C. M. O., Edwin; Kehr, Gerald; Fröhlich, Roland; Grimme, Stefan; Stephan, Douglas W.; Erker, Gerhard *Angew. Chem., Int. Ed.* **2009**, *48*, 6643-6646.

(50) Ménard, G. S., Douglas W. *J. Am. Chem. Soc.* **2010**, *132*, 1796-1797.

(51) Zhao, X.; Stephan, D. W. *Chem. Commun.* **2011**, *47*, 1833-1835.

(52) Chakraborty, S.; Zhang, J.; Krause, J. A.; Guan, H. *J. Am. Chem. Soc.* **2010**, *132*, 8872-8873.

(53) Otten, E.; Neu, R. C.; Stephan, D. W. *J. Am. Chem. Soc.* **2009**, *131*, 9918-9919.

(54) Mahdi, T.; Heiden, Z. M.; Grimme, S.; Stephan, D. W. *J. Am. Chem. Soc.* **2012**, *134*, 4088-4091.

(55) Rosorius, C.; Kehr, G.; Fröhlich, R.; Grimme, S.; Erker, G. *Organometallics* **2011**, *30*, 4211-4219.

(56) Mömming, C. M.; Frömel, S.; Kehr, G.; Fröhlich, R.; Grimme, S.; Erker, G. *J. Am. Chem. Soc.* **2009**, *131*, 12280-12289.

(57) Morton, J. G. M.; Dureen, M. A.; Stephan, D. W. *Chem. Commun.* **2010**, *46*, 8947-8949

(58) Birkmann, B.; Voss, T.; Geier, S. J.; Ullrich, M.; Kehr, G.; Erker, G.; Stephan, D. W. *Organometallics* **2010**, *29*, 5310-5319.

(59) Inés, B.; Holle, S.; Goddard, R.; Alcarazo, M. *Angew. Chem., Int. Ed.* **2010**, *49*, 8389-8391.

(60) Ménard, G.; Stephan, D. W. *Angew. Chem.* **2012**, *124*, 4485-4488.

(61) Appelt, C.; Westenberg, H.; Bertini, F.; Ehlers, A. W.; Slootweg, J. C.; Lammertsma, K.; Uhl, W. *Angew. Chem., Int. Ed.* **2011**, 3925-3928.

(62) Ménard, G.; Stephan, D. W. *Angew. Chem.* **2011**, *123*, 8546-8549.

(63) Menard, G.; Stephan, D. W. *J. Am. Chem. Soc.* **2010**, *132*, 1796-1797.

(64) Welch, G. C.; Stephan, D. W. *J. Am. Chem. Soc.* **2007**, *129*, 1880-1881.

(65) Chase, P. A.; Welch, G. C.; Jurca, T.; Stephan, D. W. *Angew. Chem., Int. Ed.* **2007**, *46*, 8050-8053.

(66) Chase, P. A.; Jurca, T.; Stephan, D. W. *Chem. Commun.* **2008**, 1701-1703.

(67) Zhao, L.; Li, H.; Lu, G.; Wang, Z.-X. *Dalton Trans.* **2010**, *39*, 4038-4047.

(68) Zhao, L.; Li, H.; Lu, G.; Huang, F.; Zhang, C.; Wang, Z.-X. *Dalton Trans.* **2011**, *40*, 1929-1937.

(69) Chen, D.; Wang, Y.; Klankermayer, J. *Angew. Chem., Int. Ed.* **2010**, *49*, 9475-9478.

(70) Spies, P.; Schwendemann, S.; Lange, S.; Kehr, G.; Frohlich, R.; Erker, G. *Angew. Chem., Int. Ed.* **2008**, *47*, 7543-7546.

(71) Harhausen, M.; Fröhlich, R.; Kehr, G.; Erker, G. *Organometallics* **2012**, *31*, 2801-2809.

(72) Theuergarten, E.; Schluns, D.; Grunenberg, J.; Daniliuc, C. G.; Jones, P. G.; Tamm, M. *Chem. Commun.* **2010**, *46*, 8561-8563.

(73) Ullrich, M. L., Alan J.; Stephan, Douglas W. *Organometallics* **2010**, *29*, 3647-3654.

(74) Ullrich, M.; Lough, A. J.; Stephan, D. W. *J. Am. Chem. Soc.* **2009**, *131*, 52-53.

(75) Stephan, D. W.; Erker, G. *Angew. Chem., Int. Ed.* **2010**, *49*, 46-76.

(76) Stephan, D. W. *Dalton Trans.* **2009**, 3129-3136.

(77) Chase, P. A.; Stephan, D. W. *Angew. Chem., Int. Ed.* **2008**, *47*, 7433-7437.

(78) Geier, S. J.; Gille, A. L.; Gilbert, T. M.; Stephan, D. W. *Inorg. Chem.* **2009**, *48*, 10466-10474.

(79) Geier, S. J.; Stephan, D. W. *J. Am. Chem. Soc.* **2009**, *131*, 3476-3477.

(80) Sumerin, V.; Schulz, F.; Nieger, M.; Leskela, M.; Repo, T.; Rieger, B. *Angew. Chem., Int. Ed.* **2008**, *47*, 6001-6003.

(81) Focante, F.; Mercandelli, P.; Sironi, A.; Resconi, L. *Coord. Chem. Rev.* **2006**, *250*, 170-188.

(82) Binding, S. C.; Zaher, H.; Mark Chadwick, F.; O'Hare, D. *Dalton Trans.* **2012**, *41*, 9061-9066.

(83) Lu, Z.; Cheng, Z.; Chen, Z.; Weng, L.; Li, Z. H.; Wang, H. *Angew. Chem., Int. Ed.* **2011**, *50*, 12227-12231.

(84) Sumerin, V.; Schulz, F.; Nieger, M.; Leskelä, M.; Repo, T.; Rieger, B. *Angew. Chem., Int. Ed.* **2008**, *47*, 6001-6003.

(85) http://evans.harvard.edu/pdf/evans_pka_table.pdf

(86) Blackwell, J. M.; Piers, W. E.; Parvez, M. *Org. Lett.* **2000**, *2*, 695-698.

(87) Shi, Y.-J.; Humphrey, G.; Maligres, P. E.; Reamer, R. A.; Williams, J. M. *Advanced Synthesis & Catalysis* **2006**, *348*, 309-312.

(88) Rokob, T. A.; Hamza, A.; Papai, I. *J. Am. Chem. Soc.* **2009**, *131*, 10701-10710.

(89) Hamza, A.; Stirling, A.; András Rokob, T.; Pápai, I. *Int. J. Quantum Chem.* **2009**, *109*, 2416-2425.

(90) Holschumacher, D.; Bannenberg, T.; Hrib, C. G.; Jones, P. G.; Tamm, M. *Angew. Chem., Int. Ed.* **2008**, *47*, 7428-7432.

(91) Flierler, U.; Leusser, D.; Ott, H.; Kehr, G.; Erker, G.; Grimme, S.; Stalke, D. *Chem. Eur. J.* **2009**, *15*, 4595-4601.

(92) Grimme, S.; Kruse, H.; Goerigk, L.; Erker, G. *Angew. Chem., Int. Ed.* **2010**, *49*, 1402-1405.

(93) Tye, J. W.; Darensbourg, M. Y.; Hall, M. B. In *Activation of Small Molecules*; Wiley-VCH Verlag GmbH & Co. KGaA: 2006, p 121-158.

(94) Pyykko, P.; Wang, C. *Phys. Chem. Chem. Phys.* **2010**, *12*, 149-155.

(95) Rokob, T. A.; Hamza, A.; Pápai, I. *J. Am. Chem. Soc.* **2009**, *131*, 10701-10710.

(96) Rokob, T. A.; Hamza, A.; Stirling, A.; Soós, T.; Pápai, I. *Angew. Chem., Int. Ed.* **2008**, *47*, 2435-2438.

(97) Guo, Y.; Li, S. *Inorg. Chem.* **2008**, *47*, 6212-6219.

(98) Schulz, F.; Sumerin, V.; Heikkinen, S.; Pedersen, B.; Wang, C.; Atsumi, M.; Leskelä, M.; Repo, T.; Pyykkö, P.; Petry, W.; Rieger, B. *J. Am. Chem. Soc.* **2011**, *133*, 20245-20257.

(99) Mömming, C. M.; Otten, E.; Kehr, G.; Fröhlich, R.; Grimme, S.; Stephan, D. W.; Erker, G. *Angew. Chem., Int. Ed.* **2009**, *48*, 6643-6646.

(100) Peuser, I.; Neu, R. C.; Zhao, X.; Ulrich, M.; Schirmer, B.; Tannert, J. A.; Kehr, G.; Fröhlich, R.; Grimme, S.; Erker, G.; Stephan, D. W. *Chem. Eur. J.* **2011**, *17*, 9640-9650.

(101) Sgro, M. J.; Domer, J.; Stephan, D. W. *Chem. Commun.* **2012**, *42*, 7253-7255.

(102) Ashley, A. E.; Herrington, T. J.; Wildgoose, G. G.; Zaher, H.; Thompson, A. L.; Rees, N. H.; Krämer, T.; O'Hare, D. *J. Am. Chem. Soc.* **2011**, *133*, 14727-14740.

(103) Gibson, V. C.; Spitzmesser, S. K. *Chem. Rev.* **2003**, *103*, 283-315.

(104) Cotton, A. F.; Wilkinson, G. *Advanced Inorganic Chemistry* 5th ed., 1988.

(105) Hammett, L. P. *J. Am. Chem. Soc.;* **1937**, *59*, 96-103

(106) McDaniel, D. H.; Brown, H. C. *J. Org. Chem.* **1958**, *23*, 420-427.

CHAPTER TWO

Synthesis and Characterisation of Three Novel *Tris*(aryl)boranes

2.1 Introduction

In 1963, Massey *et al.* reported the synthesis of *tris*(pentafluorophenyl)borane ($B(C_6F_5)_3$). They noted its tendency to form a variety of strongly bound adducts with ammonia, ethers and phosphines.[1,2]

Since then $B(C_6F_5)_3$ has found a number of applications in both inorganic chemistry (e.g. synthesis of weakly-coordinating anions, anion-binding, and activator in transition metal-mediated α-olefin polymerisations)[3-10] and organic chemistry (e.g. silylation of alcohols, hydrosilylation of ketones and imines, and reductive cleavage of alcohols and ethers).[11-16] $B(C_6F_5)_3$ has many appealing features; not only is it a powerful Lewis acid (with it Lewis acidity measured between BF_3 and BCl_3),[17,18] it is also a thermally robust solid (due to its strong B-C and C-F bonds) and is water-tolerant, making it easy to handle.[19,20] Therefore, it is not surprising that $B(C_6F_5)_3$ has been described as the 'ideal boron-based Lewis acid, due to its high acid strength, and stability, even at elevated temperatures, combined with substantial steric bulk'.[20]

The role of $B(C_6F_5)_3$ has changed significantly over the years and more recently it has been used as a Lewis acid partner in Frustrated Lewis Pair (or FLP) chemistry.[21-23] FLPs are formed when the steric hindrance between a Lewis acid and Lewis base prevents them from forming an adduct.[23] The unquenched energy in these molecules are able to facilitate the activation of small molecules, e.g. splitting of H_2,[24] and addition of CO_2,[23,25-27] addition of unsaturated systems,[28,29] and addition of aldehydes.[30] Another useful application of FLPs is their ability to add H_2 to bulky imines,[31-34] which has been

carried out enantioselectively.[35] The enhanced reactivity of H_2 in the presence of $B(C_6F_5)_3$-derived FLPs has been utilised to effect the metal-free hydrogenation of CO_2 to CH_3OH.[23]

Research has shown that in certain processes (e.g. the rate of epoxide ring-opening)[17] the strength of the Lewis acid with the FLP system is linked to its chemical activity. So by simply changing the Lewis acid, $B(C_6F_5)_3$, in an FLP system to the bulkier $B(C_6F_5)_2(Mes)$ (Mes = 2,4,6-$Me_3C_6H_2$) the catalytic reactivity of the system is altered. In this example, the $B(C_6F_5)_2(Mes)$ system has recently shown to lead to orthogonal reactivity patterns in the FLP-mediated reduction of imines.[36]

The vast majority of powerful boron-based Lewis acid systems have been built upon electron-withdrawing fluoroaryl ligands,[37] which impart strong acidity at the acceptor site. This increase in acidity witnessed in these Lewis acids can be explained by the high electronegativity of F ($\chi_{Pauling}$ = 3.98) which gives a potent inductive withdrawal *via* the σ-bonding framework from the boron centre. Effective mesomeric donation from *ortho*- and *para*-F lone pairs (2*p*-2*p* overlap) results in significant back-donation from the aromatic π-system into the acceptor orbital and can reduce the Lewis acidity. The scale to which π-electrons from aryl substituents are involved with the aromatic centre may be quantified using the Hammett equation, which derives a free energy relationship between reaction rates and equilibrium constants for various *meta*- and *para*- substituted aromatic compounds;[38] higher values indicate increasingly powerful electron-withdrawing groups, in the absence of steric effects. Although F is more electronegative than Cl ($\chi_{Pauling}$ = 3.16), its Hammett parameter ($\sigma_{para}F$ = 0.062) is considerably lower than Cl ($\sigma_{para}Cl$ = 0.227). This is as a result of weaker (3*p*-2*p*) π-overlap with Cl and the aromatic centre. As a result, substitution of C_6F_5 for perchlorophenyl groups (C_6Cl_5) should increase the

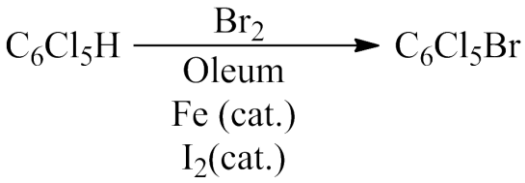
natural electron-withdrawing properties of the ligands in the resultant organoboranes, thus increasing the Lewis acidity when considered alone.

This chapter describes the successful synthesis of a systematic series of new (perhaloaryl)borane Lewis acids, $B(C_6F_5)_{3-n}(C_6Cl_5)_n$ (n = 1-3), in order to systematically examine the effects on the electrochemical and spectroscopic properties upon replacement of C_6F_5 with C_6Cl_5 groups. Furthermore, the Lewis acidity of these boranes with the parent $B(C_6F_5)_3$ is examined.

2.2 Synthesis of Novel Lewis Acids

2.2.1 Synthesis of C_6Cl_5Li

At the beginning of this project, hexachlorobenzene was readily available from main stream chemical suppliers at reasonable prices, which allowed for the facile synthesis of C_6Cl_5Li following a literature procedure.[39] However, as the project progressed it became more difficult for hexachlorobenzene to be obtained at a reasonable price as it was banned in 2005 under the Stockholm Convention on Persistent Organic Pollutants treaty,[40] requiring an alternative route to be found to C_6Cl_5Li. While an obvious replacement would be C_6Cl_5Br, this is harder to obtain then hexachlorobenzene and far more expensive, whereas, C_6Cl_5H is both readily available and much cheaper than any alternative starting material. Lithiation reactions were carried out using ^nBuLi in Et_2O but all attempts to lithiate the protio position on C_6Cl_5H led to an intractable mixture of products with lithiation seen on both the chloro and protio positions. As C_6Cl_5H has a history of reacting in an uncontrollable way,[41] focus was turned to synthesising C_6Cl_5Br from the deactivated C_6Cl_5H. After investigating a variety of different routes,[42-45] a method of synthesising C_6Cl_5Br was found by modifying a literature procedure[46] (Scheme 2.1).

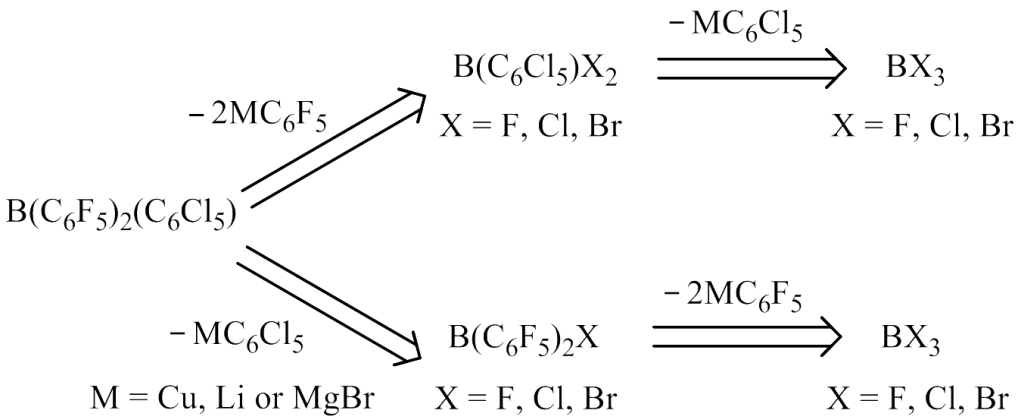


Scheme 2.1 Synthesis of C_6Cl_5Br.

C_6Cl_5Br was successfully synthesised as colourless crystalline needles, with a yield of 92%. Lithiation of C_6Cl_5Br successfully afforded C_6Cl_5Li.

2.2.2 Synthesis of $B(C_6F_5)_2(C_6Cl_5)$; 1

Retrosynthetic analysis revealed two possible routes to $B(C_6F_5)_2(C_6Cl_5)$ (**1**), depending on which perhaloaryl groups were added first (Scheme 2.2). It was rationalised that B-X metathesis with the smaller C_6F_5 moiety on a $B(C_6Cl_5)X_2$ (X = F, Cl, Br) intermediate should be carried out at the final step of the synthesis in order to minimise potential side-reactions i.e. *para*-F substitution (S_NAr) on C_6F_5 rings, which has been documented for $B(C_6F_5)_3$ in reactions with bulky nucleophiles.[47]

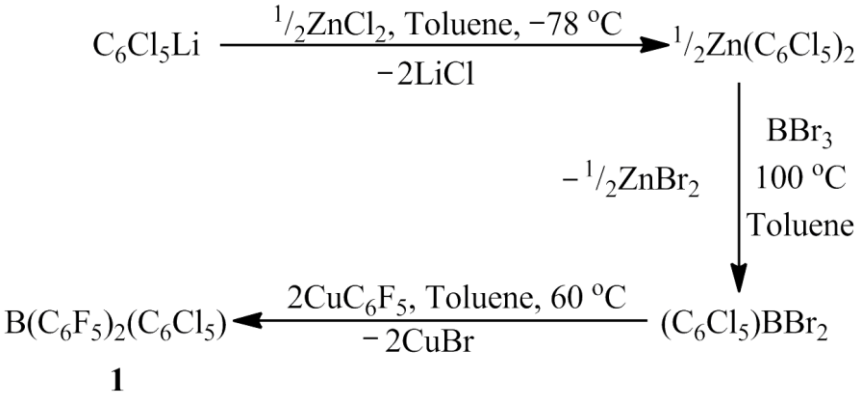


Scheme 2.2 Retrosynthetic analysis of $B(C_6F_5)_2(C_6Cl_5)$.

Previously, $(C_6Cl_5)BCl_2$ had been synthesised from $C_6Cl_5SnMe_3$ and $BCl_{3(g)}$ at 120 °C.[48] However, attempts to carry out this reaction using a less hazardous solution-

phase method led to no reaction. An alternative route, avoiding the highly toxic organotin species, was thus developed.

Previous research showed the ability of $Zn(C_6F_5)_2$ to selectively transfer C_6F_5 groups to organoboron halides.[49] Base-free $Zn(C_6Cl_5)_2$ was synthesised in a facile manner from C_6Cl_5Li and $ZnCl_2$ and then used with an excess of BBr_3 to synthesise $(C_6Cl_5)BBr_2$ as an off-colourless powder, in good yield (70%) (Scheme 2.3).

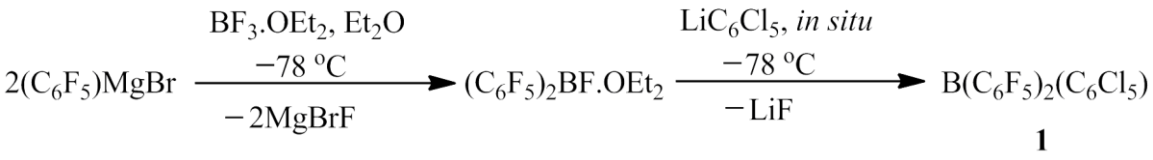


Scheme 2.3 Synthesis of $B(C_6F_5)_2(C_6Cl_5)$; **1**.

$(C_6Cl_5)BBr_2$ is an extremely moisture sensitive solid, producing HBr fumes when it makes contact with air. Attempts were made to enact the final step using C_6F_5MgBr in Et_2O. However, this led to products of solvent cleavage, which was identified by several quartet resonances between 3-4 ppm and corresponding triplets at higher field (^{1}H NMR spectroscopy), and by MS which revealed ion peaks attributable to $B(C_6Cl_5)(OEt)_2$ and $B(C_6Cl_5)(C_6F_5)OEt$. It was discovered afterwards that $(C_6Cl_5)BBr_2$ reacts with Et_2O alone to form various B-OEt containing species. Jäkle *et al*. reported the improved selectivity exhibited by CuAr (Ar = C_6F_5, 2,4,6-trimethyl-C_6H_2; Mes) in conjunction with BX_3 (X = Cl, Br) to form $ArBX_2$ or Ar_2BX, when compared to their lithium or Grignard analogues. In addition, these reactions can be carried out in donor-free solvents such as CH_2Cl_2 or

aromatics.[50] Thus, CuC_6F_5 metathesis was employed in the final stage to successfully produce **1** as a colourless powdery solid in excellent yield (81%) for this step.

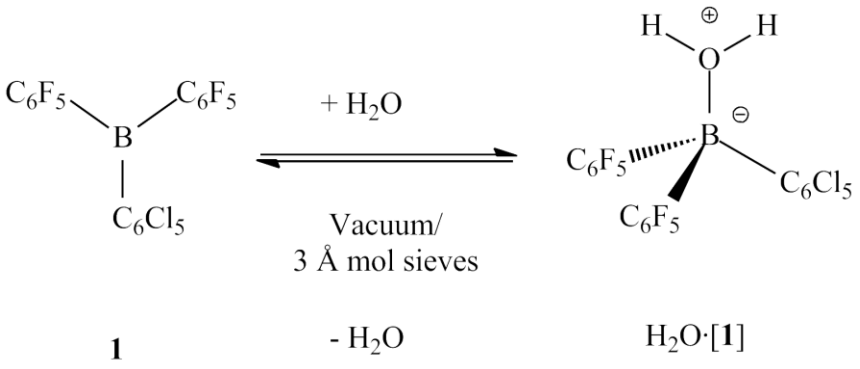
An alternative route generates $(C_6F_5)_2BX$ first and then reacts with LiC_6Cl_5. Bochmann *et al.*[51] generated $(C_6F_5)_2BF.OEt_2$ by reacting C_6F_5MgBr[52] with $BF_3.OEt_2$ (Scheme 2.4).



Scheme 2.4 Alternative synthesis of $B(C_6F_5)_2(C_6Cl_5)$; **1**.

Isolation of $(C_6F_5)_2BF.OEt_2$ proved problematic due to its rapid decomposition, and thus the subsequent reaction with LiC_6Cl_5 led to a very low yield of **1**. Whereas, the *in situ* reaction of LiC_6Cl_5 with $(C_6F_5)_2BF.OEt_2$ at −78 °C led to a higher yield of **1** (64%) as a colourless solid.

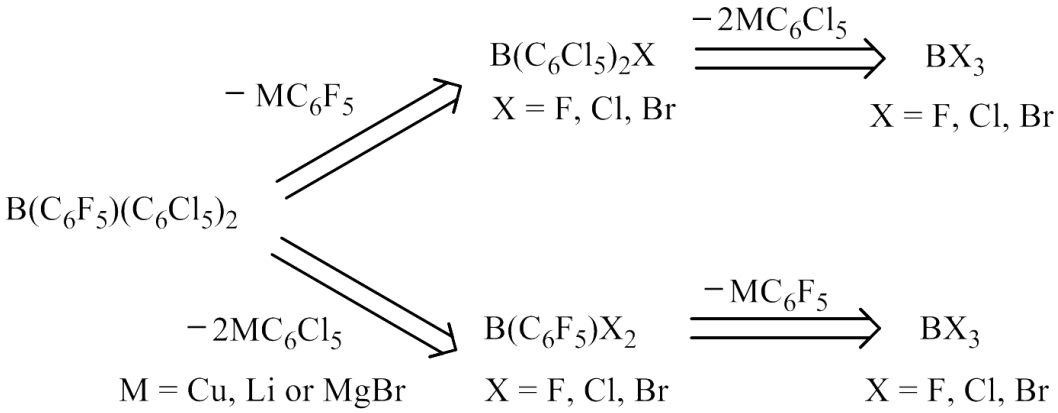
Compound **1** is moderately soluble in aliphatic hydrocarbons and extremely soluble in chlorinated and aromatic solvents, and sublimes at 125 °C (1 x 10^{-3} mbar). **1** is also oxygen stable but binds H_2O forming the dative complex $H_2O\cdot$[**1**] as shown by ^{19}F NMR spectroscopy,[53] which is a sensitive method in determining the coordination environment around the boron centre in C_6F_5-substituted boranes.[54] In comparison to $H_2O\cdot B(C_6F_5)_3$, the H_2O molecule can be rapidly and reversibly removed under vacuum, or in the solution phase upon addition of molecular sieves, forming **1** (Scheme 2.5). This difference is possibly the result of increased steric bulk around the boron centre due to the *ortho*-Cl substituents, as opposed to electronic effects (*vide infra*), resulting in a longer and thus weaker B-O interaction.



Scheme 2.5 Reversible coordination of H_2O by **1**.

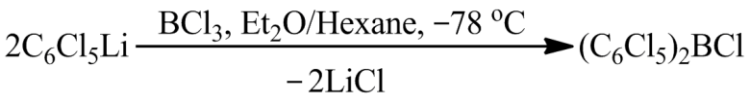
2.2.3 Synthesis of $B(C_6F_5)(C_6Cl_5)_2$; 2

As with **1**, there were two possible routes to $B(C_6F_5)(C_6Cl_5)_2$ (**2**) (Scheme 2.6).



Scheme 2.6 Retrosynthetic analysis of $B(C_6F_5)(C_6Cl_5)_2$; (**2**).

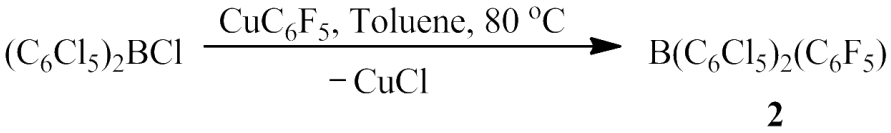
Jäkle *et al.*[50] synthesised $(C_6F_5)BBr_2$ by reacting base-free CuC_6F_5[52] with excess BBr_3 in CH_2Cl_2 at –78 ^oC. This reaction is significant as the reaction of C_6F_5MgBr with BBr_3 does not selectively produce a mono-arylated borane.[55] However, as $(C_6F_5)BBr_2$ is an oil, it proved difficult to handle. Therefore, focus was turned to synthesising $(C_6Cl_5)_2BX$. Previous use of C_6Cl_5Li as a route to $(C_6Cl_5)BX_2$ showed very poor selectivity, so it was quite a surprise when pale orange needles of $(C_6Cl_5)_2BCl$ was synthesised by reacting BCl_3 with $C_6Cl_5Li.(OEt_2)_n$ affording a yield of 54%. $C_6Cl_5Li.(OEt_2)_n$ was made from the slow addition of hexane to solution of C_6Cl_5Li in Et_2O (Scheme 2.7).



Scheme 2.7: Synthesis of $(C_6Cl_5)_2BCl$.

$(C_6Cl_5)_2BCl$ is a pale orange crystalline solid which fumes slowly in moist air (releasing HCl) and shows moderate solubility in chlorinated solvents, but is poorly soluble in aliphatics and aromatics.

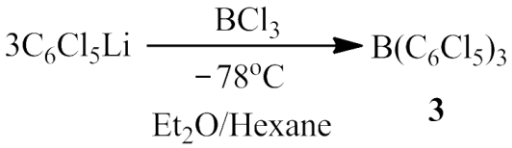
After the successful use of CuC_6F_5 in the synthesis of **1**, its reaction with $(C_6Cl_5)_2BCl$ led to the synthesis of $B(C_6Cl_5)_2(C_6F_5)$ (**2**) in good yield (70%), albeit after 72 h at 80 °C (Scheme 2.8). The slower rate of this reaction is likely due to the increased bulk of the starting haloborane $(C_6Cl_5)_2BCl$, and its replacement of a stronger B-Cl bond as opposed to B-Br, in $(C_6Cl_5)BBr_2$.



Scheme 2.8 Synthesis of $B(C_6Cl_5)_2(C_6F_5)$ (**2**).

2.2.4 Synthesis of $B(C_6Cl_5)_3$; 3

Tris(perchlorophenyl)borane (**3**) was synthesised via the stoichiometric addition of BCl_3 to C_6Cl_5Li (1:3). This is similar to the preparation of $(C_6Cl_5)_2BCl$, requiring the use of hexane as a co-solvent with Et_2O and $(C_6Cl_5)_2BCl$ is presumed to be an intermediate in the reaction. $B(C_6Cl_5)_3$ (**3**) as pale yellow crystals was isolated in moderate yield, 42% (Scheme 2.9).



Scheme 2.9 Synthesis of $B(C_6Cl_5)_3$ (**3**).

After quenching the unreacted BCl_3 and C_6Cl_5Li with H_2O, the crude product was extracted with CH_2Cl_2 using 'open bench' techniques. The orange oil was recrystallised from boiling toluene which afforded **3**·(toluene) as a pale yellow microcrystalline solid; the solvent was removed upon heating under vacuum. **3** is insoluble in aliphatic hydrocarbons, sparingly so in aromatics and moderately soluble in CH_2Cl_2. It is air and moisture stable and extraordinarily robust, remaining unchanged at temperatures up to 250 °C and does not sublime, even under high-vacuum (1×10^{-6} mbar), at these temperatures. Refluxing **3** in a toluene:H_2O mixture (1:1) for several days led to quantitative recovery of the compound and thus is remarkably hydrolytically stable.

2.3 NMR Spectroscopy

Solution phase ^{19}F, $^{11}B\{^1H\}$ and $^{13}C\{^1H\}$ NMR spectral data for **1**, **2** and **3** have been summarised and compared with $B(C_6F_5)_3$ (Tables 2.1 and 2.2). Compounds **1** and **2** exhibit three resonances in their ^{19}F NMR spectra in an intensity ratio 2:1:2 for the corresponding *ortho*, *para* and *meta* fluorine environments (to higher field respectively) for the C_6F_5 rings. The difference between the *meta* and *para* resonances, $\Delta\delta_{m,p}$, were between 17-18 ppm, and in combination with ^{11}B NMR spectroscopy the data supports the idea that the boron retains the three coordinate geometry in the solution phase for all three species.

Table 2.1 ^{19}F and $^{11}B\{^1H\}$ NMR spectral data for $B(C_6F_5)_{3-n}(C_6Cl_5)_n$; n = 0-3.

$B(C_6F_5)_{3-n}(C_6Cl_5)_n$ n = 0-3	δ(^{19}F NMR)/ppm[a]				
	***ortho*-F**	***para*-F**	***meta*-F**	$\Delta\delta_{m,p}$[c]	δ($^{11}B\{^1H\}$ NMR)/ ppm[b]
$B(C_6F_5)_3$	−128.2	−143.9	−161.1	17.2	61.2
1	−127.1	−142.8	−161.1	18.3	61.5
2	−127.4	−143.1	−160.6	17.5	66.1
3	-	-	-	-	68.2

[a]Solvent: CD_2Cl_2, $CFCl_3$ reference (external). [b]Solvent: CD_2Cl_2, $BF_3.OEt_2$ reference (external). [c]Difference between ^{19}F NMR *meta* and *para* resonances (ppm).

Table 2.2 $^{13}C\{^1H\}$ NMR spectral data for $B(C_6F_5)_{3-n}(C_6Cl_5)_n$; n = 0-2 ($C_6F_5$ ligands only).

$B(C_6F_5)_{3-n}(C_6Cl_5)_n$ n = 0-2	δ($^{13}C\{^1H\}$ NMR)/ppm[a]			
	***ortho*-C**	***para*-C**	***meta*-C**	***ipso*-C**
$B(C_6F_5)_3$	148.7	145.5	138.0	113.3
1	149.6	145.9	138.0	112.3
2	149.1	145.8	138.0	114.5

[a]Solvent: CD_2Cl_2 reference (internal).

As the number of the C_6Cl_5 ligands coordinated to the boron centre increases, the resonance in the ^{11}B NMR spectroscopy shifts to higher values. This indicates that the boron centre is becoming more electron deficient, which supports the hypothesis that a C_6Cl_5 groups are more electron withdrawing than C_6F_5. Upon addition of the first C_6Cl_5 group, a significant change is seen in the ^{19}F NMR chemical shifts, however, after the further addition of a C_6Cl_5 group, a reduced effect is seen on the ^{19}F NMR chemical shifts. It should be noted that ^{19}F NMR resonances of each of the C_6F_5 rings in **1** exhibit an averaging of aryl substituents in solution at 298 K, which is confirmed by the inequivalent C_6F_5 groups in the X-ray crystal structure of **1** (see section 2.4).

The greatest change for the $^{11}B\{^1H\}$ NMR chemical shifts occurs between compounds **1** and **2**. When one C_6F_5 ring is replaced by a C_6Cl_5 ring in $B(C_6F_5)_3$ to give **1**, the B atom experiences a stronger electron-withdrawing effect. The *ortho* and *para*- F atoms in the remaining C_6F_5 rings on **1** compensate for this effect via increased π donation, therefore the resonances for these positions become deshielded (Figure 2.1).

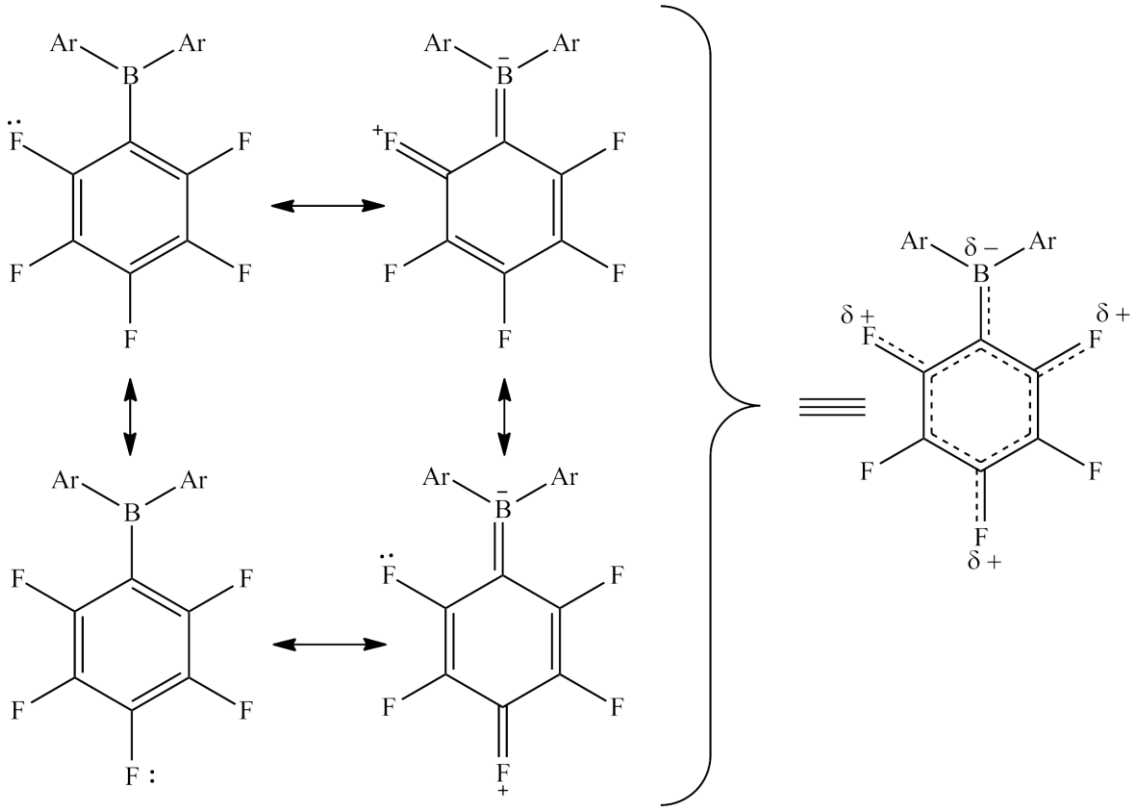


Figure 2.1 C_6F_5-ring canonical forms involving *ortho*- and *para*-F positions, contributing to enhanced π electron density at boron in compounds $B(C_6F_5)_{3-n}(C_6Cl_5)_n$ (n = 0-2).

The introduction of another bulky C_6Cl_5 group in **2** is likely to disrupt π donation through conjugation due to a sterically-induced twist of the C_6F_5 rings away from in-plane resonance with the B centre. The added inductive effect of the extra C_6Cl_5 group and a gain of electron density on the F atoms in **2** from greater electronic localisation (relative to those in **1**) allows a balance to be achieved. In general the ^{19}F NMR resonances experience a smaller change overall. This theory may be supported using the $^{13}C\{^1H\}$ NMR data, by comparing the difference between the *ipso*-C_6F_5 resonance for **1** and **2** ($\Delta\delta_i$ = +2.2), and the differences between the *ipso*-C_6F_5 resonance for $B(C_6F_5)_3$ and **1** ($\Delta\delta_i$ = −1.0). This increase in $\Delta\delta_i$ can signify an enhanced inductive withdrawal that is not as adequately compensated for by B-C_6F_5 resonance in the former C_6Cl_5-C_6F_5 substitution. The corresponding changes in the ^{13}C NMR shifts for the remaining C_6F_5

carbon atoms ($\Delta\delta_o$, $\Delta\delta_m$ and $\Delta\delta_p$; *ortho*, *meta* and *para* respectively) decreases as *n* increases, indicating that inductive effects, which become more important than resonance effects due to the ring twisting, dissipate faster with distance from the boron centre since they are mediated exclusively through the σ-framework.

2.4 Structural Characterisation

Colourless plates of **1** suitable for single crystal X-ray structure determination were grown by slow-cooling a saturated toluene solution to –35 °C.[56] Slow evaporation of a toluene solution of **2** afforded small pale-yellow blocks. Whereas, for **3**·toluene clear prisms were acquired from a saturated solution in boiling toluene (in air) that was slowly cooled to ambient temperature.

Crystallographic data was collected and solved by Dr. Amber Thompson. The solid-state structures are shown in Figures 2.2, 2.3 and 2.4 for **1**, **2** and **3** respectively. Currently no structural data exists for $B(C_6F_5)_3$ even though the Lewis acid has found widespread use in many chemical applications. Compounds $B(C_6F_5)_{3-n}(C_6Cl_5)_n$ (n = 1-3) are the first structurally characterised compounds featuring the B-C_6Cl_5 motif. All three crystallise in centrosymmetric space groups so that both left and right-handed 'propellers' are present.[57] The B atom shows trigonal planar coordination geometry as determined by the almost zero deviation of this atom from the plane of three *ipso*-C atoms, in spite of **1**, **2** and **3** having different ligand sets.[58,59] Selected bond lengths and torsion angles are shown in Table 2.3. The C-Cl bond lengths vary slightly and are comparable to those in C_6Cl_6 (range 1.713(2) - 1.724(3) Å);[60] the longest are found in the *ortho* position and are likely to reflect the high steric crowding at these sites.

In **1**, the two C_6F_5 rings are inequivalent (as mentioned in section 2.3), which is also found in the analogous $ArB(C_6F_5)_2$ (Ar = C_6H_5, Mes) species;[61] the torsion angles between the best plane of a C_6F_5 ring and the plane of the remaining B-*ipso*$(C_6X_5)_2$ (X = Cl, F) fragment best represent this difference. For steric reasons, the lowest energy conformation (minimising non-bonding interactions between *ortho*-substituents on different rings) would be a 'propeller', for which each Ar^XBAr_2 = 60° (Ar^X = C_6Cl_5, C_6F_5).[62] However, π-donation into the vacant B *p*-orbital from the C_6F_5 rings lowers the energy of the molecule and a compromise is achieved; for that reason the aryl group with the smallest torsion angle also has the shortest B-C_{ipso} bond for each $ArB(C_6F_5)_2$ (Ar = C_6H_5, Mes, C_6Cl_5) examined. By comparison, the much larger torsion angle for C_6Cl_5 in **1** is likely to be due to the poorer π-donor ability of this substituent relative to C_6F_5, in addition to its larger size; for **3** the angles now approach D_3 symmetry. Each of the solid-state structures show a trigonal planar environment around the boron centre in all the compounds (C-B-C bond angles displayed in Table 2.3), regardless of the asymmetry of the ligand set in the complexes **1** and **2**.

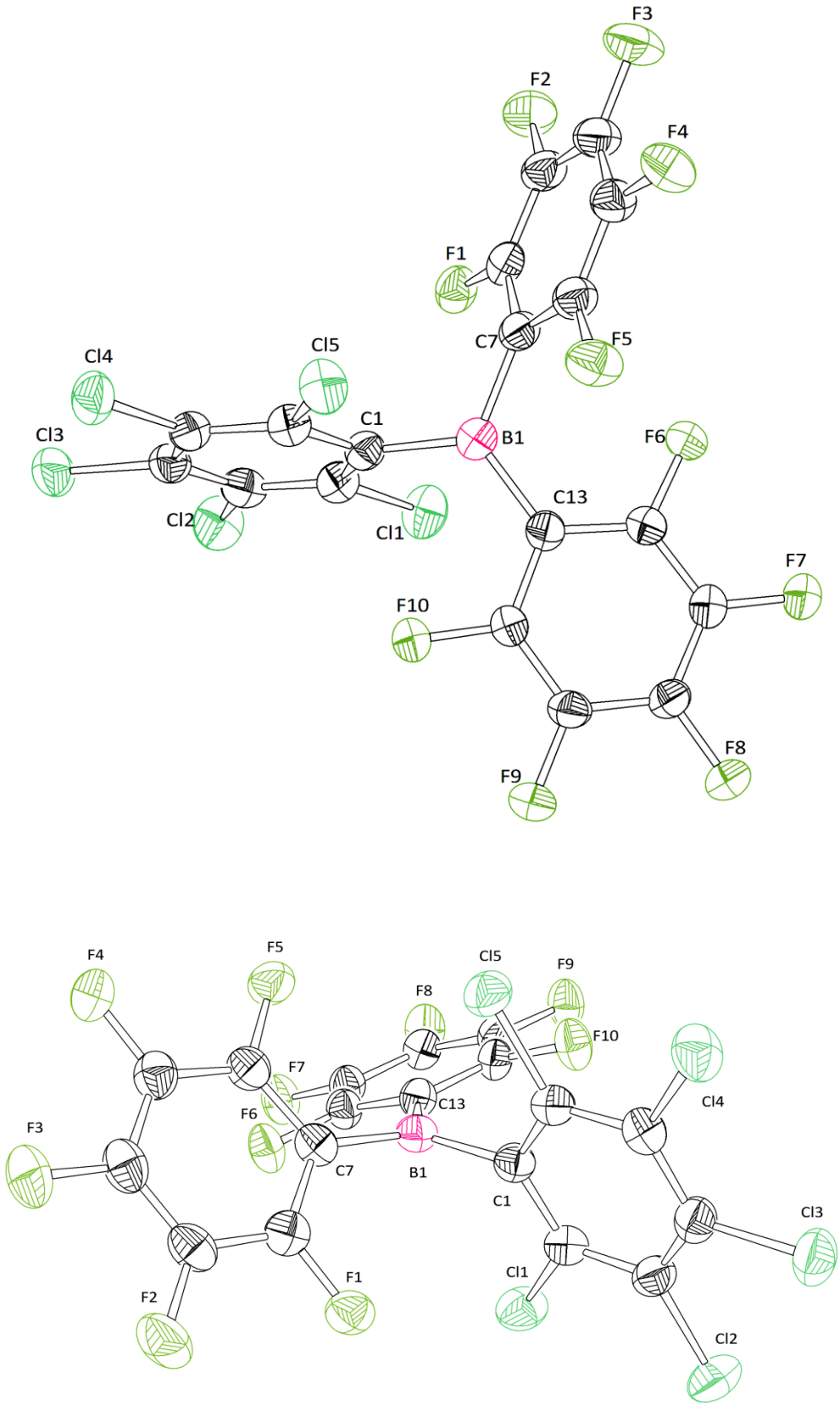


Figure 2.2 Structure of the right handed form of **1**. Orthogonal (top) and side (bottom) views of 1 (with respect to BC_3 plane); thermal ellipsoids at 50 % probability (C atoms black, Cl atoms dark green, F atoms light green and B atoms spicy pink).

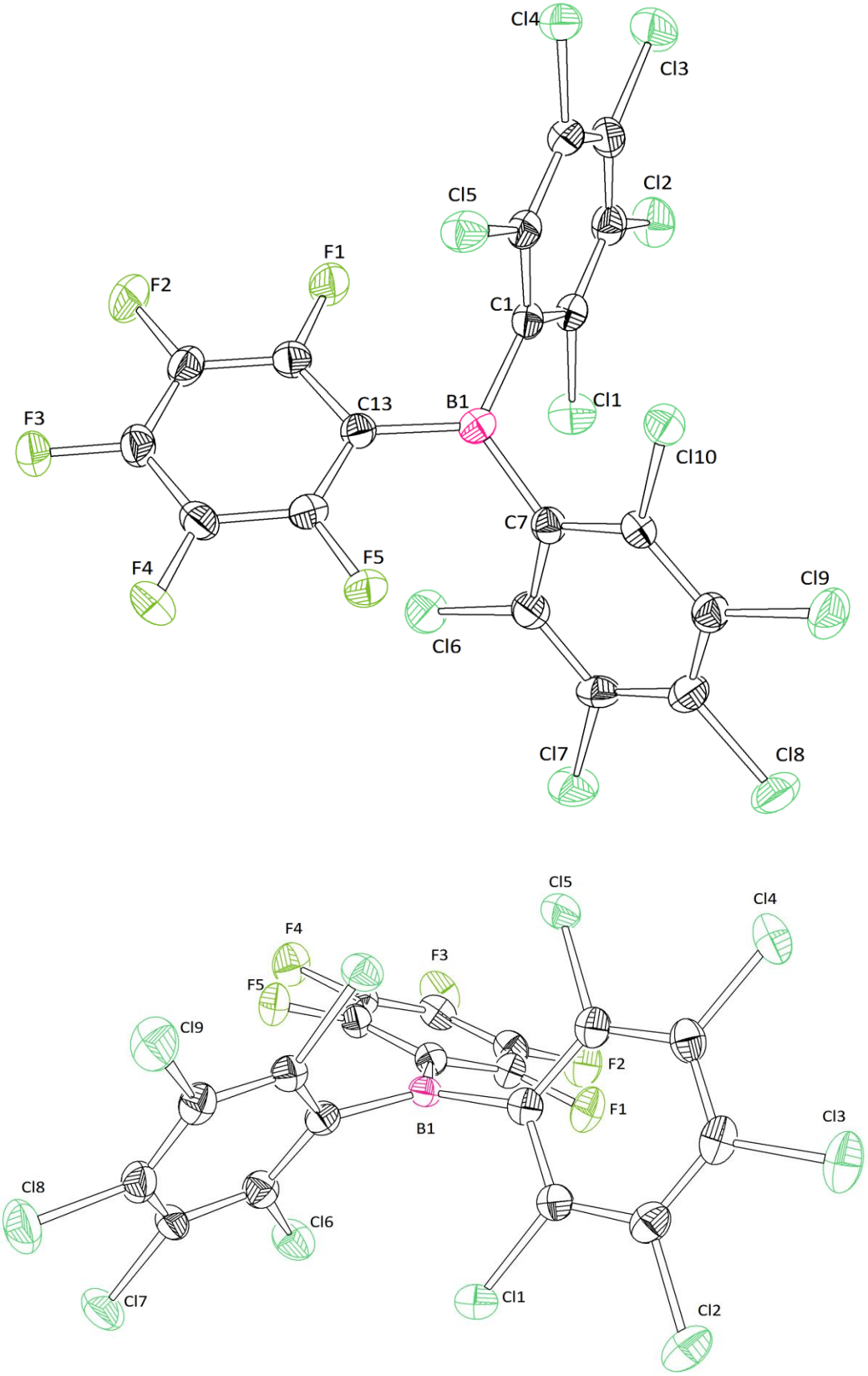


Figure 2.3 Structure of the right handed form of **2**. Orthogonal (top) and side (bottom) views with respect to BC_3 plane; thermal ellipsoids at 50 % probability (C atoms black, Cl atoms dark green, F atoms light green and B atoms spicy pink).

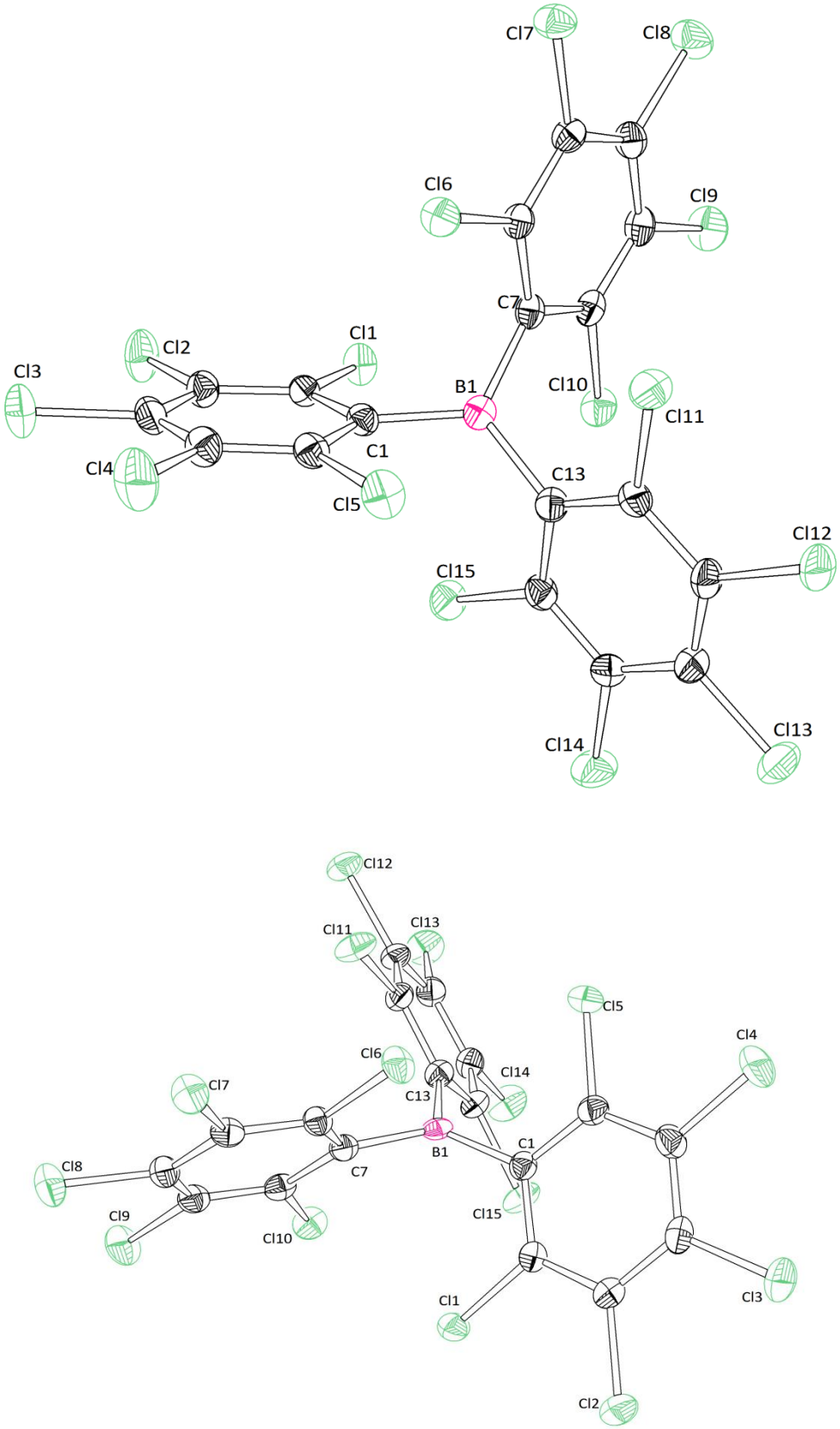


Figure 2.4 Structure of the right handed form of **3**. Orthogonal (top) and side (bottom) views with respect to BC_3 plane); thermal ellipsoids at 50 % probability (C atoms blue, Cl atoms dark green and B atoms spicy pink). Disordered toluene molecule in asymmetric unit removed for clarity.

Table 2.3 Selected bond lengths and angles for $B(C_6F_5)_3$ and compounds **1**, **2** and **3**; numbers in parentheses are estimated standard uncertainties (esu). Computed values (B3LYP/TZVP) are shown in italics.

	$B(C_6F_5)_3$	**1**	**2**	**3**
B1 – C1 (Å)	(*1.57*)	1.580(4) (*1.59*)	1.589(4) (*1.59*)	1.576(4) (*1.59*)
B1 – C7 (Å)	(*1.57*)	1.577(4) (*1.57*)	1.586(4) (*1.59*)	1.587(4) (*1.59*)
B1 – C13 (Å)	(*1.57*)	1.561(4) (*1.57*)	1.552(4) (*1.57*)	1.586(4) (*1.59*)
Range C-F (Å)	(*1.33 – 1.34*)	1.333(3)-1.352(4) (*1.33 – 1.34*)	1.330(4)-1.344(3) (*1.33 – 1.34*)	–
Range C-Cl (Å)	-	1.712(3)-1.732(3) (*1.74 – 1.76*)	1.714(3)-1.730(3) (*1.74 – 1.76*)	1.711(3)-1.732(3) (*1.74 – 1.75*)
Ar^F^BAr_2 (°)	(*40, 41,40*)	24.4, 51.9 (*24, 52*)	22.3 (*36*)	–
Ar^{Cl}^BAr_2(°)	-	69.7(*74*)	57.1, 62.0 (*57, 58*)	54.5, 55.3, 58.1 (*53, 53, 53*)
C(1)-B(1)-C(7) (°)	-	118.1(3)	118.6(3)	120.0(2)
C(1)-B(1)-C(13) (°)	-	121.4(3)	119.0(2)	122.8(3)
C(7)-B(1)-C(13) (°)	-	120.4(3)	122.2(3)	117.2(2)

Ar^X^BAr_2 (Ar^{Cl} = C_6Cl_5; Ar^F = C_6F_5) is the torsion angle, as defined in Figure 2.5.

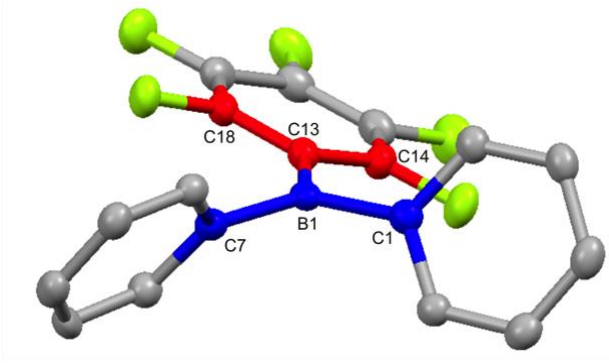


Figure 2.5 Calculation of the torsion angle for C_6F_5 ring in **2** ($C_6F_5BAr_2$; Ar = C_6Cl_5) and the $B(C_6Cl_5)_2$ unit, defined as the angle between the planes of blue (BAr_2) atoms and red (C_6F_5 ring) atoms. F atoms shown in green, Cl atoms have been omitted for clarity.

2.5 Lewis Acidity Measurements

There are a number of methods available to measure the relative Lewis acidity of compounds, which are mainly based on spectroscopic (IR, NMR) techniques.[63-67] For (fluoroaryl)boranes, there are two commonly used methods based on NMR spectroscopy. The first of these methods focuses on Gutmann's acceptor number (AN) for scaling solvent polarity, which measures the change in $^{31}P\{^{1}H\}$ NMR chemical shift ($\Delta\delta$) of uncoordinated Et_3PO *vs* that of the Lewis acid adduct. This method was subsequently modified by Beckett.[67] The second method was developed by Childs and is based upon the downfield shift of the *trans*-crotonaldeyde H_3 resonance upon forming a complex to the Lewis acid.[63] The H_3 site is considered sterically remote from the site of bonding yet electronically connected *via* conjugation (Figure 2.6).

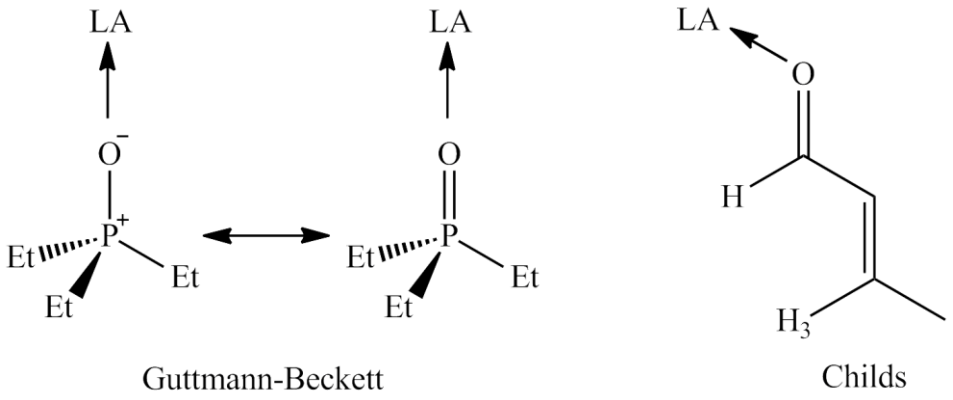


Figure 2.6 The Gutmann-Beckett and Childs Lewis acidity test (LA, Lewis acid).

The results obtained from both methods are summarised in Table 2.4; for comparison the Lewis acidity of $B(C_6F_5)_3$ has also been measured. The results from the Guttmann-Beckett method are presented in Figure 2.7, which shows that upon coordination of Et_3PO the difference in chemical shift ($\Delta\delta$ $^{31}P\{^{1}H\}$ NMR) decreases in the order $B(C_6F_5)_3$ > **1** > **2**, thus the introduction of each C_6Cl_5 group has a linear effect on the

measured Lewis acidity. There is no indication of complexation for **3**, and thus no data is reported.

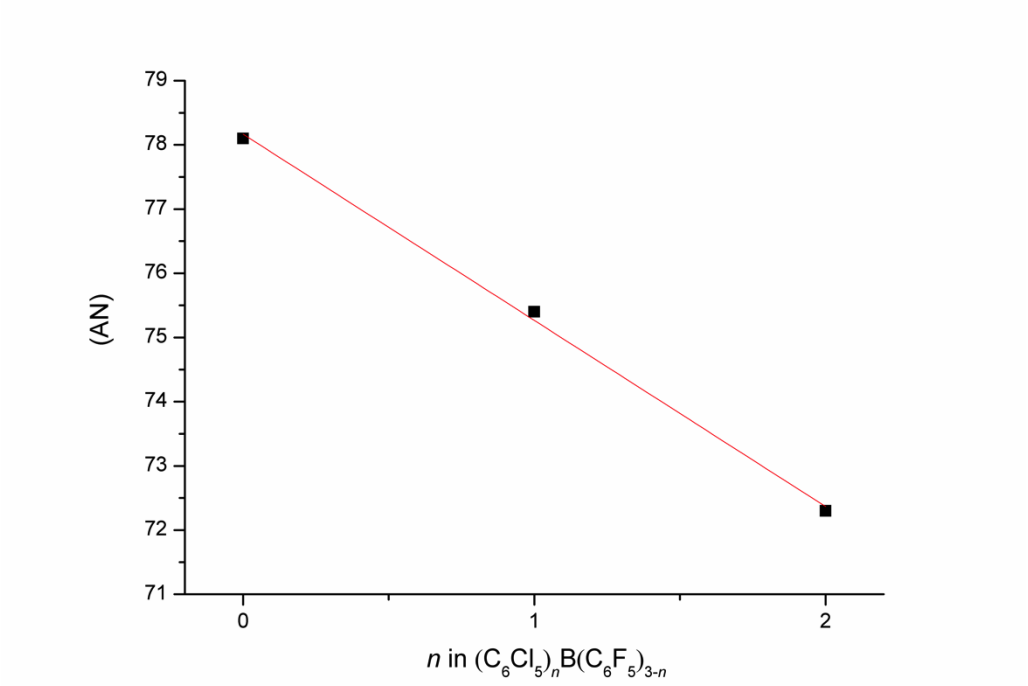


Figure 2.7 Plot of Acceptor Number (AN) *vs n* in $B(C_6F_5)_{3-n}(C_6Cl_5)_n$ (n = 0-2).

Whereas, the Child's method produced an alternative set of results with only $B(C_6F_5)_3$ and **1** showing complexation to the aldehyde. It was found that the upfield shift difference ($\Delta\delta$) in the adduct of **1** was noticeably smaller than that seen for $B(C_6F_5)_3$. Recently Stephan *et al*. proposed the idea of tuning the Lewis acidity for a series of phosphine-borane/phosphinium-borane species $R_2P(C_6F_4)B(C_6F_5)_2$ and $[R_3P(C_6F_4)B(C_6F_5)_2]^+$, and observed a linear correlation between the two techniques.[68,69] As an environment consisting of only B-C bonds was maintained throughout, the steric factors about the borane centre remained effectively unchanged and the site of electronic modulation is remote (*para*-bound P on C_6F_4 ring), the results obtained can be considered self-consistent. On the other hand, Britovsek *et al*. synthesised the series

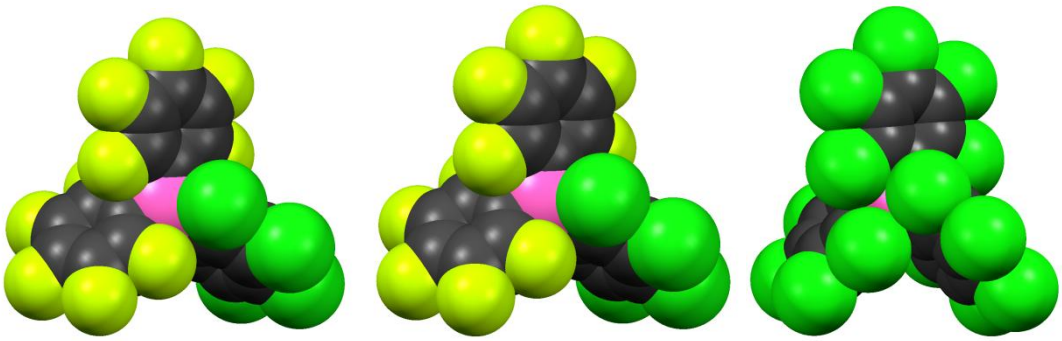
$B(C_6F_5)_{3-x}(OC_6F_5)_x$ (x = 1-3), where systematic replacement of pentafluorophenyl moieties by harder pentafluorophenoxy ligands resulted in binding preference for Et_3PO over crotonaldehyde.[70] This was rationalized using Pearson's HSAB principle where the largely covalent and softer C=O $p\pi$-$p\pi$ bond is a preferable donor to $B(C_6F_5)_3$ compared to the harder, more ionic $p\pi$-$d\pi$ P=O bond in Et_3P=O, which is favoured by $B(OC_6F_5)_3$.[71]

Table 2.4 $^{31}P\{^1H\}$ and ^1H NMR spectral data derived for Lewis acidity measurements for **1**, **2**, **3** and $B(C_6F_5)_3$.

Lewis Acid	**Et_3PO**				***trans*-Crotonaldeyde**	
	$^{31}P\{^1H\}$ NMR /ppm[a]	**Δδ /ppm[b]**	**$^{11}B\{^1H\}$ NMR /ppm[a]**	**AN[b]**	**^1H NMR /ppm[a,c]**	**Δδ /ppm[c]**
None	50.7	–	–	0	6.88	–
$B(C_6F_5)_3$	77.0	33.7	–2.5	78.1	7.93	1.05
1	75.8	32.5	–1.1	75.3	7.51	0.63
2	74.5	31.2	0.3	72.3	6.88	–
3	50.7	0.0	68.2	–	6.88	–

[a] Solvent: CD_2Cl_2. [b] See reference 69 for calculation of acceptor number (AN); $\delta = \delta[Et_3PO(coordinated)] - \delta[Et_3PO(hexane)]$. [c] $\Delta\delta = \delta[H_3(coordinated)] - \delta[H_3(free)]$

When only considering steric hindrance of the Lewis acids, the Britovsek study showed that as x increases there is a steady increase in the accessibility of the Lewis acid centre which allows for binding by both the donors examined. As a result this allows the Lewis bases to be distinguished by electronic factors caused by the replacement of B-C by B-O linkages. Examination of the space-fill diagrams for the solid-state structures of compounds **1**, **2**, and **3** (Figure 2.8) show greater screening of the boron acceptor site upon replacement of C_6F_5 moieties for C_6Cl_5.



(a) **(b)** **(c)**

Figure 2.8 Space-fill diagram of (a) **1**, (b) **2** and (c) **3**; (C atoms black, Cl atoms aquamarine, F atoms yellowgreen and B atoms spicy pink).

When determining the Lewis acidity of the compounds, moving along the series from $B(C_6F_5)_3$ to $B(C_6Cl_5)_3$, another variable needed to be taken into consideration. As well as the increase in electrophilicity there is also, simultaneously, an increase in the steric crowding around the boron centre. Due to the increase in steric crowding, one can imagine that a steric threshold exists whereby the *ortho*-ring substituents obstruct the Lewis base from forming a dative interaction which overrides the electronic factors. This effect is probably more significant for crotonaldehyde (C=O bond length 1.21 Å)[72] than the phosphine oxide (P=O 1.46(1) Å in Ph_3PO, for example)[73] at the position of complexation. Thus, for Et_3PO the adduct formation is achieved for n = 0, 1, 2 and a linear relationship is present throughout the series, whereas crotonaldehyde can only bind to n = 0 and 1; nevertheless, the results show a decrease in Lewis acidity from $B(C_6F_5)_3$. Due to the steric hindrance provided by the three C_6Cl_5 groups on **3**, neither Lewis base can successfully achieve coordination and the compound may be judged to have gone beyond the steric threshold with both Lewis bases.

2.6 Electrochemical Studies

In collaboration with Dr. Gregory Wildgoose, the reduction potentials for **1**, **2** and **3** were studied to determine the electron density at the boron acceptor orbital for each Lewis acid. As shown by Power *et al.*, reduction of $B(Mes)_3$ and subsequent X-ray structure determination of the resultant radical anion showed that minimal structural reorganisation of the trigonal planar environment of the borane occurs upon electron transfer.[61] Hence, the potentials may be viewed as an approximate measure of the Lewis acidity of $B(C_6F_5)_{3-n}(C_6Cl_5)_n$ (n = 0-3) in the absence of steric effects. In spite of the prevalent use of $B(C_6F_5)_3$ as a powerful Lewis acid no report exists that claims to directly observe the voltammetric reduction of this species, even though evidence documents its use as a one electron oxidant.[74]

An attempt was made to estimate the redox potential of $B(C_6F_5)_3$ (THF, 0.1 M $[^nBu_4N][BF_4]$ electrolyte) by Cummings *et al.*, using cyclic voltammetry (CV) on the series $B(C_6F_5)_{3-n}(Mes)_n$ (n = 1-3).[75] However, it has been documented that the mesityl-substituted boranes only weakly coordinate THF so it is reasonable that the observation of a reduction wave for these species is due to high enough concentrations of the free three-coordinate *tris*(aryl)borane electron acceptors in solution. However, the C_6Cl_5 substituted boranes were predicted to be substantially more electron-deficient, due to the C_6Cl_5 moieties being more electron withdrawing than the mesityl moieties, and indeed **1** strongly coordinates THF. The reduction of the **1**.THF coordinated species was examined using the CV (under comparable conditions). The investigation only yielded poorly defined voltammograms with no distinct waves. However, when the experiments were conducted using the weakly coordinating solvent CH_2Cl_2, recording at various scan rates (50-500 mVs^{-1}); well-defined cyclic voltammograms for all compounds were observed (Figure 2.9). A plot of the reductive peak current *vs* the square root of the voltage scan

rate was created (Figure 2.9, insets) and in all cases a linear relationship was seen, thus confirming that the reduction was operating under diffusion control.[76]

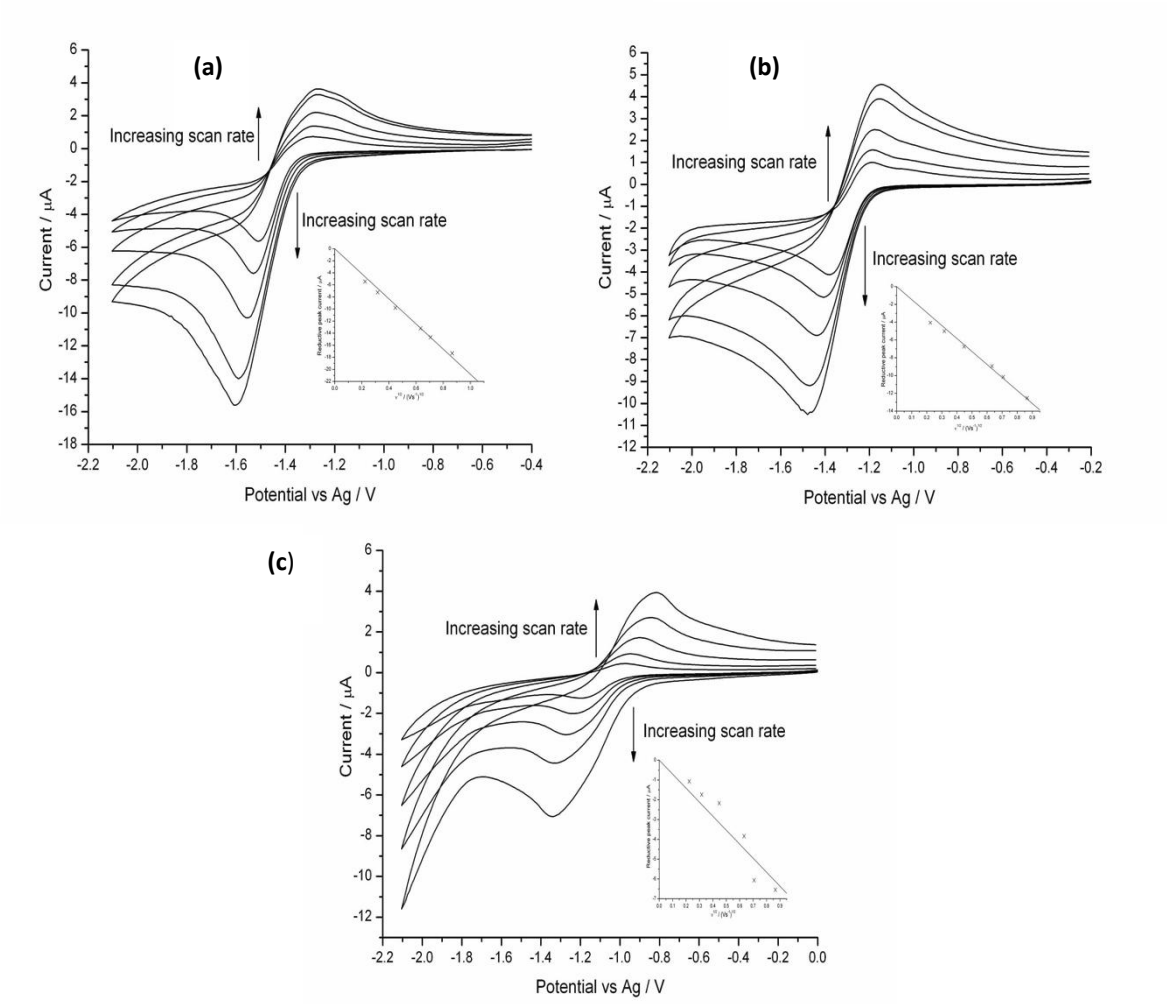


Figure 2.9 Overlaid cyclic voltammograms recorded at scan rates of 50 to 500 mVs^{-1} in CH_2Cl_2 (0.1 M [$^nBu_4N$][BF_4]) of (a) **1** (10 mM concentration); (b) **2** (10 mM concentration); (c) **3** (5 mM concentration). Insets show respective plots of reductive peak current *vs* square-root of voltage scan rate.

Intially, when the potential was scanned in a negative direction a single reduction wave was observed at every scan rate for each complex. At lower scan rates (e.g. 50 mVs^{-1}) when the direction is later reversed the corresponding oxidation waves were observed to be quite broad and smaller in height than the reduction wave. At higher scan rates, the oxidative waves became more prominent and the ratio of the oxidative to

reductive peak current increased, but was always less than 1:1 even at scan rates of up to 10 Vs^{-1}. The observed cyclic voltammetric behaviour is consistent with the reduction corresponding to an EC mechanism[77] where 'E' denotes a heterogeneous electron transfer step and 'C' denotes a follow-up homogeneous chemical step, and is comparable to the behaviour observed by Cummings *et al.* for $B(C_6F_5)_{3-n}(Mes)_n$. Once the radical anion of the parent complex had formed, the radical anion rapidly underwent further homogenous follow-up chemistry leading to decomposition of the radical anion produced at the electrode. At slow scan rates, the decomposition of the intermediate radical anion is sufficiently fast compared to the voltammetric timescale so that its corresponding re-oxidation is not observed. On increasing the scan rate, an increase in the kinetics of decomposition began to be outrun and a correspondingly larger oxidation wave is then observed until the ratio of i_{pOx}:i_{pRed} approached unity. The formal reduction potential of each compound **1**, **2** and **3** is calculated using the mid-peak potential, $E_{mid} = (E_{pOx} + E_{pRed})/2$, and are listed in Table 2.5. A trend is observable whereby the reduction peak potential of each complex was discovered to shift to increasingly less negative potentials, and the voltammetry seems to become more reversible as the number of C_6Cl_5 substituents attached to the boron centre increases. These findings support the NMR spectral data that a C_6Cl_5 group is *more* electron-withdrawing than a C_6F_5 substituent, thus causing the boron centre to become more oxidising and shows a strong relationship with the more positive Hammett parameter for aryl-bound Cl *vs* F. Additionally, the larger size of the Cl group (especially in the *ortho* position) reflects an increased shielding of the boron-centred radical anion upon reduction, which inhibits bimolecular decomposition pathways and hence increases the stability/reversibility of the voltammetry; a similar strengthening effect is attributed to the stability, and consequently the persistence of the isoelectronic $[C(C_6Cl_5)_3]^{\bullet}$.[78,79] Thus, assuming that a linear

relationship exists between these potentials and the number of C_6Cl_5 substituents attached to each boron centre gives an estimate of the reduction potential for $B(C_6F_5)_3$ of –1.92 V ± 0.1 V (*vs* $Cp_2Fe^{0/+}$).

Table 2.5 Average values of E_{mid} measured from CV data for complexes $B(C_6F_5)_{3-n}(C_6Cl_5)_n$ (n = 0-3).

$B(C_6F_5)_{3-n}(C_6Cl_5)_n$	E_{mid}/V[a]
$B(C_6F_5)_3$	–1.97 ± 0.10
1	–1.87 ± 0.05
2	–1.55 ± 0.05
3	–1.48 ± 0.02

[a]Potentials are reported *vs* $Cp_2Fe^{0/+}$ (CH_2Cl_2) at a Pt macrodisc electrode.

Prior attempts to witness the direct reduction of $B(C_6F_5)_3$ have employed either CH_2Cl_2 or THF solvent (despite the fact that $B(C_6F_5)_3$·THF is known to be a strongly bound adduct)[80] and commonly used electrolytes such as $[^nBu_4N][ClO_4]$ or $[^nBu_4N][BF_4]$; at best produced ill-defined curves.[74,75] $B(C_6F_5)_3$ has demonstrated rich oxo-anion binding chemistry which could possibly extend to ClO_4^- (reported to be more coordinating than BF_4^-),[81] and since the Lewis acidity of $B(C_6F_5)_3$ has been judged to be similar to that of BF_3, it is probable that F^- abstraction from BF_4^- to form $[FB(C_6F_5)_3]^-$ occurs;[82] in both these examples the supporting electrolyte would quench the acceptor orbital and hence inhibit reduction. With these potential drawbacks in mind; instead the $[^nBu_4N]^+$ salt of the weakly coordinating anion $[BArF_{24}]^-$ in CH_2Cl_2 was used as an electrolyte ($BArF_{24}$ = $B[3,5\text{-}(CF_3)_2C_6H_3]_4$). Figure 2.10 shows the resulting cyclic voltammetry of $B(C_6F_5)_3$, successfully obtained for the first time. At modest scan rates

(< 1 Vs^{-1}) a reduction wave is observed which corresponds to a one-electron reduction forming the $[B(C_6F_5)_3]^{\bullet-}$ radical anion, at –1.97 ± 0.1 V. The rate of decomposition of $B(C_6F_5)_3$ continues the trend observed for $B(C_6F_5)_{3-n}(C_6Cl_5)_n$ complexes (n = 1-3) and is the fastest of the series, such that a back peak corresponding to the re-oxidation of the radical anion is only observed at scan rates in excess of 1 Vs^{-1}.

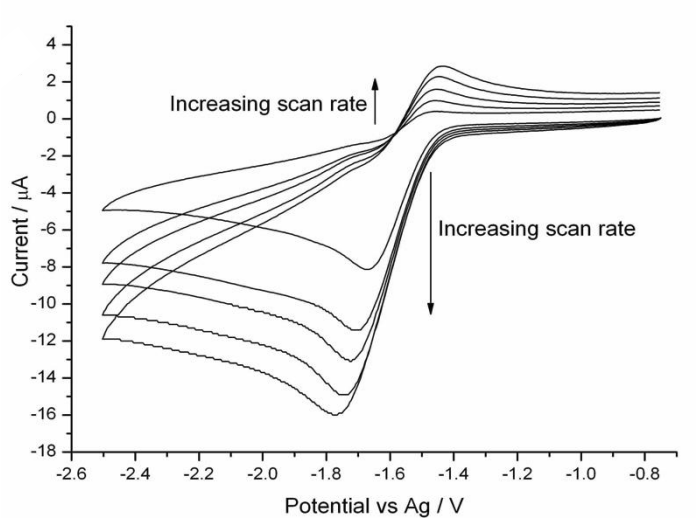


Figure 2.10: Overlaid cyclic voltammograms of $B(C_6F_5)_3$ in CH_2Cl_2 (5 mM, 0.1 M $[^nBu_4N][BArF_{24}]$; 1-5 Vs^{-1} scan rate).

Figure 2.11 combines the *measured* E_{mid} potentials of all complexes $B(C_6F_5)_{3-n}(C_6Cl_5)_n$ complexes (n = 0-3) *vs* the number of C_6Cl_5 groups in the molecule and shows a clear linear trend. The *estimated* value of the reduction potential of $B(C_6F_5)_3$ is very close to the measured value. It is also interesting to compare the estimated values from the $B(C_6F_5)_{3-n}(Mes)_n$ series used by Cummings *et al.* to estimate the potential of $B(C_6F_5)_3$, and to compare their estimate with our measured value.[75] To do this, the IUPAC convention of referencing non-aqueous potentials to the $Cp_2Fe^{0/+}$ couple in the solvent system of choice rather than the practice of referencing potentials to the aqueous SCE reference electrode was employed.[83] The data shows that the estimated reduction potential of $B(C_6F_5)_3$ in the work of Cummings *et al.* is encouragingly close to the measured value; the difference in values may be accounted for by appreciating the fact

that the studies were conducted in different solvents (CH_2Cl_2 and THF). The difference in shift of *ca*. +200 mV per C_6Cl_5 introduced compared with *ca*. –500 mV obtained for the mesityl series may be understood in that for the former case C_6F_5 (a σ-acid and π-donor) is replaced by a group of greater electron-withdrawing ability (predominantly σ-acid) whereas in the latter it is replaced by a strongly electron-donating ligand (a σ-donor); the effect on the electrode potentials is therefore appreciably greater.

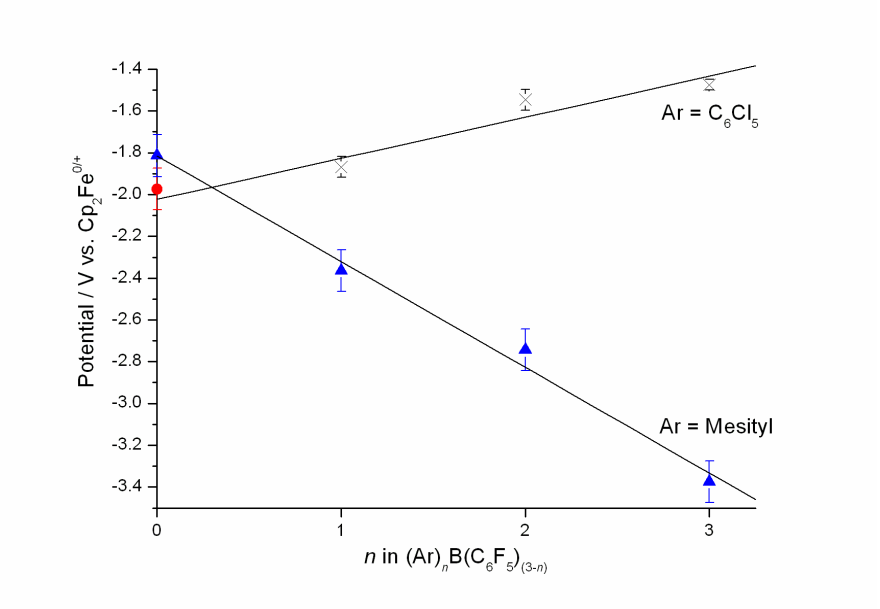


Figure 2.11 A plot showing the E_{mid} potentials of complexes $B(C_6F_5)_{3-n}(C_6Cl_5)_n$ (n = 0-3; denoted ×) *vs* the number of substituent C_6Cl_5 groups in the complex, and also the E_{mid} values determined for the series $B(C_6F_5)_{3-n}(Mes)_n$ (n = 0-3) and their estimated value for the reduction potential of $B(C_6F_5)_3$ (▲).[75] The *measured* potential, E_{mid}, for $B(C_6F_5)_3$ in CH_2Cl_2 (●) has also been included.

2.7 Electronic Structure Analysis

In collaboration with Dr. Tobias Krämer, the electronic consequences of the successive replacement of C_6F_5 with C_6Cl_5 were explored. The structures have been optimised for all four members of the series, $B(C_6F_5)_{3-n}(C_6Cl_5)_n$ (n = 0-3) using density functional theory (DFT) (B3LYP/TZVP). The bond lengths and angles at the minimum

energy structures (shown in parentheses in Table 2.3) are all fully consistent with the experimental data. Most appreciably in the context of the present study, the B-C_6F_5 distances across the series are uniformly 0.02 Å shorter than their B-C_6Cl_5 counterparts. Computed ^{11}B shielding constants also replicate the experimental trend almost quantitatively, with shifts (relative to $B(C_6F_5)_3$, n = 0) of –0.4, 4.5 and 6.6 ppm (for n = 1, 2 and 3, respectively) *c.f.* values of 0.3, 4.9 and 7.1 ppm from experiment (Table 2.1). The encouraging level of agreement with both structural and spectroscopic observables gives us confidence that the chosen methodology is capturing the essential variations in electronic structure across the series. The computed natural charges on the boron centre increase in the order n = 0 (0.81) < n = 1 (0.89) < n = 2 (1.02) < n = 3 (1.16), supporting the hypothesis that Lewis acidity increases with increasing substitution of C_6F_5 with C_6Cl_5.

2.8 Kinetics of H_2O Dissociation from H_2O.[1]

It has been shown that H_2O forms a number of aqua complexes with $B(C_6F_5)_3$, $[H_2O{\cdot}B(C_6F_5)_3]{\cdot}(H_2O)_n$, involving H_2O molecules hydrogen-bonded together beyond the primary coordination sphere of the dative 1:1 adduct.[84-86] Although coordinated water in $H_2O{\cdot}B(C_6F_5)_3$ is tightly bound and difficult to remove under vacuum (e.g. negligible loss at 10^{-3} mbar) or through heating (exceeding 60 °C results in hydrolysis to $(C_6F_5)_2BOH$ and C_6F_5H),[87] the kinetics of water dissociation have been studied by observing degenerate aqua ligand transfer between $H_2O{\cdot}B(C_6F_5)_3$ and free $B(C_6F_5)_3$ using Variable Temperature ^{19}F NMR.[88] Since **1** exhibits the ability to reversibly coordinate H_2O under similar conditions it was thought prudent to determine comparable data for H_2O dissociation from $H_2O{\cdot}$**1**; such a property is likely to be of use in true Lewis acid catalysis under aqueous regimes, in contrast to the Brønsted acidic properties of $H_2O{\cdot}B(C_6F_5)_3$

resulting from strong activation of the water molecule.[89] Due to such facile decoordination of H_2O, an analogous equilibrium was achieved by combining **1** with H_2O in a 2:1 ratio in toluene-d_8 solution.

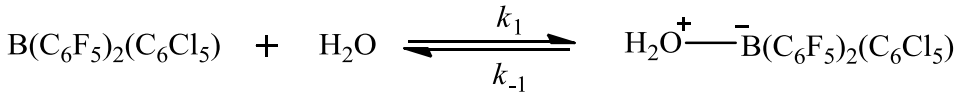


Figure 2.12 Dissociative exchange between H_2O and **1**.

At 200 K sharp resonances in the ^{19}F NMR spectrum are observed with separate resonances corresponding to a mixture of H_2O·**1** and **1**, whereas at room temperature dynamic averaging reflects fast exchange (Figures 2.12 and 2.13). With Dr. Nick Rees, line-shape analysis of the ^{19}F NMR spectra as a function of temperature enabled the rate constants, and subsequent thermodynamic parameters $\Delta H^{\ddagger}$ and $\Delta S^{\ddagger}$, to be obtained from an Eyring plot (Table 2.7).

Table 2.7 Activation parameters for H_2O dissociation from H_2O·[B] ([B] = $B(C_6F_5)_3$, and **1**) as determined by Variable Temperature ^{19}F NMR (toluene-d_8 solution); errors in parentheses.

	$\Delta H^{\ddagger}$ / kJ mol^{-1}	$\Delta S^{\ddagger}$ / J K^{-1} mol^{-1}	$\Delta G^{\ddagger}_{300}$ / kJ mol^{-1}
$H_2O{\cdot}B(C_6F_5)_3$[88]	79.50(3)	100(1)	47.49(4.5)
H_2O·**1**	41.4(0.3)	13.4(1.2)	37.2(1)

As expected, $\Delta H^{\ddagger}$ for dissociation of H_2O from **1** is less than that for $B(C_6F_5)_3$ which is consistent with the increased size of the borane, leading to a weaker B-O interaction. The considerably larger entropic value for $H_2O{\cdot}B(C_6F_5)_3$ may be rationalised by

hydrogen-bonding between the hydroxyl protons and the *ortho*-F substituents. This effect will be emphasised by the strong polarisation of the O-H bonds in the H_2O molecule from the powerfully Lewis acidic organoborane fragment, and indeed O-H···F bonding is observed in the solid-state structure of this compound.[85] In the ground state of the complex such organised bonding would more than likely restrict free rotation of bonds within the H_2O moiety, thus lowering the total entropy of the system. However, on the dissociation of H_2O, loss of ordered H-bonding leads to an overall greater entropy change than that expected for a unimolecular to bimolecular conversion alone. In comparison, for H_2O·**1** the degree of O-H···F interactions is anticipated to be smaller due to fewer C_6F_5 moieties in the borane and poorer O-H polarisation from weaker H_2O-B binding. Thus upon dissociation the entropy gain significantly diminishes in relation to that found for $H_2O{\cdot}B(C_6F_5)_3$.

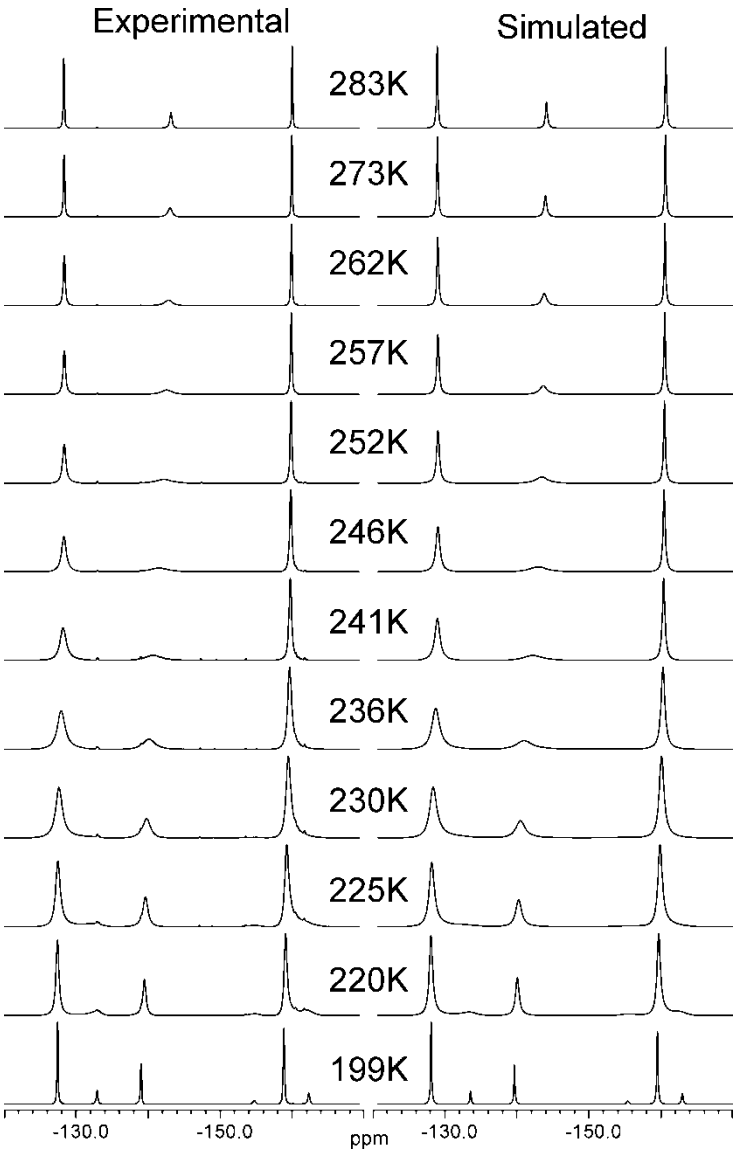


Figure 2.13 Variable-temperature ^{19}F NMR spectra (simulated and experimental) for exchange of water between H_2O·**1** and **1** (toluene-d_8 solution).

2.9 Conclusions

The complete series of perchloroaryl Lewis Acids $B(C_6F_5)_{3-n}(C_6Cl_5)_n$ (n = 1-3; **1, 2** and **3**) have been successfully synthesised and comprehensively characterised. Perchlorination of all the aryl substituents bestows substantial thermal and hydrolytic stability to **3**. The solid-state structures reveal a trigonal planar environment for boron in all the compounds, despite the asymmetry of the ligand set in the complexes **1** and **2**. Solution $^{11}B\{^1H\}$, $^{13}C\{^1H\}$ and ^{19}F NMR spectroscopy studies reveal a trend of B-C_6F_5 resonance interactions being replaced by predominantly inductive effects arising from the increasing number of C_6Cl_5 groups. A decrease in Lewis acidity has been established upon sequential substitution of C_6F_5 with C_6Cl_5 in $B(C_6F_5)_3$ for n = 0-2, as demonstrated by the Gutmann-Beckett method, and corroborated by the Childs method despite only being successful for n = 0 and 1; the acceptor properties of **3** could not be determined using either of these techniques. On the other hand, electrochemical studies show that the boron centre becomes more electron deficient (oxidising) travelling along the series, demonstrating a C_6Cl_5 substituent to be more electron withdrawing than a C_6F_5 substituent. The optimised structures of all the Lewis acid, $B(C_6F_5)_{3-n}(C_6Cl_5)_n$ (n = 0-3) using density functional theory (B3LYP/TZVP) agree fully with the experimental structural data. Computed ^{11}B shielding constants are also consistent with the experimental trend almost quantitatively, and the computed natural charges on the boron centre increase in the order n = 0 (0.81) < n = 1 (0.89) < n = 2 (1.02) < n = 3 (1.16), supporting the hypothesis that Lewis acidity should parallel electrophilicity trends upon increasing substitution of C_6F_5 with C_6Cl_5. All the results can rationalised by realising that various measurements of Lewis acidity may be dominated by either steric and/or electronic effects. While electrochemistry provides a physio-chemical measure of the electron affinity of the B centre in these compounds, it does not consider the steric cost of

B sp^2-sp^3 rehybridisation which is important for bulky boranes upon coordination of Lewis bases. In comparison, the Gutmann-Beckett/Childs' methods include both factors in their measurement and give a more reliable indication of 'chemical' Lewis acidity. Therefore, when considering these novel Lewis acids as a whole, the Lewis acidity decreases when substituting the C_6F_5 groups with C_6Cl_5 groups.

2.10 References

(1) Massey, A. G.; Stone, F. G. A.; Park, A. J. *Proc. Chem. Soc. (London)* **1963**, 212.

(2) Massey, A. G.; Park, A. J. *J. Organomet. Chem.* **1964**, *2*, 245-250.

(3) Krossing, I.; Raabe, I. *Angew. Chem. Int. Ed.* **2004**, *43*, 2066-2090.

(4) Bochmann, M.; Lancaster, S. J.; Hannant, M. D.; Rodriguez, A.; Schormann, M.; Walker, D. A.; Woodman, T. J. *Pure Appl. Chem.* **2003**, *75*, 1183-1195.

(5) Lancaster, S. J.; Walker, D. A.; Thornton-Pett, M.; Bochmann, M. *Chem. Commun.* **1999**, 1533-1534.

(6) Lancaster, S. J.; Rodriguez, A.; Lara-Sanchez, A.; Hannant, M. D.; Walker, D. A.; Hughes, D. H.; Bochmann, M. *Organometallics* **2002**, *21*, 451-453.

(7) LaPointe, R. E.; Roof, G. R.; Abboud, K. A.; Klosin, J. *J. Am. Chem. Soc.* **2000**, *122*, 9560-9561.

(8) Yang, X. M.; Stern, C. L.; Marks, T. J. *J. Am. Chem. Soc.* **1994**, *116*, 10015-10031.

(9) Bernsdorf, A.; Brand, H.; Hellmann, R.; Kockerling, M.; Schulz, A.; Villinger, A.; Voss, K. *J. Am. Chem. Soc.* **2009**, *131*, 8958-8970.

(10) Chen, E. Y. X.; Marks, T. J. *Chem. Rev.* **2000**, *100*, 1391-1434.

(11) Gevorgyan, V.; Rubin, M.; Benson, S.; Liu, J. X.; Yamamoto, Y. *J. Org. Chem.* **2000**, *65*, 6179-6186.

(12) Blackwell, J. M.; Sonmor, E. R.; Scoccitti, T.; Piers, W. E. *Org. Lett.* **2000**, *2*, 3921-3923.

(13) Parks, D. J.; Piers, W. E. *J. Am. Chem. Soc.* **1996**, *118*, 9440-9441.

(14) Morrison, D. J.; Piers, W. E. *Org. Lett.* **2003**, *5*, 2857-2860.

(15) Blackwell, J. M.; Foster, K. L.; Beck, V. H.; Piers, W. E. *J. Org. Chem.* **1999**, *64*, 4887-4892.

(16) Morrison, D. J.; Blackwell, J. M.; Piers, W. E. *Pure Appl. Chem.* **2004**, *76*, 615-623.

(17) Beckett, M. A.; Brassington, D. S.; Coles, S. J.; Hursthouse, M. B. *Inorg. Chem. Comm.* **2000**, *3*, 530-533.

(18) Jacobsen, H.; Berke, H.; Doring, S.; Kehr, G.; Erker, G.; Frohlich, R.; Meyer, O. *Organometallics* **1999**, *18*, 1724-1735.

(19) Erker, G. *Dalton Trans.* **2005**, 1883-1890.

(20) Piers, W. E.; Chivers, T. *Chem. Soc. Rev.* **1997**, *26*, 345-354.

(21) Welch, G. C.; Prieto, R.; Dureen, M. A.; Lough, A. J.; Labeodan, O. A.; Holtrichter-Rossmann, T.; Stephan, D. W. *Dalton Trans.* **2009**, 1559-1570.

(22) Kenward, A. L.; Piers, W. E. *Angew. Chem., Int. Ed.* **2008**, *47*, 38-41.

(23) Ménard, G. S., Douglas W. *J. Am. Chem. Soc.* **2010**, *132*, 1796-1797.

(24) Welch, G. C.; Stephan, D. W. *J. Am. Chem. Soc.* **2007**, *129*, 1880-1881.

(25) Stephan, D. W.; Erker, G. *Angew. Chem., Int. Ed.* **2010**, *49*, 46-76.

(26) Ashley, A. E.; Thompson, A. L.; O'Hare, D. *Angew. Chem., Int. Ed.* **2009**, *48*, 9839-9843.

(27) Zhao, X.; Stephan, D. W. *Chem. Commun.* **2011**, *47*, 1833-1835.

(28) Stirling, A.; Hamza, A.; Rokob, T. A.; Papai, I. *Chem. Commun.* **2008**, 3148-3150.

(29) Ullrich, M. L., Alan J.; Stephan, Douglas W. *Organometallics* **2010**, *29*, 3647-3654.

(30) Mömming, C. M. O., Edwin; Kehr, Gerald; Fröhlich, Roland; Grimme, Stefan; Stephan, Douglas W.; Erker, Gerhard *Angew. Chem., Int. Ed.* **2009**, *48*, 6643-6646.

(31) Chase, P. A.; Welch, G. C.; Jurca, T.; Stephan, D. W. *Angew. Chem., Int. Ed.* **2007**, *46*, 8050-8053.

(32) Chase, P. A.; Jurca, T.; Stephan, D. W. *Chem. Commun.* **2008**, 1701-1703.

(33) Zhao, L.; Li, H.; Lu, G.; Wang, Z.-X. *Dalton Trans.* **2010**, *39*, 4038-4047.

(34) Zhao, L.; Li, H.; Lu, G.; Huang, F.; Zhang, C.; Wang, Z.-X. *Dalton Trans.* **2011**, *40*, 1929-1937.

(35) Chen, D.; Wang, Y.; Klankermayer, J. *Angew. Chem., Int. Ed.* **2010**, *49*, 9475-9478.

(36) Eros, G.; Mehdi, H.; Papai, I.; Rokob, T. A.; Kiraly, P.; Tarkanyi, G.; Soos, T. *Angew. Chem. Int. Ed.* **2010**, *49*, 6559-6563.

(37) Piers, W. E.; Irvine, G. J.; Williams, V. C. *Eur. J. Inorg. Chem.* **2000**, 2131-2142.

(38) McDaniel, D. S.; Brown, H. C. *J. Org. Chem.* **1958**, *23*, 420-427.

(39) Rausch, M. D. T., F.E.; Gordon,H.B. *J. Organomet. Chem.* **1966**, *5*, 493-500.

(40) UNEP. *Stockholm Convention on Persistent Organic Pollutants* [Online Early Access].http://www.pops.int/documents/guidance/nipsfinal/i06e.pdf, http://www.pops.int/documents/guidance/beg_guide.pdf.

(41) Schlosser, M.; Marzi, E.; Cottet, F.; Büker, H. H.; Nibbering, N. M. M. *Chem. Eur. J.* **2001**, *7*, 3511-3516.

(42) Joshi, S. N.; Vyas, S. M.; Duffel, M. W.; Parkin, S.; Lehmler, H. J. *Synthesis* **2011**, *2011*, 1045-1054.

(43) Rahman, M. A.; Shito, F.; Kitamura, T. *Synthesis* **2010**, *2010*, 27-29.

(44) Do, H.-Q.; Daugulis, O. *Org. Lett.* **2008**, *11*, 421-423.

(45) Popov, I.; Do, H.-Q.; Daugulis, O. *J. Org. Chem.* **2009**, *74*, 8309-8313.

(46) Harada, K.; Hart, H.; Frank Du, C. J. *J. Org. Chem.* **1985**, *50*, 5524-5528.

(47) Welch, G. C.; Juan, R. R. S.; Masuda, J. D.; Stephan, D. W. *Science* **2006**, *314*, 1124-1126.

(48) Chivers, T.; David, B. *J. Organomet. Chem.* **1968**, *13*, 177-186.

(49) Williams, V. C.; Piers, W. E.; Clegg, W.; Elsegood, M. R. J.; Collins, S.; Marder, T. B. *J. Am. Chem. Soc.* **1999**, *121*, 3244-3245.

(50) Sundararaman, A.; Jakle, F. *J. Organomet. Chem.* **2003**, *681*, 134-142.

(51) Duchateau, R.; Lancaster, S. J.; ThorntonPett, M.; Bochmann, M. *Organometallics* **1997**, *16*, 4995-5005.

(52) Cairncross, A.; Sheppard, W. A.; Wonchoba, E. *Org. Synth.* **1988**, *50-9*, 875-882.

(53) Confirmation of the formation of a four coordinate complex is revealed by measuring $\Delta\delta_{m,p}$, the difference of the chemical shifts between the *para*-F and *meta*-F resonances, which decrease from 18.9 ppm to ca. 9 ppm upon rehybridisation from a 3- to 4-coordinate complex

(54) Horton, A. D.; deWith, J. *Organometallics* **1997**, *16*, 5424-5436.

(55) Sundararaman, A.; Jäkle, F. *J. Organomet. Chem.* **2003**, *681*, 134-142.

(56) Crystals of **3** had to be manipulated at temperatures below 0°C in order to inhibit dissolution in either Paratone® or perfluoropolyether oil.

(57) For consistency, the right-handed propeller is shown in all crystallographic figures.

(58) A common test for planarity is to sum all angles around a central atom and comparing with the ideal 360°; in this case however the sum of the angles about B is 360°. However, the sum-of-all-angles test this can be extremely insensitive to planarity and the reader is directed to reference [59] for examples of such situations.

Using the method applied in the text, the largest deviation is seen for **2** (0.0028 Å), confirming a planar assignment.

(59) Blake, A. J.; Cole, J. M.; Evans, J. S. O.; Main, P.; Parsons, S.; Watkin, D. J. *Crystal Structure Analysis: Principles and Practice*; 2nd ed.; Oxford University Press: Oxford, 2009.

(60) Tulinsky, A.; White, J. G. *Acta Crystallogr.* **1958**, *11*, 7-14.

(61) Power, P. P.; Olmstead, M. M. *J. Am. Chem. Soc.* **1986**, *108*, 4253-4236.

(62) Zettler, F.; Hausen, H. D.; Hess, H. *J. Organomet. Chem.* **1974**, *72*, 157-162.

(63) Childs, R. F.; Mulholland, D. L.; Nixon, A. *Can. J. Chem.* **1982**, *60*, 801-808.

(64) Lappert, M. F. *J. Chem. Soc.* **1961**, 817-822.

(65) Lappert, M. F. *J. Chem. Soc.* **1962**, 542-548.

(66) Mayer, U.; Gutmann, V.; Gerger, W. *Monatsh. Chem.* **1975**, *106*, 1235-1257.

(67) Gutmann, V. *Coord. Chem. Rev.* **1976**, *18*, 225-255.

(68) Welch, G. C.; Cabrera, L.; Chase, P. A.; Hollink, E.; Masuda, J. D.; Wei, P. R.; Stephan, D. W. *Dalton Trans.* **2007**, 3407-3414.

(69) Beckett, M. A.; Strickland, G. C.; Holland, J. R.; Varma, K. S. *Polymer* **1996**, *37*, 4629-4631.

(70) Britovsek, G. J. P.; Ugolotti, J.; White, A. J. P. *Organometallics* **2005**, *24*, 1685-1691.

(71) Pearson, R. G. *J. Am. Chem. Soc.* **1963**, *85*, 3533-3539.

(72) Mackle, H.; Sutton, L. E. *Trans. Faraday Soc.* **1951**, *47*, 691-699.

(73) Bandoli, G.; Bortolozzo, G.; Clemente, D. A.; Croatto, U.; Panattoni, C. *J. Chem. Soc. A* **1970**, 2778-2780.

(74) Harlan, C. J.; Hascall, T.; Fujita, E.; Norton, J. R. *J. Am. Chem. Soc.* **1999**, *121*, 7274-7275.

(75) Cummings, S. A.; Iimura, M.; Harlan, C. J.; Kwaan, R. J.; Trieu, I. V.; Norton, J. R.; Bridgewater, B. M.; Jakle, F.; Sundararaman, A.; Tilset, M. *Organometallics* **2006**, *25*, 1565-1568.

(76) Compton, R. G.; Banks, C. E. *Understanding Voltammetry*; World Scientific Publishing: Singapore, 2007.

(77) Testa, A. C.; Reinmuth, W. H. *Anal. Chem.* **1961**, *33*, 1320-1324.

(78) Ballester, M.; Riera-Figueras, J.; Castaner, J.; Badfa, C.; Monso, J. M. *J. Amer. Chem. Soc.* **1971**, *93*, 2215-2225.

(79) Ballester, M. *Acc. Chem. Res.* **1985**, *18*, 380-387.

(80) Chivers, T.; Schatte, G. *Eur. J. Inorg. Chem.* **2003**, 3314-3317.

(81) Strauss, S. H. *Chem. Rev.* **1993**, *93*, 927-942.

(82) Frohn, H. J.; Jakobs, S. *J. Chem. Soc., Chem. Commun.* **1989**, 625-627.

(83) Gritzner, G.; Kuta, J. *Pure Appl. Chem.* **1984**, *56*, 461-466.

(84) Danopoulos, A. A.; Galsworthy, J. R.; Green, M. L. H.; Cafferkey, S.; Doerrer, L. H.; Hursthouse, M. B. *Chem. Commun.* **1998**, 2529-2530.

(85) Doerrer, L. H.; Green, M. L. H. *J. Chem. Soc., Dalton Trans.* **1999**, 4325-4329.

(86) Beringhelli, T.; Maggioni, D.; D'Alfonso, G. *Organometallics* **2001**, *20*, 4927-4938.

(87) Timoshkin, A. Y.; Frenking, G. *Organometallics* **2008**, *27*, 371-380.

(88) Bergquist, C.; Bridgewater, B. M.; Harlan, C. J.; Norton, J. R.; Friesner, R. A.; Parkin, G. *J. Am. Chem. Soc.* **2000**, *122*, 10581-10590.

(89) Bergquist, C.; Parkin, G. *J. Am. Chem. Soc.* **1999**, *121*, 6322-6323.

CHAPTER THREE

Synthesis and Reactions of Novel Frustrated Lewis Pairs with H_2

3.1 Introduction

In 1996, Welch and Stephan showed the first example of a metal-free system that reversibly cleaves hydrogen using a frustrated Lewis pair (FLP). This was done using the zwitterionic phosphonium hydridoborate salt $(Mes)_2PH(C_6F_4)BH(C_6F_5)_2$.[1] FLPs have gained more prominence in recent years and are formed when the steric hindrance between a Lewis acid and Lewis base prevents them from forming an adduct.[2] The unquenched reactivity in these molecules have the ability to facilitate the activation of small molecules, e.g. splitting of H_2,[2] addition of CO_2,[3-5] addition of unsaturated systems[6-8] and addition of aldehydes.[9] Amongst the useful applications of FLPs is their ability to add H_2 to bulky imines,[8-11] which has been carried out enantioselectively[12] and to reduce CO_2 to methanol.[3,13]

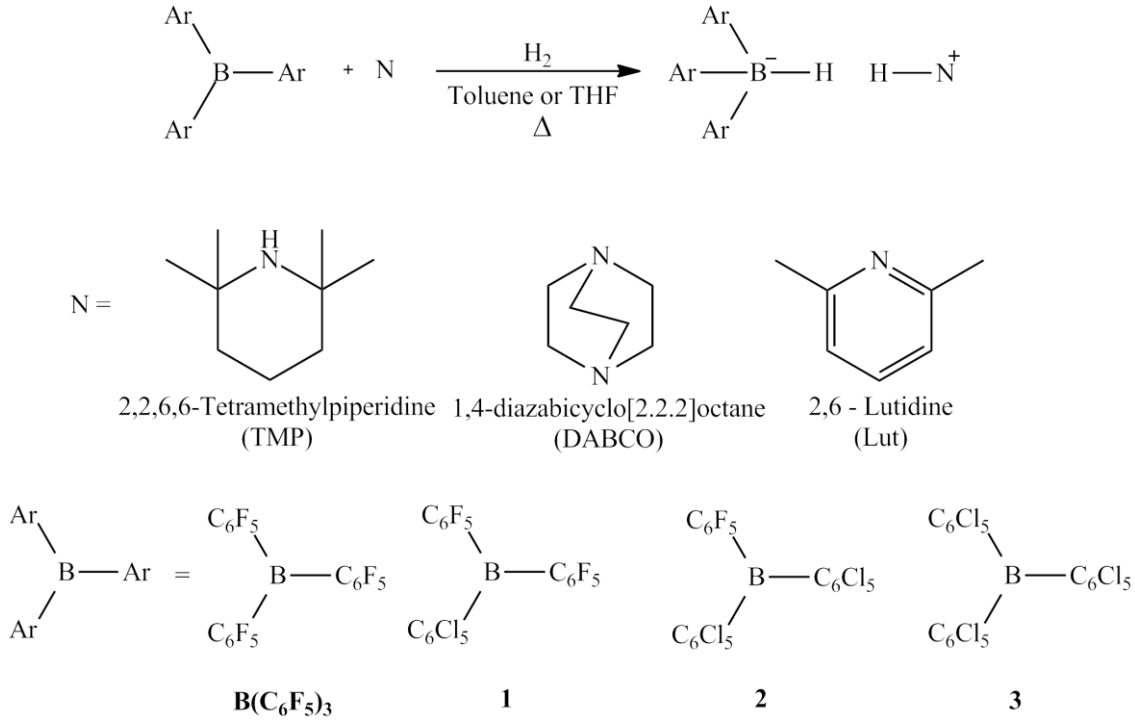
Due to their capacity to reduce CO_2 to methanol and their promise in the field of hydrogen storage via dehydrogenation and rehydrogenation processes, the use of metal-free FLPs as a method of activating H_2 has grown in popularity over the last 5 years.[3,14] There are many examples of FLPs containing boron or aluminium Lewis acids used in combination with either nitrogen or phosphine bases.[1,2,8,10,11,15-20] $B(C_6F_5)_3$, as part of an FLP system, has over 200 known H_2 activation reactions and thus is one of the most widely used Lewis acids due to its facile synthesis, steric bulk and high Lewis acidity. As one can imagine, a large number of reactions are possible with a vast array of Lewis bases that can be used in conjunction with $B(C_6F_5)_3$, for this study three Lewis bases

were selected; 2,2,6,6-tetramethylpiperidine (TMP), 2,6-lutidine (Lut) and 1,4-diazabicyclo[2.2.2]octane (DABCO). These bases encompass a wide range of steric demands and basicity that exhibit interesting reactivity. $B(C_6F_5)_3$ has already been used in combination with TMP[21,22] and Lut[22-24] as FLP systems and each has shown the ability to successfully activate H_2. However, DABCO has experienced limited use in FLP systems[25] and when added to $B(C_6F_5)_3$ forms a classical Lewis adduct.[26]

In Chapter Two a new family of electron-deficient *tris*(aryl)boranes, $B(C_6F_5)_{3-x}(C_6Cl_5)_x$ (x = 1-3) were synthesised, allowing for an exploration of the subtle interplay of electronic and steric effects, resulting from the gradual replacement of C_6F_5 with C_6Cl_5 ligands, to be studied.[27] These novel Lewis acids have been used with TMP, Lut and DABCO to create and evaluate the reactivity of novel FLP systems.

3.2 Synthesis of Novel Frustrated Lewis Pairs and Reactions with H_2

Using the Lewis acids $B(C_6F_5)_2(C_6Cl_5)$, $B(C_6F_5)(C_6Cl_5)_2$ and $B(C_6Cl_5)_3$ (**1**, **2** and **3**, respectively) together with a stoichiometric amount of TMP, Lut or DABCO, nine FLP systems were synthesised in either toluene or THF. $B(C_6F_5)_3$ and DABCO were combined in toluene to form a classical Lewis adduct that was isolated according to the literature.[26] The propensity of these 10 systems to split H_2 was evaluated (Scheme 3.1).



Scheme 3.1 H_2 splitting using the novel FLP systems.

Initially the reactions were carried out on NMR scale, using 30 mg of the Lewis acid and one equivalent of the Lewis base and placed under one atmosphere of H_2 via three freeze-pump-thaw degas cycles. This allowed each of the reactions to be monitored using ^{1}H and $^{11}B\{^{1}H\}$ NMR spectroscopy and where relevant ^{19}F NMR spectroscopy. Following splitting of H_2 a four-coordinate borohydride species is formed which gives a distinct resonance in the $^{11}B\{^{1}H\}$ NMR spectrum which appears at approximately −18 ppm, −13 ppm and −8 ppm, for Lewis acids **1**, **2**, and **3** respectively. These characteristic resonances remain constant for the Lewis acid regardless of which Lewis base is used and only shift approximately 1 ppm when the reaction is carried out in a different solvent (e.g. toluene, THF).

Upon the addition of H_2 to the $B(C_6F_5)_3$.DABCO adduct, a resonance at −25 ppm in the ^{11}B NMR spectrum was observed. This resonance is characteristic of the four-coordinate borohydride species of $[(C_6F_5)_3B\text{-}H]^-$.[21] Thus, when in solution,

$B(C_6F_5)_3$.DABCO is able to successfully activate H_2, although there are very few examples in the literature of H_2 activation using B-N adducts.[28-30]

Each system activates H_2 at different temperatures and in many of the systems H_2 splitting is observed after 24 h at 22 ^oC using $^{11}B\{^1H\}$NMR spectroscopy (the ^{11}B nuclei couples to the H with $^1J_{BH}$ ~ 90 Hz), a broad quartet is also observed in the ^1H NMR spectrum, however, initially this is difficult to detect due to the broadness and weakness of the resonance. Attempts were made to improve the B-H resonance using $^1H\{^{11}B\}$ NMR spectroscopy, however, the signal observed was still weak and $^{11}B\{^1H\}$ NMR spectroscopy proved to be the best method of monitoring H_2 activation. Even though the splitting of H_2 is observed at 22 ^oC for a number of these systems, the maximum rate of reaction/borohydride yield is usually achieved at an elevated temperature. Some of the systems required prolonged heating at 110 ^oC before H_2 activation was observed and the reaction conditions are summarised in Table 3.1.

Table 3.1 Summary of H_2 splitting reactions.

FLP/Adduct System	% Yield of Isolated [B-H][H-N] Salt	Reaction Temperature/ ^oC	Observations
$(C_6F_5)_3$B.DABCO[a]	86	65	Side reaction seen T > 65 ^oC
[**1**][DABCO] [a]	77	75	Side reaction seen T > 75 ^oC
[**2**][DABCO] [a]	45	25	Side reaction seen T > 25 ^oC
[**3**][DABCO] [a]	33	110	-
[**1**][TMP] [a]	76	110	-
[**2**][TMP] [a]	77	110	-
[**3**][TMP][b]	61	120	-
[**1**][Lut] [a]	35	65	Releases H_2 T > 65 ^oC
[**2**][Lut] [a]	18	65	Releases H_2 T > 65 ^oC
[**3**][Lut][b]	16	70	Releases H_2 T > 70 ^oC

[a]Solvent: Toluene. [b]Solvent: THF.

As Table 3.1 illustrates, the yield of the borohydride salt decreases upon substituting the perfluoro groups with perchloro groups. This can be ascribed to the increase of steric bulk in the Lewis acids,[27] which prevents the H_2 molecule entering between the Lewis acid and base. It would be expected that increasing perchloro substitution would increase the Lewis acidity and thus should split H_2 more efficiently (as described in Chapter Two). Unfortunately, the reactivity of **3** is hindered by its very poor solubility. Initially all reactions using **3** were carried out in toluene at 120 ^{o}C (**3** is soluble in boiling toluene).[27] It was found that only [**3**][DABCO] split H_2 in toluene with the resultant salt isolated with a modest yield of 33 %. As [**3**][TMP] and [**3**][Lut] were unable to split H_2 in toluene, the reactions were carried out successfully in THF and isolated with varying yields (Table 3.1). The efficiency of H_2 activation is also affected when adjusting the Lewis base in the FLP systems.

There is an increase in steric bulk exhibited on progressing from DABCO to Lut and TMP, as DABCO is able to form a classical Lewis adduct with $B(C_6F_5)_3$, whereas with Lut the system is in equilibrium[23] and TMP forms an FLP.[31] Jiang *et al.* found a correlation between the steric hindrance on the Lewis base and the reactivity of the FLP and concluded that TMP had a larger cone angle than Lut (169^{o} and 164^{o}, respectively) which prevents the formation of a TMP-$B(C_6F_5)_3$ adduct.[22] However, steric bulk is not the only factor that needs to be considered; the basicity also plays a major role in the reactivity of the FLP system. $[TMP\text{-}H]^+$ is more basic than $[Lut\text{-}H]^+$ and $[DABCO\text{-}H]^+$ (pKa = 11.07,[32] 6.75[33,34] and 8.82,[33] respectively). When considering both the sterics and the basicity of the Lewis bases, it can be concluded that upon combination of a Lewis acid with Lut, a less reactive FLP system is formed than when combined with TMP or DABCO, as is observed in the lower isolated yield of the borohydride salts from the Lut systems. However, even though TMP is an extremely bulky base, its

strong basicity allows its FLP system to successfully activate H_2 in high yields. In contrast, DABCO is a much weaker base but due to it being less sterically hindered, H_2 has easier access within the FLP and therefore is still able to split H_2 with higher yields than the Lut FLP systems. When combining DABCO, a weak sterically less demanding base, with **3** (a strong bulky acid) the reactivity of the FLP decreases, as witnessed in the yield of the borohydride salt.

The Lut FLP systems exhibit even more interesting reactivity. Unlike the TMP and DABCO systems, the Lut systems have shown to reversibly split H_2 when heated above 65 ^{o}C, i.e. H_2 is released back into the system above this temperature. As this trend is not observed for the TMP and DABCO systems it can be presumed that this is due to the weak basicity and larger steric bulk of the Lut molecule. Using the isolated [**1**-H][H-Lut], ^{1}H, ^{11}B{^{1}H} and ^{19}F NMR spectroscopy experiments were carried out on the release of H_2 at temperatures 65 – 110 ^{o}C which is discussed later.

3.3 NMR Spectroscopy

Solution phase ^{11}B{^{1}H} and ^{19}F NMR spectral data for [**1**-H][H-N], [**2**-H][H-N] and [**3**-H][H-N] have been summarised and compared with $B(C_6F_5)_3$ (Table 3.2). Compounds [**1**-H][H-N] and [**2**-H][H-N] exhibit three resonances in their ^{19}F NMR spectra in an intensity ratio 2:1:2 for the corresponding *ortho*, *para* and *meta* fluorine environments (to higher field respectively) for the C_6F_5 rings. This is consistent for all three bases. The difference between the *meta* and *para* resonances, $\Delta\delta_{m,p}$ in the ^{19}F NMR spectra of the FLP were between 17-18 ppm. However, upon splitting H_2, the *meta* resonance shifts upfield decreasing the difference between the *meta* and *para* resonances, $\Delta\delta_{m,p}$ to 2-3 ppm, which is indicative of a four-coordinate anionic boron

centre and is consistent with previously published findings by Piers *et al*.[34,35] The corresponding NMR data of the FLP is shown in *italics*.

Table 3.2 ^{19}F and $^{11}B\{^1H\}$ NMR spectral data for the Borohydride Salts; [B-H][H-N], where B = $B(C_6F_5)_3$, **1**, **2**, **3**.

[B-H]$^-$	**δ(^{19}F NMR)/ppm[a]**				**δ(^{11}B{^{1}H} NMR)/ppm[b]**
	***ortho*-F**	***para*-F**	***meta*-F**	**$\Delta\delta_{m,p}$[c]**	
$[(C_6F_5)_3B\text{-}H]^-$	−135 *(−128.2)*	−165 *(−143.9)*	−168 *(−161.1)*	3 *(17.2)*	−25 *(61.2)*
[1-H]$^-$	−134 *(−127.1)*	−165 *(−142.8)*	−168 *(−161.1)*	3 *(18.3)*	−19 *(61.5)*
[2-H]$^-$	−134 *(−127.4)*	−165 *(−143.1)*	−168 *(−160.6)*	3 *(17.5)*	−14 *(66.1)*
[3-H]$^-$	-	-	-	-	−8 *(68.2)*

[a]Solvent: CD_3CN, $CFCl_3$ reference (external). [b]Solvent: CD_3CN, $BF_3{\cdot}OEt_2$ reference (external). [c]Difference between ^{19}F NMR *meta* and *para* resonances (ppm).

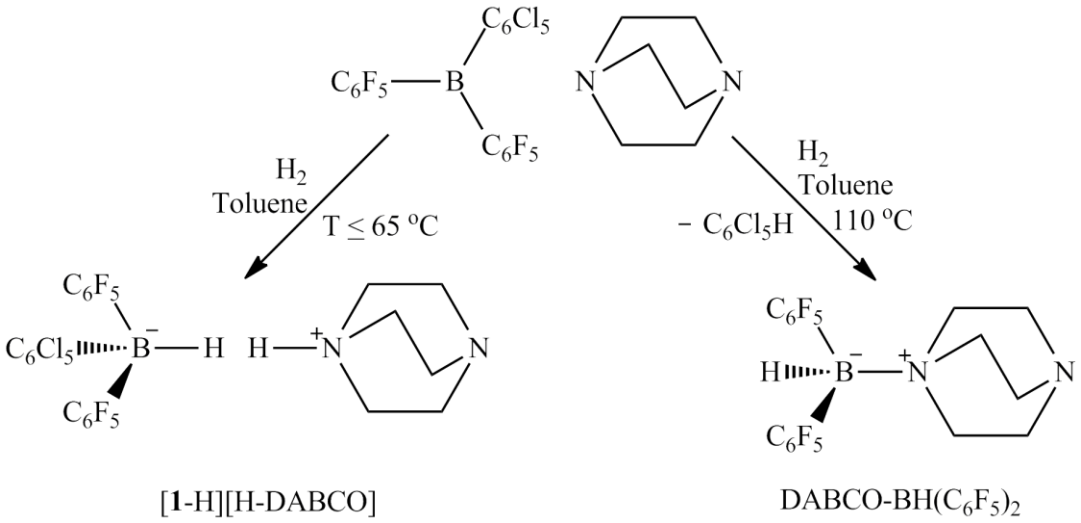
Both the $^{11}B\{^1H\}$ and ^{19}F NMR spectra suggests that the borane species becomes a four-coordinate anionic borohydride species upon cleaving H_2 and is consistent with the literature.[34,35] A trend is witnessed in the $^{11}B\{^1H\}$ NMR spectra, upon stepwise substitution of the C_6F_5 groups with C_6Cl_5 groups, the $^{11}B\{^1H\}$ resonance shifts approximately 5-6 ppm downfield,[27] which is consistent with the boron centre becoming more deshielded. This is due to the increase in electrophilicity at the boron centre caused by the addition of the more electron-withdrawing C_6Cl_5 groups, thus confirming that the Lewis acidity increases in the series; $B(C_6F_5)_{3-n}(C_6Cl_5)_n$ n = 0-3. The ^1H NMR spectra confirms the presence of a borohydride species with quartet resonance due to coupling with the quadrapolar ^{11}B ($I = \frac{3}{2}$) at 3.5 – 4 ppm, which also shifts downfield when progressing along the series.

3.4 Monitoring H_2 Reactions using $B(C_6F_5)_2(C_6Cl_5)$ FLP Systems

Attempts were made to determine the activation energy of three FLP systems consisting of [**1**][DABCO], [**1**][TMP] and [**1**][Lut]. The aim was to monitor the activation of H_2 using ^1H, ^{19}F and $^{11}B\{^1H\}$ NMR spectroscopy, plot the concentration of the borohydride species against time and using the Eyring plot to determine the activation energy of each system. Each of the experiments were carried out with 30 mg of **1** and one equivalent of the appropriate base in 0.7 ml of toluene-d_8 in a J-Young NMR tube. Each sample was heated within the NMR spectrometer under one atmosphere of H_2 and monitored over time to observe the formation of the borohydride salt.

3.4.1 H_2 Activation using [1][DABCO]

The [**1**][DABCO] system was held at temperatures between 40 – 110 ^oC, at equally spaced increments and the reactions were monitored over 10 h at each temperature. When the [**1**][DABCO] system was held between 40 – 75 ^oC, only the FLP system and the borohydride salt were observed in the NMR spectra. However, once this reaction was heated above 75 ^oC, new resonances were detected in both the $^{11}B\{^1H\}$ and ^{19}F NMR spectra. Heating the reaction at 110 ^oC did not produce the resonances which were characteristic to the borohydride salt; only the resonances attributable to the side product (DABCO-$BH(C_6F_5)_2$) were evident (Scheme 3.2). The formation of [**1**-H][H-DABCO] is observed in both the ^{19}F (−133 (*o*), −161 (*p*) and −165 ppm (*m*)) (Figure 3.1) and $^{11}B\{^1H\}$ NMR spectroscopy (−19 ppm) (Figure 3.6).



Scheme 3.2 Reactions observed using the [**1**][DABCO] FLP system and H_2.

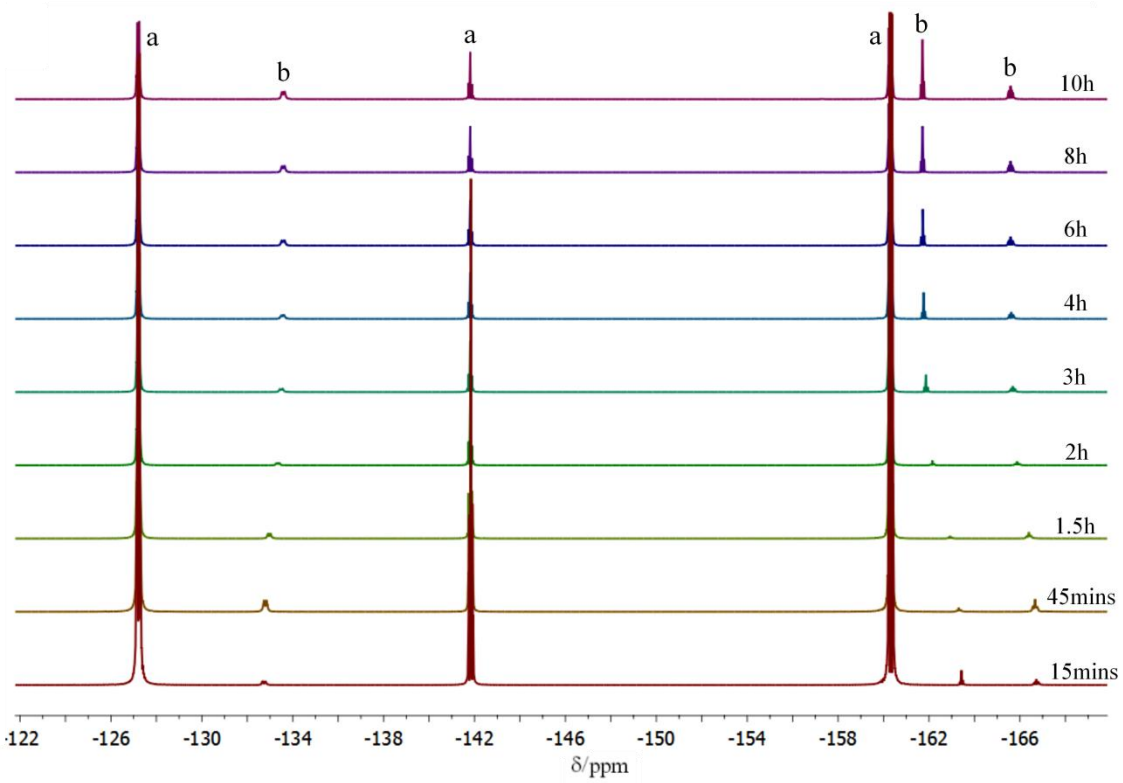


Figure 3.1 ^{19}F NMR spectra of (a) [**1**][DABCO] and the formation of (b) [**1**-H][H-DABCO] at 75 ^{o}C in toluene-d_8.

Figure 3.1 shows that when the reaction mixture of [**1**][DABCO] in toluene-d_8 (under one atmosphere of H_2) is heated at 75 ^{o}C, the production of [**1**-H][H-DABCO]

can be monitored using ^{19}F NMR spectroscopy. Initially a steady growth of the product can been observed, however, after approximately 1 h, the amount of [**1**-H][H-DABCO] begins to decrease. There could be many for reasons for this, for example the reaction is reversible or the product could be insoluble in toluene-d_8. When the reaction was left at room temperature in toluene-d_8, X-ray quality single crystals of [**1**-H][H-DABCO] grew, thus the borohydride salt is only partially soluble in toluene, as shown in Figure 3.2. This could explain the inconsistent growth of the borohydride salt resonance in the ^{19}F NMR spectra. Further heating at 75 ^{o}C allowed for the [**1**-H][H-DABCO] resonance to increase again at a steady rate. Another explanation for the inconsistent growth could be that due to the presence of the FLP in solution, the borohydride salt experiences low solubility. Once a certain amount of the FLP is consumed, this allows more of the borohydride salt to be observed in solution. To determine if the reaction was First Order or Second Order, ln[**1**] and 1/[**1**] were plotted against time (Figures 3.3 and 3.4, respectively).

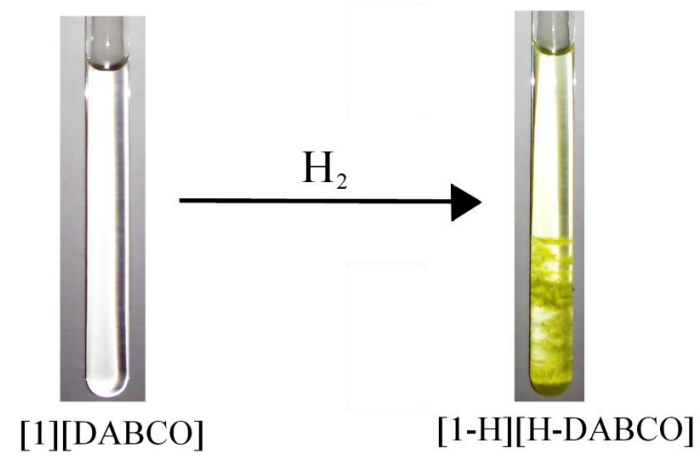


Figure 3.2 Solution of [**1**][DABCO] (left) and precipitate of [**1**-H][DABCO] (right) in toluene-d_8.

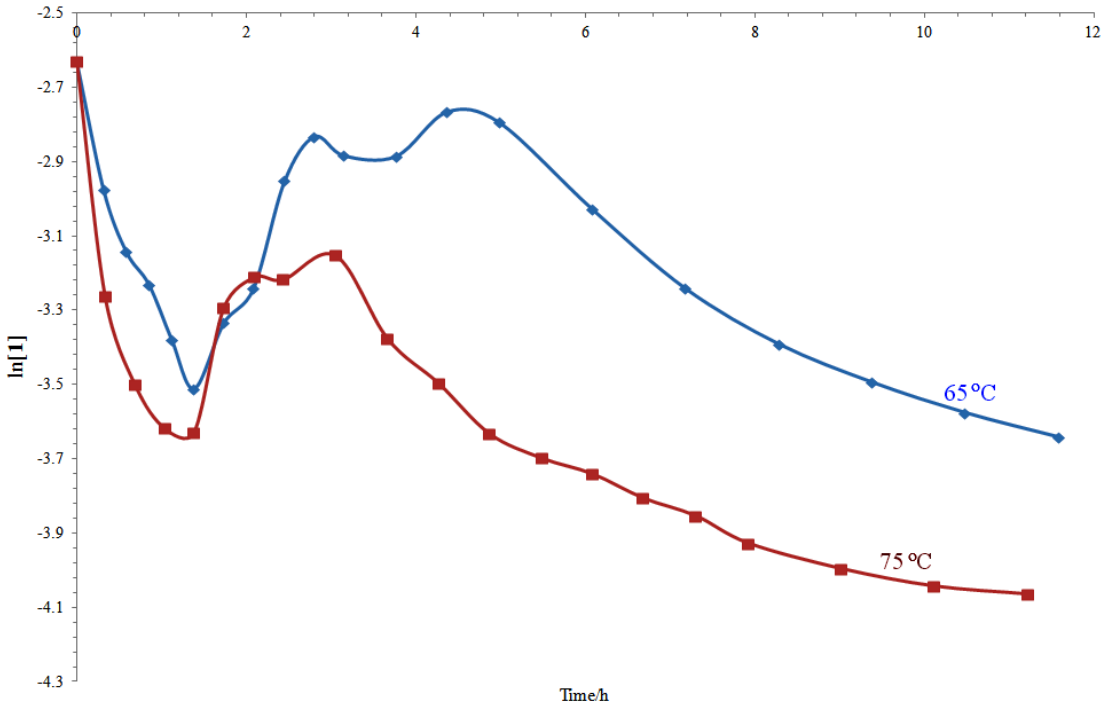


Figure 3.3 Plot of ln[**1**] vs t to determine if the [**1**][DABCO] reaction with H_2 is First Order ([**1**] = concentration of **1** in M and t = time in hours).

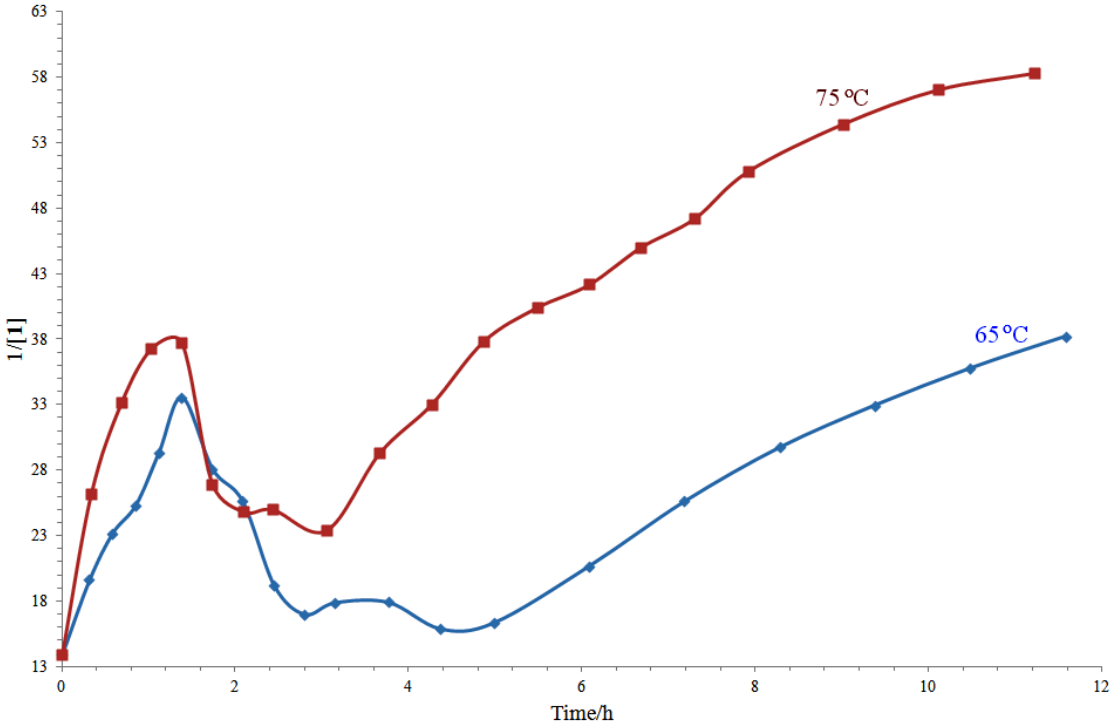


Figure 3.4 Plot of 1/[**1**] vs t to determine if the [**1**][DABCO] reaction with H_2 is Second Order ([**1**] = concentration of **1** in M and t = time in hours).

If the splitting of H_2 using [**1**][DABCO] was either First Order of Second Order, a linear plot would be expected. However, as this is not observed in Figures 3.3 and 3.4, it can be concluded that this reaction is neither First Order nor Second Order.

The plot (Figure 3.4) is in agreement with the initial observations of the ^{19}F NMR spectra, i.e. the borohydride salt does start to form, however the concentration of the salt decreases after 1 h. After approximately two hours, the concentration of the borohydride salt in solution begins to increase again. Hypothetically, precipitation could occur until enough of the FLP has been consumed which then allows for a higher concentration of the borohydride salt to be observed in solution.

When the reaction is heated at temperatures > 75 ^{o}C a resonance at approximately −8 ppm is seen in the $^{11}B\{^{1}H\}$ NMR spectrum (Figure 3.6) and in the ^{19}F NMR spectrum (−128 (*o*), −157 (*p*) and – 163 ppm (*m*)) (Figure 3.5).

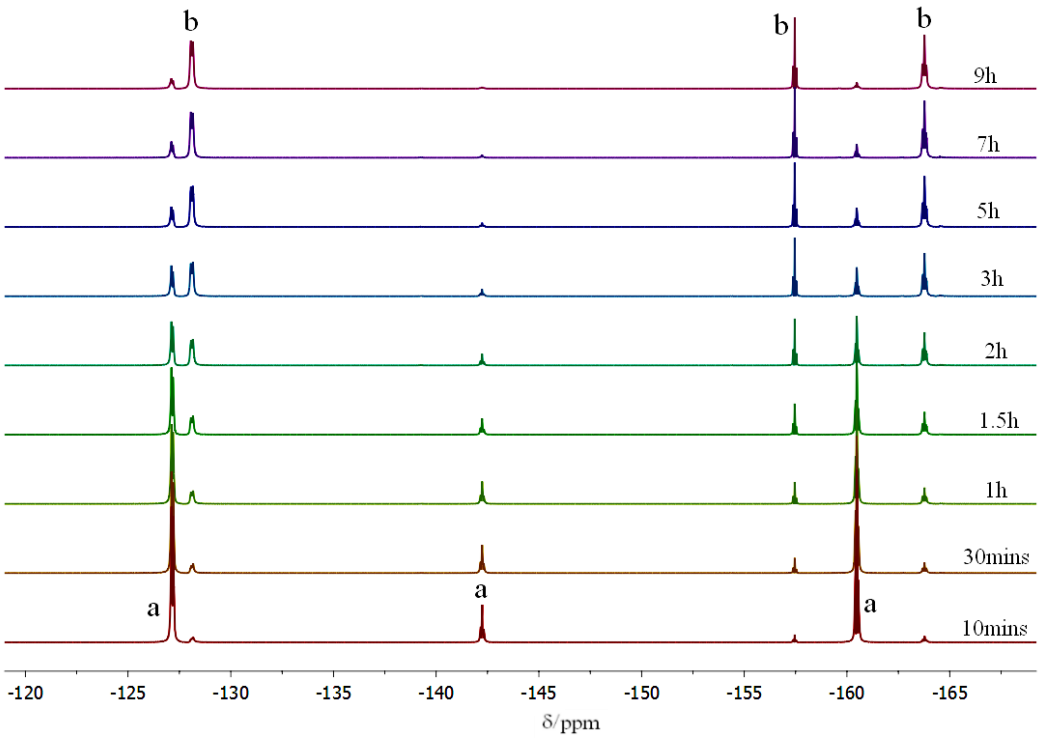


Figure 3.5 ^{19}F NMR spectra of (a) [**1**][DABCO] and the formation of (b) DABCO-BH(C_6F_5)$_2$ at 110 ^{o}C in toluene-d_8.

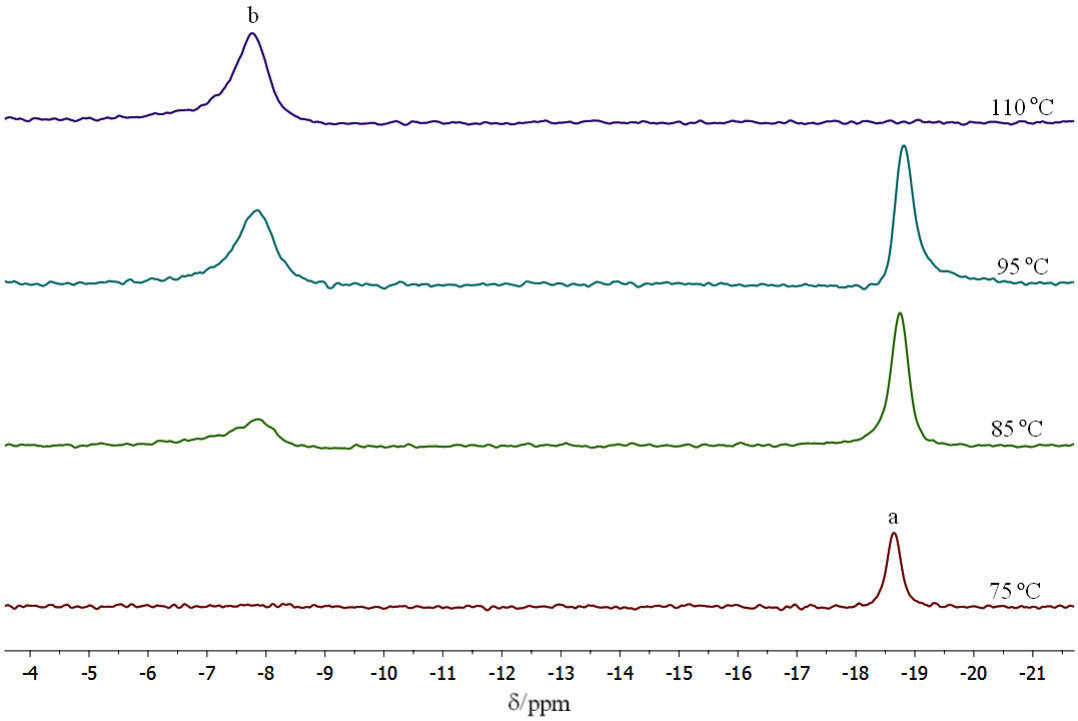


Figure 3.6 $^{11}B\{^1H\}$ NMR spectra of [**1**][DABCO] reacting with H_2 at various temperatures displaying the formation of (a) [**1**-H][H-DABCO] and the side product (b) DABCO-BH(C_6F_5)$_2$ after 10 h in toluene-d_8.

The resonances displayed in the $^{11}B\{^1H\}$ NMR spectrum for the side product, DABCO-BH(C_6F_5)$_2$, were similar to those of TMP-BH(C_6F_5)$_2$ and Lut-BH(C_6F_5)$_2$, with resonances at −11.82 ppm[36] and −7.4 ppm,[37] respectively and when coupled to ^1H, produced a doublet ($^1J_{BH}$ = 91 Hz). Recrystallisation of the side product from boiling toluene generated single X-ray quality crystals, thus confirming the structure of the side product as DABCO-BH(C_6F_5)$_2$. Attempts to synthesise DABCO-BH(C_6F_5)$_2$ from [**1**-H][H-DABCO] in toluene-d_8 at 110 ^oC did not yield the side product. Ménard *et al.* recently showed a similar rearrangement was caused by an excess of the FLP system; Al(C_6F_5)$_3$/P^{t}Bu$_3$, present in the reaction.[38] Therefore, to determine if this is the route taken by (C_6F_5)$_2$BH.DABCO, one equivalent of **1** and DABCO were placed in a J-Young NMR tube containing [**1**-H][H-DABCO] in toluene-d_8. The system was held at

110 ^{o}C for 16 h and analysis using ^{11}B NMR spectroscopy showed only the presence of [**1**-H][H-DABCO], **1** and DABCO. This suggests that the borohydride salt is not an intermediate in this reaction and thus elimination of the C_6Cl_5H group occurs quite soon after splitting H_2.

3.4.2 H_2 Activation using [1][TMP]

The [**1**][TMP] FLP system was placed under H_2 and heated between 65 – 110 ^{o}C equally spaced increments for 10 h at each temperature. It has been established that the borohydride can be observed using ^{1}H, ^{11}B{^{1}H} and ^{19}F NMR spectroscopy. However, as the resonance in the ^{1}H NMR spectrum is broad and weak and it is not possible to determine the ratio of the FLP to the borohydride in the ^{11}B{^{1}H} NMR spectrum; the formation of the borohydride, [**1**-H][H-TMP], was monitored using ^{19}F NMR spectroscopy (Figure 3.7).

To determine if the reaction was First Order or Second Order, ln[**1**] and 1/[**1**] were plotted against time (Figures 3.8 and 3.9, respectively).

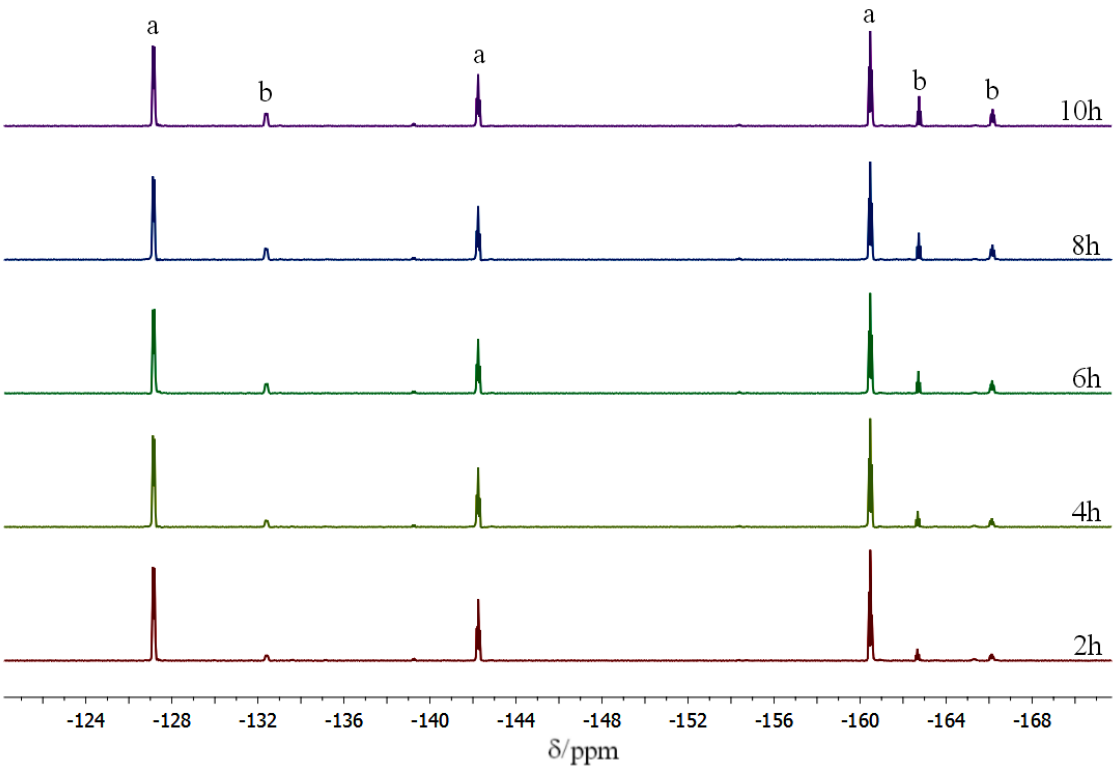


Figure 3.7 The ^{19}F NMR spectra of the (a) [**1**][TMP] and the formation of (b) [**1**-H][H-TMP] at 110 ^{o}C in toluene-d_8.

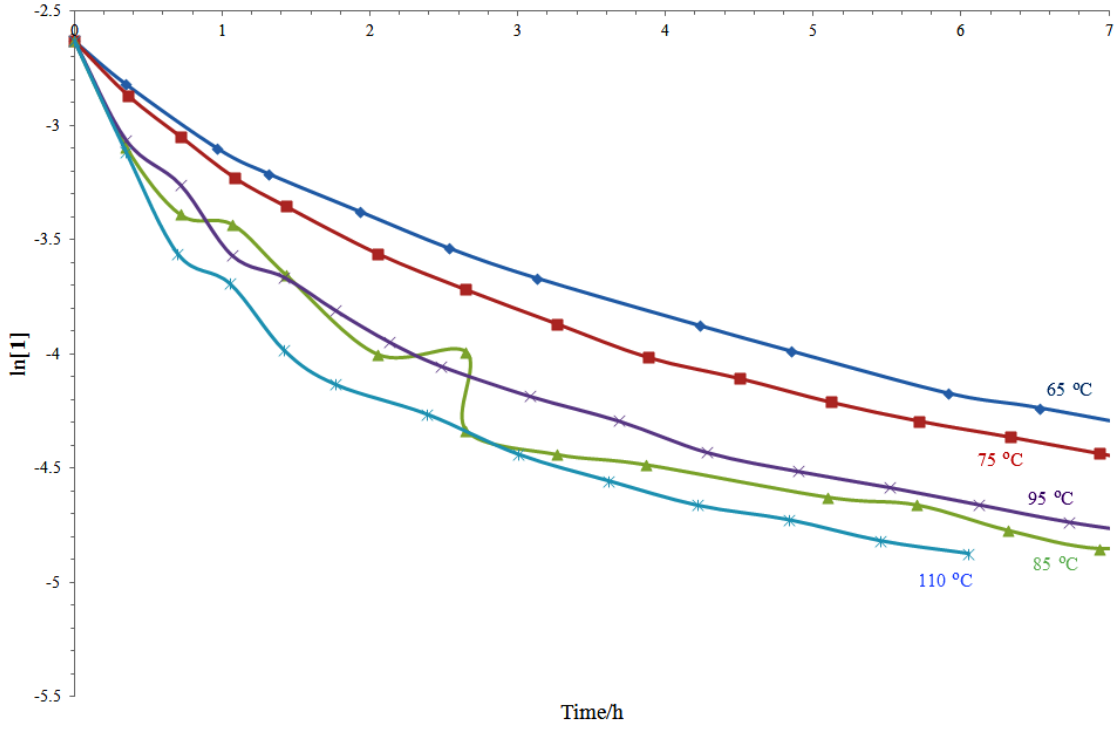


Figure 3.8 Plot of ln[**1**] vs t to determine if the [**1**][TMP] reaction with H_2 is First Order ([**1**] = concentration of **1** in M and t = time in hours).

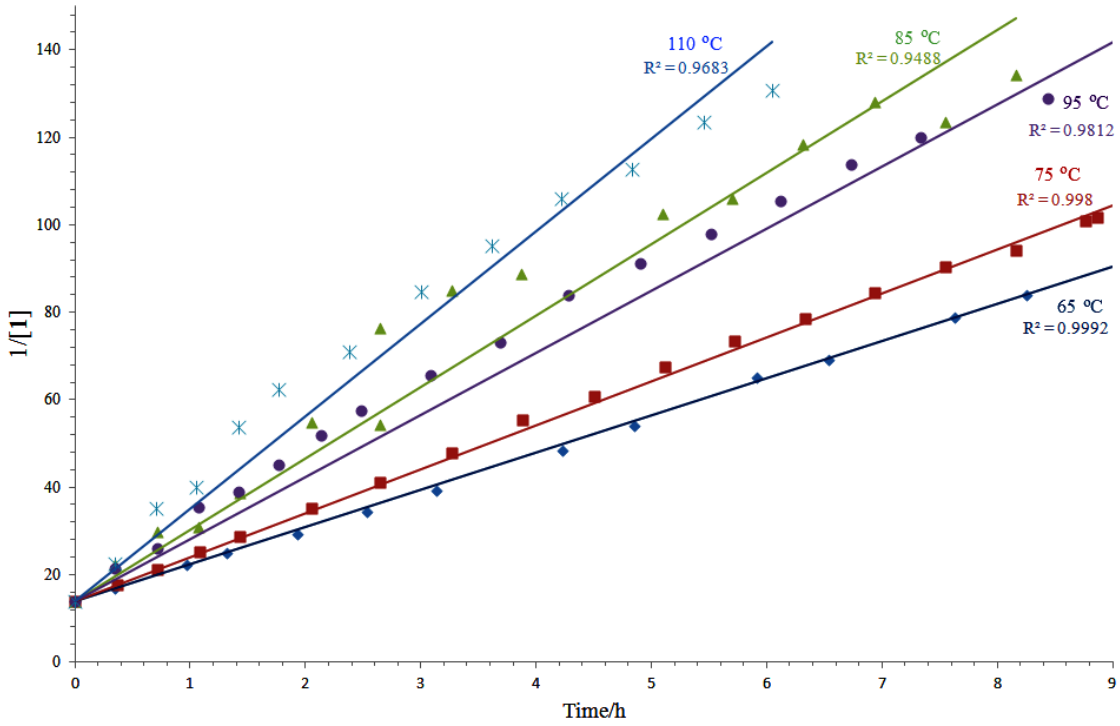


Figure 3.9 Plot of 1/[**1**] vs t to determine if the [**1**][TMP] reaction with H_2 is Second Order ([**1**] = concentration of **1** in M and t = time in hours).

Figure 3.7 shows a stack plot of ^{19}F NMR spectra, which illustrates the formation of the borohydride species; [**1**-H][H-TMP]. This demonstrates that as time increases the yield of the product increases. To determine the order of the reaction ln[**1**] (concentration of **1**) was plotted against time (hours), to give Figure 3.8, which illustrates that the splitting of H_2 using [**1**][TMP] is not a First Order reaction as the plots are not linear. Whereas, Figure 3.9 (1/[**1**] vs t) shows linear plots thus indicating that the reaction is Second Order. The plots show that the reaction steadily proceeds and that the rate of borohydride formation increases with increasing temperature, with the greatest yield found after heating at 110 ^oC for 7 h. These findings corroborate the hypothesis that increasing the bulk of the Lewis acid requires more energy to activate H_2 (with a high yield) than previously seen with TMP and the less bulky $B(C_6F_5)_3$.[21] Therefore, even though **1** is a stronger Lewis acid then $B(C_6F_5)_3$,[27] the FLP system is

less reactive, which shows the steric bulk of the Lewis acid (and base) contributes greatly to reactivity of the FLP system.

The rate constant, k, was determined from the gradient of each plot in Figure 3.9 and then ln(k/T) was plotted against 1/T, where T is the temperature in K.

However, even though the data in Figure 3.10 looked promising it was unreliable as the initial plots in Figure 3.9 were not completely linear and the integrals taken from the ^{19}F NMR spectra also have a degree of error. Therefore it was not possible to reliably calculate the activation energy of the TMP system.

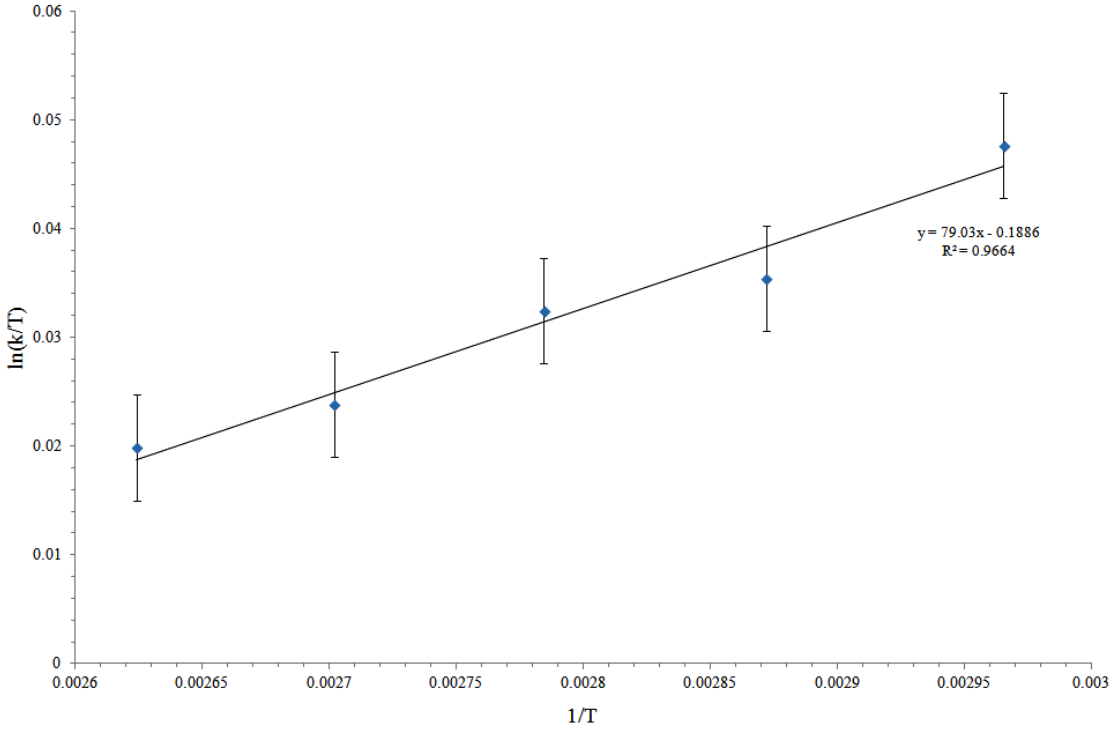


Figure 3.10 ln(k/T) vs 1/T, where k is the rate constant and T is temperature (K) of the splitting of H_2 using [**1**][TMP].

Upon splitting H_2 it was observed that the colour of the solution changes from colourless to pale pink (Figure 3.11).

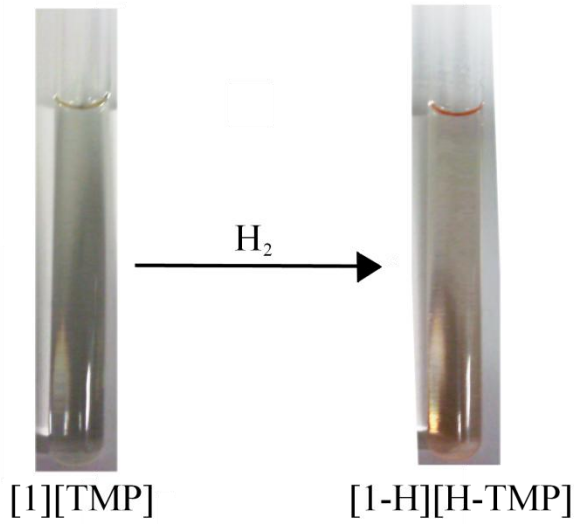


Figure 3.11 Solutions of [**1**][TMP] (left) and [**1**-H][H-TMP] (right) in toluene-d_8.

3.4.3 H_2 Activation using [1][Lut]

As mentioned before, the FLP systems containing Lut are unlike the others because they alone are all able to activate H_2 reversibly. This was first observed when the activation of H_2, using the [**1**][Lut] system, was monitored with ^{19}F and $^{11}B\{^1H\}$ NMR spectroscopy. As with the previous experiments, these were also carried out in toluene-d_8 and the reactions were monitored between 40 – 110 ^oC. As with the previous systems 1/[**1**] was plotted against time (Figure 3.12).

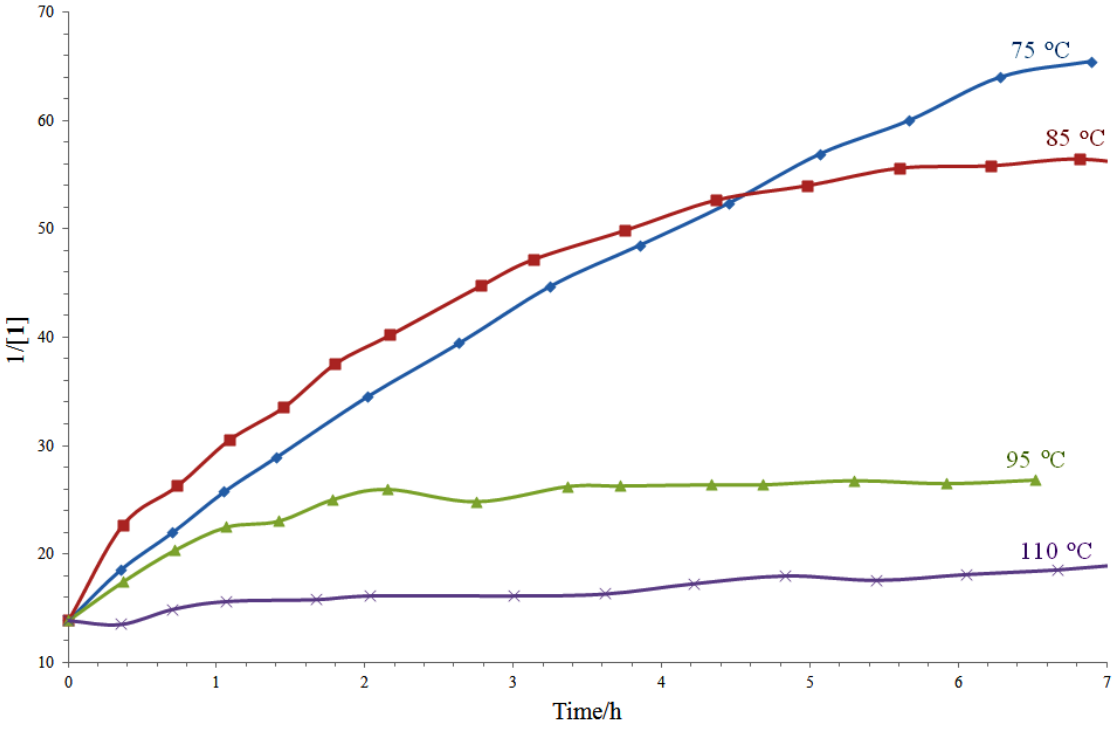


Figure 3.12 Plot of 1/[**1**] vs t to determine if the [**1**][Lut] reaction with H_2 is Second Order ([**1**] = concentration of **1** in M and t = time in hours).

It was observed that when the system was heated between 40 – 75 ^{o}C the yield of the [**1**-H][H-Lut] increased with increasing temperature, however, none of the plots appeared to be linear thus confirming that the order of the reaction could not be determined for this system. Once the system was heated above 75 ^{o}C the yield of the borohydride salt decreased (Figure 3.12). It was hypothesised, that as with some FLP systems,[2] this system might be able to reversibly split H_2. To confirm this theory, release experiments were conducted by heating 30 mg of [**1**-H][H-Lut] in toluene-d_8 at 85, 95 and 110 ^{o}C over 5 h and were monitored using ^{19}F NMR spectroscopy (Figure 3.13).

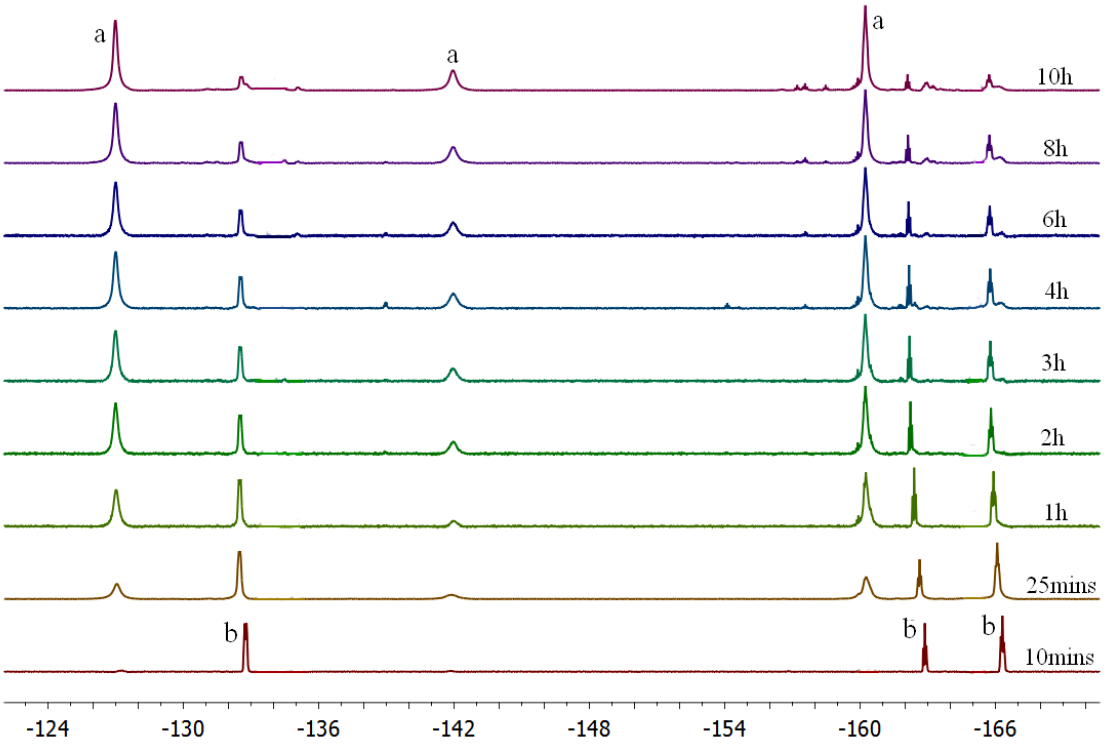


Figure 3.13 The ^{19}F NMR spectra of the production of [**1**][Lut] (a) and the loss of [**1**-H][H-Lut] (b) at 110 ^{o}C in toluene-d_8.

As Figure 3.13 shows, the borohydride resonances in the ^{19}F NMR spectra decrease over 10 h when heated at 110 ^{o}C, whilst the parent FLP increases in intensity. It was also observed that upon releasing H_2, the colourless solution develops a vibrant pink colour (Figure 3.14).

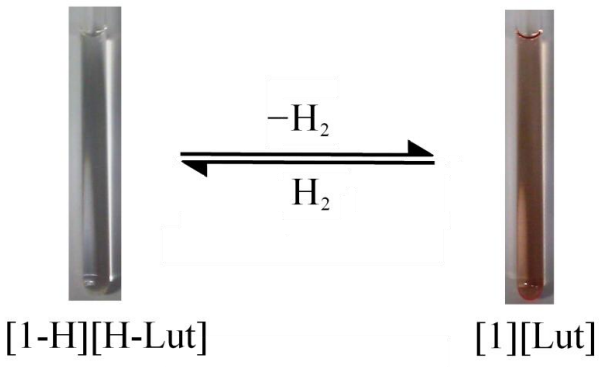


Figure 3.14 Release of H_2 from [**1**-H][H-Lut] (left) to give [**1**][Lut] (right).

The presence of H_2 was confirmed in the ^1H NMR spectrum with a resonance at 4.5 ppm, which is consistent with the literature.[39] The results of the H_2 release experiments were plotted against time and are shown in Figure 3.15.

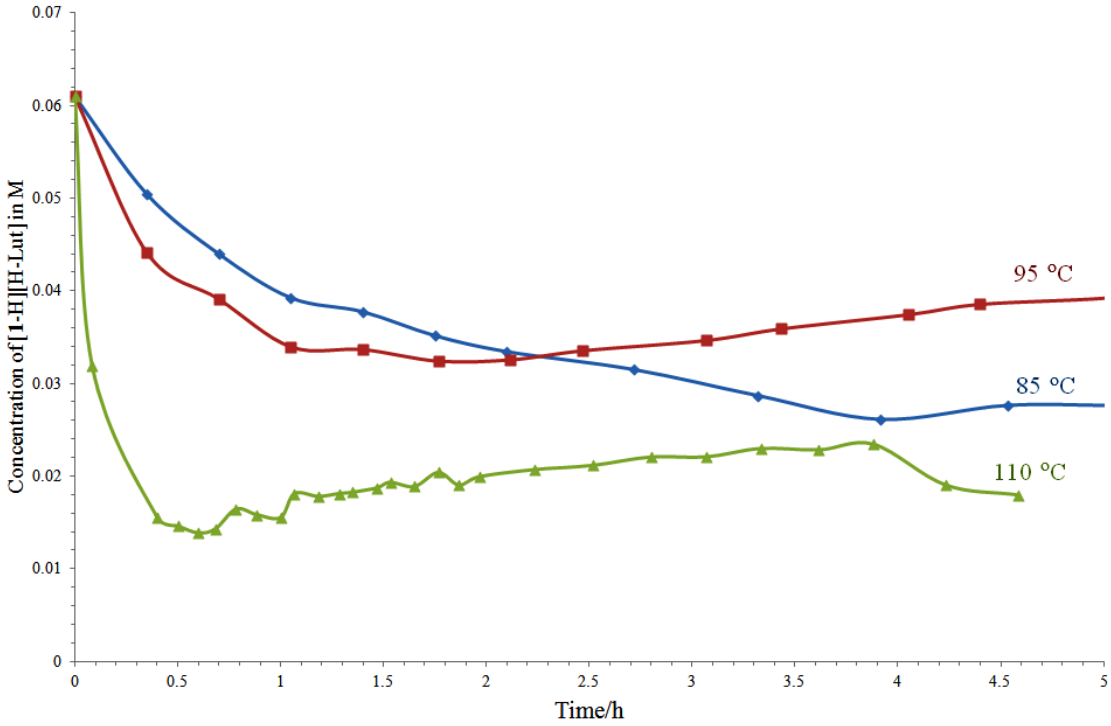


Figure 3.15 Plot of the concentration of [**1**-H][H-Lut] (in M) against t (in hours).

As displayed in Figure 3.15 the concentration of [**1**-H][H-Lut] initially decreases when heated above 75 ^oC for 5 h. After 30 minutes at 110 ^oC the concentration of the borohydride salt begins to increase which indicates that reaction has reached equilibrium. Thus this reaction does not go to completion, unlike $[(C_6F_5)_3B\text{-}H][H\text{-}Lut]$ where complete loss of H_2 is seen when heated at 100 ^oC.[23]

The results from these NMR experiments show that attempts to experimentally determine the activation energy for the splitting of H_2 using these FLP systems was far more difficult than originally imagined and therefore could not be reliably determined.

3.5 Side Reactions Observed using the DABCO FLP Systems

As mentioned previously (Table 3.1) the DABCO FLP systems show unique and interesting reactivity. Unlike the other FLP systems, these systems show the formation of a side product. However, the side product is not observed when the [**3**][DABCO] system is used to activate H_2. The data was consistent with a four-coordinate boron side product that was first observed in the NMR scale reactions using $^{11}B\{^1H\}$ NMR spectroscopy (Figure 3.6). Each borohydride salt shows a distinctive resonance in the $^{11}B\{^1H\}$ NMR spectrum ($[H\text{-}B(C_6F_5)_3]^-$ −25 ppm; [**1**-H]$^-$ −18 ppm; [**2**-H]$^-$ −14 ppm; [**3**-H]$^-$ −8 ppm), regardless of the base used. However, when some of the reactions are either heated above a certain temperature or in the case of $B(C_6F_5)_3$, the concentration was tripled (from 30 mg to 90 mg in 0.7 ml of toluene-d_8) the side product was seen (Table 3.3).

Table 3.3 Summary of the side products observed using the DABCO systems.

FLP System	Side Product	Conditions	$^{11}B\{^1H\}$ NMR Resonance (ppm)
$[B(C_6F_5)_3]$[DABCO]	DABCO-$BH(C_6F_5)_2$	T > 65 ^oC 90 mg in 0.7 ml	−8
[**1**][DABCO]	DABCO-$BH(C_6F_5)_2$	T > 75 ^oC	−8
[**2**][DABCO]	DABCO-$BH(C_6F_5)(C_6Cl_5)$	T > 25 ^oC	−3
[**3**][DABCO]	-		-

The resonances in the $^{11}B\{^1H\}$ NMR spectrum for the side products were analogous to those of TMP-$BH(C_6F_5)_2$ and Lut-$BH(C_6F_5)_2$, with resonances at −11.82 ppm[36] and −7.4 ppm,[37] respectively, indicating that a perfluoroaryl group had been eliminated to produce the four-coordinate boron species. Examination of the NMR spectra for each of the side products reveals that both the products from

$[B(C_6F_5)_3]$[DABCO] and [**1**][DABCO] exhibit similar resonances in the $^{11}B\{^1H\}$ and ^{19}F NMR spectra. Whereas, the product from [**2**][DABCO] showed a resonance at −3 ppm, indicating that due to the downfield shift (5 ppm), the boron centre is more Lewis acidic as mentioned previously in Table 3.2. Therefore, it can be concluded, with some certainty, that the side product of [**2**][DABCO] is DABCO-$BH(C_6F_5)(C_6Cl_5)$ via the elimination of C_6Cl_5H. This is confirmed by the ^1H NMR spectrum, which showed a resonance at 7.78 ppm, indicative of C_6Cl_5H, confirmed by the $^{13}C\{^1H\}$ NMR spectrum showing a resonance at 128.9 ppm (in CD_3CN).[40] The C_6Cl_5H resonance is also observed in the ^1H NMR spectrum of the side product from [**1**][DABCO], confirming initial suspicions that DABCO-$BH(C_6F_5)_2$ was produced. Similarly, upon elimination of C_6F_5H from the $[B(C_6F_5)_3]$[DABCO] reaction, a multiplet is observed at 5.84 ppm in the ^1H NMR spectrum, which is consistent with the formation of C_6F_5H (5.8 ppm according to the literature).[37] Attempts to synthesise these side products from the appropriate borohydride salt at 110 ^oC in toluene-d_8 did not yield the side product. This suggests that either the borohydride salt is not the intermediate species for the production of the side products or the atmosphere of H_2 plays a crucial role in producing the side product. The structure of these side products were confirmed using single X-ray crystallography.

3.5.1 Single X-ray Crystal Structures of the DABCO Side Products

The structure of the side products were first confirmed when the crystal structure of DABCO-BH(C_6F_5)(C_6Cl_5) (Figure 3.16) was collected (from the [**2**][DABCO] reaction). X-ray quality single crystals of DABCO-BH(C_6F_5)(C_6Cl_5) were grown from a saturated solution of toluene layered with pentane at 22 ^oC.

The X-ray structure shows the DABCO is directly bonded to the B atom, after eliminating a C_6Cl_5H molecule. Unfortunately, the single X-ray crystal structures of TMP-BH(C_6F_5)$_2$ and Lut-BH(C_6F_5)$_2$ have not been published and due to the limited use of DABCO there are no published examples of which containing the DABCO group. Therefore the closest related structure to DABCO-BH(C_6F_5)$_2$ and DABCO-BH(C_6F_5)(C_6Cl_5) is *i*Pr$_2$NH.BH(C_6F_5)$_2$.[41] A summary of the selected bond lengths and bond angles for the structures are displayed in Tables 3.4 and 3.5.

The single crystals of DABCO-BH(C_6F_5)$_2$ suitable for X-ray diffraction were grown from slow cooling a toluene-d_8 reaction mixture and analysed using single X-ray diffraction (Figure 3.17).

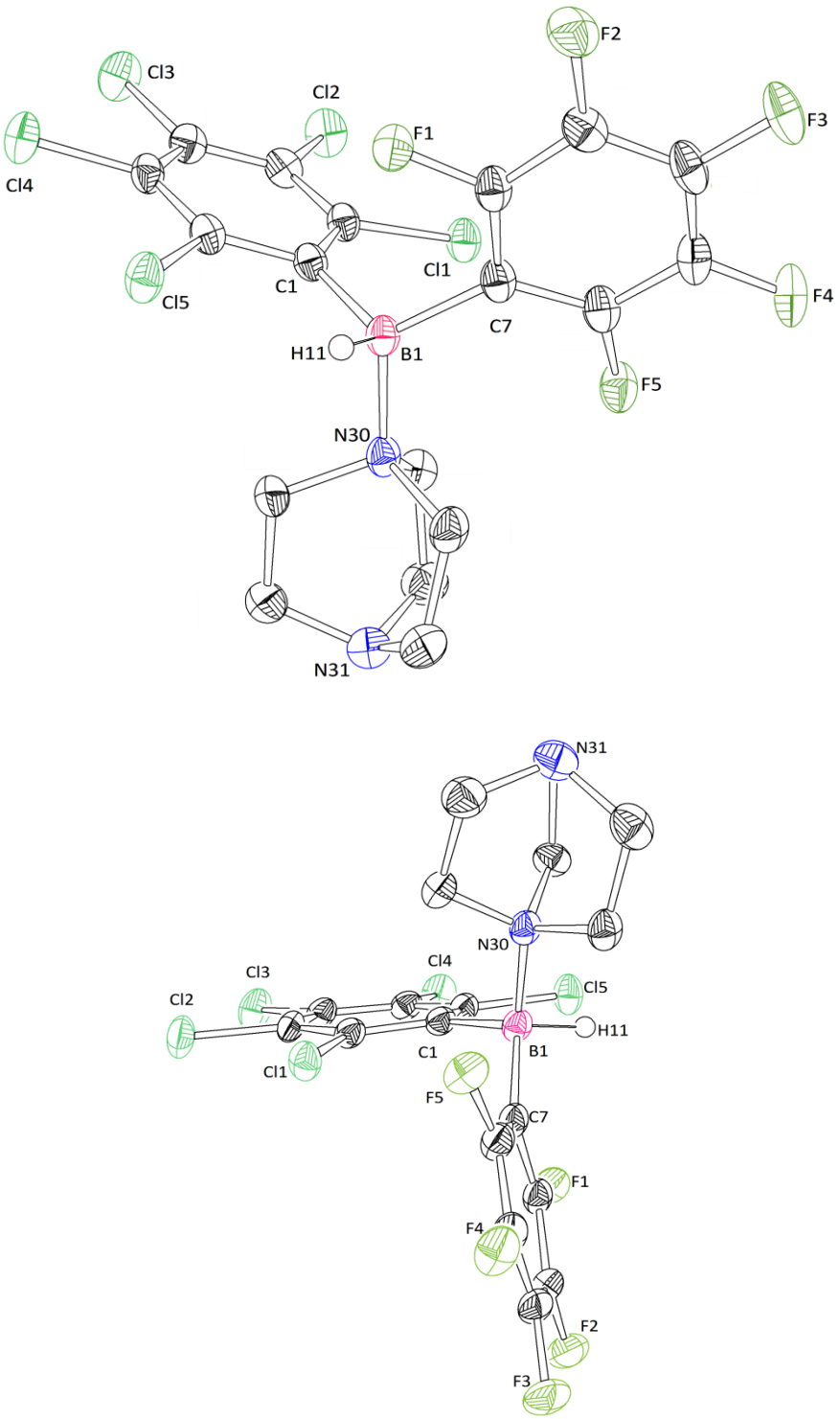


Figure 3.16 X-ray crystal **s**tructure of DABCO-BH(C_6F_5)(C_6Cl_5). Thermal ellipsoids at 50% probability (B atom spicy pink, C atoms black, Cl atoms dark green, F atoms light green, N atoms blue). H atoms on the DABCO have been omitted for clarity.

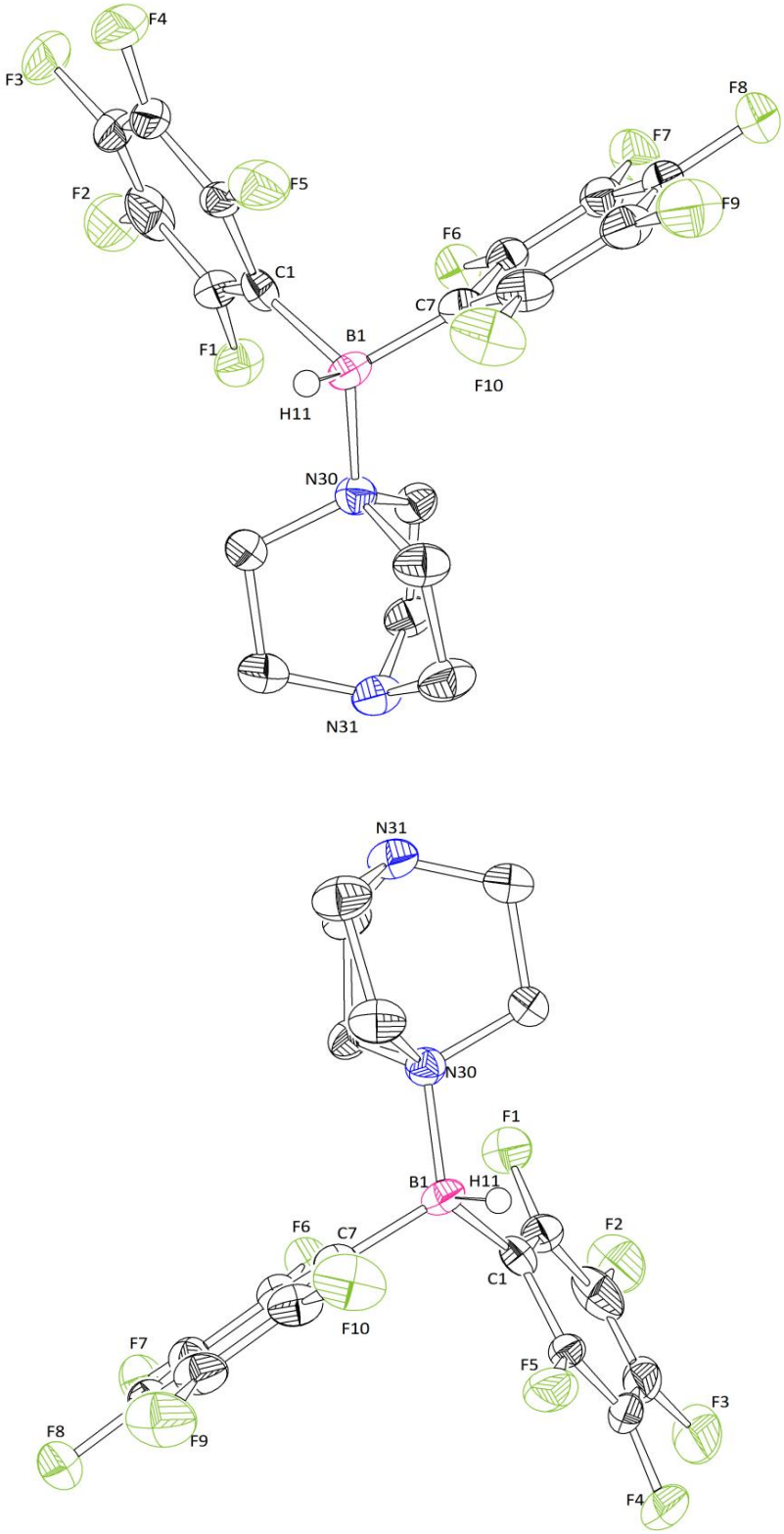


Figure 3.17 X-ray crystal **s**tructure of DABCO-BH(C_6F_5)$_2$. Thermal ellipsoids at 50% probability (B atom spicy pink, C atoms black, Cl atoms dark green, F atoms light green, N atoms blue). H atoms on the DABCO have been omitted for clarity. The minor component of the model of the disorder in the C_6F_5 ring (F1-F5) has been omitted for clarity.

Table 3.4 Selected bond lengths for DABCO-BH(C_6F_5)$_2$, DABCO-BH(C_6F_5)(C_6Cl_5) and *i*Pr_2NH.BH(C_6F_5)$_2$.[41]

Atom 1	**Atom 2**	**Bond Lengths/Å**		
		DABCO-BH(C_6F_5)$_2$	**DABCO-BH(C_6F_5)(C_6Cl_5)**	***i*Pr_2NH.BH(C_6F_5)$_2$[41]**
B1	H11	1.08(2)	1.13	1.12(2)
B1	C1	1.618(10)	1.642(2)	1.640(4)
B1	C7	1.55(2)	1.640(2)	1.632(4)
B1	N30	1.649(18)	1.636(2)	1.628(3)

Table 3.5 Selected bond angles for DABCO-BH(C_6F_5)$_2$, DABCO-BH(C_6F_5)(C_6Cl_5) and *i*Pr_2NH.BH(C_6F_5)$_2$.[41]

Atom 1	**Atom 2**	**Atom 3**	**Bond Angles/^{o}**		
			DABCO-BH(C_6F_5)$_2$	**DABCO-BH (C_6F_5)(C_6Cl_5)**	***i*Pr_2NH.BH (C_6F_5)$_2$[41]**
C(1)	B(1)	C(7)	106.8(12)	112.89(12)	107.74 (19)
C(1)	B(1)	N(30)	114.1(10)	111.29(11)	111.46(18)
C(7)	B(1)	N(30)	115.7(12)	117.75(12)	117.91(18)
C(1)	B(1)	H(11)	97.7(15)	109.2	1.628(3)
C(7)	B(1)	H(11)	118.3(18)	104.5	108.6(11)
N(30)	B(1)	H(11)	103.5(16)	99.8	107.10(11)

Analysis of the bond lengths in Table 3.4 shows that DABCO-BH(C_6F_5)$_2$ has shorter B-H and B-C bonds when compared to *i*Pr_2NH.BH(C_6F_5)$_2$. Due to the presence of different bases, the B-N bond for DABCO-BH(C_6F_5)$_2$ is longer than *i*Pr_2NH.BH(C_6F_5)$_2$. The N-C bond lengths in both DABCO-BH(C_6F_5)$_2$ and DABCO-BH(C_6F_5)(C_6Cl_5) are longer than that reported for free DABCO (1.440(7) Å).[42] Due to the H atom being geometrically placed in DABCO-BH(C_6F_5)(C_6Cl_5) it is not possible to compare the B-H bond length and angles. The B-C bond lengths in DABCO-BH(C_6F_5)(C_6Cl_5) are longer than those in DABCO-BH(C_6F_5)$_2$ which would be caused by the increased steric bulk provided by the C_6Cl_5 group.

Table 3.5 displays selected bond angles for DABCO-BH(C_6F_5)$_2$, DABCO-BH(C_6F_5)(C_6Cl_5) and *i*Pr_2NH.BH(C_6F_5)$_2$. Examination of these bond angles

shows the borohydride have a *pseudo*-tetrahedral geometry around the boron centre. As mentioned before, the [**3**][DABCO] system does not undergo a side reaction. This is likely due to the steric hindrance on **3**, which does not allow the DABCO to coordinate to the B atom.

3.6 Structural Characterisation of the Borohydride Salts

3.6.1 Structural Characterisation of the [B-H][H-DABCO] systems

Crystals of $[(C_6F_5)_3B\text{-}H][H\text{-}DABCO]$ suitable for single crystal X-ray structure determination were grown from a saturated reaction mixture in C_6D_6 (Figure 3.18).

Crystals of [**1**-H][DABCO-H-DABCO] suitable for single crystal X-ray structure determination were grown from the slow diffusion on H_2 into a saturated solution of [**1**][DABCO] in toluene-d_8 at 22 ^{o}C (Figure 3.19).

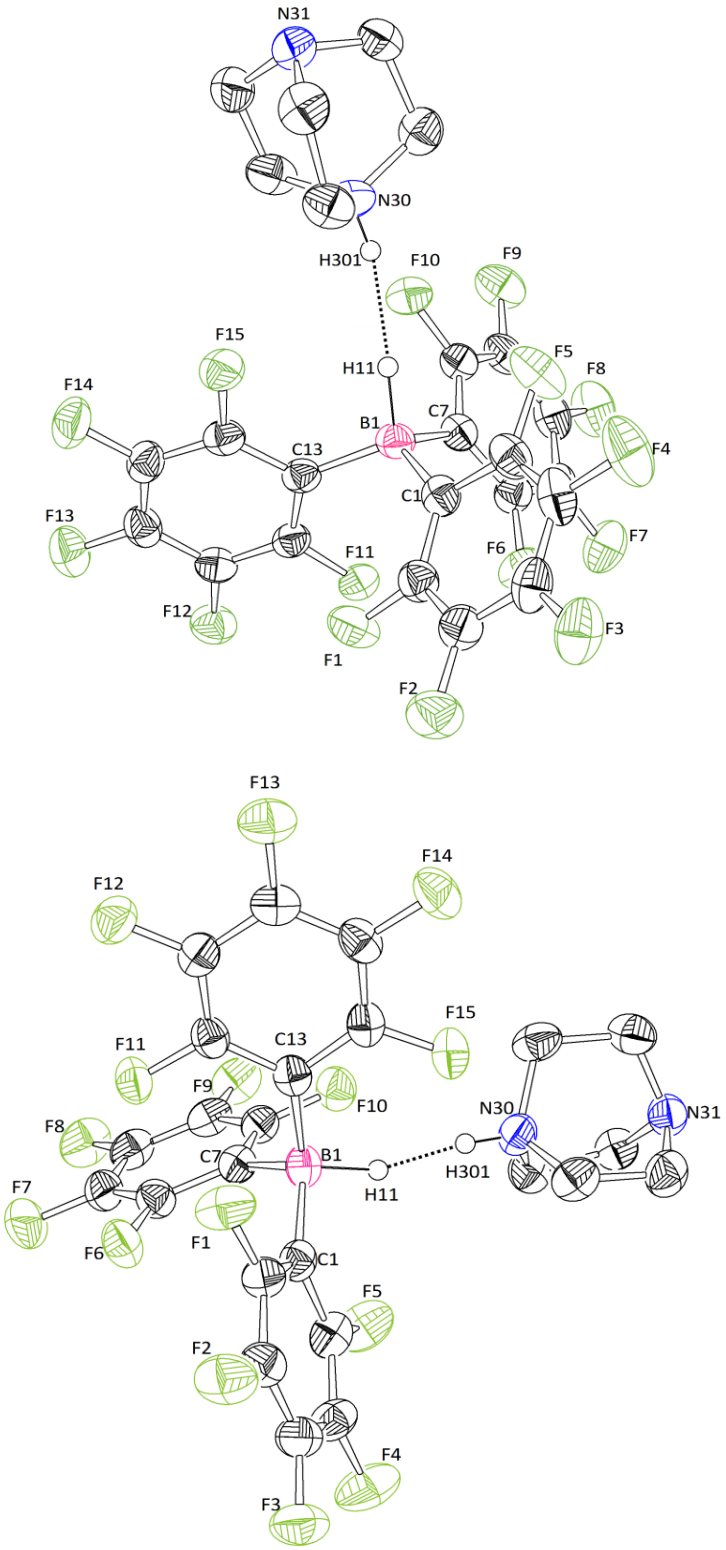


Figure 3.18 X-ray crystal **s**tructures of $[(C_6F_5)_3B\text{-}H][H\text{-}DABCO]$. Thermal ellipsoids at 50% probability (B atom spicy pink, C atoms black, Cl atoms dark green, F atoms light green, N atoms blue). H atoms on the DABCO molecules (except those bound to N atoms) have been omitted for clarity.

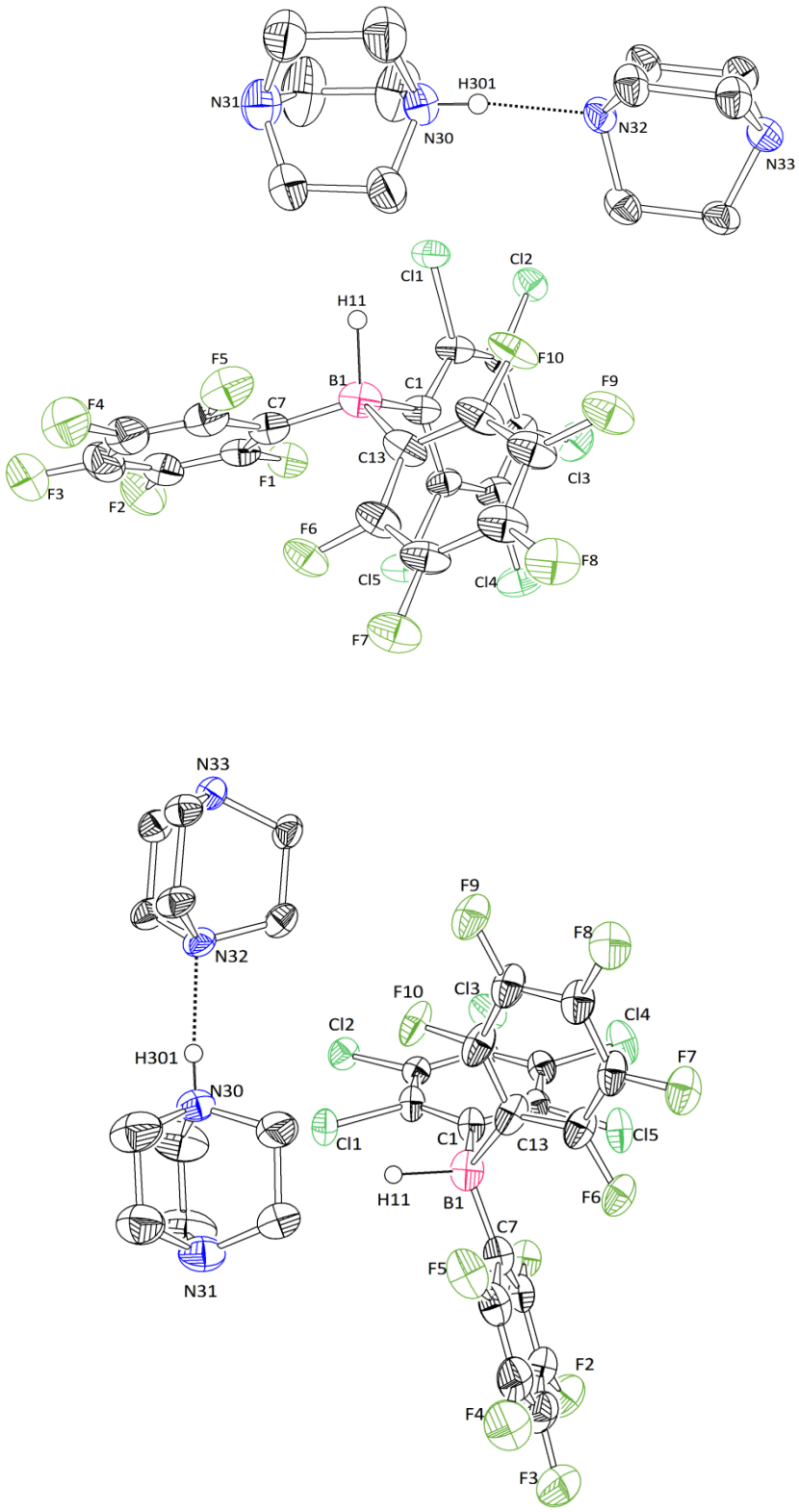


Figure 3.19 X-ray crystal **s**tructures of [**1**-H][DABCO-H-DABCO]. Thermal ellipsoids at 50% probability (B atom spicy pink, C atoms black, Cl atoms dark green, F atoms light green, N atoms blue). Disorder and H atoms on the DABCO molecules (except those bound to N atoms) have been omitted for clarity.

Crystals of [**3**-H][DABCO-H-DABCO] suitable for single crystal X-ray structure determination were grown from a saturated solution of THF layered with pentane (Figure 3.20).

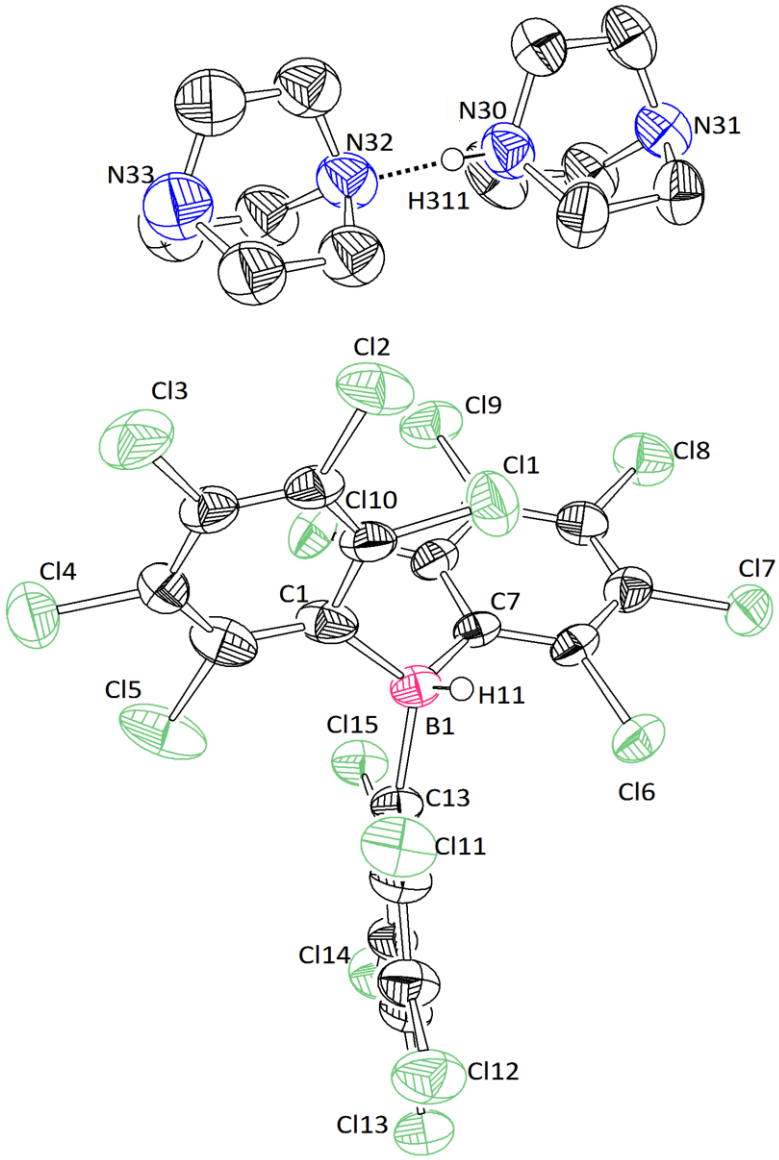


Figure 3.20 X-ray crystal **s**tructure of [**3**-H][DABCO-H-DABCO]. Thermal ellipsoids at 50% probability (B atom spicy pink, C atoms black, Cl atoms dark green, F atoms light green, N atoms blue). Disorder and H atoms on the DABCO molecules (except those bound to N atoms) have been omitted for clarity.

Figure 3.18 displays that upon splitting H_2 using $[B(C_6F_5)_3]$[DABCO], the B-H and N-H groups orientate in a manner so that they are pointing to one another, showing a possible hydrogen bond remaining between the two H atoms. Whereas, in the cases of both [**1**-H][DABCO-H-DABCO] and [**3**-H][DABCO-H-DABCO] (Figures 3.19 and 3.20, respectively), the structures seem to be stabilised by advantageous DABCO which coordinates to the $[H\text{-}DABCO]^+$ group. It is also observed in these cases the B-H group does not coordinate to the DABCO groups.

A summary of the bond lengths and angles for $[(C_6F_5)_3B\text{-}H][H\text{-}DABCO]$, [**1**-H][DABCO-H-DABCO] and [**3**-H][DABCO-H-DABCO] are displayed in Tables 3.6 and 3.7, respectively.

Table 3.6 Selected bond lengths for $[(C_6F_5)_3B\text{-}H][H\text{-}DABCO]$, [**1**-H][H-DABCO] and [**3**-H][H-DABCO].

Atom 1	**Atom 2**	**Bond Lengths/Å**		
		$[(C_6F_5)_3B\text{-}H]$ [H-DABCO]	**[1-H] [DABCO-H-DABCO]**	**[3-H] [DABCO-H-DABCO]**
B(1)	H(11)	1.238(13)	1.35	1.35
B(1)	C(1)	1.637(2)	1.639(8)	1.657(9)
B(1)	C(7)	1.640(2)	1.628(10)	1.634(5)
B(1)	C(13)	1.639(2)	1.682(13)	1.643(6)
N(30)	C(40)	1.497(2)	1.464(4)	1.462(12)
N(30)	C(42)	1.499(2)	1.498(3)	1.475(10)
N(30)	C(44)	1.498(2)	1.490(4)	1.475(10)
N(30)	H(301)	0.88(2)	0.897	0.889
H(11)	H(301)	1.797(2)	-	-

As Table 3.6 shows, the B-C bond lengths do not differ greatly, however they are longer than the parent Lewis acid, which is simply due to the three-coordinate boron centre becoming a four-coordinate species. The most notable difference in the bond lengths is that of the B-H. However, due to the disorder observed in the

[**1**-H][DABCO-H-DABCO] and [**3**-H][DABCO-H-DABCO] crystal structures it is not possible to discuss the B-H bond length.

Table 3.7 Selected bond angles for $[(C_6F_5)_3B\text{-}H][H\text{-}DABCO]$, [**1**-H][H-DABCO] and [**3**-H][H-DABCO].

Atom 1	**Atom 2**	**Atom 3**	**Bond Angles/^{o}**		
			$[(C_6F_5)_3B\text{-}H]$ [H-DABCO]	**[1-H][DABCO-H-DABCO]**	**[3-H][DABCO-H-DABCO]**
C(1)	B(1)	C(7)	111.95(12)	115.0(6)	117.4(4)
C(1)	B(1)	C(13)	115.61(11)	105.5(7)	118.5(5)
C(7)	B(1)	C(13)	110.26(12)	114.11(6)	114.9(5)
C(40)	N(30)	C(44)	109.48(12)	110.9(3)	108.0(7)
C(42)	N(30)	C(44)	109.39(13)	107.5(3)	108.3(7)
C(40)	N(30)	C(42)	110.74(14)	109.8(3)	108.5(6)
C(1)	B(1)	H(11)	101.3(6)	106.6	105.6
C(7)	B(1)	H(11)	107.2(6)	106.9	93.6
C(13)	B(1)	H(11)	109.8(6)	108.4	101.1

When comparing the bond angles of $[(C_6F_5)_3B\text{-}H][H\text{-}DABCO]$, [**1**-H][DABCO-H-DABCO] and [**3**-H][DABCO-H-DABCO], as shown in Table 3.7, it is observed that the bond angles around the boron centre (C-B-C) of [**3**-H][DABCO-H-DABCO] are noticeably larger than those on $[(C_6F_5)_3B\text{-}H][H\text{-}DABCO]$ and [**1**-H][DABCO-H-DABCO]. This is most likely due to the presence of the larger C_6Cl_5 groups (when compared to C_6F_5) and thus greater steric repulsion is observed.

All three X-ray structures display a four-coordinate boron atom centre that adopts a *pseudo*-tetrahedral coordination geometry as seen from the C-B-H and C-B-C angle ranges illustrated in Table 3.7.

3.6.2 Structural Characterisation of the [B-H][H-TMP] Systems

Crystals of [**1**-H][H-TMP] and [**2**-H][H-TMP] suitable for single crystal X-ray structure determination were both grown from a saturated solution of toluene layered with pentane (Figure 3.21 and 3.22, respectively).

Table 3.8 and 3.9 show some selected bond lengths and angles of [**1**-H][H-TMP], [**2**-H][H-TMP] and [$(C_6F_5)_3$B-H][H-TMP], as comparison.

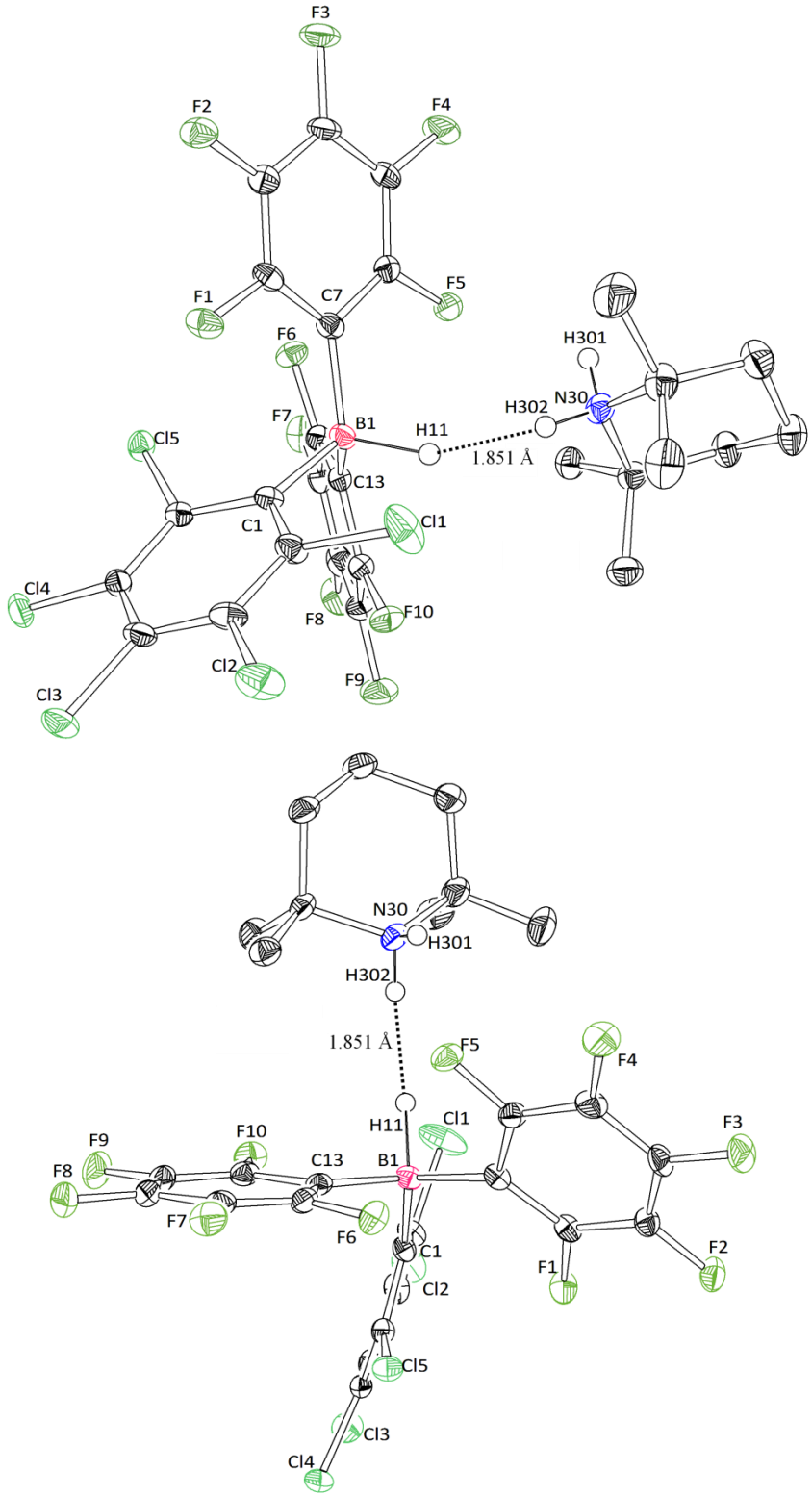


Figure 3.21 Crystal **s**tructure of [**1**-H][H-TMP]. Thermal ellipsoids at 50% probability (B atom spicy pink, C atoms black, Cl atoms dark green, F atoms light green, N atom blue). H atoms on the TMP molecules (except those bound to N atom) have been omitted for clarity.

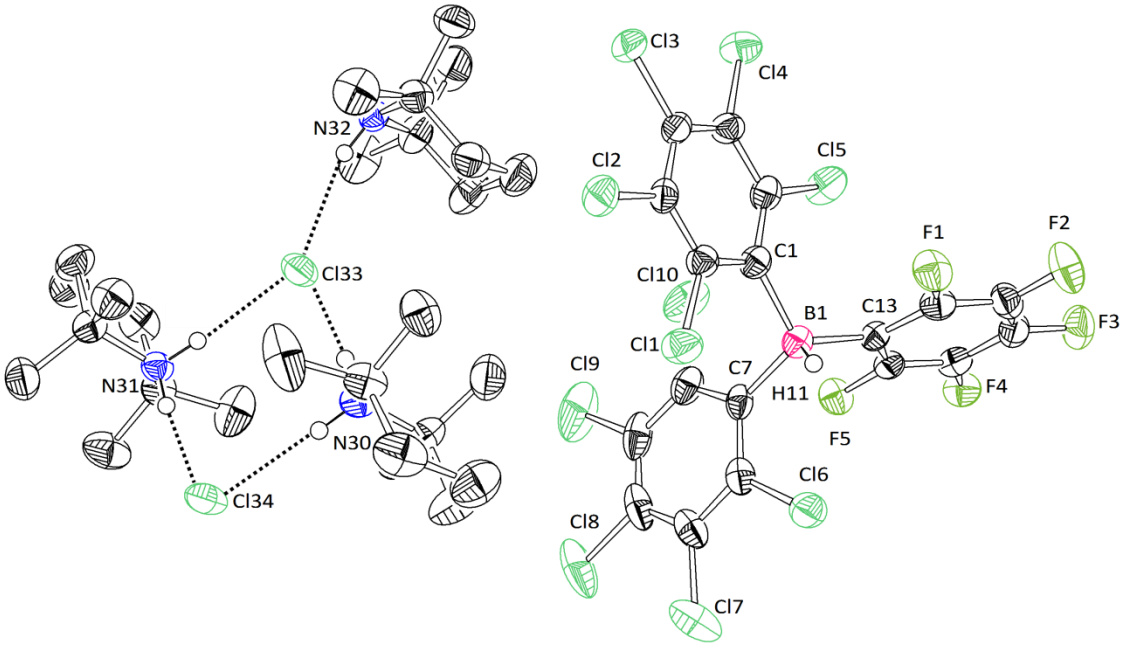


Figure 3.22 Crystal **s**tructure obtained from crystallising [**2**-H][H-TMP]. Thermal ellipsoids at 50% probability (B atom spicy pink, C atoms black, Cl atoms dark green, F atoms light green, N atoms blue). H atoms on the TMP molecules (except those bound to N atoms) have been omitted for clarity.

Figure 3.22 shows the crystal structure obtained from a sample of [**2**-H][H-TMP] is not the 'traditional' borohydride salt when compared to those that have been published, for example $[(C_6F_5)_3B\text{-}H][H\text{-}TMP]$,[14,23,43] and the previous example of [**1**-H][H-TMP]. The crystal structure of [**2**-H][H-TMP] shows that upon the splitting of H_2, Cl^- ions are formed and the $[H\text{-}TMP]^+$ coordinates to the Cl^- ions, indicating either decomposition of the Lewis acid occurs when splitting H_2 or there is another source of Cl^- present in the reaction.

Table 3.8 Selected bond lengths for $[(C_6F_5)_3B\text{-}H][H\text{-}TMP]$,[21] [**1**-H][H-TMP] and [**2**-H][H-TMP]. Computed values for [**1**–H][H-TMP] (BP86/Def2-TZVP) are shown in italics.

Atom 1	**Atom 2**	**Bond Lengths/Å**		
		$[(C_6F_5)_3B\text{-}H]$ [H-TMP][21]	**[1-H][H-TMP]**	**[2-H][H-TMP]**
B(1)	H(11)	1.18(2)	1.35 *(1.230)*	1.12
B(1)	C(1)	1.6413(3)	1.6402(17) *(1.641)*	1.651(4)
B(1)	C(7)	1.632(3)	1.6319(17) *(1.633)*	1.649(4)
B(1)	C(13)	1.639(3)	1.6486(18) *(1.639)*	1.629(4)
N(30)	H(301)	0.90(2)	0.88 *(1.030)*	0.89
N(30)	H(302)	0.92(2)	0.89 *(1.043)*	0.89

Table 3.9 Selected bond angles for $[(C_6F_5)_3B\text{-}H][H\text{-}TMP]$,[21] [**1**-H][H-TMP] and [**2**-H][H-TMP].

Atom 1	**Atom 2**	**Atom 3**	**Bond Angles/°**		
			$[(C_6F_5)_3B\text{-}H]$ [H-TMP][21]	**[1-H][H-TMP]**	**[2-H][H-TMP]**
C(1)	B(1)	C(7)	115.10(18)	114.66(10)	111.6(2)
C(1)	B(1)	C(13)	111.71(17)	106.44(9)	116.7(2)
C(7)	B(1)	C(13)	107.57(17)	116.41(10)	113.4(2)
C(1)	B(1)	H(11)	106.4(10)	108.7	102.0
C(7)	B(1)	H(11)	108.2(10)	105.3	106.7
C(13)	B(1)	H(11)	107.6(10)	104.7	105.1

Both X-ray structures display a four-coordinate boron atom which adopts a *pseudo*-tetrahedral coordination geometry as seen from the C-B-H and C-B-C angle ranges as illustrated in Figures 3.21 and 3.22 and Table 3.9. These observations are consistent with the ^{19}F and $^{11}B\{^1H\}$ NMR spectra of [**1**-H][H-TMP] and [**2**-H][H-TMP] discussed earlier. Comparison of the B-C bond lengths in Table 3.8, shows that upon substituting a C_6F_5 moiety with a C_6Cl_5 moiety, the bond lengths increase. This is expected as there

is an increase in steric hindrance conferred by the Cl groups at the *ortho*-C atoms. The C-F and C-Cl bond lengths for all three structures are comparable, with average distances of 1.3 Å and 1.7 Å, respectively.

[**1**-H][H-TMP] and [**2**-H][H-TMP] are analogous to $[(C_6F_5)_3B\text{-}H][H\text{-}TMP]$.[21] The structure of [**1**-H][H-TMP] shows the H atoms pointing towards each other, suggesting that a H···H bond remains as also seen with $[(C_6F_5)_3B\text{-}H][H\text{-}DABCO]$ (section 3.6.1). Whereas the rearrangement of [**2**-H][H-TMP], due to the stabilising presence of Cl^-, impedes the H atoms from being positioned across from another. This precludes comparison of the distances between the two hydrogen atoms of interest. [**1**-H][H-TMP] exhibits a hydrogen bond distance (N-H···H) of 1.85 Å as demonstrated in Figures 3.16 and 3.17. Sumerin *et al* reports the distance between the two similar hydrogen atoms in $[(C_6F_5)_3B\text{-}H][H\text{-}TMP]$ (B-H···H-N) as 2.97 Å.[44] This value is significantly longer than that measured for [**1**-H][H-TMP] suggesting that $[(C_6F_5)_3B\text{-}H][H\text{-}TMP]$ undergoes rearrangement after splitting H_2.

Recently, Schulz *et al.*, showed that by using Neutron diffraction, NMR spectroscopy and IR spectroscopy, that the distance between the split H_2 molecule was determined to be 1.67 Å using an ansa-aminoborane; 1-N-TMPH-CH_2-2-$[HB(C_6F_5)_2]C_6H_4$.[45] This result was very encouraging as it confirms the insertion of H_2 within the intramolecular FLP and that a hydrogen bond between the split H_2 molecule was still present. Promoted by this, and the crystal structures obtained of the borohydride salts showing the H atoms pointing towards each other, suggesting that a H···H interaction remains, the mechanism of H_2 activation using an intermolecular FLP was investigated by growing single crystals of [**1**-H][H-TMP] suitable for neutron diffraction.

3.7 Mechanism of H_2 Activation

The exact mechanism by which intermolecular FLPs activate H_2 is still under investigation. The mechanistic and structural details of these FLP systems are highly important in helping to improve future systems. The theory that H-H bond cleavage is mediated by a linear [LA]-H···H-[LB] transition state has recently been discredited because the theory did not allow for the interaction between large substituents.[46] Erker proposed a bimolecular process, demonstrated for the FLP system compiled of $^{t}Bu_3P$ and $B(C_6F_5)_3$, whereby the reaction is thought to be asymmetric-concerted with the LA-H bond forming a little earlier than that of H-LB. This suggests that FLPs activate H_2 *via* polarisation due to the electric field created by their donor/acceptor atoms (Figure 3.23).

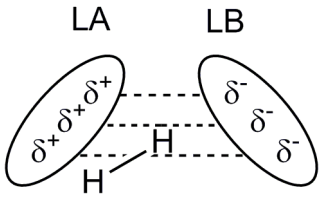


Figure 3.23 Postulated electric field polarisation of the H_2 molecule involving FLPs.

Schulz *et al.* demonstrated using single crystal Neutron diffraction and IR and NMR spectroscopy that a weak hydrogen bond interaction (1.67 Å) was present after H_2 was split using an intramolecular FLP system.[45] These findings have helped improve the understanding of the mechanism of H_2 splitting using intramolecular FLPs. However, as their FLP system contains a bridge that forces the Lewis acidic and basic centres together, it can be argued that this H···H distance is not a true representative of the transition state. Therefore, H_2 activation using intermolecular FLP systems (e.g. $B(C_6F_5)_3$/TMP) are still under investigation, as upon crystallisation there is a greater possibility for the rearrangement of the salt.[44]

3.7.1 Single Crystal Neutron Diffraction of [1-H][H-TMP]

The X-ray crystal structure of [**1**-H][H-TMP] has been determined (section 3.6.2) and shows that after splitting H_2 the orientation of the salt displays a possible hydrogen bond (B-H···H-N). However, as X-ray diffraction only allows one to see electron density and due to the low electron density on a H atom, it is not possible for the precise positions and distances of the H atoms to be determined. Therefore, to accurately determine the geometry of B-H···H-N, a neutron diffraction measurement was conducted using a single crystal grown from a saturated toluene solution layered with pentane (Figure 3.24).

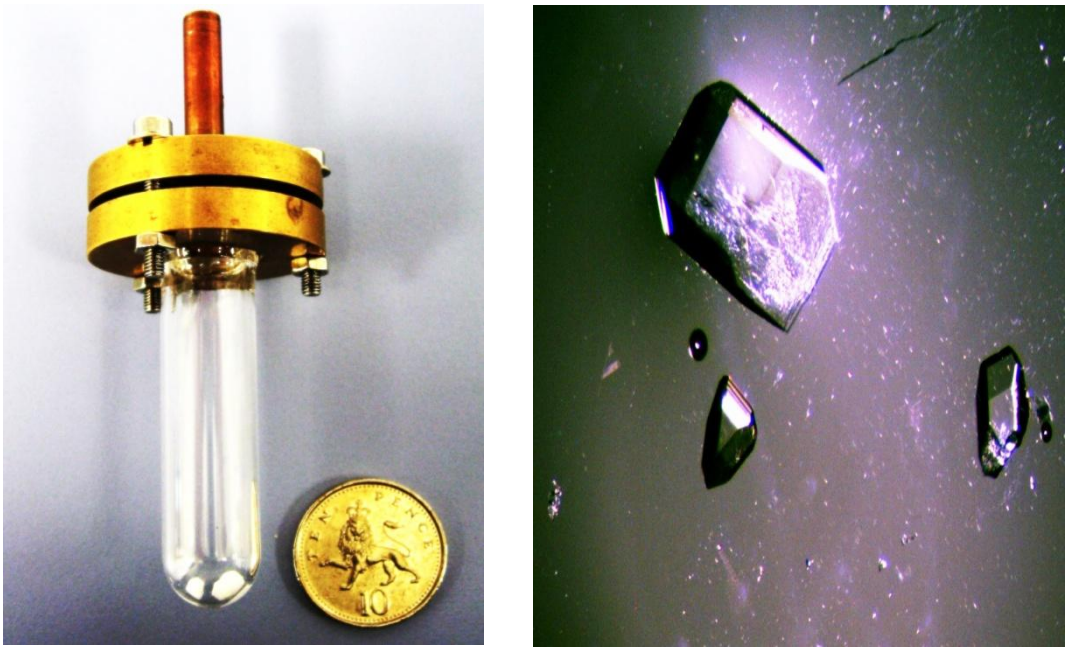


Figure 3.24 Single crystals of [**1**-H][H-TMP] in the neutron diffraction sample holder (left) and single crystals used for X-ray diffraction (right).

A differerence map displaying the H atoms located using from the neutron diffraction experiment is shown in Figure 3.25.

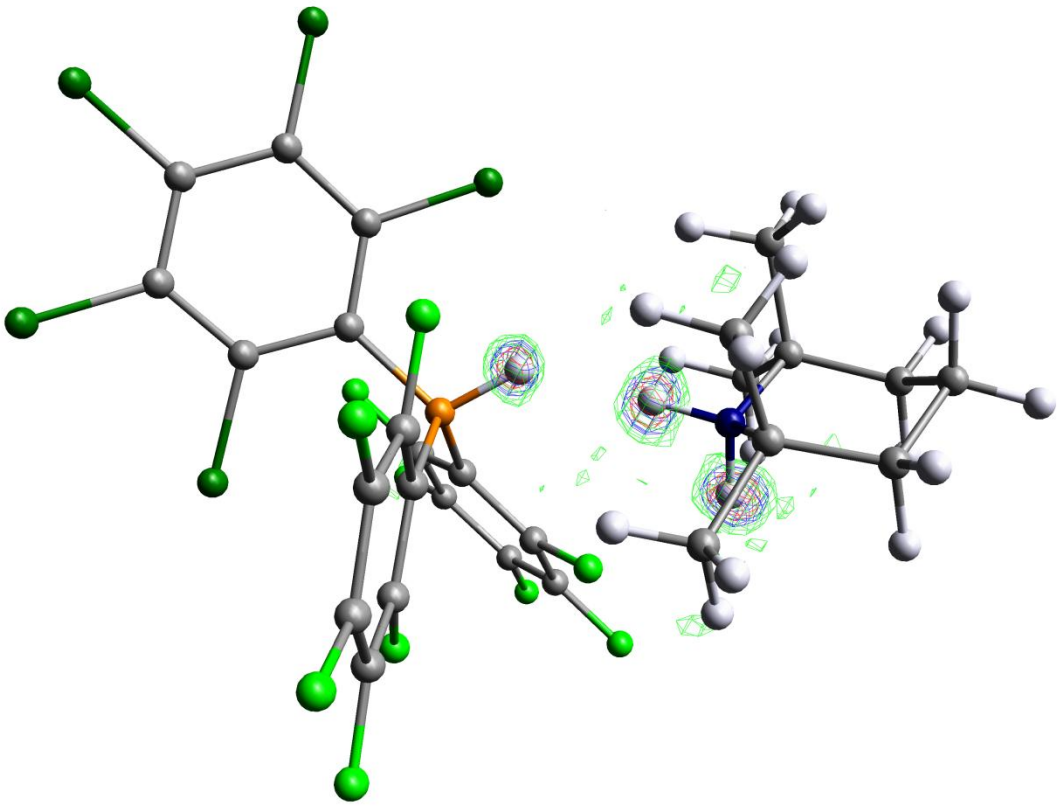


Figure 3.25 Difference map of the [**1**-H][H-TMP] Neutron structure.

The difference map in Figure 3.25 shows that unlike X-ray diffraction, where the diffracted X-ray intensity is bigger for atoms with a large atomic number, neutrons directly interact with the nucleus of the atom so that atoms with a low atomic number e.g. hydrogen, can strongly contribute to the diffraction intensity even in the presence of atoms with a large atomic number. Figure 3.26 shows the neutron diffraction structure of [**1**-H][H-TMP].

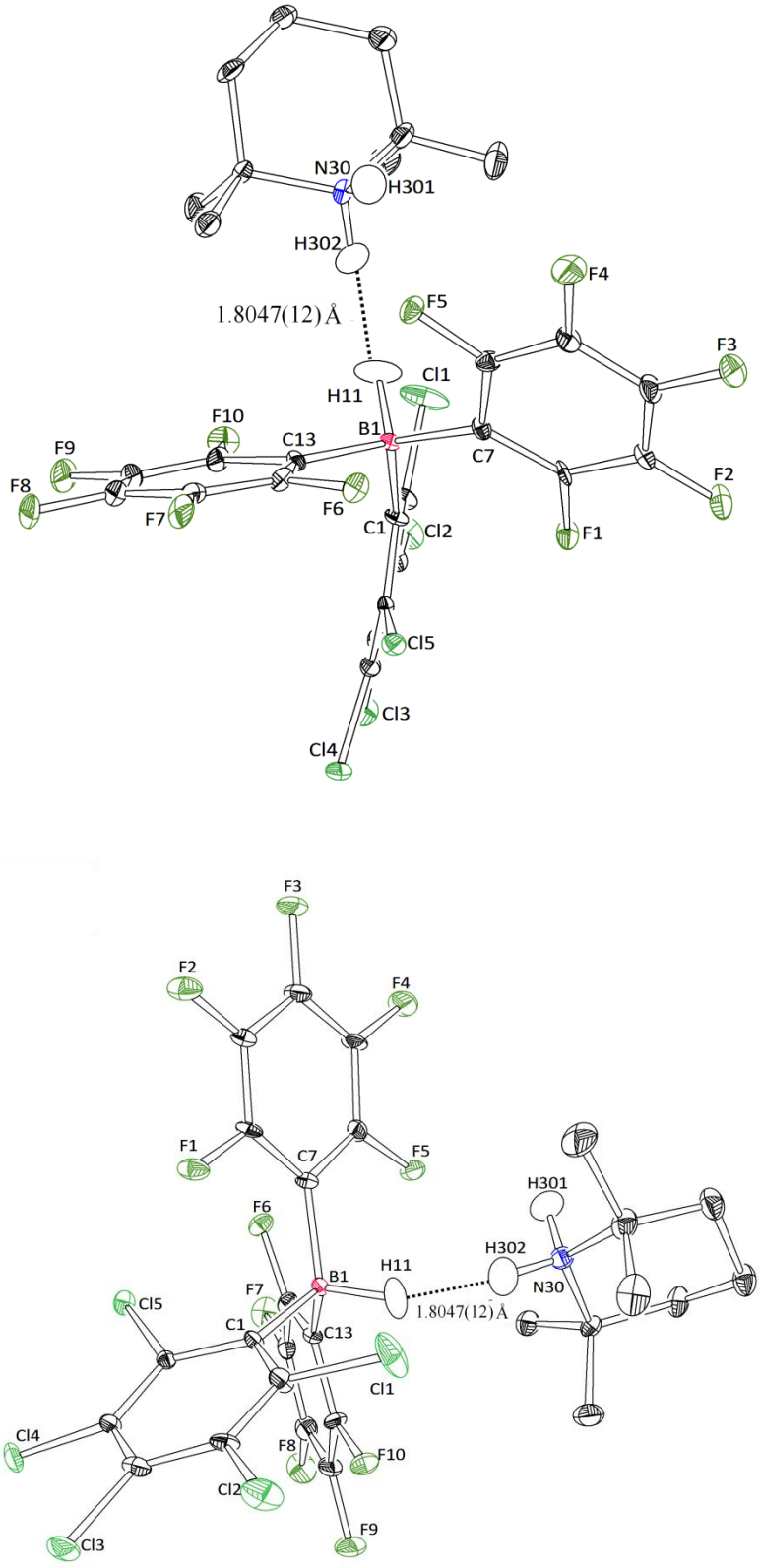


Figure 3.26 Neutron structure of [**1**-H][H-TMP] at 100 K. Thermal ellipsoids at 50% probability (B atom spicy pink, C atoms black, Cl atoms dark green, F atoms light green, N atom blue). H atoms on the TMP molecules (except those bound to N atom) have been omitted for clarity.

The neutron structure (Figure 3.26) agrees well with the X-ray structure (Figure 3.21) displaying a four-coordinate boron atom which adopts a *pseudo*-tetrahedral coordination geometry as seen from the C-B-H and C-B-C angle ranges. Table 3.10 and 3.11 show selected bond lengths and bond angles from DFT and the X-ray and neutron diffraction studies carried out on [**1**-H][H-TMP]. The C-F and C-Cl bond lengths for both structures are comparable, with average distances of 1.3 Å and 1.7 Å, respectively.

Table 3.10 Selected bond lengths for [**1**-H][H-TMP] from DFT, X-ray diffraction and neutron diffraction experiments.

Atom 1	**Atom 2**	**Bond Lengths/Å**		
		DFT	**X-ray Diffraction**	**Neutron Diffraction**
H(1)	H(302)	1.766	1.85	1.8047(12)
B(1)	H(11)	1.230	1.35	1.203(9)
B(1)	C(1)	1.641	1.6402(17)	1.636(5)
B(1)	C(7)	1.633	1.6319(17)	1.632(5)
B(1)	C(13)	1.639	1.6486(18)	1.644(6)
N(30)	H(301)	1.030	0.88	1.030(8)
N(30)	H(302)	1.043	0.89	1.038(9)

Table 3.11 Selected bond angles for [**1**-H][H-TMP] from DFT, X-ray diffraction and neutron diffraction experiments.

Atom 1	**Atom 2**	**Atom 3**	**Bond Angles/^{o}**		
			DFT	**X-ray Diffraction**	**Neutron Diffraction**
C(1)	B(1)	C(7)	114.51	114.66(10)	115.0(3)
C(1)	B(1)	C(13)	109.67	106.44(9)	106.8(3)
C(7)	B(1)	C(13)	117.10	116.41(10)	116.0(3)
C(1)	B(1)	H(11)	106.25	108.7	108.9(5)
C(7)	B(1)	H(11)	104.80	105.3	105.4(6)
C(13)	B(1)	H(11)	103.14	104.7	104.1(7)

Using neutron diffraction the distances between the split H_2 atoms could be accurately be determined as 1.8047(12) Å. This distance is slightly longer than that predicted by DFT and shorter than the calculated distance using X-ray diffraction

(Table 3.10). The results from the neutron diffraction study also shows that the B-H bond length was overestimated with X-ray diffraction but is in good agreement with the DFT study. In the case of the N-H bond length, the neutron diffraction experiment shows that bond length is slightly longer than calculated using X-ray diffraction but just like the B-H bond length, is very similar to the result from the DFT study.

The B-H and N-H bond lengths (1.24 and 1.03 Å, respectively) for 1-*N*-TMPH-CH_2-2-[$HB(C_6F_5)_2$]C_6H_4 measured by Schulz *et al.* are comparable to those determined for [**1**-H][H-TMP] (1.20 and 1.03 Å). However, the distances between the H atoms for 1-*N*-TMPH-CH_2-2-[$HB(C_6F_5)_2$]C_6H_4 are significantly shorter than that determined for [**1**-H][H-TMP] (1.67 Å and 1.80 Å, respectively).[45] One main reason for this could be that the bridge between the borane and N-base on 1-*N*-TMPH-CH_2-2-[$HB(C_6F_5)_2$]C_6H_4 only allows limited space for the H atoms to exist, with a B-N distance of 3.35 Å compared to [**1**-H][H-TMP] which has a B-N distance of 3.8228(5) Å. Therefore the FLP field for an intermolecular species is larger than that for an intramolecular FLP. The H to H distance measured for [**1**-H][H-TMP] is considerably shorter than that previously measured for [$(C_6F_5)_3$B-H][H-TMP] which displayed an elongated N-H···H-B distance of 2.97 Å.[44] According to Steiner a "moderate" or "normal" hydrogen bond has a distance of 1.5 – 2.2 Å.[47] Therefore the B-H···H-N measured for [**1**-H][H-TMP] is within the accepted range for a hydrogen bond and is the first B-H···H-N distance measured for an intermolecular borohydride salt.

3.7.2 Electronic Structure Analysis of [1-H][H-TMP]

In collaboration with Dr. Tobias Krämer, the electronic structure of [**1**-H][H-TMP] was explored. The structure has been optimised using density functional theory (DFT) (BP86/Def2-TZVP). The bond lengths and angles at the minimum energy structure (shown in Tables 3.10 and 3.11) are all fully consistent with the experimental data, displaying a four-coordinate *pseudo*-tetrahedral boron centre. The B-H···H-N intermolecular distance was determined to be 1.766 Å.

Analysis of the *infra-red* stretching modes show that the B-H frequency is at 2307 cm^{-1} and the N-H frequency is found at 3144 cm^{-1} (shown in parentheses in Table 3.12) This is in agreement with the solid state measurement of the IR spectrum of [**1**-H][H-TMP] (see section 3.8).

3.7.3 NMR Studies of [1-H][H-TMP]

To compare every variable discussed by Schulz *et al.* attempts were made to determine the H(11) to H(302) distance using T1 relaxation measurements and 1D NOE experiments as a collaboration with Dr. Nick Rees.

After trying the most common NMR solvents, it was found that the B-H and N-H resonances resolved best in CD_3CN. Unfortunately, the freezing point for CD_3CN is −40 ^oC, which limited the experiment to temperatures greater than −40 ^oC.

The ^1H NMR spectrum of [**1**-H][H-TMP] in CD_3CN with well resolved N-H (6.22 ppm) and B-H (3.96 ppm) resonances is displayed in Figure 3.27.

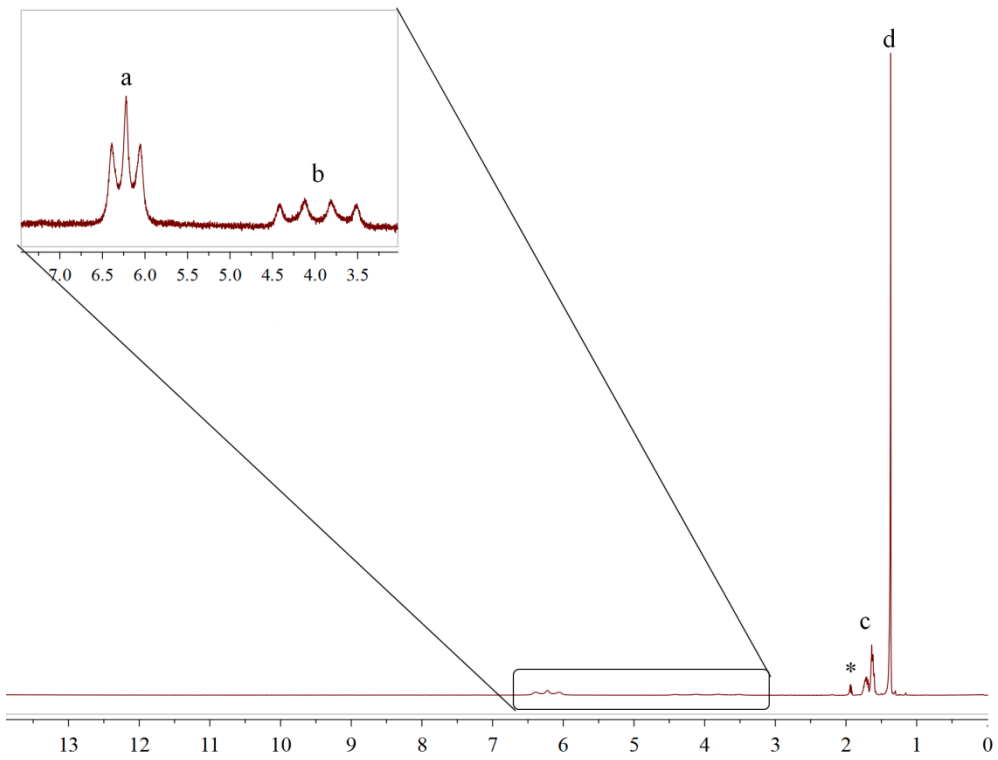


Figure 3.27 ^{1}H NMR spectrum of [**1**-H][H-TMP] showing N-H **a**, B-H **b**, TMP **c** and **d**, in CD_3CN (*).

Schulz *et al.* conducted their 1D NOE experiments by pulsing two resonances (N-H and a methyl group) which have a known distance obtained from neutron diffraction and then extrapolating this information to give the B-H···H-N distance, which agreed with their previous measurements. Fortunately for them, their chosen resonances were well spaced and showed good resolution, which was aided by having a rigid structure. Regrettably the ^{1}H NMR spectrum of [**1**-H][H-TMP] does not provide a fixed point to determine a calibration distance due to the fluxional TMP group.

Attempts were made to emulate the T1 experiments carried out by Schulz *et al.* unfortunately, just like with the 1D NOE experiment, the T1 experiment was found to be too complicated and difficult to resolve. Therefore, attempts to determine the H(11) to H(302) distance using NMR spectroscopy proved fruitless.

3.8 FT-IR SPECTROSCOPY

The FT-IR spectra of the borohydride salts were measured in the solid state to study the structure of the salts in attempt to further understand the hydrogen bonding in B-H···H-N. Recently Schulz *et al.* have successfully shown the use of FT-IR spectroscopy to support their findings from neutron diffraction. They demonstrated that the broadening of the vibration proves the existence of hydrogen bonding in the solid state, which additionally supports the findings of the neutron diffraction study.[45,48] A summary of the frequencies observed for each of the borohydride salts are exhibited in Table 3.12.

Table 3.12 Frequencies observed for the B-H and N-H *infra-red* stretching modes in the solid state of the borohydride salts (cm^{-1}).

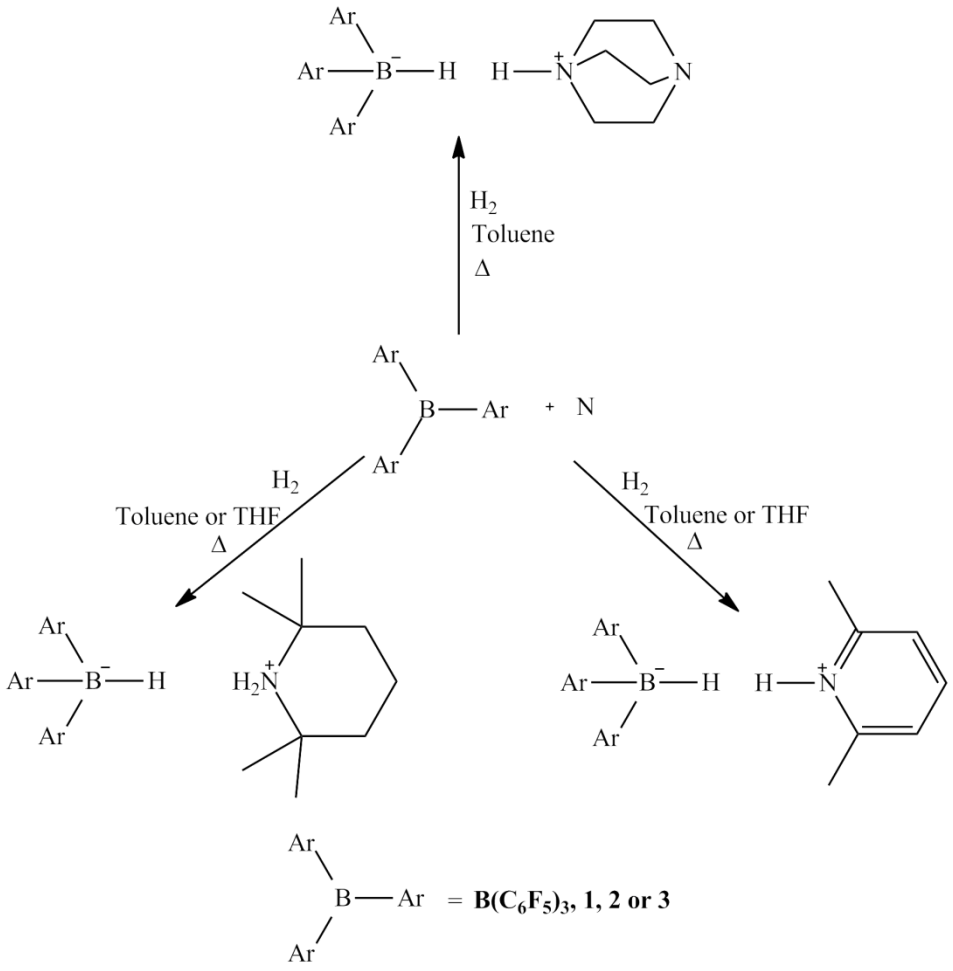
Salt	*v* (B-H) (cm^{-1})	*v* (N-H) (cm^{-1})
$[(C_6F_5)_3B\text{-}H][H\text{-}DABCO]$	2371	2972
[**1**-H][H-TMP]	2262 *(2307)*	2959 *(3144)*
[**2**-H][H-TMP]	1959	2970
[**3**-H][H-TMP]	2266	2959
[**1**-H][H-DABCO]	2362	2972
[**2**-H][H-DABCO]	2206	2945
[**3**-H][H-DABCO]	2204	2943
[**1**-H][H-Lut]	2345	2962
[**2**-H][H-Lut]	2347	2978
[**3**-H][H-Lut]	2258	2961

As Table 3.12 shows the B-H and N-H *infra-red* stretching modes are in agreement with each other and the theoretical studies (section 3.7.2), as well as the literature.[45] They display broad vibrational modes, which concurs with Schulz *et al.* findings.

The stretching vibration of the hydrogen bond between B-H···H-N is assumed to be located between 600-100 cm^{-1},[45] however, due to a large number of other stretches observed within this region, an exact assignment could not be made.

3.9 Conclusions

The synthesis of nine novel FLPs have been accomplished and have all shown to successfully split H_2 under various conditions as summarised in Scheme 3.2.



Scheme 3.2 Summary of reactions.

The FLP systems containing TMP exhibit the simplest reactions, by irreversibly splitting H_2 without any side reactions. Whereas the DABCO and Lut systems

demonstrate interesting reactivity, with the DABCO system showing the loss of a C_6X_5 (X = F or Cl) group and coordination of the DABCO to the B atom with H_2 activation, once heated above 65 ^oC. Whereas the Lut FLP systems are all able to reversibly activate H_2. Each borohydride salt has been fully characterised spectroscopically. Some of the reactions were monitored using NMR spectroscopy in an attempt to experimentally determine the activation of energy of splitting H_2 with these systems. The experiments gave a great insight into the ideal reaction conditions for each of the systems.

Using five of the borohydride salts their structures were determined using single crystal X-ray diffraction. The X-ray structures show that in some cases the H atoms from the split H_2 molecules point to one another suggesting a hydrogen bond still exists between the molecules. These could be the transition state of the reactions indicating that upon polarising H_2, the molecule positions itself between the B and N atoms. To determine the exact positions of the H atoms, single crystal neutron diffraction and DFT experiments were carried out on [**1**-H][H-TMP]. Data from the single crystal neutron diffraction and DFT experiments were consistent. It was determined from neutron diffraction that the H(11) to H(302) distance was 1.8047(12) Å. This is much shorter than what previously reported for $[(C_6F_5)_3B\text{-}H][H\text{-}TMP]$ (2.97 Å)[44] and is the first B-H···H-N distance to be measured for an intermolecular borohydride salt which is also within the accepted range for a hydrogen bond.[47]

This is a significant step towards the elucidation of the nature of the key transition state in the splitting of H_2.

3.10 References

(1) Welch, G. C.; Juan, R. R. S.; Masuda, J. D.; Stephan, D. W. *Science* **2006**, *314*, 1124-1126.
(2) Stephan, D. W.; Erker, G. *Angew. Chem., Int. Ed.* **2010**, *49*, 46-76.
(3) Ashley, A. E.; Thompson, A. L.; O'Hare, D. *Angew. Chem., Int. Ed.* **2009**, *48*, 9839-9843.
(4) Menard, G.; Stephan, D. W. *J. Am. Chem. Soc.* **2010**, *132*, 1796-1797.
(5) Zhao, X.; Stephan, D. W. *Chem. Commun.* **2011**, *47*, 1833-1835.
(6) Stirling, A.; Hamza, A.; Rokob, T. A.; Papai, I. *Chem. Commun.* **2008**, 3148-3150.
(7) Stute, A.; Kehr, G.; Frohlich, R.; Erker, G. *Chem. Commun.* **2011**, *47*, 4288-4290.
(8) Ullrich, M. L., Alan J.; Stephan, Douglas W. *Organometallics* **2010**, *29*, 3647-3654.
(9) Momming, C. M.; Otten, E.; Kehr, G.; Frohlich, R.; Grimme, S.; Stephan, D. W.; Erker, G. *Angew. Chem., Int. Ed.* **2009**, *48*, 6643-6646.
(10) Chase, P. A.; Welch, G. C.; Jurca, T.; Stephan, D. W. *Angew. Chem., Int. Ed.* **2007**, *46*, 8050-8053.
(11) Chase, P. A.; Jurca, T.; Stephan, D. W. *Chem. Commun.* **2008**, 1701-1703.
(12) Chen, D.; Wang, Y.; Klankermayer, J. *Angew. Chem., Int. Ed.* **2010**, *49*, 9475-9478.
(13) Sgro, M. J.; Domer, J.; Stephan, D. W. *Chem. Commun.* **2012**, *42*, 7253-7255.
(14) Jiang, C.; Blacque, O.; Fox, T.; Berke, H. *Dalton Trans.* **2011**, *40*, 1091-1097.
(15) Harhausen, M.; Fröhlich, R.; Kehr, G.; Erker, G. *Organometallics* **2012**.
(16) Welch, G. C.; Stephan, D. W. *J. Am. Chem. Soc.* **2007**, *129*, 1880-1881.
(17) Theuergarten, E.; Schluns, D.; Grunenberg, J.; Daniliuc, C. G.; Jones, P. G.; Tamm, M. *Chem. Commun.* **2010**, *46*, 8561-8563.
(18) Ullrich, M.; Lough, A. J.; Stephan, D. W. *J. Am. Chem. Soc.* **2009**, *131*, 52-53.
(19) Stephan, D. W. *Dalton Trans.* **2009**, 3129-3136.
(20) Chase, P. A.; Stephan, D. W. *Angew. Chem., Int. Ed.* **2008**, *47*, 7433-7437.
(21) Sumerin, V.; Schulz, F.; Nieger, M.; Leskela, M.; Repo, T.; Rieger, B. *Angew. Chem., Int. Ed.* **2008**, *47*, 6001-6003.
(22) Jiang, C.; Blacque, O.; Fox, T.; Berke, H. *Organometallics* **2011**, *30*, 2117-2124.
(23) Geier, S. J.; Stephan, D. W. *J. Am. Chem. Soc.* **2009**, *131*, 3476-3477.
(24) Tran, S. D. T., T. A.; Kaminsky, W.; Heinekey, D. M.; Mayer, J. M. *Inorg. Chim. Acta* **2011**, *369*, 126-132.
(25) Binding, S. C.; Zaher, H.; Mark Chadwick, F.; O'Hare, D. *Dalton Trans.* **2012**, *41*, 9061-9066.
(26) Lu, Z.; Cheng, Z.; Chen, Z.; Weng, L.; Li, Z. H.; Wang, H. *Angew. Chem., Int. Ed.* **2011**, *50*, 12227-12231.
(27) Ashley, A. E.; Herrington, T. J.; Wildgoose, G. G.; Zaher, H.; Thompson, A. L.; Rees, N. H.; Krämer, T.; O'Hare, D. *J. Am. Chem. Soc.* **2011**, *133*, 14727-14740.
(28) Rokob, T. A.; Hamza, A.; Pápai, I. *J. Am. Chem. Soc.* **2009**, *131*, 10701-10710.
(29) Rokob, T. A.; Hamza, A.; Stirling, A.; Papai, I. *J. Am. Chem. Soc.* **2009**, *131*, 2029-2036.
(30) Privalov, T. *Eur. J. Inorg. Chem.* **2009**, *2009*, 2229-2237.
(31) Sumerin, V.; Schulz, F.; Nieger, M.; Leskelä, M.; Repo, T.; Rieger, B. *Angew. Chem., Int. Ed.* **2008**, *47*, 6001-6003.
(32) http://evans.harvard.edu/pdf/evans_pka_table.pdf.
(33) Shi, Y.-J.; Humphrey, G.; Maligres, P. E.; Reamer, R. A.; Williams, J. M. *Advanced Synthesis & Catalysis* **2006**, *348*, 309-312.

(34) Blackwell, J. M.; Piers, W. E.; Parvez, M. *Org. Lett.* **2000**, *2*, 695-698.
(35) Di Saverio, A.; Focante, F.; Camurati, I.; Resconi, L.; Beringhelli, T.; D'Alfonso, G.; Donghi, D.; Maggioni, D.; Mercandelli, P.; Sironi, A. *Inorg. Chem.* **2005**, *44*, 5030-5041.
(36) Jiang, C.; Blacque, O.; Berke, H. *Chem Commun (Camb)* **2009**, 5518-5520.
(37) O'Hare, D.; Ashley, A. E.; Organization, W. I. P., Ed. 2011; Vol. WO2011/045605 A1.
(38) Ménard, G.; Stephan, D. W. *Angew. Chem., Int. Ed.* **2012**, *51*, 8272-8275.
(39) Chen, J. Y. C.; Martí, A. A.; Turro, N. J.; Komatsu, K.; Murata, Y.; Lawler, R. G. *J. Phys. Chem. B* **2010**, *114*, 14689-14695.
(40) Takeuchi, Y. *J. Chem. Soc. Perkin Trans. II* **1985**, 175-177.
(41) Jiang, C. B., Olivier; Berke, Heinz *Organometallics* **2009**, *28*, 5233-5239.
(42) Nimmo, J. K.; Lucas, B. W. *Acta Crystallographica Section B* **1976**, *32*, 348-353.
(43) Welch, G. C.; Cabrera, L.; Chase, P. A.; Hollink, E.; Masuda, J. D.; Wei, P. R.; Stephan, D. W. *Dalton Trans.* **2007**, 3407-3414.
(44) Sumerin, V. PhD Thesis, University of Helsinki, 2011.
(45) Schulz, F.; Sumerin, V.; Heikkinen, S.; Pedersen, B.; Wang, C.; Atsumi, M.; Leskelä, M.; Repo, T.; Pyykkö, P.; Petry, W.; Rieger, B. *J. Am. Chem. Soc.* **2011**, *133*, 20245-20257.
(46) Flierler, U.; Leusser, D.; Ott, H.; Kehr, G.; Erker, G.; Grimme, S.; Stalke, D. *Chem. Eur. J.* **2009**, *15*, 4595-4601.
(47) Steiner, T. *Angew. Chem., Int. Ed.* **2002**, *41*, 48-76.
(48) Nibbering, E. T. J.; Elsaesser, T. *Chem. Rev.* **2004**, *104*, 1887-1914.

CHAPTER FOUR

Conversion of CO_2 to Methanol using the [B-H][H-N] Salts

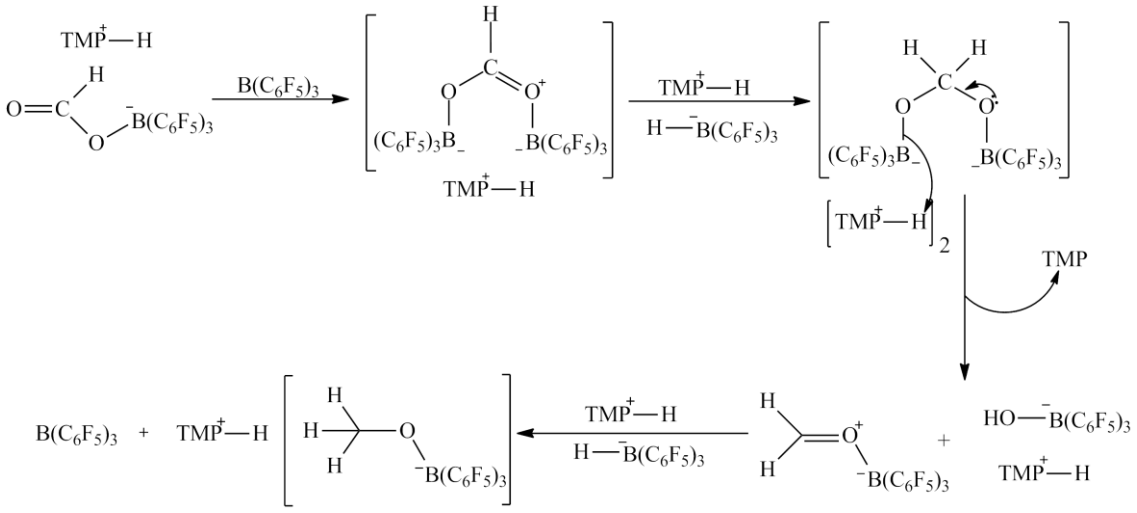
4.1 Introduction

For the last 200 years, since the industrial revolution, the global concentration of atmospheric carbon dioxide has increased rapidly, thus contributing to global warming and climate change.[1] This is a highly debated topic which has generated a considerable amount of attention internationally.[2] Attempts are being made to reduce carbon dioxide emissions via various methods including capturing the non-polar CO_2 molecule[3-5] with the use of high-surface-area macro- and microporous materials, for example, complex metal–organic frameworks (MOFs), organic materials (e.g. activated carbon materials), and inorganic materials (e.g. alumina, silicas, and zeolites).[6-10] A more attractive result than capture and storage, would be converting CO_2 into useful chemicals which could be used both in energy generation and as chemical feedstocks. Not only would this sequester CO_2 from atmospheric release and help limit the effects of global warming, but it would also provide the planet with a renewable fuel. One idea that tackles both the capture of CO_2 and its utilisation as an alternative to fossil fuels is the methanol economy proposed by Olah.[1,11-13] This approach allows for CO_2 to be "recycled" to a C1 fuel source, which in principle could result in a "carbon neutral" fuel, especially if "green" hydrogen, sourced from splitting water, is used.[14]

Homogeneous and heterogeneous processes have been studied, using transition metals, which employ CO_2 to produce CO as well as formic acid and its derivatives.[15-17] However, these reactions are far from perfect as they exhibit poor selectivity and produce a mixture of products. Therefore further breakthroughs are required.

Recent studies have looked into exploiting the exciting reactivity of FLPs in the activation of small molecules to achieve the desirable reduction of CO_2 to methanol.[18-20]

Research by Tran *et al.* showed that CO_2 was able to insert into the B-H bond of $[(C_6F_5)_3B\text{-}H][H\text{-}Lut]$ at 22 ^oC.[21] Ashley *et al.* were able to take the reaction one step further using the $B(C_6F_5)_3$/TMP system and successfully reduce CO_2 and isolate methanol; however, the reaction was low yielding.[22] This method takes advantage of the equilibria that exist between the borane, borohydride, and formatoborate to activate the substrate and act as a hydride delivery source. It was found that major decomposition of the FLP system occurred which prevented any attempt for the system to be catalytic. A mechanism was proposed on the method of decomposition (Scheme 4.1).



Scheme 4.1 Proposed mechanism for the decomposition of the $B(C_6F_5)_3$/TMP system.[22]

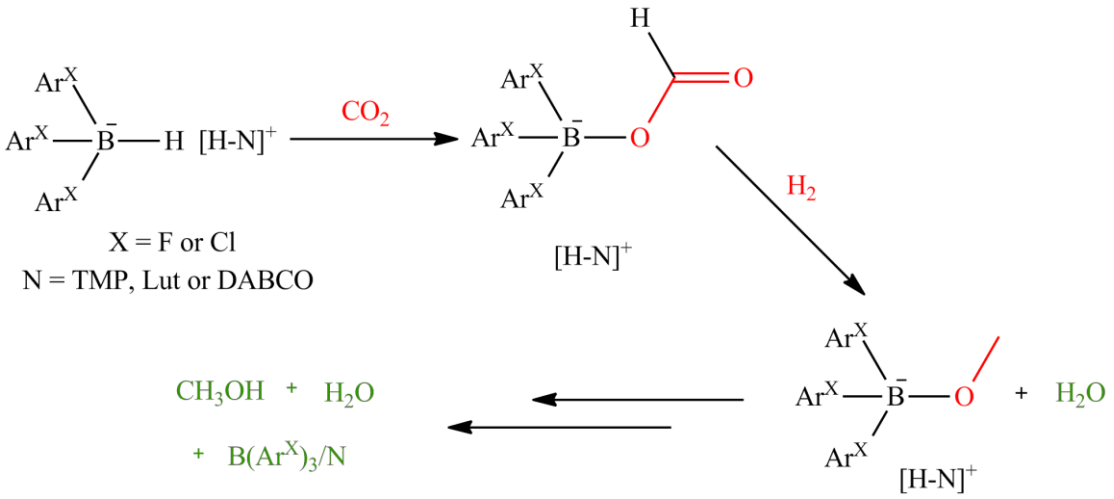
The decomposition products were identified using NMR spectroscopy.[22] Due to the decay of the Lewis acid, it was concluded that if the Lewis acid could be hydrolytically stable then the system might become catalytic, thus finding an efficient method of reducing CO_2.

In 2012, Sgro *et al.* achieved the reduction of CO_2 using a bis-borane-based FLP.[23] They successfully synthesised methanol from CO_2 with a yield of 57 % in 1 h. These

findings are extremely encouraging as this opens up alternative routes to finding a highly efficient method of catalytically reducing CO_2 to methanol.

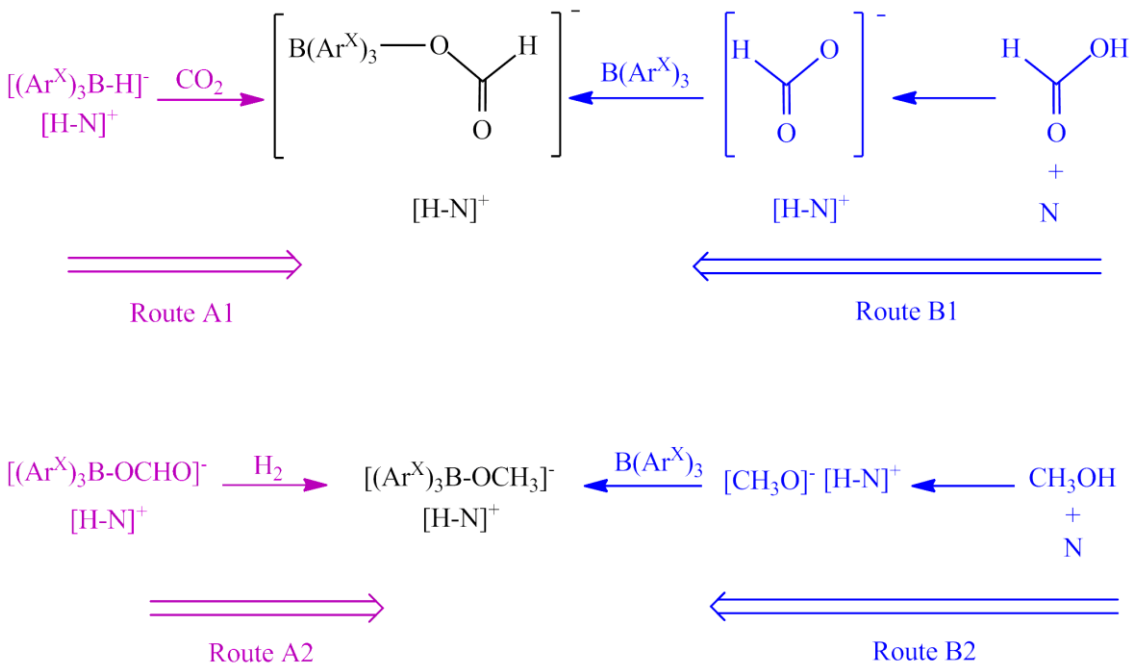
4.2 Reducing CO_2 to Methanol

The main reason that the $B(C_6F_5)_3$/TMP system was unable to catalytically reduce CO_2 to methanol was due to the decomposition of the Lewis acid. Therefore, in attempt to make a more stable Lewis acid, three novel Lewis acids were synthesised (as described in Chapter Two). These were then used to synthesise nine new FLPs, as well as the $B(C_6F_5)_3$/DABCO adduct. All of these were able to successfully split H_2 (as described in Chapter Three), which is the first step in reducing CO_2 (Scheme 4.2).



Scheme 4.2 Reduction of CO_2 using a borohydride salt.

Reducing CO_2 using a borohydride species is a convenient route to synthesising methanol, as the reactions can easily be monitored using ^{1}H, $^{11}B\{^{1}H\}$ and $^{13}C\{^{1}H\}$ NMR spectroscopy, especially when using $^{13}CO_2$. The formatoborate and the methoxyborate can also be independently synthesised using formic acid and methanol, respectively (Scheme 4.3), providing a helpful guide to where these species would appear in the NMR spectra.



Scheme 4.3 Synthetic routes to the formatoborate and the methoxyborate species, where X = F or Cl and N is DABCO, TMP or Lut.

Using route B1 (Scheme 4.3) all of the FLPs containing $B(C_6F_5)_3$, **1** and **2**, from Chapter Three, successfully reacted to give the formatoborate. Each of the salts were fully characterised using NMR spectroscopy and mass spectrometry. Synthesis of the methoxyborates via route B2 was only successful using FLPs $B(C_6F_5)_3$/DABCO, **1**/TMP and **1**/DABCO. FLPs containing **2** did not react with methanol to give the methoxyborates.

The borane **3** did react with $[CO_2H][H\text{-DABCO}]$ to give the formatoborate, which was first established by ESI^- mass spectrometry followed by full characterisation. Unfortunately, **3** did not react with $[^{13}CO_2H][H\text{-TMP}]$, $[^{13}CO_2H][H\text{-Lut}]$ or methanol. Initial analysis of the isolated products using NMR spectroscopy showed confusing results as the integrals did not correspond to what was expected and some important resonances were missing. The measured mass spectra showed that the products contained only the 'free borane' and not the formatoborates or the methoxyborates.

This limited reactivity was an early indication that these systems were too bulky to form a B-O bond and thus is unlikely to reduce CO_2. However, to make certain that this is the case, all ten of the borohydride salts were reacted with CO_2.

4.3 Reduction of $^{13}CO_2$ using $[(C_6F_5)_3B\text{-}H][H\text{-}DABCO]$

Upon addition of two equivalents of $^{13}CO_2$ to $[(C_6F_5)_3B\text{-}H][H\text{-}DABCO]$ in toluene-d_8 in a J-Young's tap NMR tube, insertion of $^{13}CO_2$ was not observed at 22 ^oC. The reaction was heated overnight at 65 ^oC resulting in insertion of the $^{13}CO_2$ into the B-H bond to give the formatoborate species, as observed in the ^1H, $^{11}B\{^1H\}$ and $^{13}C\{^1H\}$ NMR spectra (Table 4.1). Using $^{13}C\{^1H\}$ NMR spectroscopy, the relative distribution for B-O^{13}CHO:$^{13}CO_2$ was determined to be 3:7.

Table 4.1 Selected resonances from the NMR spectra for the reduction of $^{13}CO_2$ using $[(C_6F_5)_3B\text{-}H][H\text{-}DABCO]$.

Salt	δ/ppm[a]		
	^1H	**$^{13}C\{^1H\}$**	**$^{11}B\{^1H\}$**
$[(C_6F_5)_3B\text{-}H]$ $[H\text{-}DABCO]$	3.60 (br. q)	-	−25.50
$[(C_6F_5)_3B\text{-}O^{13}CHO]$ $[H\text{-}DABCO]$	8.22 (d)	170.07	−2.57
$[(C_6F_5)_3B\text{-}O^{13}CH_3]$ $[H\text{-}DABCO]$	3.53 (br. d)	50.82	2.83

[a]Solvent: toluene-d_8, $BF_3{\cdot}OEt_2$ reference (external).

With further heating at 65 ^oC for 48 h, the relative distribution changed to 1:1 for B-O^{13}CHO:$^{13}CO_2$, producing more of the formatoborate species. After 5 days, additional insertion of $^{13}CO_2$ was not observed and according to the $^{11}B\{^1H\}$ NMR spectrum, the borohydride had been completely utilised. Therefore, due to the lack of borohydride present in the system, the reaction was carried forward and H_2 was

admitted to the system to give a $^{13}CO_2/H_2$ atmosphere, in an attempt to reduce the formatoborate to the methoxyborate. Following heating at 65 ^oC for 48 h, and then at 95 ^oC for 24 h no reduction of the formatoborate was observed. Formation of the methoxyborate was finally seen in $^{13}C\{^1H\}$ NMR spectrum after heating the reaction at 100 ^oC for 48 h (Figure 4.1).

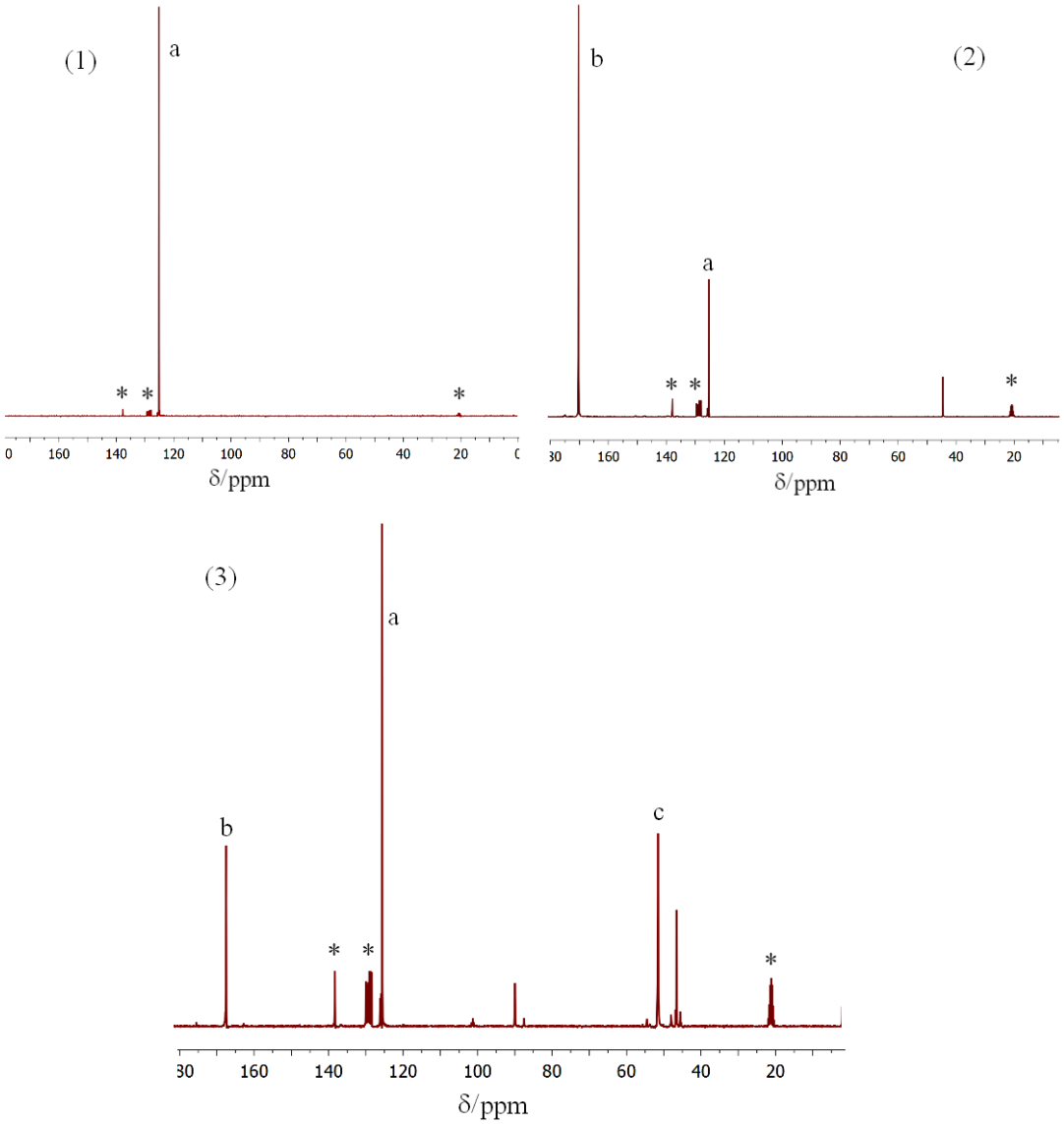


Figure 4.1 $^{13}C\{^1H\}$ NMR spectra showing (1) the addition of 'free' $^{13}CO_2$, **a** to $[(C_6F_5)_3B\text{-}H][H\text{-}DABCO]$; (2) $^{13}CO_2$ inserts into the B-H bond at 100 ^oC to produce the formatoborate species, **b**; (3) reduction of **b** with H_2 to give the methoxyborate, **c**, in toluene-d_8 (*).

Figure 4.1 shows the resonances of $^{13}CO_2$ (120 ppm), B-O^{13}CHO (170 ppm) and B-O$^{13}CH_3$ (51 ppm) in the $^{13}C\{^1H\}$ NMR spectra and how easily the reactions can be monitored. Unfortunately, with the production of the methoxyborate came the decomposition of the Lewis acid, producing $(C_6F_5)_2$B-O$^{13}CH_3$ and C_6F_5H as observed in the ^1H, $^{13}C\{^1H\}$ and ^{19}F NMR spectra as shown in Figure 4.2, which is consistent with the literature.[24] This was an early but very strong indication that the reduction of $^{13}CO_2$ would not be catalytic with this FLP system.

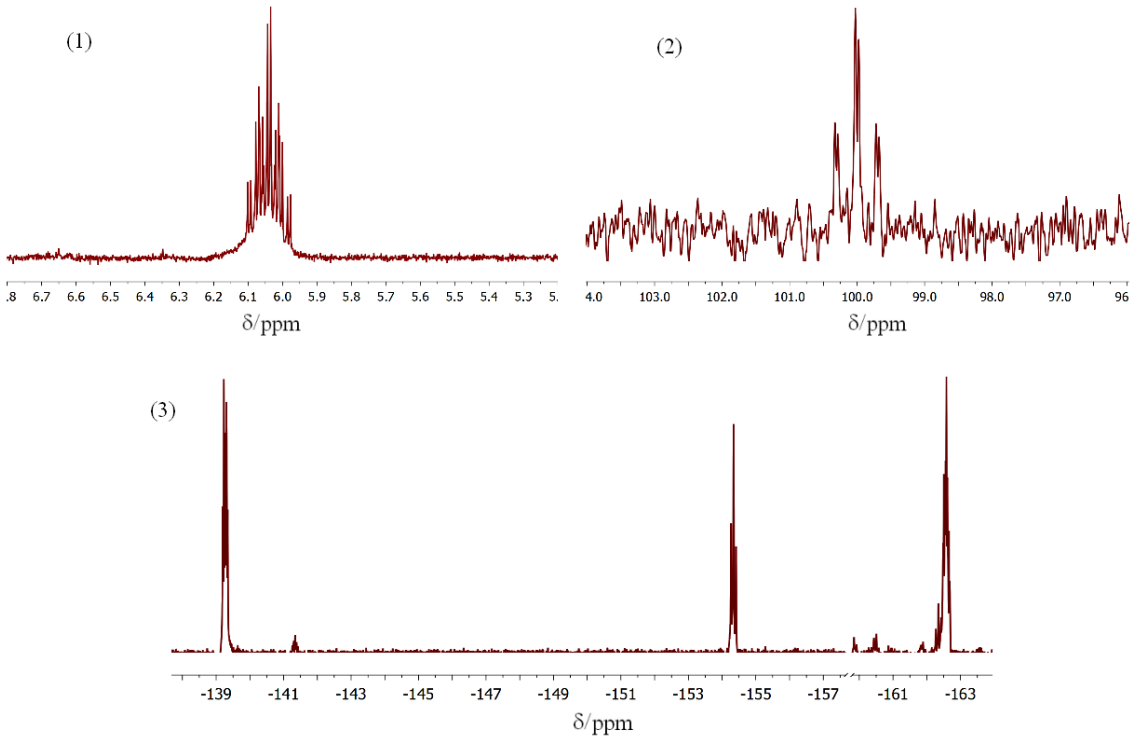


Figure 4.2 (1) ^1H, (2) $^{13}C\{^1H\}$ and (3) ^{19}F NMR spectra of the decomposition product, C_6F_5H in toluene-d_8.[24]

The reaction was heated for one more week at 130 ^oC, until no change in the reaction was seen (by ^{13}C NMR spectroscopy). The system underwent vacuum distillation at 130 ^oC, using Cp_2Fe as an internal reference, in an attempt to break the B-O bond and isolate any 'free' methanol present in the system. Analysis of the ^1H, $^{13}C\{^1H\}$ and ^{19}F NMR spectra of the distillate showed only the presence of the $^{13}CO_2$, C_6F_5H, uncoordinated DABCO and Cp_2Fe as displayed in Figure 4.3.

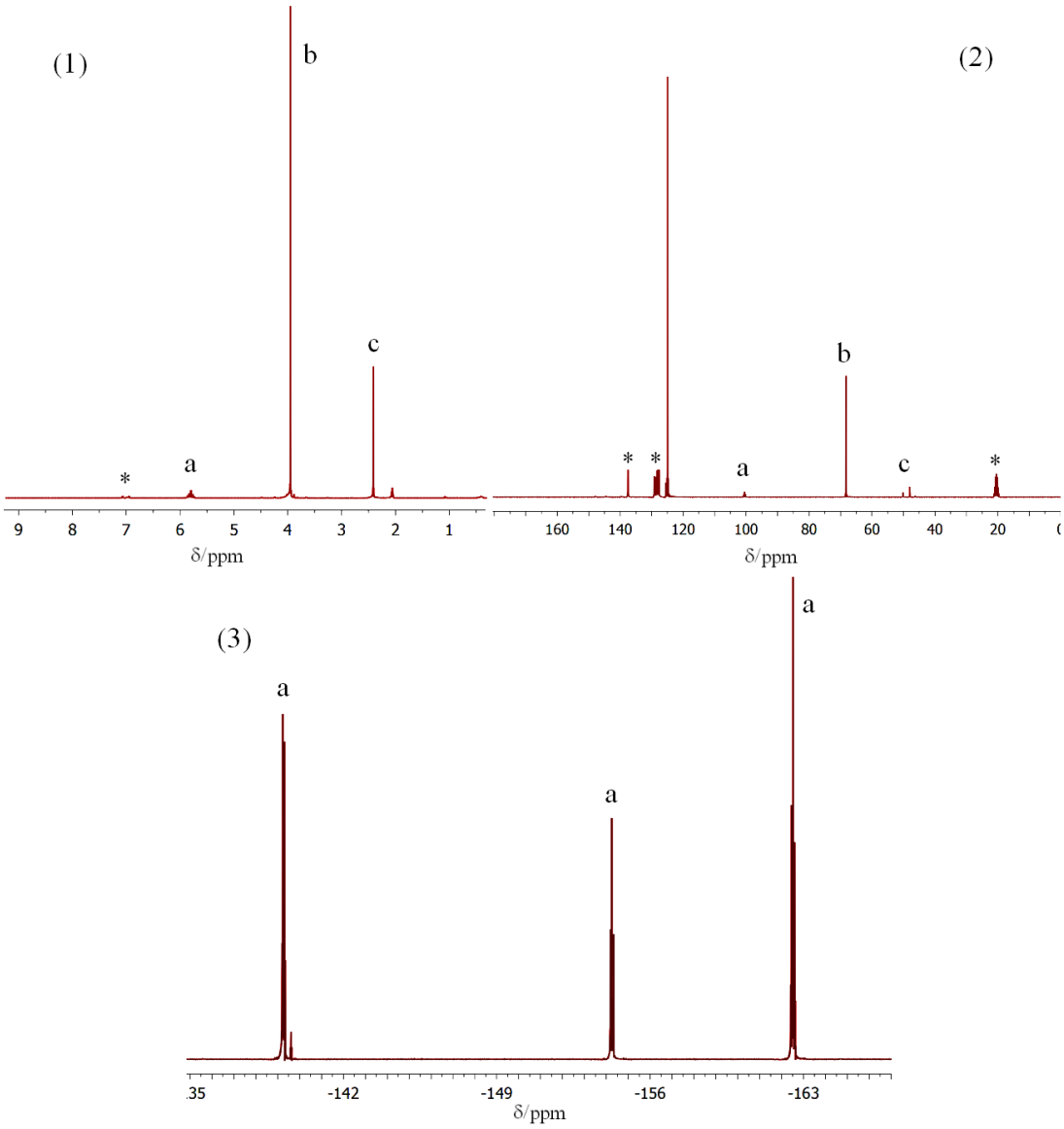


Figure 4.3 (1) ^{1}H, (2) $^{13}C\{^{1}H\}$ and (3) ^{19}F NMR spectra of the distillate from the reduction of $^{13}CO_2$ using $[(C_6F_5)_3B\text{-}H][H\text{-}DABCO]$ reaction showing C_6F_5H, **a** Cp_2Fe, **b** and uncoordinated DABCO, **c** in toluene-d_8 (*).

Examination of the residue by NMR spectroscopy and mass spectrometry revealed the remaining $B(C_6F_5)_3$ complexes; $[(C_6F_5)_3B\text{-}H]^-$, $[(C_6F_5)_3B\text{-}OCHO]^-$ and $[(C_6F_5)_3B\text{-}OMe]^-$. The adduct $B(C_6F_5)_3$/DABCO behaved in a similar way to $B(C_6F_5)_3$/TMP, successfully reducing CO_2 to the methoxyborate species.[22] However, unlike with $B(C_6F_5)_3$/TMP, methanol was not isolated from this FLP system.

4.4 Attempts to Reduce CO_2 to Methanol using [1-H][H-N]

As seen in Chapter Three, all FLPs containing **1** successfully split H_2. Therefore all three systems ([**1**-H][H-DABCO], [**1**-H][H-TMP] and [**1**-H][H-Lut]) were taken further and used to reduce CO_2 to the formatoborate. Addition of one equivalent of $^{13}CO_2$ to all three borohydride salts resulted in the production of the formatoborate species, as observed with new resonances in the ^{1}H, $^{11}B\{^{1}H\}$ and $^{13}C\{^{1}H\}$ NMR spectra (Table 4.2). Analysis of the ^{19}F NMR spectra showed similar resonances to that of the borohydride species.

Table 4.2 Selected resonances from the NMR spectra for the reduction of $^{13}CO_2$ using [**1**-H][H-N].

Formatoborate Species	**δ/ppm**		
	^{1}H	**$^{13}C\{^{1}H\}$**	**$^{11}B\{^{1}H\}$**
[**1**OCHO][HDABCO][a]	8.01	160.44	2.84
[**1**OCHO][HTMP][b]	8.19	169.63	0.69
[**1**OCHO][HLut][b]	8.24	170.93	1.82

[a]Solvent: THF-d_8, $BF_3{\cdot}OEt_2$ reference (external). [b]Solvent: toluene-d_8, $BF_3{\cdot}OEt_2$ reference (external).

The yield of the formatoborate and the reaction conditions for reduction of $^{13}CO_2$ vary with each borohydride salt.

4.4.1 [1-H][H-DABCO]

Due to the low solubility of [**1**-H][H-DABCO], the reduction of $^{13}CO_2$ was carried out in THF-d_8 in a J-Young NMR tube at 22 ^{o}C over two days. The progress of the reaction was monitored using $^{13}C\{^{1}H\}$ NMR spectroscopy. As the B-O^{13}CHO species was not observed at 22 ^{o}C, the system was heated at 60 ^{o}C for 18 h, however the

formate was still not observed. The reaction was heated further at 125 ^{o}C for 48 h, which yielded a colourless precipitate and the first evidence of the formatoborate species in the ^{1}H, ^{11}B{^{1}H} and ^{13}C{^{1}H} NMR spectra. The development of the colourless precipitate coincided with observations in the NMR spectra suggesting that [**1**-OCHO][H-DABCO] has low solubility in THF and reaches an equilibrium. To push this equilibrium to produce more [**1**-OCHO][H-DABCO], the reaction was heated for one week at 145 ^{o}C. A great deal of decomposition was observed in the ^{1}H and ^{19}F NMR spectra, with the formation of both C_6Cl_5H and C_6F_5H, with resonances at 7.90 ppm and 7.16 ppm, respectively in the ^{1}H NMR spectrum. As decomposition of the Lewis acid had already been observed at this early stage, it was concluded that despite reducing CO_2 to the formatoborate, the system could not operate catalytically.

H_2 was admitted to the system to give a $^{13}CO_2/H_2$ atmosphere in an attempt to reduce the formatoborate to the methoxyborate and to push the equilibrium further. After 24 h at 145 ^{o}C, the methoxyborate was observed in the ^{13}C{^{1}H} NMR spectrum, with a resonance at 54.27 ppm. The reaction was heated for a further 48 h at 145 ^{o}C, and growth of the resonance at 54.27 ppm was observed with the development of additional resonances due to decomposition products. The reaction was heated for one week, until no more change was observed in the NMR spectra. In an attempt to determine if 'free' methanol was present in the system, it underwent trap-to-trap distillation at 145 ^{o}C. Analysis of the NMR spectra of the distillate showed only the presence of THF-d_8 and $^{13}CO_2$ as presented in Figure 4.4 (1). Whereas, Figure 4.4 (2) shows the presence of various decomposition products as well as B-O$^{13}CH_3$ and DABCO.

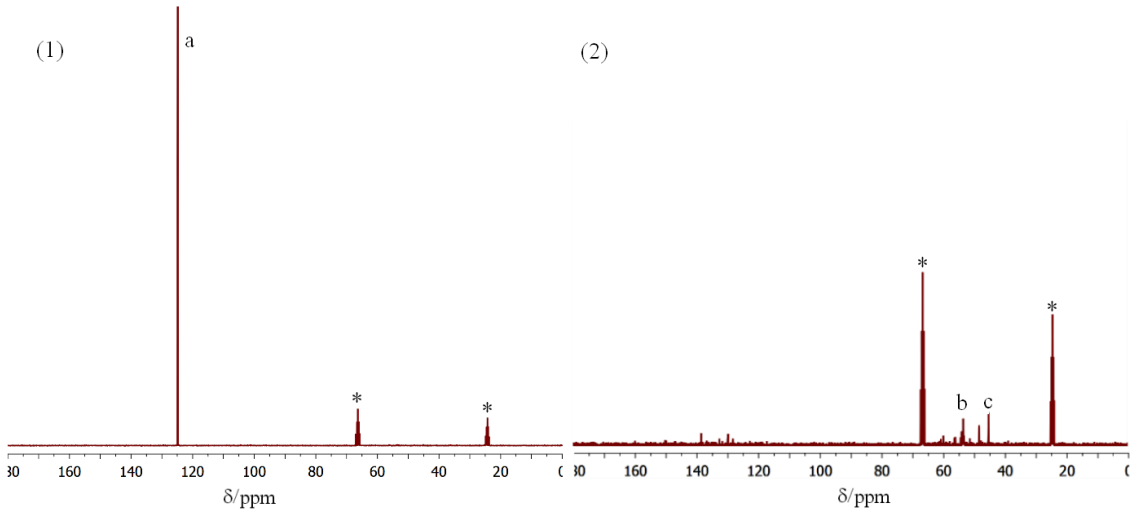


Figure 4.4 $^{13}C\{^1H\}$ NMR spectra of (1) the distillate and (2) the residue from the trap-to-trap distillation of the [**1**][DABCO] system, showing $^{13}CO_2$, **a**, B-O$^{13}CH_3$, **b**, and DABCO, **c**, in THF-d_8 (*).

Full analysis of the ^1H and $^{11}B\{^1H\}$ NMR spectra and mass spectrum of the residue showed that the major species was [**1**-H][H-DABCO] with much smaller amounts of [**1**-OCHO][H-DABCO], [**1**-OMe][H-DABCO] and the decomposition products C_6Cl_5H and C_6F_5H. It is not surprising that the majority of the residue consisted of the [**1**-H][H-DABCO] as the insertion reaction of $^{13}CO_2$ did not progress as far as observed with $[(C_6F_5)_3B\text{-}H][H\text{-}DABCO]$.

4.4.2 [1-H][H-Lut]

Unlike the [**1**-H][H-DABCO] system the [**1**-H][H-Lut], was found to release H_2 when heated above 70 ^oC. Therefore, the reduction of $^{13}CO_2$ using the [**1**-H][H-Lut] system was limited to temperatures below 70 ^oC. Initially, the [**1**-H][H-Lut] was heated at 65 ^oC with one equivalent of $^{13}CO_2$ in toluene-d_8 for 24 h. Preliminary observations showed the presence of the formatoborate species in the ^1H, $^{11}B\{^1H\}$ and $^{13}C\{^1H\}$ NMR spectra. The reaction was continued at 65 ^oC for 72 h under the assumption that the reaction would proceed further. However, monitoring of the reaction using $^{13}C\{^1H\}$

NMR spectroscopy showed that $^{13}CO_2$ was released back into the system upon sustained heating. Therefore it was decided to leave the reaction at 22 ^{o}C for 24 h and then determine the outcome of the reaction using NMR spectroscopy. As the formatoborate resonance grew, the $^{13}CO_2$ resonance decreased in the $^{13}C\{^{1}H\}$ NMR spectrum as illustrated in Figure 4.5.

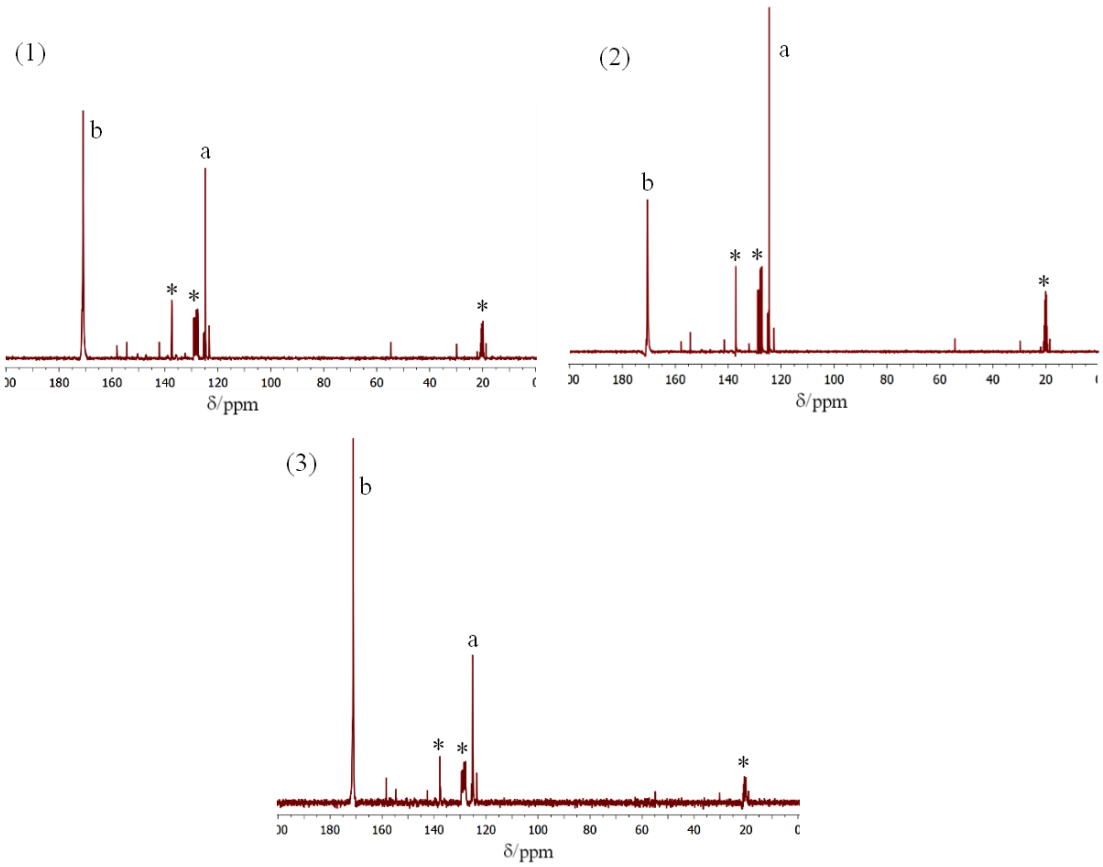


Figure 4.5 $^{13}C\{^{1}H\}$ NMR spectra showing the reduction of $^{13}CO_2$ using [**1**-H][H-Lut] to give the (1) formatoborate, **b**, after 24 h at 65 ^{o}C, (2) 72 h at 65 ^{o}C and (3) 24 h at 22 ^{o}C in toluene-d_8 (*).

The system was left at 22 ^{o}C for a further 24 h to allow the reaction to proceed further. However, after recording the $^{13}C\{^{1}H\}$ NMR spectrum of the reaction, more $^{13}CO_2$ was observed, which suggests that the reaction is in equilibrium (Figure 4.6).

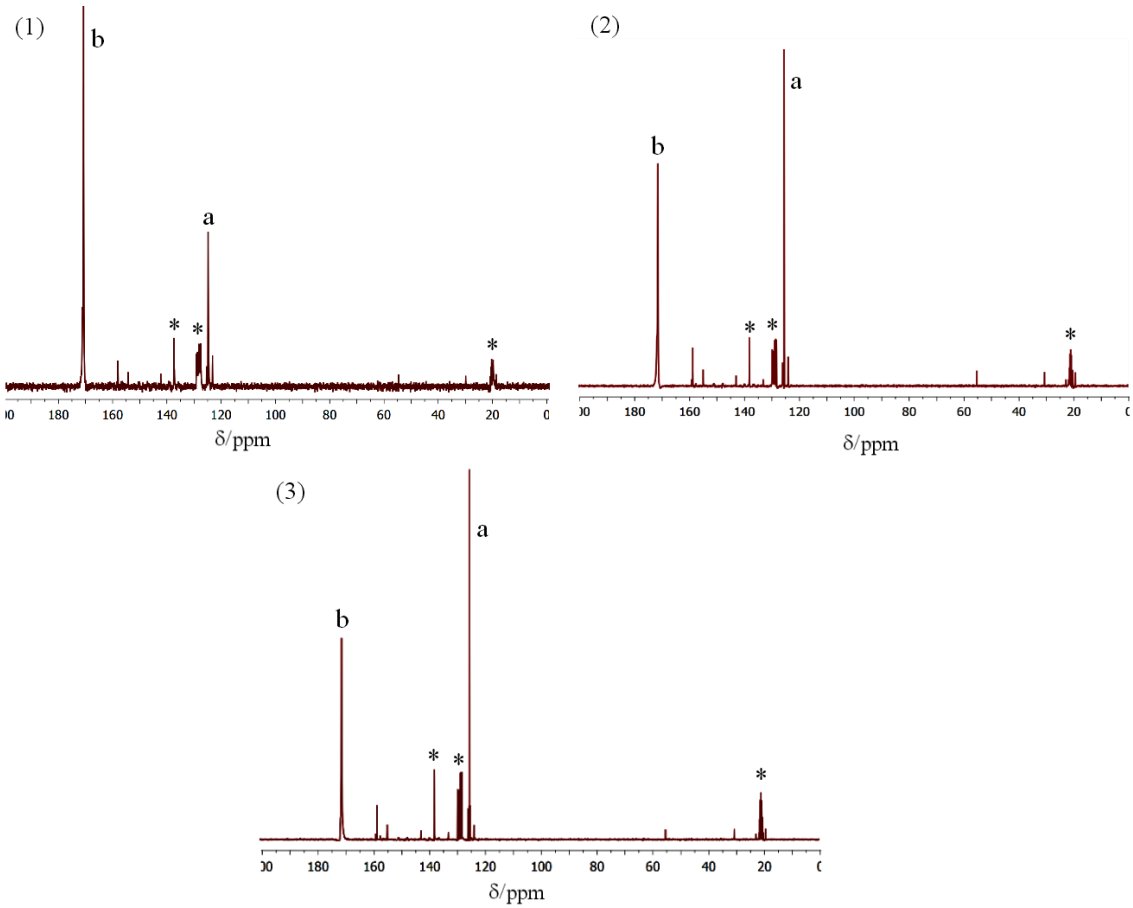


Figure 4.6 $^{13}C\{^{1}H\}$ NMR spectra showing the equilibrium between $^{13}CO_2$, **a**, and [**1**-OCHO][H-Lut], **b**, (1) after 24 h at 22 ^{o}C, (2) 48 h at 22 ^{o}C and (3) 72 h at 22 ^{o}C in toluene-d_8 (*).

As the salt [**1**-OCHO][H-Lut] exists at equilibrium with higher temperatures favouring the borohydride, it was concluded that any attempts to force the equilibrium by heating risked breaking the B-H bond and releasing H_2 to give the 'free' FLP. Therefore H_2 was added to the system give a $^{13}CO_2/H_2$ atmosphere. However, no reaction was observed after 16 h at both 22 ^{o}C and 65 ^{o}C. Heating at 125 ^{o}C in an attempt to push the formation of the methoxyborate and sacrifice any [**1**-H][H-Lut] still within the system. Overnight the reaction turned from a colourless solution to an orange/pink solution, consistent with the observation in Chapter Three, where H_2 is released from [**1**-H][H-Lut]. Analysis using NMR spectroscopy confirmed the presence

of the 'free' FLP along with products from the decomposition of the borane. The $^{13}C\{^1H\}$ NMR spectrum showed the loss of the formatoborate resonance (Figure 4.7).

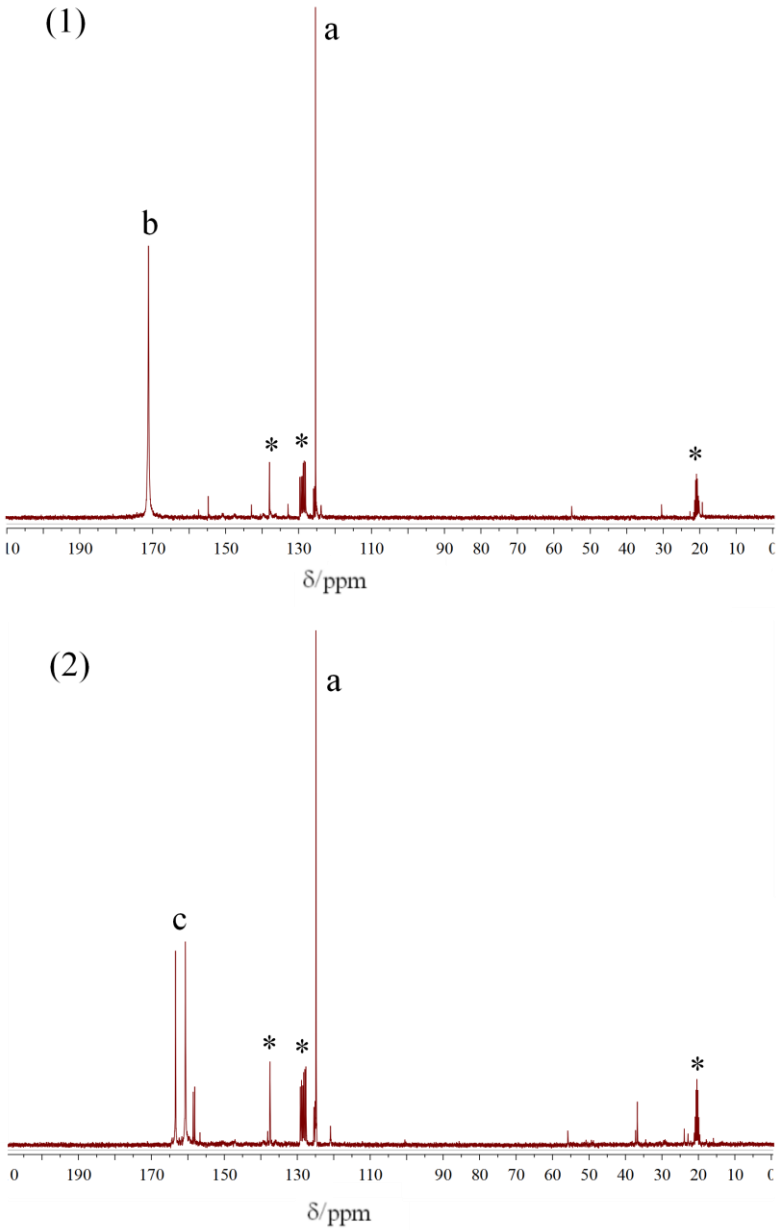
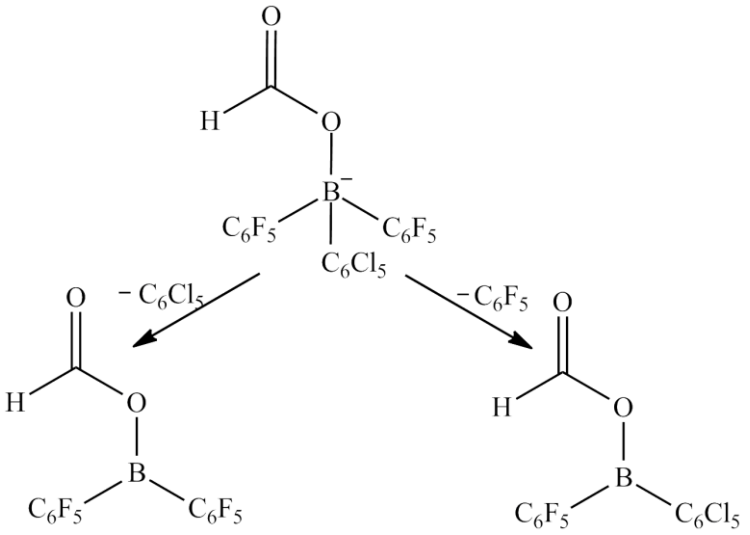


Figure 4.7 $^{13}C\{^1H\}$ NMR spectra displaying $^{13}CO_2$, **a**, and [**1**-OCHO][H-Lut], **b**, (1) after 24 h at 65 ^oC under $^{13}CO_2/H_2$ atmosphere, (2) 24 h at 125 ^oC showing the decomposition products, **c** in toluene-d_8 (*).

Figure 4.7 displays the complete loss of the formatoborate resonance at 170 ppm and the development of two new resonances at 163.14 ppm and 161.54 ppm, suggesting the decomposition products contained a C=O group. The complimentary $^{11}B\{^1H\}$ NMR

spectrum showed a resonance at 21.88 ppm suggesting the decomposition products consist of a three-coordinate formatoborate species via the loss of either a C_6F_5 or C_6Cl_5 group (Scheme 4.4).



Scheme 4.4 Decomposition routes of [**1**-O^{13}CHO][H-Lut] via loss of C_6Cl_5 or C_6F_5.

As there was no evidence in the NMR spectra for the reduction of the formatoborate to the methoxyborate and any further heating would have yielded more of the 'free' FLP and H_2, the reaction was terminated. Full analysis using ESI$^-$ mass spectrometry showed evidence of borohydride, hydroborate and methoxyborate species (Figure 4.8). This was surprising given their complete absence in the NMR studies.

Unfortunately due to the 'messy' ESI$^+$ mass spectrum, the decomposition products cannot be confirmed.

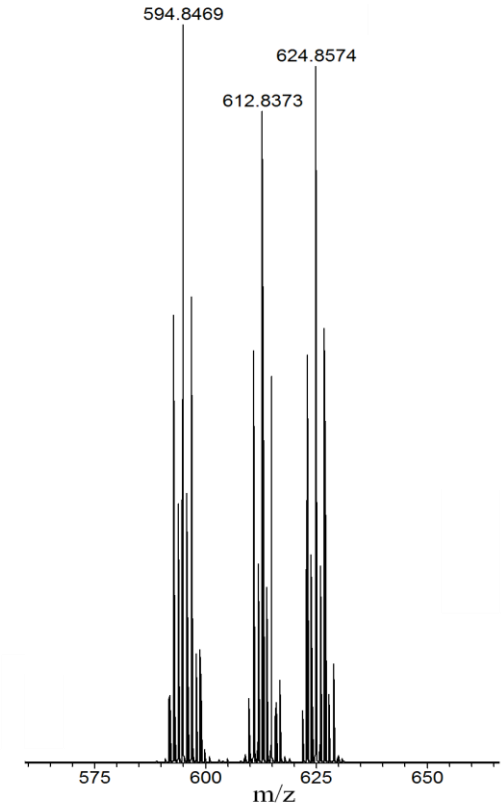


Figure 4.8 Select ESI¯ mass spectrum of the residue from the reduction of $^{13}CO_2$ using [**1**-H][H-Lut] displaying three species; [**1**-H][H-Lut] (594.8469), [**1**-OH][H-Lut] (612.8373), [**1**-OCH_3][H-Lut] (624.8574).

4.4.3 [1-H][H-TMP]

The [**1**-H][H-TMP] behaved in a similar way to [**1**-H][H-Lut], showing the ability to insert $^{13}CO_2$ at 22 ^{o}C with immediate precipitation of a colourless solid. However, unlike the Lut system, [**1**-H][H-TMP] does not release H_2 when heated (this was tested up to 160 ^{o}C in a closed system). The vast majority of 'free' $^{13}CO_2$ was consumed to give the formatoborate species after reacting for 24 h at 22 ^{o}C as observed in the $^{11}B\{^{1}H\}$ and $^{13}C\{^{1}H\}$ NMR spectra displayed in Figure 4.9 (1).

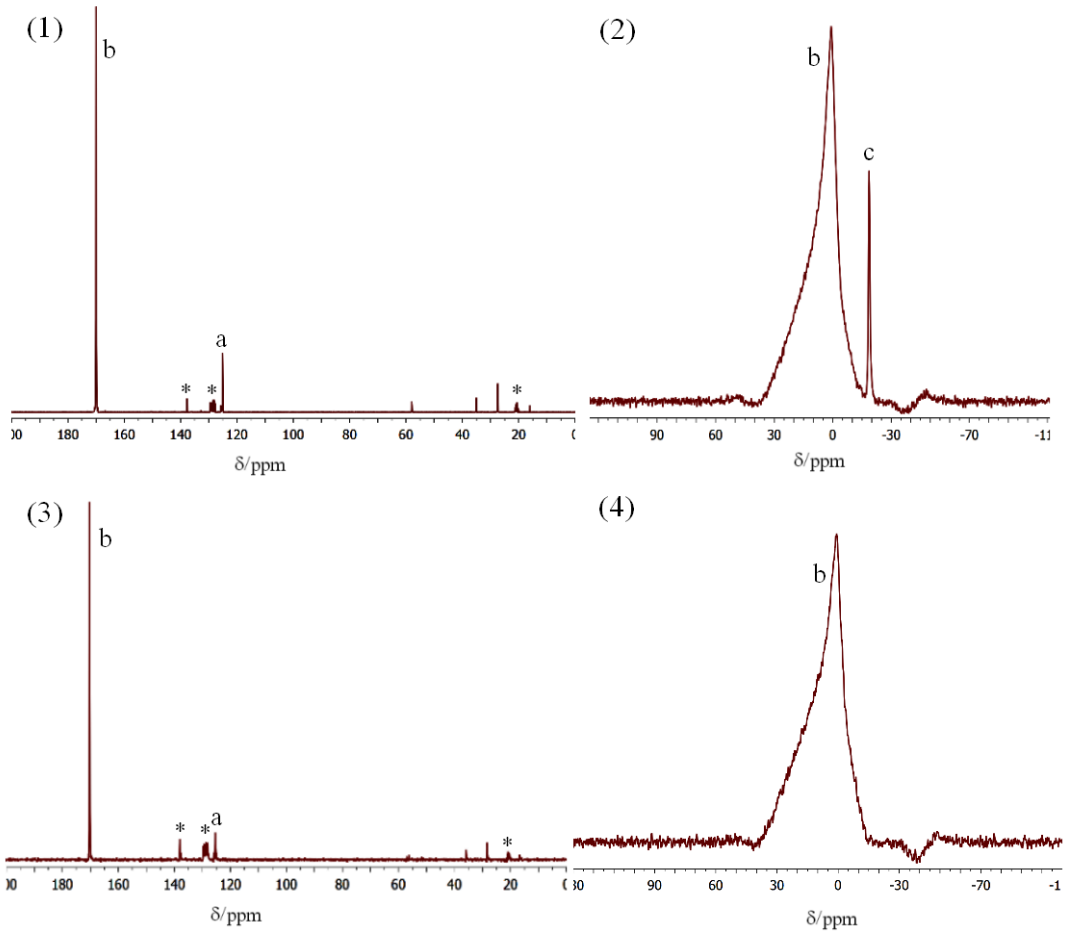


Figure 4.9 (1) $^{13}C\{^{1}H\}$ and (2) $^{11}B\{^{1}H\}$ spectra show the reduction of $^{13}CO_2$, **a**, and the production of [**1**-OCHO][H-TMP], **b**, after 24 h at 22 ^{o}C. (3) $^{13}C\{^{1}H\}$ and (4) $^{11}B\{^{1}H\}$ NMR spectra show the full consumption after 7 days at 120 ^{o}C of the borohydride, **c**, >95% consumption of $^{13}CO_2$ to produce the [**1**-OCHO][H-TMP], **b**, in toluene-d_8 (*).

Efforts to force the equilibrium in favour of the formatoborate required heating the reaction at 120 ^{o}C for 7 days. This resulted in stoichiometric conversion of the borohydride to the formatoborate, as shown in Figure 4.9 (3 and 4). Attempts to further reduce the formatoborate to the methoxyborate were made by admitting H_2 to the system. After 24 h at 22 ^{o}C, a large amount of colourless precipitate was found in the NMR tube. As the formatoborate salt was soluble in toluene-d_8, this gave hope that the methoxyborate had been synthesised. The solvent was removed under vacuum and replaced with THF-d_8 and further analysis showed that only the formatoborate salt was present and none had been reduced to the methoxyborate. Thus admission of H_2 could

have facilitated the precipitation of the formatoborate. The reaction was heated at 60 ^{o}C overnight and the first signs of the methoxyborate were observed in the $^{13}C\{^{1}H\}$ NMR spectrum. Upon increasing the temperature to 120 ^{o}C and heating for 16 h, $^{13}CO_2$ was released from the [**1**-OCHO][H-TMP] system giving back the 'free' $^{13}CO_2$ and the borohydride salt. Therefore, the reduction of $^{13}CO_2$ is reversible at 120 ^{o}C, which requires higher temperatures than [$(C_6F_5)_3$B-OCHO][H-TMP] (releases CO_2 at 80 ^{o}C),[22] which suggests the B-O is stronger in [**1**-OCHO][H-TMP].

Repeating the reaction using the formatoborate species formed via route B1 (Scheme 4.3), [**1**-O^{13}CHO][H-TMP] at 135 ^{o}C showed the subsequent reduction as witnessed by the formation of the methoxyborate. However, a three-coordinate methoxyborate was observed instead of four-coordinate species with either concomitant observations of C_6Cl_5H or C_6F_5H in the ^{1}H and ^{19}F NMR spectra, consistent with heating other FLP systems. The relative intensities for C_6F_5H and C_6Cl_5H were found to be 1:3, reflecting the differences in stability, observed previously in the decomposition experiment of **1**.H_2O (Chapter Two). The reaction was monitored every 2 h until the concentration of methoxyborate in $^{13}C\{^{1}H\}$ NMR studies equilibrated at a final relative distribution of $^{13}CO_2$ to B-O$^{13}CH_3$ of 7:13. Unfortunately, $^{13}CH_3OH$ could not be detected. This could be due to the experiment being performed in a closed system and the formation may have been inhibited which forces the decomposition, despite dissociation occurring. Attempts to force the conversion by suspending 4 Å molecular sieves (both a CH_3OH and H_2O scavenger)[25] above the reaction medium using a glass wool plug as support, led to no change as it was found that the sieves also scavenged $^{13}CO_2$.

4.4.3.1 Single X-ray Crystal Structure of [1-OCHO][H-TMP]

A colourless solid precipitated immediately upon addition of CO_2 to [**1**-H][H-TMP], suggests facile insertion at ambient temperature. The reaction was stored at 22 ^{o}C under an atmosphere of CO_2 for 7 days, which gave colourless X-ray quality single crystals. Analysis of the crystal structure displayed a four-coordinate boron atom which adopts a pseudo-tetrahedral coordination geometry as seen from the C-B-O and C-B-C angle ranges as illustrated in Figure 4.10 and Table 4.4. These observations are consistent with the ^{19}F and ^{11}B{^{1}H} NMR spectra of the [**1**-OCHO][H-TMP] discussed earlier.

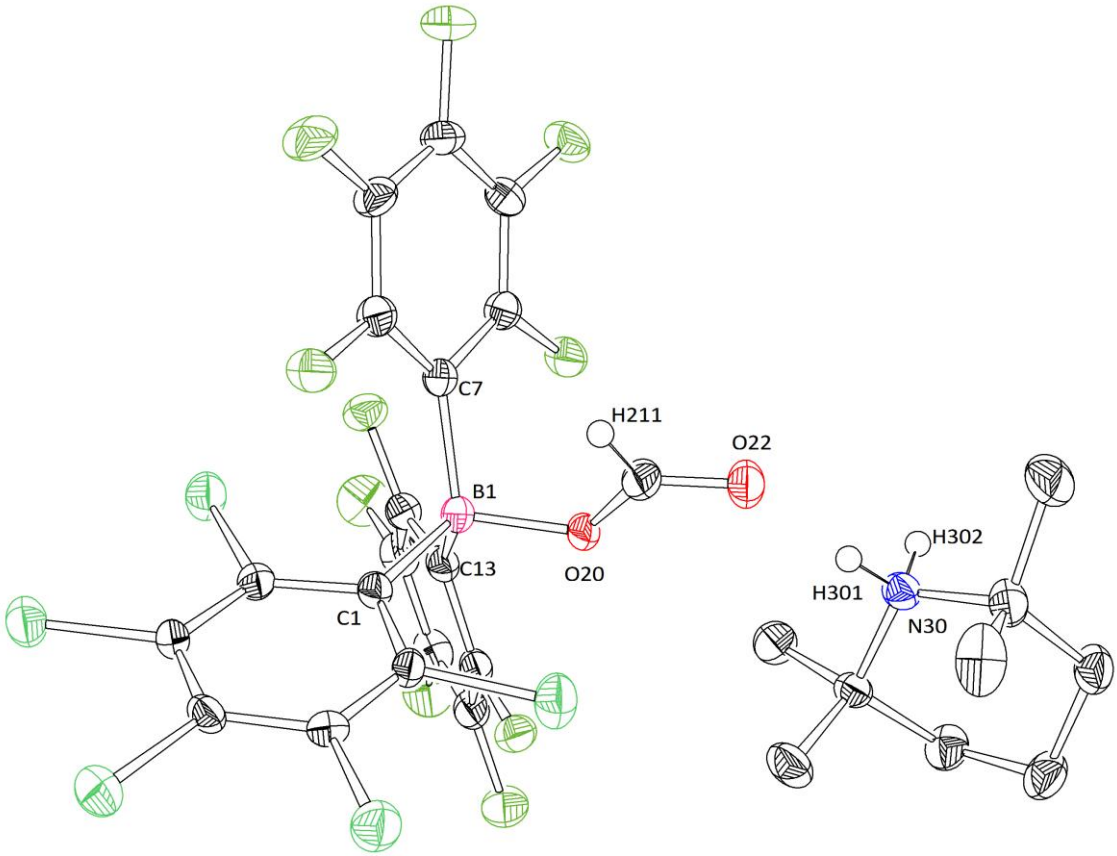


Figure 4.10 Crystal structure of [**1**-OCHO][H-TMP]. Thermal ellipsoids at 50% probability (B atom spicy pink, C atoms black, Cl atoms dark green, F atoms light green, N atoms blue, O atoms red). H atoms are omitted for clarity, except for those bound to C21 and N30. Disordered toluene molecule in asymmetric unit removed for clarity.

Table 4.3 Selected bond lengths/distances for [**1**-OCHO][H-TMP] and $[(C_6F_5)_3B\text{-OCHO}][H\text{-TMP}]$.[22]

Atom 1	**Atom 2**	**Bond Lengths/Distances (Å)**	
		[1-OCHO][H-TMP]	**$[(C_6F_5)_3B\text{-OCHO}][H\text{-TMP}]$[22]**
H301	O22	1.889	2.04
B1	O20	1.533(3)	1.546(3)
B1	C1	1.667(3)	1.645(4)
B1	C7	1.656(3)	1.639(4)
B1	C13	1.648(3)	1.648(4)
C21	O20	1.295(3)	1.288(3)
C21	O22	1.218(3)	1.236(3)
C21	H211	0.935	0.986
N30	H301	0.877	0.931

Table 4.4 Selected bond angles for for [**1**-OCHO][H-TMP] and $[(C_6F_5)_3B\text{-OCHO}][H\text{-TMP}]$.[22]

Atom 1	**Atom 2**	**Atom 3**	**Bond Angles/^{o}**	
			[1-OCHO][H-TMP]	**$[(C_6F_5)_3B\text{-OCHO}][H\text{-TMP}]$[22]**
C(1)	B(1)	C(7)	113.54(17)	113.5(2)
C(1)	B(1)	C(13)	107.79(17)	112.4(2)
C(7)	B(1)	C(13)	115.21(18)	110.8(2)
C(1)	B(1)	O(20)	113.72(17)	104.1(2)
C(7)	B(1)	O(20)	104.21(16)	111.6(2)
C(13)	B(1)	O(20)	101.90(16)	104.0(2)

[**1**-OCHO][H-TMP] is analogous to $[(C_6F_5)_3B\text{-OCHO}][H\text{-TMP}]$[22] and $[(C_6F_5)_3B\text{-OCHO}][H\text{-Lut}]$,[21] which show a hydrogen bond distance (N-H···O) of 2.04 and 1.90 Å, respectively. Whereas, [**1**-OCHO][H-TMP] shows a hydrogen bond distance (N-H···O) of 1.889 Å as demonstrated in Figure 4.10 and Table 4.3. This closer packing of ions is surprising as **1** is bulkier than $B(C_6F_5)_3$, so one would expect the N-H···O to be longer. When comparing the equivalent bond lengths of [**1**-OCHO][H-TMP] with $[(C_6F_5)_3B\text{-OCHO}][H\text{-TMP}]$ (Table 4.3) it can be seen that the B–O bond is shorter in [**1**-OCHO][H-TMP] as well as the C=O bond, supporting the idea that the boron centre in **1** is more electron deficient than $B(C_6F_5)_3$. An increase in the B-C bond lengths is observed in [**1**-OCHO][H-TMP], which is understandable due to the increase of steric bulk on the aryl groups. Overall the greatest difference is seen

in the intermolecular hydrogen bond, which is much shorter and thus stronger in [**1**-OCHO][H-TMP] than in [$(C_6F_5)_3$B-OCHO][HTMP]. The range of C-F lengths of [$(C_6F_5)_3$B-OCHO][HTMP] (1.345(4)-1.357(3) Å) are all similar to [**1**-OCHO][H-TMP] (1.346(2)-1.353(2) Å).

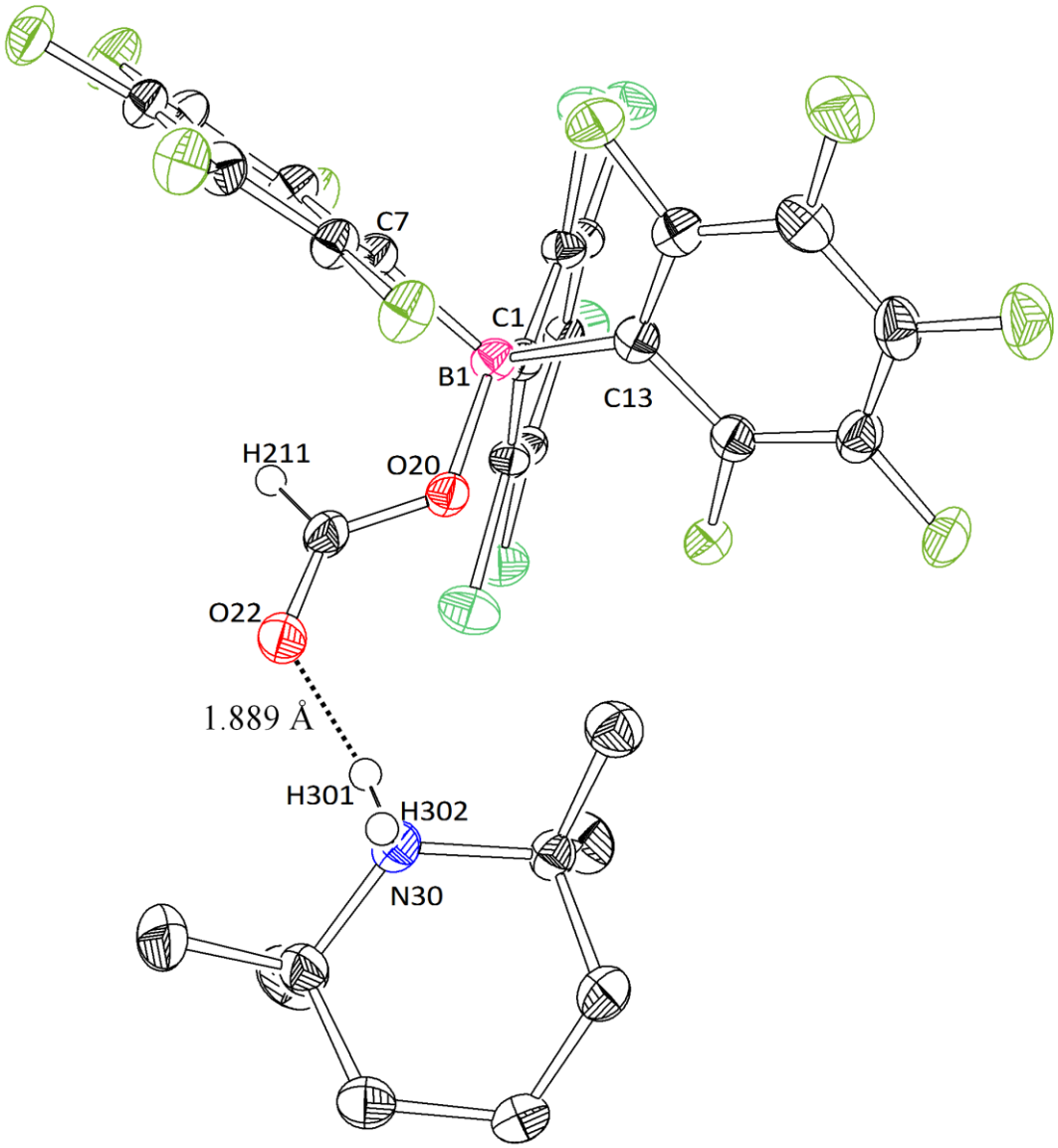


Figure 4.11 Crystal **s**tructure of [**1**-OCHO][H-TMP] showing the N-H···O distance of 1.889 Å. Thermal ellipsoids at 50% probability (B atom spicy pink, C atoms black, Cl atoms dark green, F atoms light green, N atoms blue, O atoms red). H atoms are omitted for clarity, except for those bound to C21 and N30. Disordered toluene molecule in asymmetric unit removed for clarity.

4.5 Reduction of CO_2 Using [2-H][H-N]

All FLPs containing **2** successfully split H_2, as shown in Chapter Three. Therefore CO_2 reduction was attempted with all three systems ([**2**-H][H-DABCO], [**2**-H][H-TMP] and [**2**-H][H-Lut]). The formatoborate was successfully formed by the addition of 1 atm of $^{13}CO_2$ to all three borohydride salts, as observed with new resonances in the ^{1}H, $^{11}B\{^{1}H\}$ and $^{13}C\{^{1}H\}$ NMR spectra (Table 4.5).

Table 4.5 Selected resonances from the NMR spectra for the reduction of $^{13}CO_2$ using [**2**-H][H-N].

Formatoborate Species	**δ/ppm**		
	^{1}H	**^{13}C**	**$^{11}B\{^{1}H\}$**
[**2**-OCHO][H-DABCO][a]	8.14 (dm)	165.62	0.67
[**2**-OCHO][H-TMP][b]	7.92 (dm)	165.26	−0.61
[**2**-OCHO][H-Lut][b]	7.96 (dm)	170.24	2.66

[a]Solvent: CD_3CN, $BF_3.OEt_2$ reference (external).

Analysis of these salts by ^{19}F NMR spectroscopy revealed two different *ortho* F-environments. Furthermore the ^{1}H NMR spectra for the B-OC*H*O proton appears as a doublet of doublets (approximately $^{1}J_{CH}$ = 208 Hz and J_{HF} = 8 Hz) showing long-range coupling to F on the C_6F_5 ring (Figure 4.12).[26]

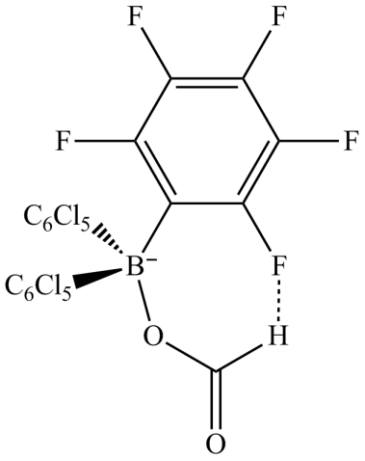


Figure 4.12 Proposed coupling of *ortho*-F in [**2**-OCHO]$^-$.

4.5.1 [2-H][H-DABCO]

As with [**1**-H][H-DABCO], it was found that [**2**-H][H-DABCO] had modest solubility in toluene-d_8, therefore THF-d_8 was used for NMR reactions. One equivalent of $^{13}CO_2$ was admitted to a J-Young NMR tube containing the borohydride solution, and the system was left at 22 ^oC for 24 h (which saw no reaction) and then heated at 95 ^oC for another 18 h. A new resonance at 2.52 ppm ($^{11}B\{^1H\}$), which could be indicative of insertion of $^{13}CO_2$ appeared. However, neither the ^1H nor the $^{13}C\{^1H\}$ NMR spectra showed any evidence of the formatoborate. Examination of the ^{19}F NMR spectrum displayed decomposition in the form of C_6F_5H, as previously observed with the $B(C_6F_5)_3$ and **1** systems.

The temperature was increased to 130 ^oC, in an attempt to force the insertion, and after 24 h showed precipitation of a colourless solid in the NMR tube; possibly the formatoborate as the amount of borohydride in system had decreased. Unfortunately, the ^1H NMR spectrum showed the presence of more decomposition in the form of both C_6F_5H and C_6Cl_5H.[24] This decomposition indicates that this [**2**-H][H-DABCO] is unstable and the system is unlikely to be catalytic. Continued heating at 140 ^oC for 5

days with regular monitoring by NMR spectroscopy, revealed an equilibrium had been reached with no apparent change in the concentration of the species of interest. The reaction was placed under a $^{13}CO_2/H_2$ atmosphere and heated at 140 ^{o}C for 24 h. Initial analysis of the ^{13}C NMR spectrum showed the first signs of the methoxyborate at 54 ppm. It is likely this is formed once the precipitate of the formatoborate is dissolved by heating at 140 ^{o}C.

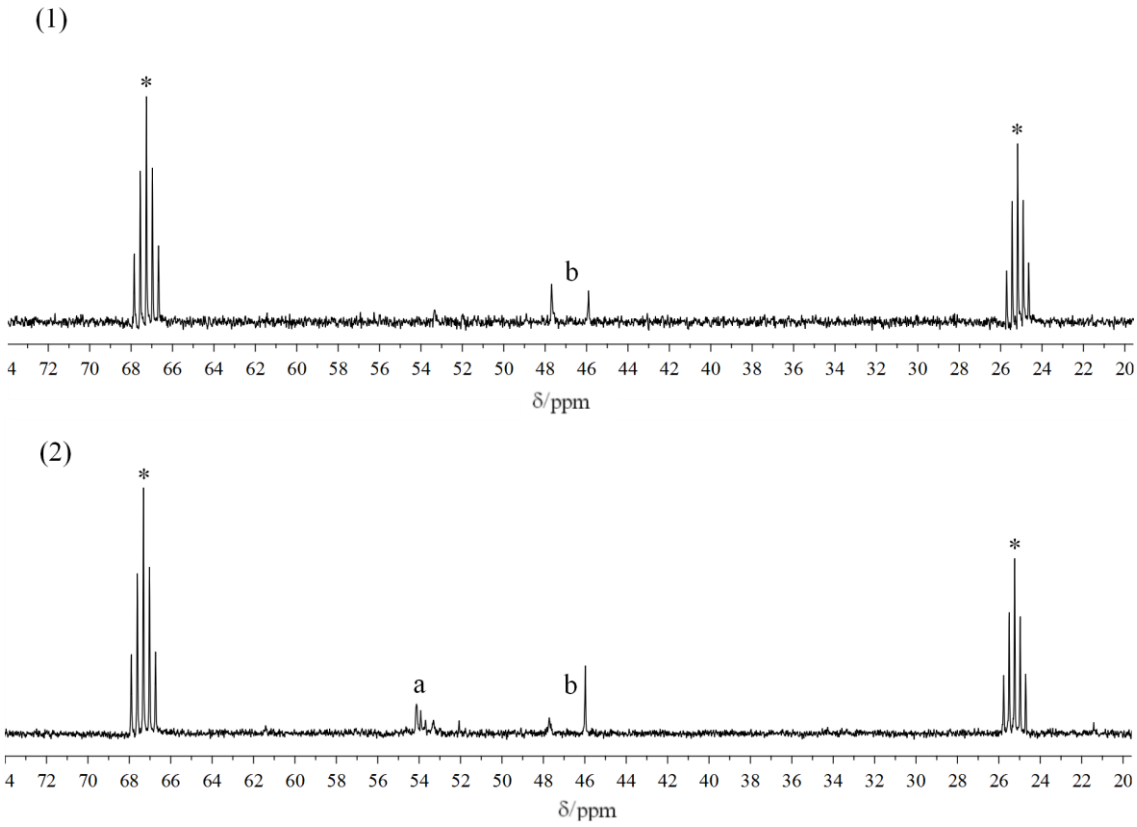


Figure 4.13 $^{13}C\{^{1}H\}$ NMR spectra from the [**2**-H][H-DABCO]/$^{13}CO_2$ reaction (1) before H_2 was added and (2) after heating at 140 ^{o}C, under a $^{13}CO_2/H_2$ atmosphere showing the methoxyborate, **a** and DABCO, **b** in THF-d_8 (*).

After 2 weeks of further heating the reaction at 140 ^{o}C, no significant change was observed in the NMR spectra, with both the borohydride and $^{13}CO_2$ present in large amounts in the system. The insolubility of the formatoborate in THF-d_8 made it very difficult to determine the percentage of $^{13}CO_2$ that was converted to the formatoborate. Therefore it was concluded that neither the insertion nor the subsequent reduction goes

to completion. Both the ^{1}H and ^{13}C NMR spectra show strong indications that methoxyborate decomposition products had been synthesised. The system was distilled under vacuum at 140 ^{o}C to irrefutably determine whether or not methanol had been formed.

Upon distillation, it was observed that some of the borohydride was transferred as well as the solution. Analysis of the distillate showed that as well as the borohydride, C_6Cl_5H and C_6F_5H were present in the system (in a ratio of 1:6; showing that the C_6F_5 group is more prone to protonation). Examination by ^{19}F NMR spectroscopy showed only the presence of two species; C_6F_5H and [**2**-H][H-DABCO], consistent with degradation of the borane species via preferential loss of the C_6F_5 group. Further analysis by EI mass spectrometry displayed a m/z = 32.0376, consistent with CH_3OH. However, as the spectrometer is not calibrated to detect m/z below 100, it cannot definitely be said that the species detected is methanol. The ^{1}H NMR spectrum exhibited a range of multiplets from 3.4 to 3.7 ppm, symptomatic of a methanol species. However the very low intensity of these resonances in ^{1}H and $^{13}C\{^{1}H\}$ NMR spectra led to the conclusion that if any methanol was produced it was an immeasurable amount.

Analysis of the residue displayed similar NMR spectra to the distillate, but with less decomposition.

4.5.2 [2-H][H-Lut]

The majority of the borohydride systems were synthesised with a decent yield, whereas [**2**-H][H-Lut] could only be obtained with a yield of 6%. Addition of $^{12}CO_2$ to [**2**-H][H-Lut] showed the successful ambient insertion of $^{12}CO_2$. However, due to the low yield of [**2**-H][H-Lut] it made it very difficult to add one equivalent of $^{13}CO_2$ to the

system. Therefore, as it had been determined that [**2**-H][H-Lut] inserts $^{12}CO_2$, the preformed formatoborate, [**2**-O^{13}CHO][H-Lut], was used in an attempt to produce methanol. A known amount of [**2**-O^{13}CHO][H-Lut] and toluene-d_8 were placed in a J-Young NMR tube under an atmosphere of H_2 and heated at 140 ^{o}C. As with the previous reactions, all progress was monitored using ^{1}H, ^{11}B{^{1}H}, and ^{13}C{^{1}H} NMR spectroscopy. Initial observations showed the presence of $^{13}CO_2$, which suggests decarboxylation occurs, releasing $^{13}CO_2$. Unfortunately, analysis did not show the formation of the methoxyborate. The closed system was heated at 160 ^{o}C for 7 days and following analysis using NMR spectroscopy it was determined that the system was unable to reduce the formatoborate to the methoxyborate. Instead, the observation of [**2**-H]$^{-}$ and **2** in the ^{11}B{^{1}H} and ^{19}F NMR spectra reveal decarboxylation dominates at this temperature. Therefore this system was deemed unsuitable.

4.5.3 [2-H][H-TMP]

The use of [**2**-O^{13}CHO][H-Lut], synthesised via route B1 (Scheme 4.3), as a method of monitoring the reduction of the formatoborate was extremely useful due to the initial presence of only one salt in the system and only required an atmosphere of hydrogen and not $^{13}CO_2/H_2$. Therefore, even though [**2**-H][H-TMP] is produced with good yields, it was decided that it would be simpler to use [**2**-O^{13}CHO][H-TMP]. The reaction was carried out in toluene-d_8 and initially heated at 80 ^{o}C under an atmosphere of H_2. Analysis of the reaction after 24 h gave a result analogous to the [**2**-O^{13}CHO][H-Lut] system; decarboxylation dominated, producing the borohydride and releasing $^{13}CO_2$, as observed in the ^{11}B{^{1}H} (−14 ppm) and ^{13}C{^{1}H} (124.9 ppm) NMR spectra, respectively. The temperature was raised to 130 ^{o}C which showed subsequent reduction of the formatoborate as evidenced by the development of

^{13}C-coupled resonances centred at 3.3-3.6 ppm in the ^{1}H NMR spectrum characteristic of the $^{13}CH_3O$-B species. The reaction was monitored at 2 h intervals until no change was obseved in the intensity ratio for $^{13}CO_2$ (δ = 124.9 ppm) and $^{13}CH_3O$-B species (δ ~ 57 ppm) by $^{13}C\{^{1}H\}$ NMR spectroscopy.

For [**2**-O^{13}CHO][H-TMP], termination was slower than witnessed with [**1**-O^{13}CHO][H-TMP], occurring 24 h later. Similarly, the [**2**-O^{13}CHO][H-TMP] reaction also gave two methoxy species (due to loss of C_6F_5H and C_6Cl_5H from the prospective $CH_3OH{\cdot}B(C_6F_5)(C_6Cl_5)_2$). However, it was observed that the final C_6F_5H:C_6Cl_5H ratio was moving towards unity. The relative distribution of $^{13}CO_2$ to $^{13}CH_3O$-B was determined to be approximately 1:2 from the $^{13}C\{^{1}H\}$ NMR spectrum. Unfortunately no $^{13}CH_3OH$ could be isolated upon distillation of the reaction. Its formation may be inhibited by performing such an experiment in a closed system, such that decomposition is forced despite dissociation occurring.

4.6 Reduction of CO_2 Using [3-H][H-N]

4.6.1 [3-H][H-DABCO]

As with all the FLP systems previously discussed, attempts were made to synthesise [**3**-OCHO][H-DABCO] and [**3**-OMe][H-DABCO], however only [**3**-OCHO][H-DABCO] could be isolated. This is not surprising as the isolated yields of the methoxy salts previously discussed have been low. As the other DABCO systems showed low solubility in toluene-d_8, it was not surprising that the borohydride salt was found to be completely insoluble. As with all the isolated borohydride salts, full NMR characterisation was carried out in CD_3CN (see Chapter Five). A preliminary reaction was carried out using $^{12}CO_2$ and [**3**-H][H-DABCO] in CD_3CN. After 24 h at 22 ^{o}C, a precipitate was observed. As [**3**-H][H-DABCO] is soluble in CD_3CN, it is possible that

the formatoborate is only partially soluble in CD_3CN and therefore the precipitate could contain the formatoborate. To determine what was present in the system, CD_3CN was removed under vacuum and replaced with THF-d_8. Analysis using ^{1}H and $^{11}B\{^{1}H\}$ NMR spectroscopy revealed new resonances at 7.9 ppm and 2.12 ppm, respectively. The 7.9 ppm resonance in the ^{1}H NMR is indicative of the formation of C_6Cl_5H, thus decomposition has occurred. Addition of $^{13}CO_2$ to the system with subsequent heating to 140 ^{o}C saw the release of H_2 as witnessed in the ^{1}H NMR spectrum (Figure 4.14), reforming the original FLP as well as decomposition products.

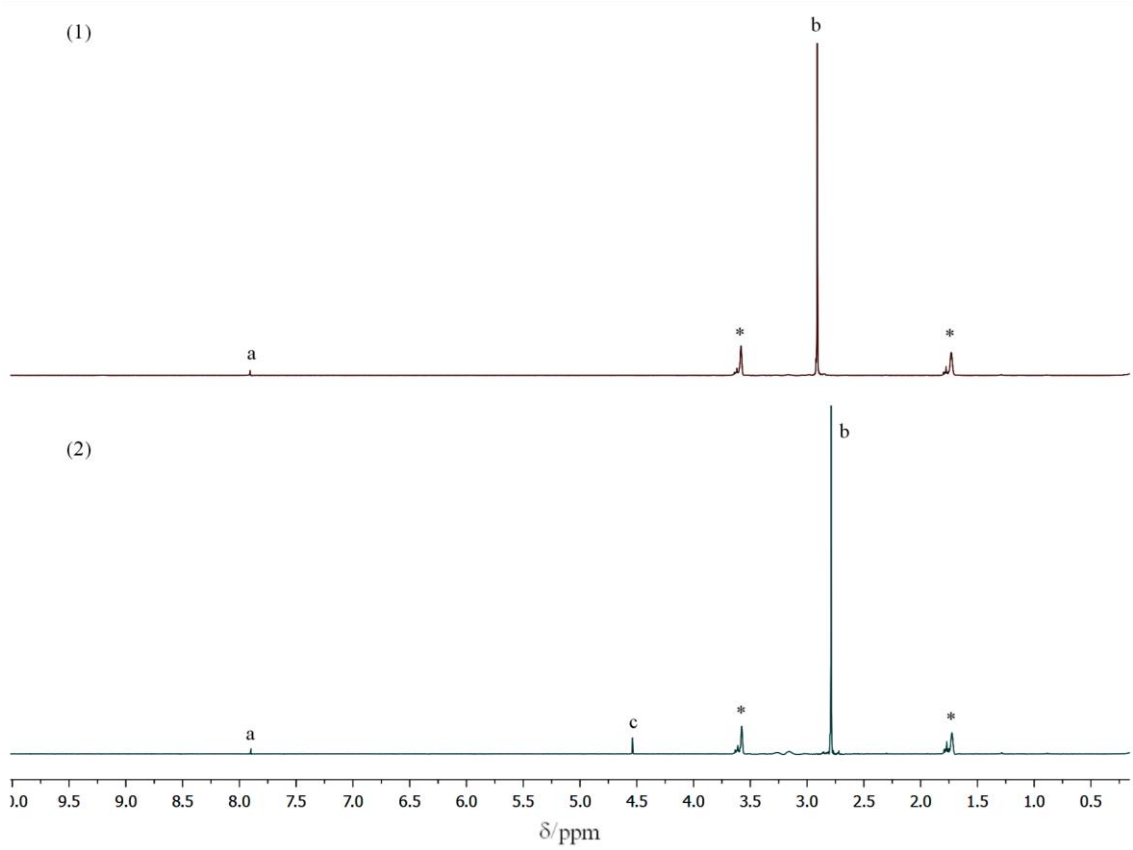


Figure 4.14 ^{1}H NMR spectrum of (1) the [**3**-H][H-DABCO]/$^{13}CO_2$ system < 80 ^{o}C, showing C_6Cl_5H, **a**, and DABCO, **b**; (2) the [**3**-H][H-DABCO]/ $^{13}CO_2$ system after heating at 140 ^{o}C for 24 h releasing H_2, **c**, in THF-d_8 (*).

This is the first observation of hydrogen being released from a borohydride salt containing DABCO. Further heating at 145 ^{o}C of the system saw only more H_2 released and without any indications of $^{13}CO_2$ inserting into the B-H bond. After a month of

heating, the reaction was terminated as a large amount of H_2 had been released and even more decomposition, as C_6Cl_5H, was observed without any of $^{13}CO_2$ inserting into the B-H bond. Therefore it was determined that the [**3**-H][H-DABCO] salt is unable to reduce $^{13}CO_2$. This could be due to the increased steric hindrance around the B-H bond, combined with the possibility of a stronger B-H bond in [**3**-H][H-DABCO] compared to [**1**-H][H-DABCO] or [**2**-H][H-DABCO], due to the stronger electron withdrawing C_6Cl_5 groups.[27]

4.6.2 [3-H][H-Lut]

Efforts to synthesise the formatoborate and methoxyborate salts via route B1 (Scheme 4.3) using [**3**][Lut] proved to be unfruitful and therefore expectations were not high for [**3**-H][H-Lut] as a reducing agent. As with [**2**-H][H-Lut], [**3**-H][H-Lut] was also low yielding. However, due to the inability to synthesise the formatoborate, direct studies on its reduction required going via route A1 (Scheme 4.3). A known amount of the FLP system in THF-d_8 was placed in a J-Young NMR tube filled with H_2 via freeze-pump-thaw degas. The system was heated at 120 ^oC for one week and monitored using NMR spectroscopy. Once it was determined that the reaction had reached equilibrium, the H_2 atmosphere was replaced with one equivalent of $^{13}CO_2$. Unfortunately, before $^{13}CO_2$ was added, decomposition of the borohydride was observed as the C_6Cl_5H resonance was detected in the ^1H NMR spectrum at 7.9 ppm. Addition of $^{13}CO_2$ and subsequent heating of the system only produced more decomposition without reducing $^{13}CO_2$. The reaction was stopped and the residue analysed using ESI mass spectrometry, which revealed no presence of either the formatoborate or the methoxyborate species.

4.6.3 [3-H][H-TMP]

Originally, it was planned that [**3**-O^{13}CHO][H-TMP] isolated via route B1 would be used in the same way as [**2**-O^{13}CHO][H-TMP] to determine if methanol could be produced from the [**3**][TMP] system. However, just like [**3**-O^{13}CHO][H-Lut], [**3**-O^{13}CHO][H-TMP] could not be synthesised by this route. Unlike [**3**-H][H-Lut], [**3**-H][H-TMP] is produced with a higher yield and therefore was dissolved in THF-d_8 in a J-Young NMR tube, followed by the addition of one equivalent of $^{13}CO_2$. Heating the system at 100 ^{o}C for 24 h, the first hint of decomposition was detected in the ^{1}H NMR spectrum at 7.9 ppm (C_6Cl_5H). Further heating at 130 ^{o}C produced more C_6Cl_5H and reduced $^{13}CO_2$ was not observed. After heating for two weeks at 140 ^{o}C, only three species were identifiable in the NMR spectra; [**3**-H][H-TMP], C_6Cl_5H and the $[(C_6Cl_5)_2BH]_2$ dimer which is consistent with the $[(C_6F_5)_2BH]_2$ dimer (Figure 4.15).[28]

Once the reaction was terminated, analysis was carried out using ESI$^-$ mass spectrometry. Examination of the mass spectrum showed that the major species present was [**3**-H][H-TMP] (Figure 4.16).

Full analysis of the reaction residue shows that just like the other systems containing **3**, this system is also unable to reduce $^{13}CO_2$ and shows major decomposition of the Lewis acid, producing C_6Cl_5H as the by-product.

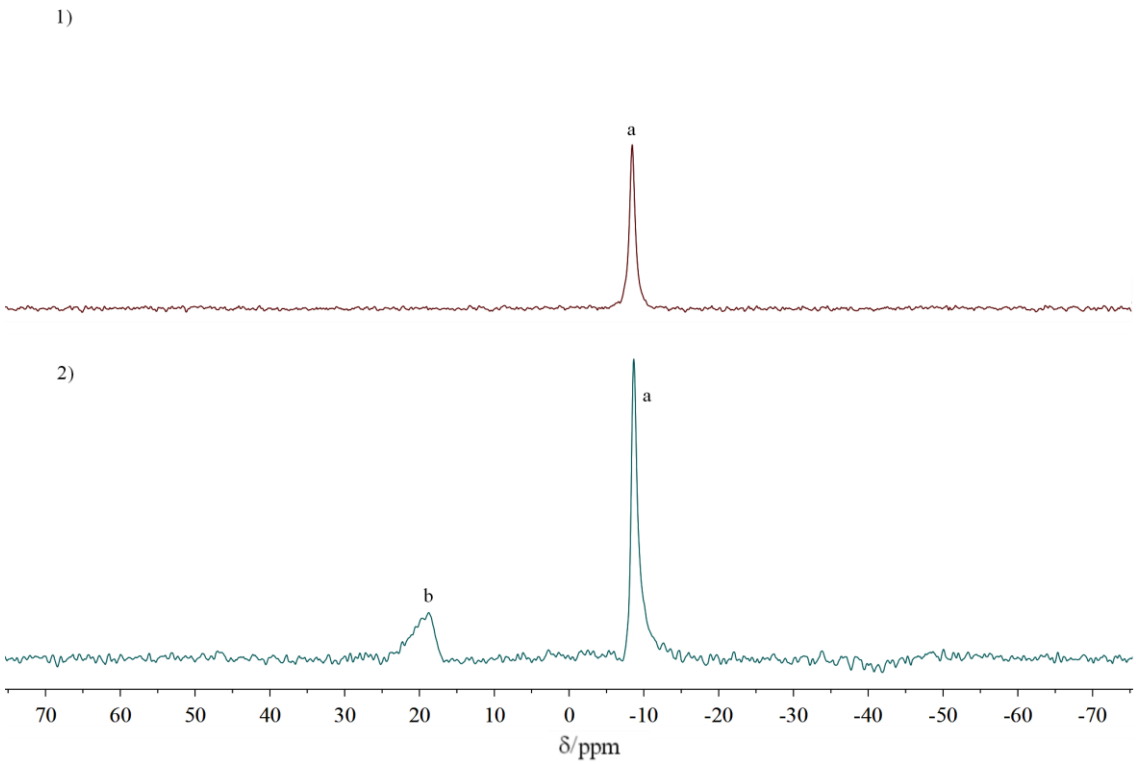


Figure 4.15 $^{11}B\{^{1}H\}$ NMR spectra (1) before addition of $^{13}CO_2$ showing [**3**-H][H-TMP], **a**; (2) two weeks after heating at 140 ^{o}C displaying [**3**-H][H-TMP], **a**, and $(C_6Cl_5)_2BH$, **b**.

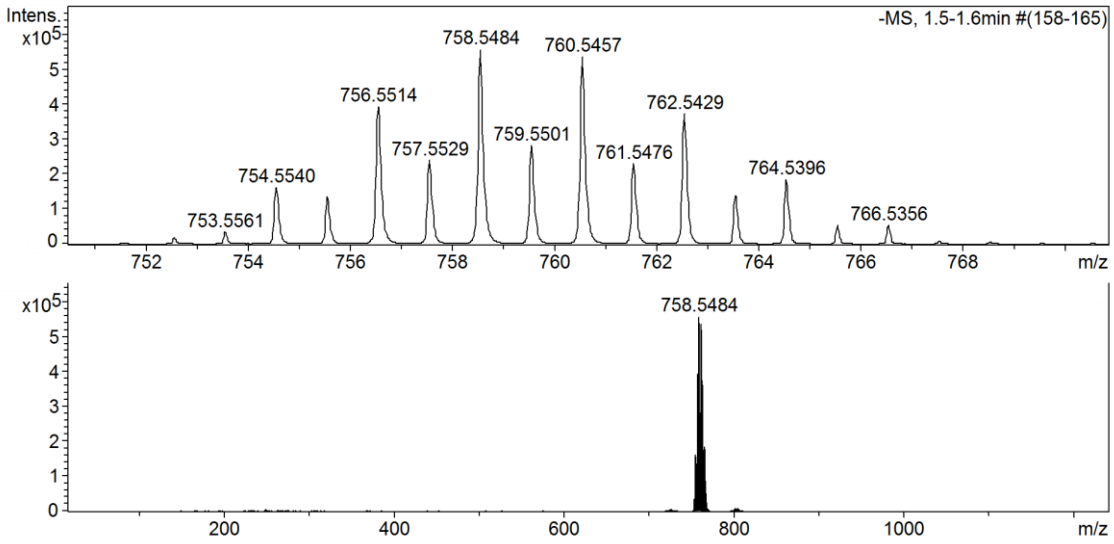
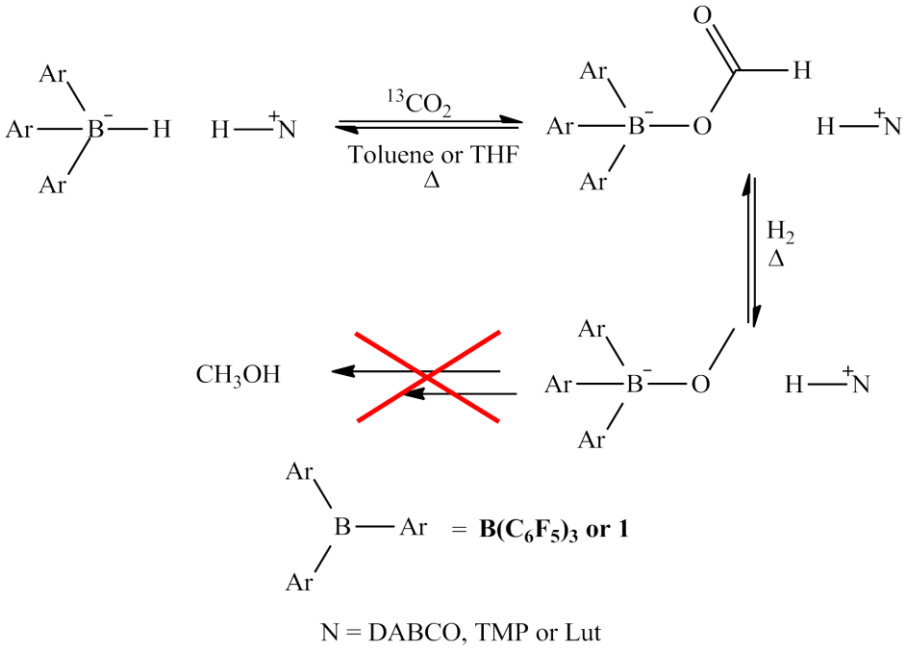


Figure 4.16 ESI$^-$ mass spectrum of the reaction residue showing the major species in the residue was [**3**-H][H-TMP].

4.7 Conclusion

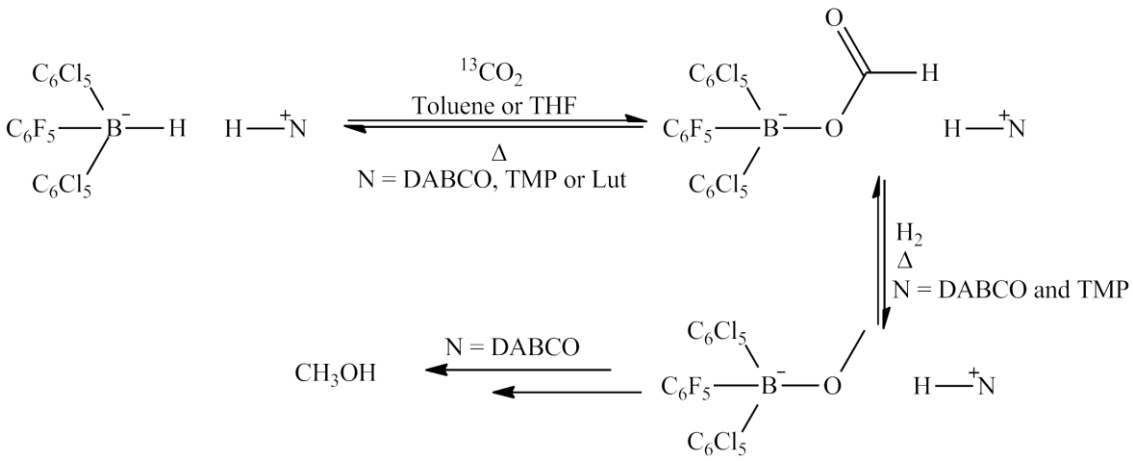
Attempts to reduce $^{13}CO_2$ using the ten novel borohydride salts gave various results. The $[(C_6F_5)_3B\text{-}H][H\text{-}DABCO]$, [**1**-H][H-DABCO], [**1**-H][H-Lut] and [**1**-H][H-TMP] systems all successfully insert $^{13}CO_2$ to give the formatoborate followed by further reduction to the methoxyborate, with varying degrees of success. However, attempts to isolate methanol by distillation did not yield any 'free' methanol as shown in Scheme 4.5.



Scheme 4.5 Summary of $^{13}CO_2$ reduction using $[(C_6F_5)_3B\text{-}H][H\text{-}DABCO]$ and [**1**-H][H-N].

All systems were pushed to their limits by heating to high temperatures, which saw a large amount of decomposition to C_6F_5H or C_6Cl_5H, observed using ^1H and ^{19}F NMR spectroscopy, which were consistent with the literature.

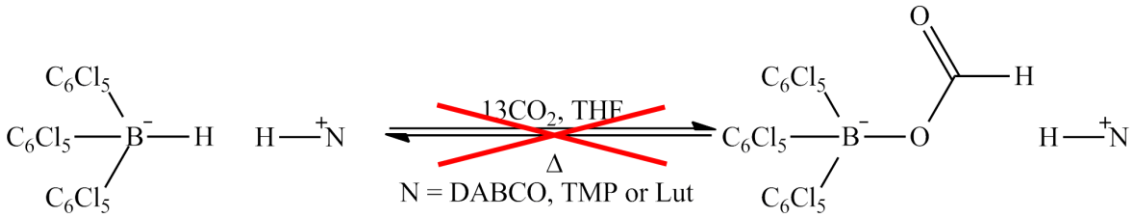
Attempts to reduce $^{13}CO_2$ were repeated using [**2**-H][H-DABCO], [**2**-H][H-Lut] and [**2**-H][H-TMP] as displayed in Scheme 4.6.



Scheme 4.6 Summary of $^{13}CO_2$ reduction using [**2**-H][H-N].

Each system displayed varying reactivity, with [**2**-H][H-DABCO] showing the greatest success in producing methanol, which, due to the small amount generated, made it incredibly difficult to determine the yield. This system also showed a high degree of decomposition of the Lewis acid, confirming that the reduction of [**2**-H][H-DABCO] is not catalytic. Efforts were made to reduce [**2**-O^{13}CHO][H-Lut], however, only the release of $^{13}CO_2$ was observed. Heating the system at higher temperatures only yielded more $^{13}CO_2$, as well as [**2**-H]$^-$, **2**, and H_2, determined by NMR spectroscopy. Therefore, it is not viable to use [**2**-H][H-Lut] to reduce $^{13}CO_2$ to methanol. Due to the ease of use of [**2**-O^{13}CHO][H-Lut], the preformed formatoborate, [**2**-O^{13}CHO][H-TMP], was successfully reduced to [**2**-O^{13}CH$_3$][H-TMP] with relative distribution of 1:2. Attempts were made to try and release methanol via vacuum distillation at 140 ^{o}C, but unfortunately 'free' methanol was not observed in the distillate after analysis using NMR spectroscopy and mass spectrometry. The production and isolation of methanol may be inhibited by performing such an experiment in a closed system, such that decomposition is forced despite dissociation occurring.

Finally, attempts to synthesise the formatoborate and methoxyborate species with **3** (Scheme 4.3, route B1 and B2) only produced [**3**-OCHO][H-DABCO]. Efforts were made to reduce $^{13}CO_2$ to methanol using [**3**-H][H-DABCO], [**3**-H][H-Lut] and [**3**-H][H-TMP] in THF-d_8 as shown in Scheme 4.7.



Scheme 4.7 Summary of $^{13}CO_2$ reduction using [**3**-H][H-N].

However, unlike the other borohydride systems, none of these were able to insert $^{13}CO_2$ into the B-H bond. In each case, decomposition was observed in the form of C_6Cl_5H, consistent with the literature. When [**3**-H][H-DABCO] was heated at 140 ^oC, H_2 was released reproducing [**3**][DABCO], making the system incompatible with $^{13}CO_2$ reduction. This is the only system containing DABCO that releases H_2 upon heating.

Unfortunately, none of the systems investigated were able to produce methanol with the same efficiency as those found by Ashley *et al.*[22] and Sgro *et al.*[23] Similarly to the $B(C_6F_5)_3$/TMP system,[22] decomposition of the Lewis acid was observed with every system as either C_6F_5H or C_6Cl_5H in the ^1H and ^{19}F NMR spectra, leaving either the three-coordinate borohydride, formatoborate or methoxyborate by products.

While the borohydride salts of $B(C_6F_5)_3$, **1** and **2** were able to reduce CO_2 by insertion into the B-H bond, some (almost), quantitatively, subsequent reduction to the methoxyborate was severely hampered both by degradation of the borane species, and by reversal of the CO_2 insertion at elevated temperatures. This lead to none of the ten FLPs investigated being successful candidates for the catalytic reduction of CO_2 to methanol.

4.8 References

(1) Olah, G. A. *Angew. Chem., Int. Ed.* **2005**, *44*, 2636-2639.
(2) Jakob, M. *Nature Clim. Change* **2012**, *2*, 488-489.
(3) Wadsworth, J. *Metall. Mater. Trans. A* **2010**, *41*, 1047-1062.
(4) Grossmann, W. D.; Grossmann, I.; Steininger, K. *Environ. Sci. Technol.* **2010**, *44*, 4849-4855.
(5) Kothari, R.; Tyagi, V. V.; Pathak, A. *Renew. Sust. Energ. Rev.* **2010**, *14*, 3164-3170.
(6) Lee, K. B.; Beaver, M. G.; Caram, H. S.; Sircar, S. *Ind. Eng. Chem. Res.* **2008**, *47*, 8048-8062.
(7) Demessence, A.; D'Alessandro, D. M.; Foo, M. L.; Long, J. R. *J. Am. Chem. Soc.* **2009**, *131*, 8784-8786.
(8) Fletcher, A. J.; Cussen, E. J.; Prior, T. J.; Rosseinsky, M. J.; Kepert, C. J.; Thomas, K. M. *J. Am. Chem. Soc.* **2001**, *123*, 10001-10011.
(9) Surble, S.; Millange, F.; Serre, C.; Duren, T.; Latroche, M.; Bourrelly, S.; Llewellyn, P. L.; Ferey, G. *J. Am. Chem. Soc.* **2006**, *128*, 14889-14896.
(10) Vaidhyanathan, R.; Iremonger, S. S.; Dawson, K. W.; Shimizu, G. K. H. *Chem. Commun.* **2009**, 5230-5232.
(11) Olah, G. A.; Doggweiler, H.; Felberg, J. D.; Frohlich, S.; Grdina, M. J.; Karpeles, R.; Keumi, T.; Inaba, S.; Ip, W. M.; Lammertsma, K.; Salem, G.; Tabor, D. C. *J. Am. Chem. Soc.* **1984**, *106*, 2143-2149.
(12) Olah, G. A.; Goeppert, A.; Prakash, G. K. S. *J. Org. Chem.* **2008**, *74*, 487-498.
(13) Olah, G. A.; Prakash, G. K. S.; Goeppert, A. *J. Am. Chem. Soc.* **2011**, *133*, 12881-12898.
(14) Navarro Yerga, R. M.; Álvarez Galván, M. C.; del Valle, F.; Villoria de la Mano, J. A.; Fierro, J. L. G. *ChemSusChem* **2009**, *2*, 471-485.
(15) Jessop, P. G.; Ikariya, T.; Noyori, R. *Chem. Rev.* **1995**, *95*, 259-272.
(16) Jessop, P. G.; Joo, F.; Tai, C. C. *Coord. Chem. Rev.* **2004**, *248*, 2425-2442.
(17) Sakakura, T.; Choi, J. C.; Yasuda, H. *Chem. Rev.* **2007**, *107*, 2365-2387.
(18) Birkmann, B.; Voss, T.; Geier, S. J.; Ullrich, M.; Kehr, G.; Erker, G.; Stephan, D. W. *Organometallics* **2010**, *29*, 5310-5319.
(19) Stephan, D. W.; Erker, G. *Angew. Chem., Int. Ed.* **2010**, *49*, 46-76.
(20) Geier, S. J.; Stephan, D. W. *J. Am. Chem. Soc.* **2009**, *131*, 3476-3477.
(21) Tran, S. D.; Tronic, T. A.; Kaminsky, W.; Michael Heinekey, D.; Mayer, J. M. *Inorg. Chim. Acta* **2011**, *369*, 126-132.
(22) Ashley, A. E.; Thompson, A. L.; O'Hare, D. *Angew. Chem., Int. Ed.* **2009**, *48*, 9839-9843.
(23) Sgro, M. J.; Domer, J.; Stephan, D. W. *Chem. Commun.* **2012**, *42*, 7253-7255.
(24) Kremlev, M. M.; Mushta, A. I.; Tyrra, W.; Yagupolskii, Y. L.; Naumann, D.; Möller, A. *J. Fluorine Chem.* **2012**, *133*, 67-71.
(25) Quaranta, E.; Carafa, M.; Trani, F. *Appl. Catal. B-Environ.* **2009**, *91*, 380-388.
(26) Blackwell, J. M.; Piers, W. E.; Parvez, M. *Org. Lett.* **2000**, *2*, 695-698.

(27) Ashley, A. E.; Herrington, T. J.; Wildgoose, G. G.; Zaher, H.; Thompson, A. L.; Rees, N. H.; Krämer, T.; O'Hare, D. *J. Am. Chem. Soc.* **2011**, *133*, 14727-14740.
(28) Parks, D. J.; Piers, W. E.; Yap, G. P. A. *Organometallics* **1998**, *17*, 5492-5503.

CHAPTER FIVE

Experimental Details and Characterisation Data

5.1 General Procedures and Physical Measurements

5.1.1 General Procedures

All reactions and compounds were manipulated under N_2 using either an MBraun Unilab glovebox or using standard Schlenk line techniques[1] on a dual manifold vacuum/inert gas line, unless stated otherwise. For the manipulation of moisture sensitive compounds, all glassware was heated to 170 °C before use. Solvents and solutions were transferred using a positive pressure of nitrogen through stainless steel or Teflon cannulae, or via plastic syringes for volumes less than 20 mL. Filtrations were performed using either glassware containing sintered glass frits or modified stainless steel cannulae fitted with glass microfiber filters. Hexane, pentane, toluene and dichloromethane were dried using an MBraun SPS-800 solvent purification system, whereas THF and Et_2O were distilled from purple Na/benzophenone diketyl; all except CH_2Cl_2 and THF were stored over K-mirrored ampoules. Methanol was purchased from Sigma Aldrich, dried and stored over activated 4 Å molecular sieves under N_2. Deuterated solvents for NMR spectroscopy of air sensitive materials were dried over the appropriate drying agent, and purified by trap-to-trap distillation: potassium (C_6D_6, C_7D_8), calcium hydride (THF-d_8). CD_3CN and CD_2Cl_2 were dried and stored over activated 4 Å molecular sieves under N_2.

5.1.2 Elemental Analysis

Elemental analyses for all samples were carried out by Mr. Stephen Boyer of the Elemental Analysis Service, London Metropolitan University, London.

5.1.3 Mass Spectrometry

Samples were analysed by Mr. Colin Sparrow and Mr. James Wickens of the Mass Spectrometry Service, Chemistry Research Laboratory, University of Oxford.

5.1.4 NMR Spectroscopy

^{1}H and ^{13}C NMR spectra were recorded on a Varian VX-Works spectrometer operating at 300 MHz or a Bruker AVII operating at 500 MHz with a ^{13}C cryoprobe. ^{19}F and ^{11}B NMR spectra were recorded on a Varian VX-Works spectrometer operating at 300 MHz. ^{1}H and ^{13}C chemical shifts are given relative to $SiMe_4$ and referenced internally to the residual proton shift in the deuterated solvent employed. ^{11}B, ^{19}F and ^{31}P chemical shifts were referenced externally to $BF_3{\cdot}OEt_2$, $CFCl_3$ and 85% H_3PO_4.

5.1.5 Infrared Spectroscopy

All IR spectra were recorded on a Bio-Rad FTS 6000 FTIR Spectrometer equipped with a DuraSamplIR II diamond accessory in attenuated total reflectance (ATR) mode in the range of 400 - 4000 cm^{-1}; 100 scans at 4 cm^{-1} resolution were collected. The weak absorbance in the range 2200 - 1900 cm^{-1} is from the DuraSamplIR II diamond surface and therefore is not reported.

5.1.6 Electrochemistry

Electrochemical experiments were performed by Dr. Gregory Wildgoose, using an Autolab PGSTAT 30 computer-controlled potentiostat. Cyclic voltammetry (CV) was performed using a three-electrode configuration consisting of a Pt disc working electrode (GoodFellow, Cambridge, UK 99.99% area 1.7 ± 0.3 x 10^{-3} cm^2), a Pt gauze counter electrode and a Ag wire pseudoreference electrode. Pt working electrodes were polished between experiments using successive grades of alumina slurries from 1.0 to 0.3 μm rinsed in distilled water and subjected to brief ultrasonication to remove any adhered alumina microparticles. The electrodes were then dried in an oven at 120 °C to remove any residual traces of water. For either cell arrangement the potentials of the Ag wire pseudoreference electrodes were found to drift by as much as 100 mV between experimental runs and therefore calibrated to the ferrocene/ferrocenium couple in CH_2Cl_2 in the absence of any borane complexes at the end of each run. All electrochemical measurements were performed at ambient temperatures under an inert N_2 atmosphere containing either 0.1 M [$^nBu_4N$][BF_4] or 0.1 M [$^nBu_4N$][$B(C_6H_3(CF_3)_2)_4$] in CH_2Cl_2.

5.1.7 Crystal Structure Determinations

Data collection, structure determination and refinements, using X-ray diffraction, were undertaken by Dr. Amber Thompson, of the Chemical Crystallography Laboratory, Chemistry Research Laboratory, University of Oxford, and Mr. Mark Irwin. Crystals were mounted on a glass fibre using perfluoropolyether oil and cooled rapidly to 150 K in a stream of cold N_2 using an Oxford Cryosystems CRYOSTREAM unit.[2] Data collection was performed using either: an Enraf-Nonius FR590 KappaCCD

diffractometer using graphite-monochromated MoK_α X-ray radiation (λ = 0.71073 Å) and intensity data was processed using the DENZO-SMN package; or Single-crystal X-ray diffraction data were collected using an Oxford Diffraction Supernova dual-source diffractometer equipped with a 135 mm Atlas CCD area detector. Data were collected at 150 K using mirror monochromated Cu Kα radiation (λ = 1.5418 Å) and processed using the CrysAlisPro package, including unit cell parameter refinement and inter-frame scaling (which was carried out using SCALE3 ABSPACK within CrysAlisPro).[3] Equivalent reflections were merged and diffraction patterns processed with the CrysAlisPro suite. The structures were then solved using the direct-methods program SIR92. Subsequent full-matrix least-squares refinement was carried out using the CRYSTALS program suite.[4,5] Neutron diffraction data were collected by Dr. Amber Thompson and Dr. Matthias Gutmann at 100 K using the time-of-flight Laue diffractometer SXD at the ISIS spallation neutron source.[6] The structure from the X-ray solutions were refined in each case, using SHELXL.[7] Crystallographic data and CIF files may be found in the electronic appendix.

5.1.8 Determination of Lewis Acidities

Assessment of Lewis acidity using the gutmann-Beckett method[8] followed a modification described by D.W. Stephan *et al.*[9] which used an excess of Lewis acid to Et_3PO (3:1), dissolved in CD_2Cl_2. For accuracy, the solution was placed in an NMR tube along with a sealed reference capillary containing uncoordinated phosphine oxide. The ^{31}P NMR shifts were recorded at 298 K. The Childs Method was performed as described by Childs *et al.*[10] and Lewis acid and *trans*-crotonaldehyde were mixed in a 1:1 ratio and

placed in an NMR tube. The ^{1}H NMR chemical shift of the H^{3} proton of crotonaldehyde was then recorded.

5.1.9 Computational Details

Calculations were performed by Dr. Tobias Krämer, using DFT with the B3LYP functional[11-14] and the TZVP basis set[15] of Ahlrichs *et al.*, as implemented in gaussian03.[16] The structures of stationary points were fully optimized without any symmetry constraints and confirmed to be minima by the absence of imaginary frequencies. Where crystallographic data were available, the experimental coordinates were used as the start point for the structure. ^{11}B NMR shielding constants were calculated with the gauge-Independent Atomic Orbital (GIAO) method,[17,18] using the geometries obtained at the B3LYP/TZVP level. These calculations employed the B3LYP functional in conjunction with a polarizable continuum model (PCM),[19] using dichloromethane ($\varepsilon = 8.93$) as the solvent. The TZVP basis set on boron was replaced by a basis set optimized for shielding constants, aug-pcS-2(triple-ζ quality),[20] while the TZVP basis set was retained for the other atoms (C, F, Cl). Relative chemical shifts (δ_{calc}) were obtained by referencing the isotropic nuclear magnetic shielding constant of the probe atom (σ_X) against the shielding constant (σ_{ref}) of the B atom in $B(C_6F_5)_3$ with δ_{ref} (^{11}B NMR) = 61.2 ppm, thus $\delta_{calc} = \sigma_{ref} - \sigma_X + \delta_{ref}$.

5.2 Source of Starting Materials

5.2.1 Commercially Available Starting Material

H_2 gas (>99.95%) was obtained from Sigma Aldrich and connected directly to a dual manifold Schlenk line. CO_2 gas (99.99%) was obtained from ARGO International

Ltd. and $^{13}CO_2$ gas was purchased from Cambridge Isotope Laboratories Inc. (99%). Both gases were passed directly into a dual manifold Schlenk line.

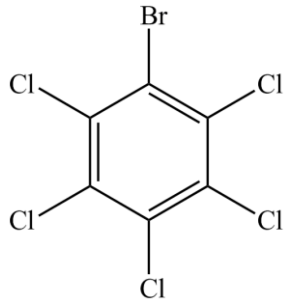
Fe powder was purchased from East Anglia chemicals; $Br_{2(l)}$ and $I_{2(s)}$ were obtained from Fisher Scientific; BBr_3 (99.9%), BCl_3 (1.0 M in heptane), $BF_3.OEt_2$, C_6Cl_5H (98%), C_6Cl_6 (99.9%), ^{n}BuLi (2.5 M in hexanes), *trans*-crotonaldehyde (> 99%), triethylphosphine oxide, Oleum (20%), formic acid and $[^nBu_4N][BF_4]$ were purchased from Sigma Aldrich; C_6F_5Br was obtained from fluorochem; all were used as received. 2,6-lutidine (98%) was purchased from Alfa Aesar and was dried and stored over activated 4 Å molecular sieves under N_2. 2,2,6,6-tetramethylpiperidine (> 99%) and 1,4-diazabicyclo[2.2.2]octane were purchased from Sigma Aldrich. 2,2,6,6-tetramethylpiperidine (> 99%) was dried and stored over activated 4 Å molecular sieves under N_2. 1,4-diazabicyclo[2.2.2]octane was dissolved in toluene and dried over activated 4 Å molecular sieves. The solution was filtered and the solvent was removed under vacuum to give spectroscopically dry 1,4-diazabicyclo[2.2.2]octane which was stored under N_2.

5.2.2 Literature Preparations

CuC_6F_5[21] and $B(C_6F_5)_3$[22] were prepared according to literature procedures.

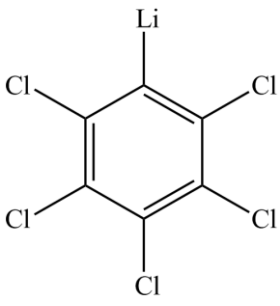
5.3 Experimental Details for Chapter Two

5.3.1 Synthesis of C_6Cl_5Br (2.1)



This is adapted from a literature procedure.[23] A solution of C_6Cl_5H (10 g, 40 mmol), bromine (4.0 mL, 77 mmol), and a catalytic amount of iron (5%, 220 mg) and iodine (5%, 220 mg) in oleum (50 mL, 25% SO_3) were stirred in a 100 mL RBF fitted with a condenser at 70 ^oC for 16 h. The mixture was poured into ice water and the precipitated solid was filtered and washed with aqueous $NaHCO_3$ (2 x 10 mL), aqueous $Na_2S_2O_3$ (2 x 10 mL) and H_2O (2 x 10 mL). Recrystallisation using a minimum quantity of hexane at 65 °C followed by rapid filtration through glass wool afforded C_6Cl_5Br (12 g, 92%) as colourless needles. **$^{13}C\{^1H\}$ NMR ($CDCl_3$, 75 MHz):** δ 134.20, 132.98, 132.04 (s, *ortho, para and meta*-C_6Cl_5); δ 123.76 (s, *ipso*-C). **HRMS (FI, *m*/*z*):** for C_6Cl_5Br **Calcd:** 325.7626. **Found:** 325.7617. **IR (cm^{-1}):** 1707 (w), 1506 (w), 1409 (s), 1327 (w), 1211 (w), 1078 (w), 922 (w), 727 (s), 689 (s), 652 (s).

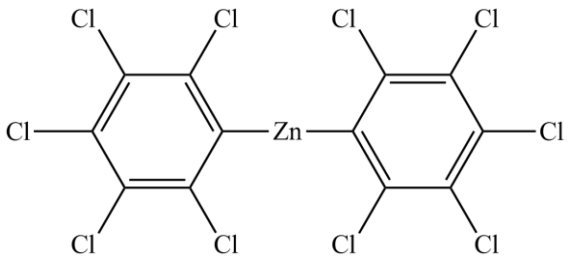
5.3.2 Synthesis of C_6Cl_5Li



This is adapted from a literature procedure.[24] A 500 mL Schlenk was charged under a nitrogen flush with C_6Cl_6 (5.70 g, 20 mmol) or C_6Cl_5Br (6.58 g, 20 mmol) and placed under dynamic vacuum for 20 minutes to remove any moisture. Following the addition of Et_2O (150 mL), the slurry was cooled to –78 °C. With rapid stirring ^{n}BuLi (18.2 mL, 20.4 mmol, 2.5 M in hexanes) was added. The contents were allowed to warm to –10 °C until solid C_6Cl_6 or C_6Cl_5Br was no longer

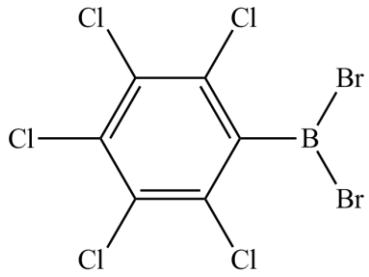
visible, and a translucent amber solution of C_6Cl_5Li had formed *in situ*. The contents were cooled to –78°C and used *in situ* as a source for $[C_6Cl_5]^-$ for later reactions.

5.3.2 Synthesis of $Zn(C_6Cl_5)_2$ (2.2)



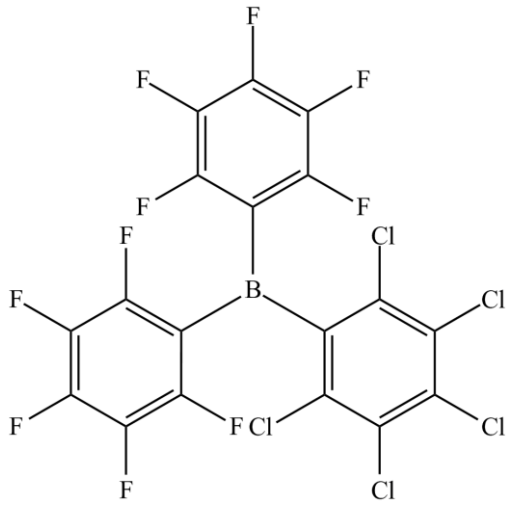
C_6Cl_5Li (28 mmol) in Et_2O at –78 °C was rapidly transferred via cannula to a stirred Et_2O (100 mL) solution of $ZnCl_2$ (1.91 g, 14 mmol) at –20 °C. The yellow reaction mixture was then slowly warmed to room temperature (22 ^oC) over the course of 3 h whereupon a precipitate began to form, which was stirred for a further 12 h. Filtration through Celite to remove LiCl, washing with Et_2O (2 × 50 mL), and subsequent removal of the solvent under reduced pressure produced a pale yellow solid, which was washed with cold (–78 °C) Et_2O (2 × 50 mL) until the washings became colourless. Drying *in vacuo* for 12 h whilst slowly heating to 60 °C afforded base-free $Zn(C_6Cl_5)_2$ as a colourless powder (6.51 g, 82%, 11.5 mmol). **HRMS (EI, *m*/*z*):** for $ZnC_{12}Cl_{10}$ **Calcd:** 557.6177. **Found:** 557.6163. **IR (Nujol, cm^{-1}):** 1700 (m), 1653 (m), 1559 (m), 1533 (m), 1465 (m), 1334 (s), 1311 (s), 1230 (m), 1128 (m), 982 (s), 659 (s), 524 (w). **Anal. Calcd.** for $ZnC_{12}Cl_{10}$: C 25.55. **Found:** C 25.43.

5.3.3 Synthesis of $B(C_6Cl_5)Br_2$ (2.3)



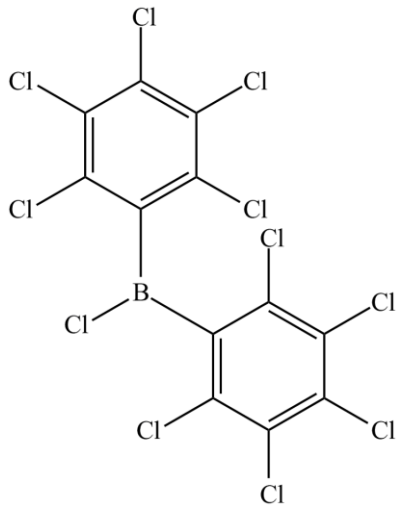
A 250 mL ampoule was charged with a magnetic stirrer bar, $Zn(C_6Cl_5)_2$ (6.51 g, 11.5 mmol), toluene (150 mL), and BBr_3 (7.20 g, 2.77 mL, 28.8 mmol). The sealed reaction mixture was heated to 100 ^oC for 12 h. The suspension was then cooled to room temperature and filtered through Celite, before stripping the solvent under vacuum to produce a solid. Washing this residue with pentane (2 × 50 mL) afforded $B(C_6Cl_5)Br_2$ as an off-colourless powder (6.78 g, 70%, 16.1 mmol). **$^{13}C\{^1H\}$ NMR (CD_2Cl_2, 75 MHz):** δ 135.6 (s, *para*-C_6Cl_5); 132.8, 130.0 (s, *meta*-C_6Cl_5 and *ortho*-C_6Cl_5). Resonance for *ipso*-C_6Cl_5 not observed. **^{11}B NMR (CD_2Cl_2, 128 MHz):** δ 55.8 (br. s). **HRMS (EI, *m*/*z*):** for $BC_6Cl_5Br_2$ **Calcd:** 415.6902. **Found:** 415.6912. **IR (Nujol, cm^{-1}):** 1700 (w), 1653 (w), 1539 (s), 1457 (s), 1377 (w), 1338 (s), 1303 (s), 1235 (s), 1132 (s), 976 (s), 920 (w), 888 (s), 861 (s), 814 (s), 715 (s). **Anal. Calcd.** for $BC_6Cl_5Br_2$: C 17.16. **Found:** C 17.23.

5.3.4 Synthesis of 1; $B(C_6Cl_5)(C_6F_5)_2$ (2.4)



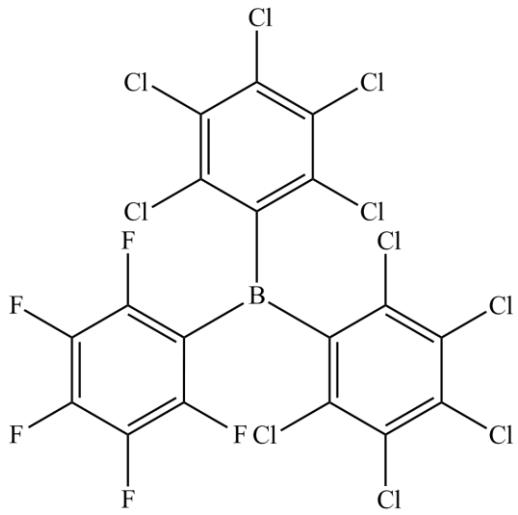
Toluene (150 mL) was added to a stirred mixture of $B(C_6Cl_5)Br_2$ (6.78 g, 16.1 mmol) and CuC_6F_5 (7.61 g, 33.0 mmol), followed by heating to 60 °C for 4 h. The initially translucent solution rapidly became cloudy, producing a colourless precipitate of CuBr. Upon cooling, the solution was filtered through Celite and the residue washed with toluene (2 × 50 mL), before removing the solvent under vacuum. The resultant off-colourless solid was then sublimed (125 °C, 0.01 mbar) to produce analytically pure **1** ($B(C_6Cl_5)(C_6F_5)_2$) as a colourless powder (7.80 g, 81%, 13.1 mmol). Crystals suitable for X-ray diffraction were grown from slow-cooling of a toluene solution to –30 °C. **$^{13}C\{^1H\}$ NMR (CD_2Cl_2, 75 MHz):** δ 149.7 (dm, $^1J_{CF}$ = 251 Hz, *ortho*-C_6F_5); 145.9 (dm, $^1J_{CF}$ = 262 Hz, *para*-C_6F_5); 141.0 (br, *ipso*-C_6Cl_5); 138.0 (dm, $^1J_{CF}$ = 249.5 Hz, *meta*-C_6F_5); 135.1 (s, *para*-C_6Cl_5); 132.3, 131.3 (both s, *meta*-C_6Cl_5 and *ortho*-C_6Cl_5); 112.2 (br, *ipso*-C_6F_5). **^{11}B NMR (C_7D_8, 128 MHz):** δ 63.6 (br. s). **^{19}F NMR (C_7D_8, 282.2 MHz):** δ –127.3 (d, 4F, $^3J_{FF}$ = 22 Hz, *ortho*-C_6F_5), –141.0 (t, 2F, $^3J_{FF}$ = 23 Hz, *para*-C_6F_5), –159.9 (m, 4F, *meta*-C_6F_5). **HRMS (EI, *m/z*):** for $BC_{18}Cl_5F_{10}$ **Calcd:** 591.8378. **Found:** 591.8376. **IR (Nujol, cm^{-1}):** 1700 (m), 1653 (m), 1646 (m), 1559 (m), 1549 (m), 1521 (s), 1507 (w), 1482 (s), 1437 (m), 1382 (m), 1336 (m), 1322 (m), 1235 (w), 1167 (m), 1142 (w), 1015 (w), 979 (s), 674 (m), 668 (m), 659 (w). **Anal. Calcd.** for $BC_{18}Cl_5F_{10}$: C 36.38. **Found:** C 36.27. **X-ray data:** HZ2_4.cif.

5.3.5 Synthesis of $B(C_6Cl_5)_2Cl$ (2.5)



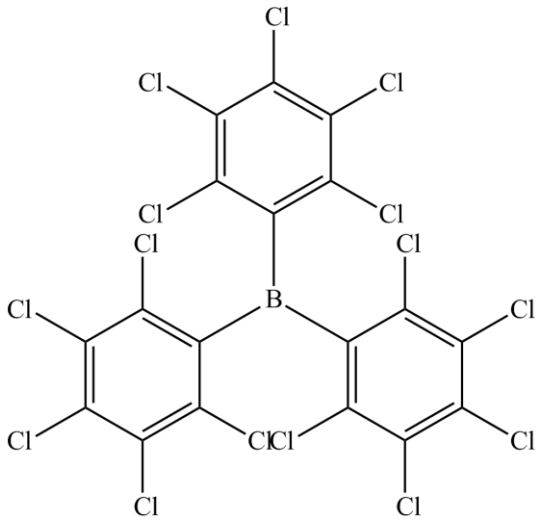
Hexane (100 mL) was slowly added to a stirred solution of C_6Cl_5Li (from 29.0 mmol of C_6Cl_6) at –78 °C, resulting in the formation of a precipitate. BCl_3 (14 mL, 14.0 mmol, 1.0 M in heptane) was then syringed into this suspension and the reaction mixture allowed to slowly warm up to room temperature (22 ^oC) in the $CO_{2(s)}$/acetone cooling bath, followed by further stirring for 12 h. The solvent was then removed under vacuum and the orange residue extracted with CH_2Cl_2 (2 × 100 mL) and filtered through Celite. The solution was then reduced to minimum volume (approximately 30 mL) and cooled to –35 °C, affording an orange powder after washing with cold (–35 °C) CH_2Cl_2 (20 mL) and drying under vacuum. Two further crops were isolated from the mother liquor following the latter procedure. A final recrystallisation from slow-cooling a saturated CH_2Cl_2 solution to –35 °C afforded pale orange needles of $B(C_6Cl_5)_2Cl$, which were dried in vacuo (4.09 g, 54%, 7.5 mmol). **$^{13}C\{^1H\}$ NMR (CD_2Cl_2, 75 MHz):** δ 136.4 (s, *para*-C_6Cl_5); 134.7, 133.1 (s, *meta*-C_6Cl_5 and *ortho*-C_6Cl_5). Resonance for *ipso*-C_6Cl_5 not observed. **^{11}B NMR (CD_2Cl_2, 128 MHz):** δ 62.9 (br. s). **HRMS (EI, *m*/*z*):** for $BC_{12}Cl_{11}$ **Calcd:** 539.6667. **Found:** 539.6660. **IR (Nujol, cm^{-1}):** 1700 (m), 1684 (m), 1653 (m), 1559 (w), 1540 (w), 1521 (w), 1457 (s), 1377 (s), 1322 (s), 1298 (s), 668 (w). **Anal. Calcd.** for $BC_{12}Cl_{11}$: C 26.45. **Found:** C 26.57.

5.3.6 Synthesis of 2; $B(C_6Cl_5)_2(C_6F_5)$ (2.6)



A ampoule was charged with a stirrer bar, $B(C_6Cl_5)_2Cl$ (4.09 g, 7.5 mmol), CuC_6F_5 (1.82 g, 7.9 mmol) and toluene (100 mL). The vessel was sealed and heated to 80 °C (temperatures above this result in decomposition of CuC_6F_5) with stirring for 72 h before being cooled and the solvent removed *in vacuo*. Extraction with CH_2Cl_2 (2 × 50 mL) was followed by filtering through Celite and solvent removal *in vacuo*. The resultant residue was recrystallised from toluene/hexane (1:2) at –78 °C, producing an orange microcrystalline solid which was washed with cold (–78 °C) pentane (2 x 20 mL) and dried under vacuum to yield **2** ($B(C_6Cl_5)_2(C_6F_5)$) (3.39 g, 70%, 5.0 mmol). Crystals suitable for X-ray diffraction were grown from slow evaporation of a saturated toluene solution. **$^{13}C\{^1H\}$ NMR (CD_2Cl_2, 75 MHz):** δ 149.0 (dm, $^1J_{CF}$ = 253 Hz, *ortho*-C_6F_5); 145.9 (dm, $^1J_{CF}$ = 261 Hz, *para*-C_6F_5); 138.0 (dm, $^1J_{CF}$ = 251 Hz, *meta*-C_6F_5); 139.6 (br, *ipso*-C_6Cl_5); 136.6 (s, *para*-C_6Cl_5); 133.0 (s, *meta*-C_6Cl_5 and *ortho*-C_6Cl_5); 114.5 (br, *ipso*-C_6F_5). **^{11}B NMR (C_7D_8, 128 MHz):** δ 64.1 (br. s). **^{19}F NMR (C_7D_8, 282.2 MHz):** δ –127.2 (d, 2F, $^3J_{FF}$ = 21 Hz, *ortho*-C_6F_5); –141.4 (t, 1F, $^3J_{FF}$ = 21 Hz, *para*-C_6F_5); –159.7 (m, 2F, *meta*-C_6F_5). **HRMS (EI, *m/z*):** for $BC_{18}Cl_{10}F_5$ **Calcd:** 675.6899. **Found:** 675.6774**. IR (Nujol, cm^{-1}):** 1700 (m), 1653 (m), 1559 (m), 1540 (w), 1521 (m), 1507 (w), 1481 (s), 1465 (s), 1394 (m), 1332 (s), 1313 (s), 1237 (m), 1190 (w), 1147 (m), 1127 (w), 1104 (w), 973 (s), 876 (w), 668 (m), 642 (w). **Anal. Calcd. for $BC_{18}Cl_{10}F_5$:** C 31.96. **Found:** C 32.27. **X-ray data:** HZ2_6.cif

5.3.7 Synthesis of 3; $B(C_6Cl_5)_3$ (2.7)

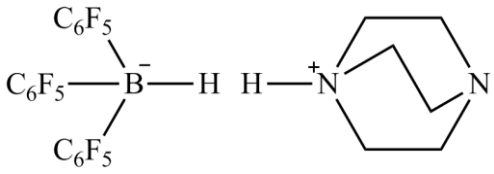


Hexane (100 mL) was added to a stirred solution of C_6Cl_5Li (from 31.2 mmol of C_6Cl_6) at –78 °C. To this slurry was added BCl_3 (10 mL, 10 mmol, 1.0 M in heptane) via syringe at –78 °C. The solution was allowed to warm slowly to –10 °C and stirred for 1 h before the cloudy orange suspension was allowed to warm to room temperature (22 ^{o}C) and stirred for a further 12 h. After quenching the reaction by addition of H_2O (0.5 mL), the solvent was removed *in vacuo* and subsequent work-up performed in air. CH_2Cl_2 (150 mL) was used to extract the crude product, the slurry being filtered through Celite and the filter pad washed with further CH_2Cl_2 (2 × 50 mL). Solvent was removed under reduced pressure to yield an amber solid. Recrystallisation using a minimum quantity of toluene at 100 °C followed by rapid filtration through glass wool and slow cooling to room temperature led to the formation of pale yellow crystals of $B(C_6Cl_5)_3$·(toluene). The toluene supernatant was decanted off and the crystals washed with pentane (2 x 40 mL), followed by drying for 16h under vacuum (1 x 10^{-3} mbar) to remove the co-crystallised toluene. Yield 3.26 g (42%, 4.3 mmol). X-ray quality crystals were produced by a second toluene recrystallisation. **$^{13}C\{^{1}H\}$ NMR (CD_2Cl_2, 75 MHz):** δ 140.6 (br, *ipso*-C_6Cl_5); 136.7 (s, *para*-C_6Cl_5); 135.3, 133.0 (both s, *meta*-C_6Cl_5 and *ortho*-C_6Cl_5). **^{11}B NMR (C_7D_8, 128 MHz):** δ 65.6 (br. s). **HRMS (EI, *m/z*):** for $BC_{18}Cl_{15}$ **Calcd:** 751.5421. **Found:** 751.5177. **IR (Nujol, cm^{-1}):** 1700 (m), 1684 (m), 1652 (m), 1558 (m), 1540 (m), 1507 (m), 1468 (s), 1334 (m), 1313 (m), 1232

(m), 1130 (w), 991 (w), 668 (m), 636 (w). **Anal. Calcd.** for $BC_{18}Cl_{15}$: C 28.49. **Found:** C 28.63. **X-ray data:** HZ2_7.cif

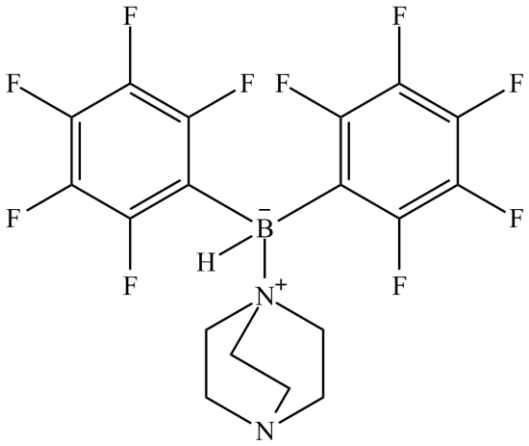
5.4 Experimental Details for Chapter Three

5.4.1 Synthesis of [$(C_6F_5)_3$B-H][H-DABCO] (3.1)



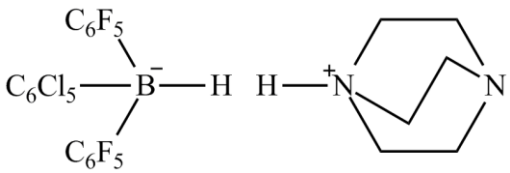
A 50 mL ampoule was charged with a magnetic stirrer bar, $B(C_6F_5)_3$ (500 mg, 0.97 mmol), DABCO (108 mg, 0.97 mmol) and toluene (15 mL). The reaction was freeze-pump-thaw degassed (x3) before H_2 (1 atm) was added to the ampoule and the reaction mixture was heated at 65 ^oC for 7 days with stirring. The precipitate was washed with pentane (2 x 10 mL), collected and dried under vacuum (10^{-2} mbar) at 80 ^oC to afford [$(C_6F_5)_3$B-H][H-DABCO] as a colourless powdery solid (522 mg, 86%, 0.83 mmol). Single X-ray quality crystals were grown by recrystallisation using benzene (70 ^oC). **^{1}H NMR (CD_3CN, 300 MHz):** δ 7.41 (s, 1H, N*H*); 3.60 (br q, 1H, $^1J_{BH}$ = 94 Hz, B*H*); 3.03 (s, 12H, CH_2N). **^{11}B NMR (CD_3CN, 128 MHz):** δ −25.50 (d, $^1J_{BH}$ = 90 Hz). **^{13}C{^{1}H} NMR (CD_3CN, 75 MHz):** δ 148.82 (dm, $^1J_{CF}$ = 234 Hz, *ortho*-C_6F_5); 138.76 (dm, $^1J_{CF}$ = 242 Hz, *para*-C_6F_5); 137.51 (dm, $^1J_{CF}$ = 245 Hz, *meta*- C_6F_5); 126.28 (s, *ipso*-C_6F_5); 45.98 (s, N*C*H_2). **^{19}F NMR (CD_3CN, 282 MHz):** δ −134.66 (d, 6F, $^3J_{FF}$ = 21 Hz, *ortho*-C_6F_5); −164.91 (t, 3F, $^3J_{FF}$ = 20 Hz, *para*-C_6F_5); −168.27 (m, 6F, *meta*- C_6F_5). **HRMS (ESI^-, *m/z*):** for $C_{18}HBF_{15}$ **Calcd:** 512.9937. **Found:** 512.9941. **IR (cm^{-1}):** 2972 (w), 2370 (w), 1703 (w), 1641 (w), 1510 (s), 1450 (s), 1373 (s), 1325 (w), 1055 (m), 995 (w), 960 (s), 893 (s), 837 (s), 798 (s), 756 (s), 727 (w) 659 (s). **Anal. Calcd.** for $C_{24}H_{14}BCl_5F_{10}N_2$: C 46.04; H 2.25; N 4.47. **Found:** C 45.91; H 2.16; N 4.39. **X-ray data:**HZ3_1.cif

5.4.2 Synthesis of DABCO-BH(C_6F_5)$_2$ (3.2)



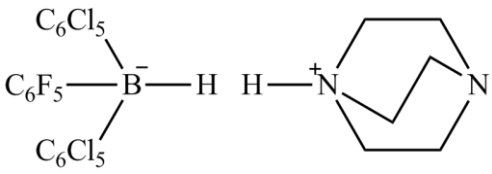
A J-Young's NMR tube was charged with B(C_6F_5)$_3$ (80 mg, 0.16 mmol), DABCO (18 mg, 0.16 mmol) and toluene-d_8 (0.7 mL). The reaction was freeze-pump-thaw degassed (x3) before H_2 (1 atm) was added to the ampoule and the reaction mixture was heated at 65 ^{o}C for 7 days and monitored using ^{1}H, ^{19}F and ^{11}B NMR spectroscopy. Upon cooling single X-ray quality crystals grew from the reaction mixture. The precipitate was isolated and analysis showed full conversion to DABCO-BH(C_6F_5)$_2$ and C_6F_5H. Due to the loss of material for single X-ray crystallography, the yield could not be determined. **^{1}H NMR (CD_3CN, 300 MHz):** δ 3.25 (br m, 1H, B*H*); 2.37 (s, 12H, CH_2N). **^{11}B NMR (CD_3CN, 128 MHz):** δ −8.25 (d, $^{1}J_{BH}$ = 91 Hz). **^{13}C{^{1}H} NMR (CD_3CN, 75 MHz):** δ 148.92 (dm, $^{1}J_{CF}$ = 238 Hz, *ortho*-C_6F_5); 146.17 (dm, $^{1}J_{CF}$ = 250 Hz, *para*-C_6F_5); 137.61 (dm, $^{1}J_{CF}$ = 250 Hz, *meta*-C_6F_5); 45.54 (s, N*C*H$_2$). **^{19}F NMR (CD_3CN, 282 MHz):** δ −128.55 (br d, 4F, $^{3}J_{FF}$ = 22 Hz, *ortho*-C_6F_5); −157.15 (t, 2F, $^{3}J_{FF}$ = 20 Hz, *para*-C_6F_5); −163.50 (m, 4F, *meta*-C_6F_5). **HRMS (ESI$^-$, *m/z*):** for $C_{18}H_{13}BF_{10}N_2Na$ **Calcd:** 481.0904. **Found:** 481.0909. **IR (cm^{-1}):** 2959 (s), 2892 (w), 2439 (br. s), 1643 (s), 1514 (s), 1459 (s), 1378 (w), 1319 (s), 1278 (s), 1259 (s), 1131 (s), 1074 (br. m), 970 (s), 892 (s), 834 (m), 736 (s). **X-ray data:** HZ3_2.cif.

5.4.3 Synthesis of [1-H][H-DABCO] (3.3)



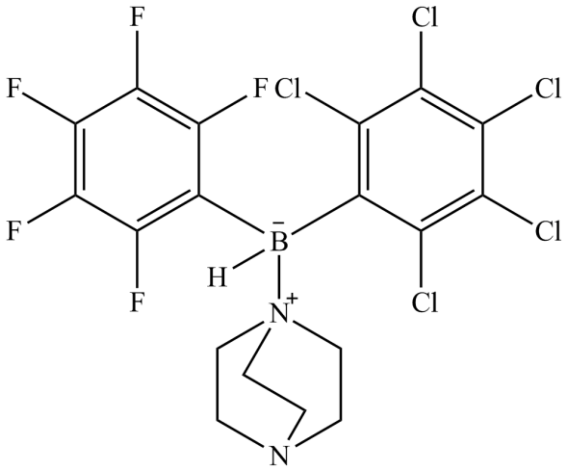
A 50 mL ampoule was charged with a magnetic stirrer bar, **1** ($B(C_6F_5)_2(C_6Cl_5)$) (577 mg, 0.97 mmol), DABCO (108 mg, 0.97 mmol) and toluene (15 mL). The reaction was freeze-pump-thaw degassed (x3) before H_2 (1 atm) was added to the ampoule and the reaction mixture was heated at 65 ^oC for 7 days with stirring. The precipitate was washed with pentane (2 x 10 mL), collected and dried under vacuum (10^{-2} mbar) at 80 ^oC to give [**1**-H][H-DABCO] as a yellow microcrystalline solid (530 mg, 77%, 0.75 mmol). **^{1}H NMR (CD_3CN, 300 MHz):** δ 8.65 (s, 1H, N*H*); 4.11 (br q, 1H, $^1J_{BH}$ = 90 Hz, B*H*); 2.95 (s, 12H, CH_2N). **^{11}B NMR (CD_3CN, 128 MHz):** δ −19.73 (d, $^1J_{BH}$ = 94 Hz). **^{13}C{^{1}H} NMR (CD_3CN, 75 MHz):** δ 149.49 (dm, $^1J_{CF}$ = 234 Hz, *ortho*-C_6F_5); 138.97 (s, *para*-C_6Cl_5); 139.04 (dm, $^1J_{CF}$ = 242 Hz, *para*- C_6F_5); 137.81 (dm, $^1J_{CF}$ = 251 Hz, *meta*- C_6F_5); 130.45, 129.98 (both s, *meta*-C_6Cl_5 and *ortho*-C_6Cl_5); 45.98 (s, N*C*H_2). *Ipso*-C_6F_5 and *ipso*-C_6Cl_5 were not observed. **^{19}F NMR (CD_3CN, 282 MHz):** δ −134.52 (d, 4F, $^3J_{FF}$ = 21 Hz, *ortho*-C_6F_5); −165.24 (t, 2F, $^3J_{FF}$ = 19 Hz, *para*-C_6F_5); −168.41 (m, 4F, *meta*-C_6F_5). **HRMS (ESI$^-$, *m/z*):** for $C_{18}HBCl_{10}F_5$ **Calcd:** 592.8460. **Found:** 592.8466. **IR (cm^{-1}):** 2972 (w), 2362 (w), 1701 (br), 1643 (s), 1602 (w), 1512 (s), 1496 (m), 1462 (m), 1178 (w), 1053 (s). **Anal. Calcd.** for $C_{24}H_{14}BCl_5F_{10}N_2$: C 40.69; H 1.99; N 3.95. **Found:** C 40.80; H 1.94; N 3.88. **X-ray data:** HZ3_3.cif.

5.4.4 Synthesis of [2-H][H-DABCO] (3.4)



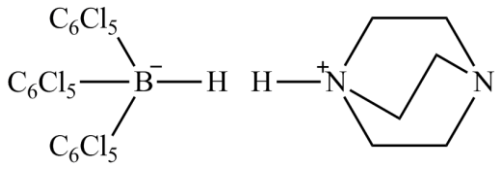
A 50 mL ampoule was charged with a magnetic stirrer bar, **2** ($B(C_6F_5)(C_6Cl_5)_2$) (300 mg, 0.39 mmol), DABCO (45.7 mg, 0.39 mmol) and toluene (15 mL). The reaction was freeze-pump-thaw degassed (x3) before H_2 (1 atm) was added to the ampoule and the reaction mixture was stirred at 22 ^oC for 5 days. The precipitate was washed with pentane to remove any starting material (2 x 10 mL), collected and dried under vacuum (10^{-2} mbar) to yield [**2**-H][H-DABCO] as a pale yellow solid (156 mg, 45%, 0.19 mmol). **^{1}H NMR (CD_3CN, 300 MHz):** δ 4.21 (br q, 1H, $^1J_{BH}$ = 90 Hz, B*H*); 2.88 (s, 12H, CH_2N). N*H* peak was not observed. **^{11}B NMR (CD_3CN, 128 MHz):** δ −14.47 (d, $^1J_{BH}$ = 90 Hz). **^{13}C{^{1}H} NMR (CD_3CN, 75 MHz):** δ 149.09 (dm, $^1J_{CF}$ = 240 Hz, *ortho*-C_6F_5); 139.29 (s, *ipso*-C_6Cl_5); 138.91 (dm, $^1J_{CF}$ = 234 Hz, *para*-C_6F_5); 137.56 (dm, $^1J_{CF}$ = 244 Hz, *meta*- C_6F_5); 131.24 (s, *para*-C_6Cl_5); 130.30 (both s, *meta*-C_6Cl_5 and *ortho*-C_6Cl_5); 46.62 (s, N*C*H_2). *Ipso*-C_6F_5 was not observed. **^{19}F NMR (CD_3CN, 282 MHz):** δ −133.78 (v. br m, 2F, *ortho*-C_6F_5); −165.16 (t, 1F, $^3J_{FF}$ = 21 Hz, *para*- C_6F_5); −168.41 (br s, 2F, *meta*- C_6F_5). **HRMS (ESI$^-$, *m/z*):** for $C_{18}HBCl_{10}F_5$ **Calcd:** 672.6982. **Found:** 672.7000. **IR (cm^{-1}):** 2945 (w), 2207 (w), 1510 (s), 1458 (s), 1301 (m), 1215 (w), 1107 (s), 1078 (s), 1056 (s), 1010 (w), 964 (s), 916 (w), 850 (w), 800 (w), 769 (s), 734 (s). **Anal. Calcd.** for $C_{24}H_{14}BCl_{10}F_5N_2$: C 36.46; H 1.78; N 3.54. **Found:** C 36.56; H 1.70; N 3.57.

5.4.5 Synthesis of DABCO-BH(C_6F_5)(C_6Cl_5) (3.5)



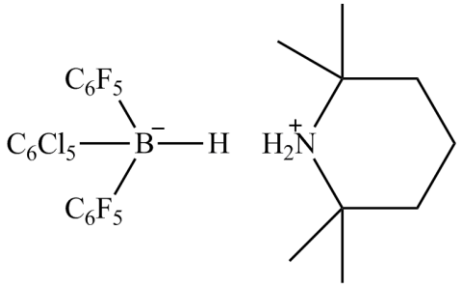
A J-Young's NMR tube was charged with **2** ($B(C_6Cl_5)_2(C_6F_5)$) (30 mg, 0.04 mmol), DABCO (4.5 mg, 0.04 mmol) and toluene-d_8 (0.7 mL). The reaction was freeze-pump-thaw degassed (x3) before H_2 (1 atm) was added to the ampoule and the reaction mixture was heated at 65 ^oC for 7 days and monitored using ^1H, ^{19}F and ^{11}B NMR spectroscopy. Single X-ray quality crystals were grown from a saturated solution of toluene layered with pentane. The precipitate was isolated and analysis showed a mixture of **2**, DABCO-BH(C_6F_5)(C_6Cl_5) and C_6Cl_5H. Due to the loss of material for single X-ray crystallography, the yield could not be determined. **^{1}H NMR (CD_3CN, 300 MHz):** δ 2.31 (s, 12H, CH_2N). B*H* resonance was not observed. **^{11}B NMR (CD_3CN, 128 MHz):** δ −3.18 (d, $^1J_{BH}$ = 80 Hz). **^{13}C{^{1}H} NMR (CD_3CN, 75 MHz):** δ 50.40 and 45.54 (both s, NCH_2). Resonances for the C_6F_5 and C_6Cl_5 rings were not observed. **^{19}F NMR (CD_3CN, 282 MHz):** *δ* −127.00 (br d, 2F, $^3J_{FF}$ = 23 Hz, *ortho*-C_6F_5); −159.13 (t, 1F, $^3J_{FF}$ = 20 Hz, *para*-C_6F_5); −164.10 (m, 2F, *meta*- C_6F_5). **IR (cm^{-1}):** 1703 (w), 1510 (s), 1458 (s), 1325 (w), 1215 (w), 1057 (s), 966 (s), 916 (w), 800 (m), 772 (s), 660 (s). **X-ray data:** HZ3_5.cif. HRMS using ESI or ES could not be obtained.

5.4.6 Synthesis of [3-H][H-DABCO] (3.6)



A 50 mL ampoule was charged with a magnetic stirrer bar, **3** ($B(C_6Cl_5)_3$) (300 mg, 0.39 mmol), DABCO (45.7 mg, 0.39 mmol) and toluene (15 mL). The reaction was freeze-pump-thaw degassed (x3) before H_2 (1 atm) was added to the ampoule and the reaction mixture was heated at 110 ^oC for 2 days with stirring. The precipitate was washed with hot toluene (110 ^oC) (2 x 10 mL), collected and dried under vacuum (10^{-2} mbar) at 120 ^oC to give [**3**-H][H-DABCO] as a yellow solid (114 mg, 33%, 0.13 mmol). **^{1}H NMR (CD_3CN, 300 MHz):** δ 8.52 (s, 1H, N*H*); 4.17 (br q, 1H, $^1J_{BH}$ = 86 Hz, B*H*); 2.87 (s, 12H, CH_2N). **^{11}B NMR (CD_3CN, 128 MHz):** δ −8.83 (d, $^1J_{BH}$ = 86 Hz). **^{13}C{^{1}H} NMR (CD_3CN, 75 MHz):** δ 139.22 (s, *ipso*-C_6Cl_5); 132.76 (d, *para*-C_6Cl_5); 130.79, 130.30 (both s, *meta*-C_6Cl_5 and *ortho*-C_6Cl_5); 46.87 (s, NCH_2). **HRMS (ESI^-, *m/z*):** for $C_{18}HBCl_{10}F_5$ **Calcd:** 752.5505. **Found:** 752.5509. **IR (cm^{-1}):** 2943 (w), 2204 (w), 1525 (s), 1456 (w), 1321 (m), 1315 (m), 1300 (m), 1222 (s), 1165 (w), 1178 (s), 1056 (s), 1008 (br), 972 (s), 833 (s), 800 (s), 771 (m), 705 (s). **Anal. Calcd.** for $C_{24}H_{14}BCl_{15}N_2$: C 33.02; H 1.62; N 3.21. **Found:** C 33.09; H 1.62; N 3.26. **X-ray data:** HZ3_6.cif

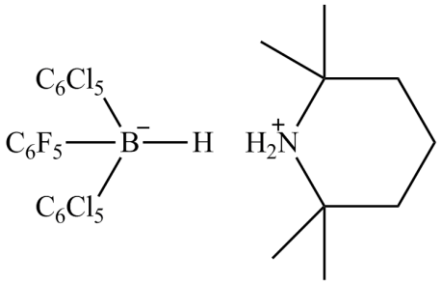
5.4.7 Synthesis of [1-H][H-TMP] (3.7)



A 50 mL ampoule was charged with a magnetic stirrer bar, **1** ($B(C_6F_5)_2(C_6Cl_5)$) (300 mg, 0.84 mmol), TMP (118 mg, 0.84 mmol) and toluene (15 mL). The reaction was freeze-pump-thaw degassed (x3) before H_2 (1 atm) was added to the ampoule and the reaction mixture

was heated at 110 °C for 7 days with stirring. The solvent was removed under vacuum and the residue was washed with pentane (2 x 10 mL), collected and dried under vacuum (10^{-2} mbar) at 80 °C to afford [**1**-H][H-TMP] as a colourless solid (284 mg, 76%, 0.38 mmol). **^{1}H NMR (CD_3CN, 300 MHz):** δ 6.21 (br t (1:1:1), 2H, $^{1}J_{NH}$ = 51 Hz, N*H*$_2$); 3.81 (br q, 1H, $^{1}J_{BH}$ = 90 Hz, B*H*); 1.73 (m, 2H, C*H*$_2$); 1.63 (m, 4H, C*H*$_2$); 1.39 (s, 12H, C*H*$_3$). **^{11}B NMR (CD_3CN, 128 MHz):** δ −19.81 (d, $^{1}J_{BH}$ = 90 Hz). **^{13}C{^{1}H} NMR (CD_3CN, 75 MHz):** δ 149.49 (dm, $^{1}J_{CF}$ = 234 Hz, *ortho*-C_6F_5); 144.96 (br s, *ipso*-C_6Cl_5); 139.30 (s, *ipso*-C_6Cl_5); 139.06 (dm, $^{1}J_{CF}$ = 242 Hz, *para*-C_6F_5); 137.89 (dm, $^{1}J_{CF}$ = 243 Hz, *meta*- C_6F_5); 131.27 (s, *para*-C_6Cl_5); 129.79, 126.16 (both s, *meta*-C_6Cl_5 and *ortho*-C_6Cl_5); 126.16 (br s, *ipso*-C_6F_5); 59.76 (s, N*C*$(CH_3)_2CH_2$); 35.73 (s, $NC(CH_3)_2CH_2$); 27.68 (s, $NC(CH_3)_2CH_2$); 17.01 (s, $NC(CH_3)_2CH_2CH_2$). *ipso*-C_6F_5 was not observed. **^{19}F NMR (CD_3CN, 282 MHz):** δ −134.51 (d, 4F, $^{3}J_{FF}$ = 22 Hz, *ortho*-C_6F_5); −165.29 (t, 2F, $^{3}J_{FF}$ = 19 Hz, *para*-C_6F_5); −168.39 (m, 4F, *meta*-C_6F_5). **HRMS (ESI$^-$, *m/z*):** for $C_{18}HBCl_{10}F_5$ **Calcd:** 592.8471. **Found:** 592.8471. **IR (cm^{-1}):** 2959 (w), 2262 (w), 1639(w), 1573 (s), 1512 (s), 1452 (s), 1384 (s), 1327 (w), 1301 (s), 1259 (s), 1076 (br m), 958 (s), 893 (s), 785 (br s). **Anal. Calcd.** for $C_{27}H_{21}BCl_5F_{10}N$: C 43.97; H 2.87; N 1.90. **Found:** C 44.07; H 2.78; N 2.04. **X-ray data:** HZ3_7.cif. **Neutron Data:** HZ3_7_neutron.cif.

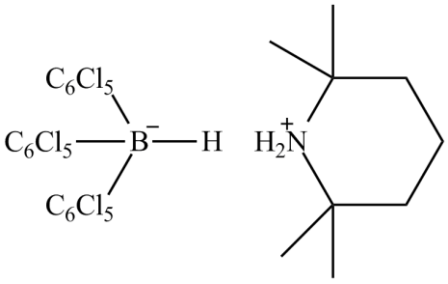
5.4.8 Synthesis of [2-H][H-TMP] (3.8)



A 50 mL ampoule was charged with a magnetic stirrer bar, **2** ($B(C_6F_5)(C_6Cl_5)_2$) (500 mg, 0.84 mmol), TMP (118 mg, 0.84 mmol) and toluene (15 mL). The reaction was freeze-pump-thaw degassed (x3) before H_2 (1 atm) was added to the ampoule and the reaction mixture was

heated at 110 °C for 7 days with stirring. Washing the precipitate with toluene (2 x 10 mL), collected and dried under vacuum (10^{-2} mbar) at 80 °C afforded [**2**-H][H-TMP] as an orange solid (530 mg, 77%, 0.75 mmol). **^{1}H NMR (CD_3CN, 300 MHz):** δ 4.03 (br q, 1H, $^{1}J_{BH}$ = 86 Hz, B*H*); 1.72 (br s, 2H, CH_2); 1.63 (br s, 4H, CH_2); 1.41 (br s, 12H, CH_3). NH_2 peak was not observed. **^{11}B NMR (CD_3CN, 128 MHz):** δ −14.52 (d, $^{1}J_{BH}$ = 90 Hz). **^{19}F NMR (CD_3CN, 282 MHz):** δ −134.73 (v. br m, 2F, *ortho*-C_6F_5); −165.24 (t, 3F, $^{3}J_{FF}$ = 19 Hz, *para*-C_6F_5); −168.55 (br s, 2F, *meta*-C_6F_5). **^{13}C{^{1}H} NMR (CD_3CN, 75 MHz):** δ 149.45 (dm, $^{1}J_{CF}$ = 237 Hz, *ortho*-C_6F_5); 139.52 (dm, $^{1}J_{CF}$ = 242 Hz, *para*-C_6F_5); 139.07 (s, *ipso*-C_6Cl_5); 138.79 (dm, $^{1}J_{CF}$ = 246.05 Hz, *meta*-C_6F_5); 131.24 (s, *para*-C_6Cl_5); 130.79, 130.30 (both s, *meta*-C_6Cl_5 and *ortho*-C_6Cl_5); 59.09 (s, N*C*$(CH_3)_2CH_2$); 35.82 (s, NC$(CH_3)_2$*C*H_2); 27.78 (s, NC(*C*$H_3)_2CH_2$); 17.14 (s, NC$(CH_3)_2CH_2$*C*H_2). *Ipso*-C_6F_5 was not observed. **HRMS (ESI$^-$, *m/z*):** for $C_{18}HBCl_{10}F_5$ **Calcd:** 672.6982. **Found:** 672.6985. **IR (cm^{-1}):** 2970 (w), 1959 (w), 1681 (m), 1585 (s), 1533 (s), 1512 (s), 1498 (s), 1429 (s), 1186 (m), 1058 (m). **Anal. Calcd.** for $C_{27}H_{21}BCl_{10}F_5N$: C 39.61; H 2.46; N 1.71. **Found:** C 39.66; H 2.41; N 1.74. **X-ray data:** HZ3_8.cif

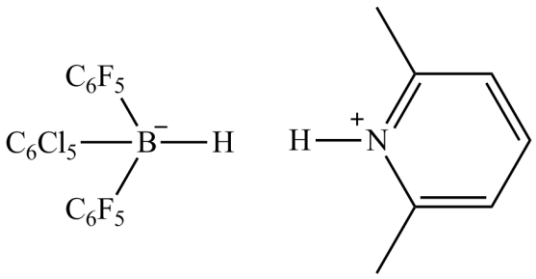
5.4.9 Synthesis of [3-H][H-TMP] (3.9)



A 50 mL ampoule was charged with a magnetic stirrer bar, **3** ($B(C_6Cl_5)_3$) (500 mg, 0.66 mmol), TMP (93 mg, 0.66 mmol) and THF (10 mL). The reaction was freeze-pump-thaw degassed (x3) before H_2 (1 atm) was added to the ampoule and the reaction mixture was heated at 70 °C for 8 days with stirring. The precipitate was washed with hot toluene (110 °C) (2 x 10 mL), collected and dried under vacuum (10^{-2} mbar) at 120 °C to yield [**3**-H][H-TMP] as a yellow solid (360 mg, 61%, 0.40 mmol). **^{1}H NMR (CD_3CN, 300**

MHz): δ 4.17 (br q, 1H, $^{1}J_{BH}$ = 86 Hz, B*H*); 1.71 (br m, 2H, CH_2); 1.57 (br m, 4H, CH_2); 1.33 (br s, 12H, CH_3). NH_2 peak was not observed. **^{11}B NMR (CD_3CN, 128 MHz):** δ −8.83 (d, $^{1}J_{BH}$ = 90 Hz). **^{13}C{^{1}H} NMR (CD_3CN, 75 MHz):** δ 139.18 (br s, *ipso*-C_6Cl_5); 131.18 (s, *para*-C_6Cl_5); 130.93, 129.01 (both s, *meta*-C_6Cl_5 and *ortho*-C_6Cl_5); 57.91 (s, N*C*$(CH_3)_2CH_2$); 36.37 (s, NC$(CH_3)_2$*C*H_2); 28.56 (s, NC(*C*$H_3)_2CH_2$); 17.49 (s, NC$(CH_3)_2CH_2$*C*H_2). **HRMS (ESI$^-$, *m/z*):** for $C_{18}HBCl_{10}F_5$ **Calcd:** 752.5505. **Found:** 752.5496. **IR (cm^{-1}):** 2943 (w), 2204 (w), 1562 (w), 1525 (s), 1452 (w), 1384 (w), 1298 (m), 1222 (m), 1165 (w), 1110 (br), 987 (s), 794 (w), 769 (s), 754 (w), 705 (s). **Anal. Calcd.** for $C_{27}H_{21}BCl_5F_{10}N$: C 35.95; H 2.35; N 1.55. **Found:** C 36.19; H 2.21; N 1.53.

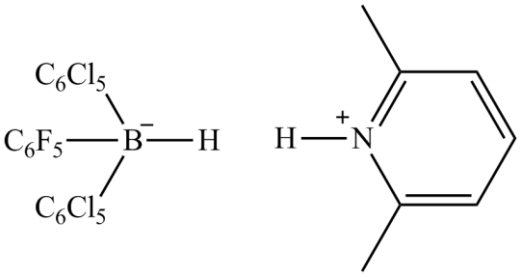
5.4.10 Synthesis of [1-H][H-Lut] (3.10)



A 50 mL ampoule was charged with a magnetic stirrer bar, **1** ($B(C_6Cl_5)(C_6F_5)_2$) (1 g, 1.69 mmol), Lut (180 mg, 1.69 mmol) and toluene (30 mL). The reaction was freeze-pump-thaw degassed (x3) before H_2 (1 atm) was added to the ampoule and the reaction mixture was heated at 65 ^{o}C for 7 days with stirring. Washing the precipitate with pentane (2 x 10 mL), collected and dried under vacuum (10^{-2} mbar) at 80 ^{o}C afforded [**1**-H][H-Lut] as a colourless solid (415 mg, 35%, 0.59 mmol). **^{1}H NMR (CD_3CN, 300 MHz):** δ 8.18 (t, $^{3}J_{HH}$ = 8 Hz, NC(CH_3)CHC*H*); 7.53 (d, $^{3}J_{HH}$ = 8 Hz, NC(CH_3)C*H*CH); 3.78 (br q, 1H, $^{1}J_{BH}$ = 86 Hz, B*H*); 2.64 (s, NC(CH_3)CHCH). NH_2 peak was not observed. **^{11}B NMR (CD_3CN, 128 MHz):** δ −19.72 (d, $^{1}J_{BH}$ = 90 Hz). **^{19}F NMR (CD_3CN, 282 MHz):** δ −134.47 (br d, 4F, $^{3}J_{FF}$ = 21 Hz, *ortho*-C_6F_5); −165.32 (t, 2F, $^{3}J_{FF}$ = 20 Hz, *para*-C_6F_5); −168.50 (br s, 4F, *meta*-C_6F_5). **^{13}C{^{1}H} NMR (CD_3CN, 75 MHz):** δ 154.66 (s, N*C*(CH_3)CHCH); 148.77 (dm, $^{1}J_{CF}$ = 240 Hz, *ortho*-C_6F_5);

146.61 (s, NC(CH_3)CH*C*H); 139.01 (s, *ipso*-C_6Cl_5); 138.77 (dm, $^1J_{CF}$ = 246 Hz, *para*-C_6F_5); 137.68 (dm, $^1J_{CF}$ = 245 Hz, *meta*-C_6F_5); 130.97 (s, *para*-C_6Cl_5); 129.99 and 129.49 (both s, *meta*-C_6Cl_5 and *ortho*-C_6Cl_5); 129.33 (s, NC(CH_3)*C*HCH); 126.33 (s, *ipso*-C_6F_5); 30.61 (s, NC(*C*H_3)CHCH). **HRMS (ESI$^-$, *m/z*):** for $C_{18}HBCl_{10}F_5$ **Calcd:** 592.8460. **Found:** 592.8468. **IR (cm^{-1}):** 2963 (w), 2345 (w), 1633.70 (w), 1510.26 (w), 1452.39 (s), 1257.58 (2), 1002.98 (m), 781.17 (s). **Anal. Calcd.** for $C_{25}H_{11}BCl_5F_{10}N$: C 42.69; H 1.58; N 1.99. **Found:** C 42.86; H 1.64; N 2.05.

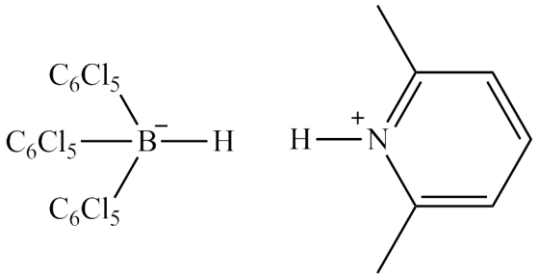
5.4.11 Synthesis of [2-H][H-Lut] (3.11)



A 50 mL ampoule was charged with a magnetic stirrer bar, **2** ($B(C_6Cl_5)_2(C_6F_5)$) (300 mg, 0.44 mmol), Lut (62.6 mg, 0.44 mmol) and toluene (10 mL). The reaction was freeze-pump-thaw degassed (x3) before H_2 (1 atm) was added to the ampoule and the reaction mixture was stirred at 22 ^oC for 7 days. The precipitate was washed with toluene (2 x 10 mL), collected and dried under vacuum (10^{-2} mbar) at 80 ^oC afforded [**2**-H][H-Lut] as an orange solid (62 mg, 18%, 0.08 mmol). **^{1}H NMR (CD_3CN, 300 MHz):** δ 8.17 (t, 1H, $^3J_{HH}$ = 8 Hz, NC(CH_3)CHC*H*); 7.53 (d, 2H $^3J_{HH}$ = 8 Hz, NC(CH_3)C*H*CH); 4.01 (br q, 1H, $^1J_{BH}$ = 89 Hz, B*H*); 2.71 (s, 6H NC(CH_3)CHCH). NH_2 peak was not observed. **^{11}B NMR (CD_3CN, 128 MHz):** δ −14.51 (d, $^1J_{BH}$ = 86 Hz). **^{19}F NMR (CD_3CN, 282 MHz):** δ −132.97 (v. br m, 2F, *ortho*-C_6F_5); −158.59 (t, 1F, $^3J_{FF}$ = 19 Hz, *para*-C_6F_5); −165.77 (br s, 2F, *meta*-C_6F_5). **^{13}C{^{1}H} NMR (CD_3CN, 75 MHz):** δ 155.14 (s, NC(CH$_3$)CHCH); 149.82 (dm, $^1J_{CF}$ = 240 Hz); 146.52 (s, NC(CH_3)CH*C*H), *ortho*-C_6F_5); 138.77 (dm, $^1J_{CF}$ = 246 Hz, *para*-C_6F_5); 138.13 (s, *ipso*-C_6Cl_5); 137.75 (dm, $^1J_{CF}$ = 245 Hz, *meta*-C_6F_5); 133.25 (s, *para*-C_6Cl_5); 131.23 and 130.30 (both s, *meta*-C_6Cl_5 and *ortho*-C_6Cl_5); 125.90

(s, NC(CH_3)*C*HCH); 27.77 (s, NC(*C*H_3)CHCH). *ipso*-C_6F_5 was not observed. **HRMS (ESI$^-$, *m/z*):** for $C_{18}HBCl_{10}F_5$ **Calcd:** 676.6928. **Found:** 676.6976. **IR (cm^{-1}):** 2978 (w), 2347 (w), 1643 (s), 1506 (br s), 1465 (s), 1382 (w), 1317 (m), 1263 (w), 1230 (s), 1188 (w), 1153 (s), 1132 (w), 10911 (br s), 968 (s), 873 (w), 788 (br s), 758 (w), 709 (s). **Anal. Calcd.** for $C_{25}H_{11}BCl_{10}F_5N$: C 38.22; H 1.41; N 1.78. **Found:** C 38.17; H 1.50; N 1.86.

5.4.12 Synthesis of [3-H][H-Lut] (3.10)



A 50 mL ampoule was charged with a magnetic stirrer bar, **3** ($B(C_6Cl_5)_3$) (500 mg, 0.66 mmol), 2,6 - Lutidine (71 mg, 0.66 mmol) and THF (15 mL). The reaction was freeze-pump-thaw degassed (x3) before H_2 (1 atm) was added to the ampoule and the reaction mixture was heated at 70 ^oC for 8 days with stirring. The supernatant was decanted off and the colourless precipitate was collected, washed with Et_2O and dried under vacuum (10^{-2} mbar) at 120 ^oC afforded [**3**-H][H-Lut] as an orange/yellow solid (91 mg, 16%, 0.11 mmol). **^{1}H NMR (CD_3CN, 300 MHz):** δ 7.85 (t, 1H, $^3J_{HH}$ = 8 Hz, NC(CH_3)CHC*H*); 7.28 (d, 2H, $^1J_{HH}$ = 8 Hz, NC(CH_3)C*H*CH); 4.23 (br q, 1H, $^1J_{BH}$ = 88 Hz, B*H*); 2.56 (s, 6H, NC(CH_3)CHCH); N*H* peak was not observed. **^{11}B NMR (CD_3CN, 128 MHz):** δ −8.75 (d, $^1J_{BH}$ = 90 Hz). **^{13}C{^{1}H} NMR (CD_3CN, 75 MHz):** δ 156.99 (s, N*C*(CH_3)CHCH); 142.52 (s, NC(CH_3)CH*C*H); 139.19 (br s, *ipso*-C_6Cl_5); 131.18 (s, *para*-C_6Cl_5); 130.94 and 129.01 (both s, *meta*-C_6Cl_5 and *ortho*-C_6Cl_5); 123.65 (s, NC(CH_3)*C*HCH); 22.56 (s, NC(*C*H_3)CHCH). **HRMS (ESI$^-$, *m/z*):** for $C_{18}HBCl_{10}F_5$ **Calcd:** 752.5505. **Found:** 752.3365. **IR (cm^{-1}):** 2961 (w), 2259 (w), 1525 (s), 1327 (s), 1300 (m), 1257 (w), 1224 (s), 1192 (s), 1126 (s), 1062 (br m), 989 (s), 871 (w), 794 (s),

742 (w), 705 (s). **Anal. Calcd.** for $C_{25}H_{11}BCl_{15}N$: C 34.59; H 1.28; N 1.61. **Found:** C 34.71; H 1.38; N 1.71.

5.5 Experimental Details for Chapter Four

5.5.1 Synthesis of the Formatoborates using Route A1

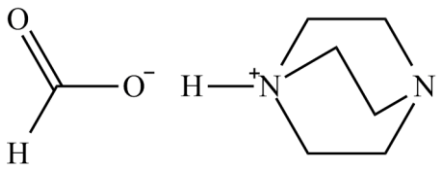
A J-Young's NMR tube containing a borohydride salt in either THF-d_8 or C_7D_8 (0.7 mL) was freeze-pump-thaw degassed (x3) and to this was added $^{13}CO_2$ (2.4 mL), via trap-to-trap transfer using a calibrated J-Young's NMR tube. The reaction mixtures were heated at various temperatures for 1-2 weeks and were monitored using ^{1}H, ^{11}B and ^{13}C NMR spectroscopy.

Borohydride Salt	**m (mg)**	**n (mmol)**	**Equiv. of $^{13}CO_2$**	**Solvent**	**T (^{o}C)**
[$(C_6F_5)_3$B-H][H-DABCO]	30	0.045	2	Toluene-d_8	65
[1-H][H-DABCO]	70	0.099	1	THF-d_8	145
[2-H][H-DABCO]	78	0.099	1	THF-d_8	145
[3-H][H-DABCO]	86	0.099	1	THF-d_8	145
[1-H][H-TMP]	73	0.099	1	Toluene-d_8	25
[2-H][H-TMP]	81	0.099	1	Toluene-d_8	120
[3-H][H-TMP]	89	0.099	1	THF-d_8	145
[1-H][H-Lut]	69	0.099	1	Toluene-d_8	25
[2-H][H-Lut]	77	0.099	1	Toluene-d_8	120
[3-H][H-Lut]	85	0.099	1	THF-d_8	145

All the borohydride salts containing $B(C_6F_5)_3$, **1** or **2** successfully inserted $^{13}CO_2$ into the B-H bond to produce the formatoborate species. None of the borohydride salts containing **3** were able to reduce $^{13}CO_2$. See Chapter 4 for full details of each reaction.

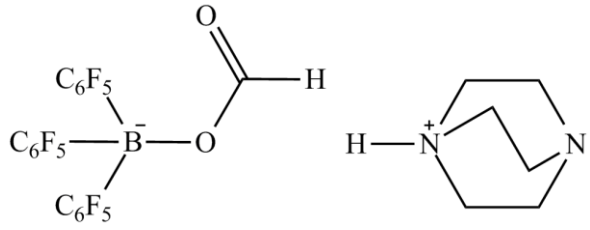
5.5.2 Synthesis of the Formatoborates using Route B1

5.5.2.1 Synthesis of [HCO_2][H-DABCO] (4.1)



HCO_2H (0.20 mL, 5.19 mmol) was added drop-wise to a stirred solution of DABCO (950 mg 6.73 mmol) in toluene (20 mL). The colourless precipitate was filtered, washed with toluene (3 x 10 mL) and dried (12 h) under vacuum to afford a colourless solid. Yield: 0.938 g (96%). **^{1}H NMR (CD_3CN, 300 MHz):** δ 8.26 (s, 1H, OC*H*O); 3.03 (s, 12H, CH_2N). N*H* was not observed. **^{13}C{^{1}H} NMR (CD_3CN, 75 MHz):** δ 167.05 (s, oCOH); 45.00 (s, *C*H_2N). **IR (cm^{-1}):** 2943 (m), 1591 (s), 1458 (m), 1323 (s), 1180 (s), 1053 (s), 986 (m), 839 (s), 804 (s), 750 (s). **Anal. Calcd.** for $C_7H_{14}N_2O_2$: C 53.15; H 8.92; N 17.71. **Found:** C 53.00; H 9.06; N 17.63.

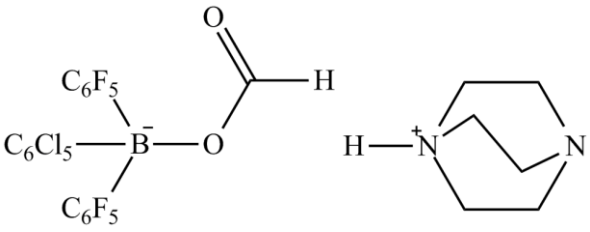
5.5.2.2 Synthesis of [$(C_6F_5)_3$B-OCHO][H-DABCO] (4.2)



A 50 mL Schlenk was charged with a magnetic stirrer bar, $B(C_6F_5)_3$ (405 mg, 0.79 mmol), HCO_2HDABCO (125 mg, 0.79 mmol) and toluene (10 mL) and was stirred at room temperature for 24 h under N_2. The solvent was removed under vacuum to give a colourless solid, which was washed with pentane (2 x 10 mL). The colourless solid was collected and dried under vacuum to give [$(C_6F_5)_3$B-OCHO][H-DABCO] (388 mg, 73%, 0.58 mmol). **^{1}H NMR (CD_3CN, 300 MHz):** δ 8.07 (s, 1H, OC*H*O); 3.08 (s, 12H, CH_2N). N*H* was not observed. **^{11}B{^{1}H} NMR (CD_3CN, 128 MHz):** δ −4.33 (s). **^{13}C{^{1}H} NMR (CD_3CN, 75 MHz):** δ 165.03 (s, BO*C*HO); 148.82 (dm, $^1J_{CF}$ = 234 Hz, *ortho*-C_6F_5); 139.74 (dm, $^1J_{CF}$ = 245 Hz, *para*-C_6F_5); 138.06 (dm, $^1J_{CF}$ = 243 Hz, *meta*-C_6F_5); 45.47 (s, N*C*H_2). *ipso*-C_6F_5 was not observed. **^{19}F NMR**

(CD_3CN, 282 MHz): δ −135.35 (d, 6F, $^3J_{FF}$ = 18 Hz, *ortho*-C_6F_5); −162.38 (t, 3F, $^3J_{FF}$ = 20 Hz, *para*- C_6F_5); −167.62 (td, 6F, $^3J_{FF}$ = 23 and 7 Hz, *meta*-C_6F_5). **HRMS (ESI⁻, *m/z*):** for **[**$HCO_2BC_{18}F_{15}]^-$ **Calcd:** 556.9836. **Found:** 556.9854. **IR (cm^{-1}):** 1662 (s), 1645 (w), 1517 (s), 1452 (s), 1373 (w), 1317 (w), 1209 (w), 1072 (w), 1053 (s), 981 (s), 966 (s), 906 (s), 835 (w), 783 (s), 773 (s), 744 (s), 692 (s), 665 (w). **Anal. Calcd.** for $C_{25}H_{14}BF_{15}N_2O_2$: C 44.89; H 2.11; N 4.18. **Found:** C 44.89; H 2.09; N 4.26.

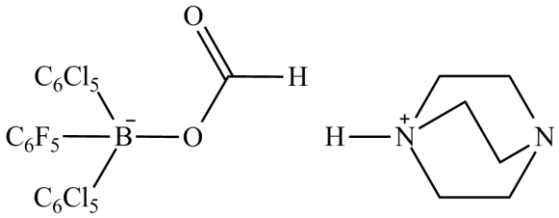
5.5.2.3 Synthesis of [1-OCHO][H-DABCO] (4.3)



A 50 mL Schlenk was charged with a magnetic stirrer bar, **1** ($B(C_6F_5)_2(C_6Cl_5)$) (470 mg, 0.79 mmol), $HCO_2HDABCO$ (125 mg, 0.79 mmol) and toluene (10 mL) and was stirred at room temperature for 24 h under N_2. The solvent was removed under vacuum to yield a pink solid, which was washed with pentane (2 x 10 mL) and dried under vacuum (10^{-2} mbar) at 60 °C to yield [**1**-OCHO][H-DABCO] as a colourless solid (474 mg, 80%, 0.63 mmol). **^{1}H NMR (CD_3CN, 300 MHz):** δ 8.07 (s, 1H, OC*H*O); 7.14 (s, 1H, N*H*), 3.03 (s, 12H, CH_2N). **$^{11}B\{^1H\}$ NMR (CD_3CN, 128 MHz):** δ 1.65 (s).**$^{13}C\{^1H\}$ NMR (CD_3CN, 75 MHz):** δ 165.59 (s, BO*C*HO); 148.95 (d, $^1J_{CF}$ = 238.8 Hz, *ortho*-C_6F_5); 140.06 (d, $^1J_{CF}$ = 245.7 Hz, *para*- C_6F_5); 138.14 (dm, $^1J_{CF}$ = 244 Hz, *meta*- C_6F_5); 137.92 (s, *ipso*-C_6Cl_5); 132.10 (s, *para*-C_6Cl_5); 131.35 and 129.95 (both s, *meta*-C_6Cl_5 and *ortho*-C_6Cl_5); 45.98 (s, NCH_2). *ipso*-C_6F_5 was not observed. **^{19}F NMR (CD_3CN, 282 MHz):** δ −134.81 (d, 4F, $^3J_{FF}$ = 21 Hz, *ortho*-C_6F_5); −162.35 (t, 2F, $^3J_{FF}$ = 19 Hz, *para*-C_6F_5); −167.53 (m, 4F, *meta*-C_6F_5). **HRMS (ESI⁻, *m/z*):** for **[**$HCO_2BC_{18}Cl_5F_{10}]^-$ **Calcd:** 636.8358. **Found:** 636.8383. **IR (cm^{-1}):** 1728 (w), 1649 (s), 1516 (s), 1450 (s), 1352 (w), 1317 (w), 1215 (w), 1076 (w), 1053 (s), 979 (s),

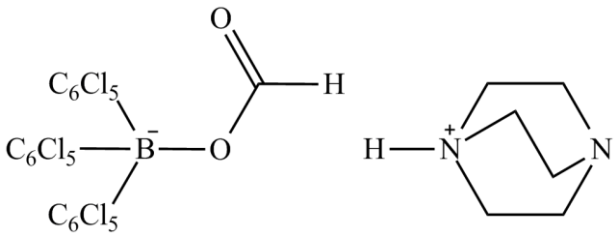
968 (s), 920 (s), 900 (s), 844 (s), 771 (w), 758 (s), 729 (w), 667 (s). **Anal. Calcd.** for $C_{25}H_{14}BCl_5F_{10}N_2O_2$: C 39.91; H 1.88; N 3.72. **Found:** C 40.03; H 1.83; N 3.81.

5.5.2.4 Synthesis of [2-OCHO][H-DABCO] (4.4)



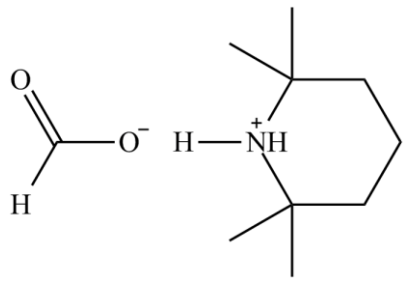
A 50 mL Schlenk was charged with a magnetic stirrer bar, $B(C_6F_5)(C_6Cl_5)_2$ (530 mg, 0.79 mmol), $HCO_2HDABCO$ (125 mg, 0.79 mmol) and toluene (10 mL) and was stirred at room temperature for 24 h under N_2. The solvent was removed under vacuum to yield a yellow solid, which was washed with pentane (2 x 10 mL). The yellow solid was collected and dried under vacuum (10^{-2} mbar) at 60 °C to give [**2**-OCHO][H-DABCO] (515 mg, 79%, 0.62 mmol). **^{1}H NMR (CD_3CN, 300 MHz):** δ 9.24 (s, 1H, N*H*), 8.14 (s, 1H, OC*H*O), 3.04 (s, 12H, CH_2N). **^{11}B{^{1}H} NMR (CD_3CN, 128 MHz):** δ 0.67 (s). **^{13}C{^{1}H} NMR (CD_3CN, 75 MHz):** δ 165.62 (s, BO*C*HO); 138.27 (s, *ipso*-C_6Cl_5); 133.42 (s, *para*-C_6Cl_5); 132.54 and 130.57 (both s, *meta*-C_6Cl_5 and *ortho*-C_6Cl_5); δ 46.13 (s, N*C*H_2). Resonances for the C_6F_5 group were not observed. **^{19}F NMR (CD_3CN, 282 MHz):** δ −130.31 (m, 1F, *ortho*-C_6F_5), −134.33 (m, 1F, *ortho*-C_6F_5), −162.45 (t, 1F, $^3J_{FF}$ = 20 Hz, *para*- C_6F_5), −167.78 (m, 2F, *meta*-C_6F_5). **HRMS (ESI^-, *m/z*):** for **[**$[HCO_2BC_{18}Cl_{10}F_5]^-$ **Calcd:** 716.6881. **Found:** 716.6913. **IR (cm^{-1}):** 1705 (m), 1651 (s), 1516 (s), 1498 (s), 1460 (m), 1350 (w), 1321 (s), 1201 (s), 1157 (w), 1053 (m), 987 (m), 798 (s), 669 (s). **Anal. Calcd.** for $C_{25}H_{14}BCl_{10}F_5N_2O_2$: C 35.97; H 1.69; N 3.36. **Found:** C 35.61; H 1.75; N 3.47.

5.5.2.5 Synthesis of [3-OCHO][H-DABCO] (4.5)



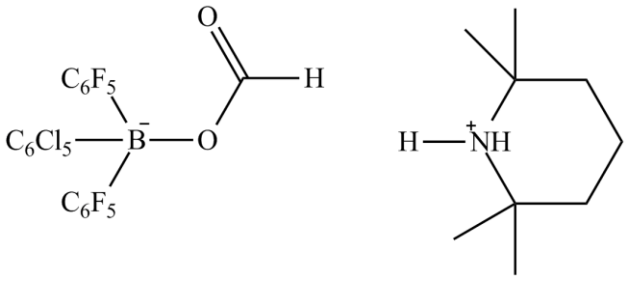
A 50 mL Schlenk was charged with a magnetic stirrer bar, **3** ($B(C_6Cl_5)_3$) (300 mg, 0.40 mmol), $HCO_2HDABCO$ (63 mg, 0.40 mmol) and THF (10 mL) and was stirred at room temperature for 24 h under N_2. The solvent was removed under vacuum to yield a yellow solid, which was dissolved in toluene (10 mL). The solution was filtered and the solvent was removed under vacuum to afford a yellow solid, which was collected and dried under vacuum (10^{-2} mbar) at 60 ^{o}C to yield [**3**-OCHO][H-DABCO] (251 mg, 70%, 0.28 mmol). **^{1}H NMR (CD_3CN, 300 MHz):** δ 8.43 (s, 1H, OC*H*O); 7.98 (s, 1H, N*H*); 3.03 (s, 12H, CH_2N). **^{11}B{^{1}H} NMR (CD_3CN, 128 MHz):** δ 2.86 (s). **^{13}C{^{1}H} NMR (CD_3CN, 75 MHz):** δ 166.32 (s, BO*C*HO); 138.92 (s, *ipso*-C_6Cl_5); 133.23 (s, *para*-C_6Cl_5); 130.92 and 130.41 (both s, *meta*-C_6Cl_5 and *ortho*-C_6Cl_5); 45.79 (s, N*C*H_2). **HRMS (ESI$^-$, *m/z*):** for **[**$HCO_2BC_{18}Cl_{15}]^-$ **Calcd:** 796.5403. **Found:** 796.5403. **IR (cm^{-1}):** 1728 (w), 1645 (s), 1506 (w), 1460 (w), 1321 (s), 1197 (m), 1051 (m), 1008 (s), 908 (s), 796 (s), 671 (s). **Anal. Calcd.** for $C_{25}H_{14}BCl_{15}N_2O_2$: C 32.74; H 1.54; N 3.06. **Found:** C 32.64; H 1.48; N 3.18.

5.5.2.6 Synthesis of [HCO_2][H-TMP] (4.6)



$H^{13}CO_2H$ (0.20 mL, 5.19 mmol) was added drop-wise to a stirred solution of TMP (950 mg 6.73 mmol) in Et_2O (20 mL). The precipitate was collected by filtration, washed with cold Et_2O (3 x 10 mL) and dried for 12 h under vacuum to afford a colourless powder (938 mg, 96%, 6.46 mmol). **^{1}H NMR (CD_3CN, 300 MHz):** δ 9.16 (br. s, 2H, NH_2); 8.52 (dd, 1H, $^1J_{HC}$ = 187 Hz, oC*H*O); 1.69 (m, 2H, NC(CH_3)$_2$CH_2CH_2); 1.59 (m, 4H, NC(CH_3)$_2$CH_2CH_2); 1.37 (s, 12H, CH_3). **^{13}C{^{1}H} NMR (CD_3CN, 75 MHz):** δ 167.45 (s, oCHO); 55.66 (s, N*C*(CH_3)$_2$CH_2); 36.04 (s, NC(CH_3)$_2$*C*H_2); 28.06 (s, NC(*C*H_3)$_2$CH_2); 17.36 (s, NC(CH_3)$_2$CH_2*C*H_2). **IR (cm^{-1}):** 2588 (m), 1705 (w), 1539 (s), 1323 (m), 1227 (m), 1082 (m), 1018 (s), 916 (w), 748 (s). **Anal. Calcd.** for $C_{10}H_{21}NO_2$: C 64.13; H 11.30; N 7.48. **Found:** C 64.08; H 11.24; N 7.56.

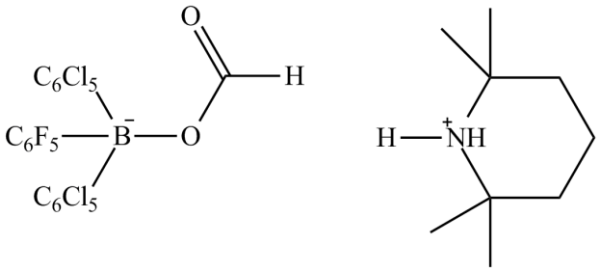
5.5.2.7 Synthesis of [1-O^{13}CHO][H-TMP] (4.7)



To a 125 mL Schlenk tube charged with **1** ($B(C_6F_5)_2(C_6Cl_5)$) (297 mg, 0.50 mmol) in toluene (20 mL) was added [$H^{13}CO_2$][TMPH] (95 mg, 0.50 mmol). The resulting colourless precipitate was collected by filtration, washed with pentane (2 x 20 mL) and dried under vacuum to afford [**1**-O^{13}CHO][HTMP] **(**362 mg, 93%, 0.47 mmol) as a colourless solid. **^{1}H NMR (C_7D_8, 300 MHz):** δ 8.15 (d, 1H, $^1J_{HC}$ = 210 Hz, oC*H*O); 7.50 (br, 2H, NH_2); 0.98 (m, 6H, CH_2); 0.87 (s, 12H, CH_3). **^{11}B NMR (CD_3CN, 128 MHz):** δ 1.37 (br. s). **^{13}C{^{1}H} NMR (CD_3CN, 75 MHz):** δ 166.18

(s, oCHO); 148.90 (dm, $^{1}J_{CF}$ = 234 Hz, *ortho*-C_6F_5); 139.86 (dm, $^{1}J_{CF}$ = 247 Hz, *para*-C_6F_5); 137.98 (dm, $^{1}J_{CF}$ = 247 Hz, *meta*-C_6F_5); 137.66 (s, *para*-C_6Cl_5); 131.91 and 131.15 (both s, *meta*-C_6Cl_5 and *ortho*-C_6Cl_5); 59.09 (s, N*C*$(CH_3)_2CH_2$); 35.32 (s, NC$(CH_3)_2$*C*H_2); 27.44 (s, NC(*C*$H_3)_2CH_2$); 16.68 (s, NC$(CH_3)_2CH_2$*C*H_2). Resonances for *ipso*-C_6F_5 and *ipso*-C_6Cl_5 not observed. **^{19}F NMR (CD_3CN, 282.2 MHz):** δ –134.13 (br. d, 4F, *ortho*-C_6F_5, $^{3}J_{FF}$ = 21 Hz); –162.10 (t, 2F, $^{3}J_{FF}$ = 20 Hz, *para*-C_6F_5); –167.35 (m, 4F, *meta*-C_6F_5). **HRMS (ESI$^-$, *m/z*):** for **[**$HCO_2BC_{18}Cl_5F_{10}]^-$ **Calcd:** 637.8353. **Found:** 637.9232. **IR (cm^{-1}):** 2968 (m), 1641 (s), 1597 (w), 1516 (s), 1462 (m). **Anal. Calcd.** for $C_{28}H_{21}BCl_5F_{10}NO_2$: C 43.03; H 2.71; N 1.79. **Found:** C 42.94; H 2.68; N 1.84. **X-ray data:** HZ4_7cif

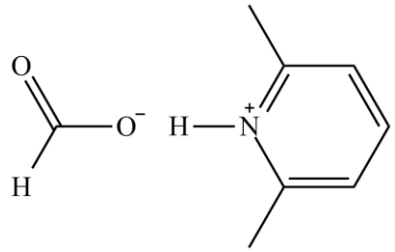
5.5.2.8 Synthesis of [2-O^{13}CHO][H-TMP] (4.8)



To a 125 mL Schlenk tube charged with **2** ($B(C_6F_5)(C_6Cl_5)_2$) (336 mg, 0.50 mmol) in toluene (20 mL) was added [TMPH][H$^{13}CO_2$] (95 mg, 0.50 mmol). The resulting colourless precipitate was collected by filtration, washed with pentane (2 x 20 mL) and dried under vacuum to afford [**2**-O^{13}CHO][HTMP] (354 mg, 82%, 0.41 mmol) as a colourless solid. **^{1}H NMR (CD_3CN, 300 MHz):** δ 7.92 (dd, 1H, $^{1}J_{HC}$ = 208 Hz, J_{HF} = 8 Hz, OC*H*O); 7.78 (br, 2H, NH_2), 1.65 (m, 2H, CH_2), 1.38 (m, 4H, CH_2), 1.15 (s, 12H, CH_3). **^{11}B NMR (CD_3CN, 128 MHz):** δ −0.61 (br. s). **^{13}C{^{1}H} NMR (CD_2Cl_2, 75 MHz):** δ 165.26 (s, oCHO); 138.12 (*para*-C_6Cl_5); 131.91 and 131.15 (both s, *meta*-C_6Cl_5 and *ortho*-C_6Cl_5); 125.83 (*ipso*-C_6Cl_5); 52.48 (s, N*C*$(CH_3)_2CH_2$); 38.11 (s, NC$(CH_3)_2$*C*H_2); 30.90 (s, NC(*C*$H_3)_2CH_2$); 18.51 (s, NC$(CH_3)_2CH_2$*C*H_2). Resonances from C_6F_5 ring were not observed. **^{19}F NMR (CD_3CN, 282.2 MHz):** δ –

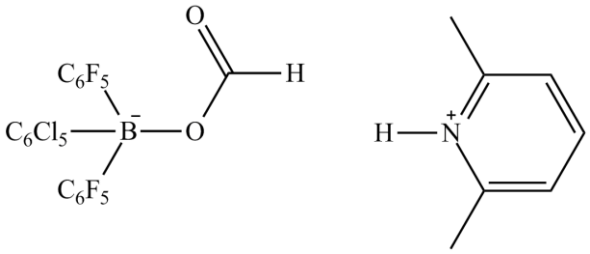
130.23 (m, 1F, *ortho*-C_6F_5), δ –134.21 (m, 1F, *ortho*-C_6F_5), δ –162.31 (t, 2F, $^3J_{FF}$ = 20 Hz, *para*-C_6F_5), δ –167.56 (m, 2F, *meta*-C_6F_5). **HRMS (ESI⁻, *m/z*):** for **[**$HCO_2BC_{18}Cl_{10}F_5]^-$ **Calcd:** 717.6914. **Found:** 717.6905. **IR (cm^{-1}):** 2939 (m), 1705 (m), 1624 (s), 1516 (s), 1462 (s), 1375 (s), 1319 (m), 1201 (s), 1070 (s), 975 (m), 798 (m), 671 (s). **Anal. Calcd.** for $C_{28}H_{21}BCl_{10}F_5NO_2$: C 38.93; H 2.45; N 1.62. **Found:** C 38.87; H 2.51; N 1.66.

5.5.2.9 Synthesis of [H^{13}CO$_2$][H-Lut] (4.9)



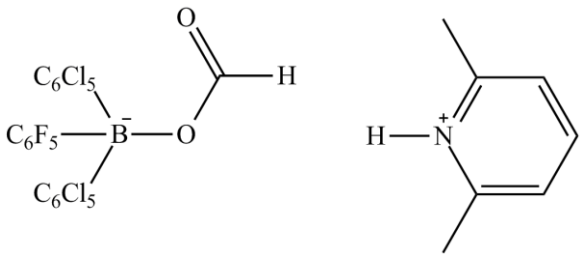
$H^{13}CO_2H$ (0.20 mL, 5.19 mmol) was added drop-wise to an ampoule containing a stirring solution of lutidine (556 mg, 5.19 mmol) in Et_2O (20 mL). The ether was subsequently removed *in vacuo* to yield [LutH][$H^{13}CO_2$] as a colourless oil (725 mg, 91%, 4.72 mmol), and stored under N_2. **^{1}H NMR (CDCl$_3$, 300 MHz):** *δ* 8.27 (t, 1H, $^1J_{HN}$ = 65 Hz, N*H*); 8.27 (d, 1H, $^1J_{HC}$ = 210 Hz, OC*H*O); 7.98 (t, 1H, $^3J_{HH}$ = 8 Hz, NHCHC*H*), 7.34 (t, 2H, $^3J_{HH}$ = 8 Hz, NHC*H*), 2.73 (s, 6H, CH_3). **^{13}C{^{1}H} NMR (CDCl$_3$, 75 MHz):** *δ* 166.33 (s, oCHO); 154.77 (s, N*C*(CH_3)CHCH); 143.20 (s, NC(CH_3)CH*C*H); 124.02 (s, NC(CH_3)*C*HCH); 20.17 (s, NC(*C*H_3)CHCH). **IR (cm^{-1}):** 2854 (m), 1655 (s), 1579 (m), 1450 (m), 1354 (m), 1188 (s), 956 (m), 777 (s), 692 (s). **Anal. Calcd.** for $C_8H_{11}NO_2$: C 62.73; H 7.24; N 9.14. **Found:** C 62.62; H 7.03; N 8.90.

5.5.2.10 Synthesis of [1-O^{13}CHO)][H-Lut] (4.10)



To a 125 mL Schlenk tube charged with a stirring solution of **1** ($B(C_6F_5)_2(C_6Cl_5)$) (297 mg, 0.50 mmol) in toluene (20 mL) was added $[H^{13}CO_2][LutH]$ (77 mg, 0.50 mmol). Removal of the solvent under vacuum afforded a yellow residue, which was washed with pentane (2 x 20 mL) and dried under vacuum to afford [1-O^{13}CHO)][LutH] (342 mg, 91%, 0.46 mmol) as a colourless powdery solid. **^{1}H NMR (CD_3CN, 300 MHz):** δ 12.86 (t, 1H, $^1J_{HN}$ = 65 Hz, N*H*); 8.76 (d, 1H, $^1J_{HC}$ = 270 Hz, OC*H*O); 8.27 (t, 1H, $^3J_{HH}$ = 8 Hz, NHCHC*H*), 7.61 (t, 2H, $^3J_{HH}$ = 8 Hz, NHC*H*), 2.68 (s, 6H, CH_3). **^{13}C{^{1}H} NMR (CD_3CN, 75 MHz):** δ 164.89 (O*C*HO); 154.79 (N*C*(CH_3)CHCH); 147.88 (dm, $^1J_{CF}$ = 245 Hz, *ortho*-C_6F_5); 143.26 (dm, $^1J_{CF}$ = 250 Hz, *para*-C_6F_5); 138.58 (dm, $^1J_{CF}$ = 241 Hz, *meta*-C_6F_5); 137.98 (s, *para*-C_6Cl_5); 130.69 (NC(CH_3)CH*C*H); 133.54 and 133.16 (both s, *ortho* and *meta*-C_6Cl_5); 126.28 (NC(CH_3)*C*HCH); 19.90 (NC(*C*H_3)CHCH). Resonances for *ipso*-C_6F_5 and *ipso*-C_6Cl_5 rings were not observed. **^{11}B NMR (CD_3CN, 128 MHz):** δ 1.96 (s). **^{19}F NMR (CD_3CN, 282.2 MHz):** δ –135.25 (m, 4F, *ortho*-C_6F_5); –159.62 (m, 2F, *para*-C_6F_5); –166.54 (m, 4F, *meta*-C_6F_5). **HRMS (ESI$^-$, *m*/*z*):** for **[**$HCO_2BC_{18}Cl_5F_{10}]^-$ **Calcd:** 637.8353. **Found:** 637.9645. **IR (cm^{-1}):** 3186 (m), 1705 (s), 1643 (s), 1514 (s), 1458 (s), 1377 (m), 1327 (s), 1192 (s), 1072 (s), 966 (m), 785 (m), 669 (m). NMR analysis showed the presence of a small impurity (<5%), therefore a satisfactory elemental analysis could not be obtained.

5.5.2.11 Synthesis of [2-O^{13}CHO)][H-Lut] (4.11)



To a 125 mL Schlenk tube charged with **2** ($B(C_6F_5)(C_6Cl_5)_2$) (336 mg, 0.50 mmol) in toluene (20 mL) was added $[H^{13}CO_2][LutH]$ (77 mg, 0.50 mmol). Removal of the solvent under vacuum afforded a yellow residue, which once washed with pentane (2 x 20 mL) and dried under vacuum afforded [2-O^{13}CHO)][LutH] (367 mg, 88%, 0.44 mmol) as a pale yellow powdery solid. **^{1}H NMR (CD_3CN, 300 MHz):** δ 7.96 (dd, 1H, $^{1}J_{HC}$ = 210 Hz, J_{HF} = 9 Hz, OC*H*O); 7.78 (s, 1H, N*H*); 7.56 (t, 1H, $^{2}J_{HH}$ = 8 Hz, NHCHC*H*), 7.07 (t, 1H, $^{2}J_{HH}$ = 8 Hz, NHC*H*), 2.51 (s, 6H, CH_3). **^{13}C{^{1}H} NMR (CD_2Cl_2, 75 MHz):** δ 170.24 (s, oCHO); 154.10 (s, N*C*(CH_3)CHCH); 145.8 (s, NC(CH_3)CH*C*H); 137.4 (s, *para*-C_6Cl_5); 131.9 and 131.2 (both s, *meta*-C_6Cl_5 and *ortho*-C_6Cl_5); 125.10 (s, NC(CH_3)*C*HCH); 19.60 (s, NC(*C*H_3)CHCH). Resonances from C_6F_5 rings and *ipso*-C_6Cl_5 were not observed. **^{11}B NMR (CD_2Cl_2, 128 MHz):** δ 2.66 (br. s). **^{19}F NMR (CD_2Cl_2, 282.2 MHz):** δ –130.25 (m, 1F, *ortho*-C_6F_5), –134.31 (m, 1F, *ortho*-C_6F_5), –162.26 (t, 1F, $^{3}J_{FF}$ = 20 Hz, *para*-C_6F_5), –167.73 (m, 2F, *meta*-C_6F_5). **HRMS (ES^-, *m/z*):** for **[**$HCO_2BC_{18}Cl_{10}F_5]^-$ **Calcd:** 717.6875. **Found:** 717.8179. **IR (CH_2Cl_2, cm^{-1}):** 2962 (m), 1705 (s), 1527 (s), 1423 (s), 1352 (m), 1319 (s), 1217 (s), 1037 (m), 989 (s), 796 (m), 665 (s). NMR analysis showed the presence of a small impurity (<5%), therefore a satisfactory elemental analysis could not be obtained.

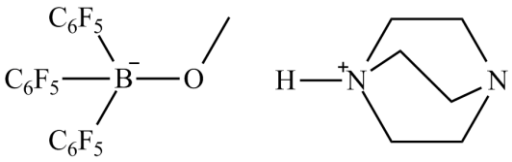
5.5.3 Synthesis of the Methoxyborates using Route A2

Using the formatoborate systems successfully synthesised using route A1, attempts were made to reduce the formatoborates to methoxyborates using H_2.

To a J-Young's NMR tube containing the equilibrium mixtures of the borohydride and formatoborate salts was freeze-pump-thaw degassed and placed under H_2 (1 atm). The reaction was heated up to 145 ^{o}C and monitored using ^{1}H and ^{13}C NMR spectroscopy. Once it was determined that no more of the methoxyborate or methanol was formed, the volatiles were distilled to another J-Young's NMR tube. Any $^{13}CH_3OH$ isolated was intergrated against internal ferrocene as described by Ashley *et al.*[25]

5.5.4 Synthesis of the Methoxyborates using Route B2

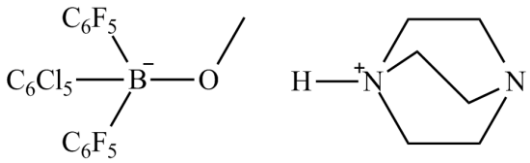
5.5.4.1 Synthesis of $[(C_6F_5)_3B\text{-}OMe][H\text{-}DABCO]$ (4.12)



A 50 mL Schlenk was charged with a magnetic stirrer bar, $B(C_6F_5)_3$ (302 mg, 0.59 mmol), DABCO (66 mg, 0.59 mmol) and toluene (10 mL), to which methanol (24 µl, 0.59 mmol) was added. The solution first became orange and then turned colourless. The reaction was stirred at 22 ^{o}C for 24 h under N_2. The solvent was removed under vacuum to afford a colourless solid, which was washed with pentane (2 x 10 mL). The colourless solid was collected and dried under vacuum to give $[(C_6F_5)_3B\text{-}OMe][H\text{-}DABCO]$ (363 mg, 94%, 0.55 mmol). **^{1}H NMR (CD_3CN, 300 MHz):** δ 3.27 (s, 3H, BOCH_3), 3.02 (s, 12H, CH_2N). N*H* was not observed. **$^{11}B\{^{1}H\}$ NMR (CD_3CN, 128 MHz):** δ 2.65 (s). **$^{13}C\{^{1}H\}$ NMR (CD_3CN, 75 MHz):** δ 148.82 (dm, $^{1}J_{CF}$ = 236 Hz, *ortho*-C_6F_5), 139.58 (dm, $^{1}J_{CF}$ = 255 Hz, *para*-C_6F_5), 137.31 (dm, $^{1}J_{CF}$ = 245 Hz, *meta*-C_6F_5), 52.60 (s, oCH_3); 45.32 (s, NCH_2). *Ipso*-C_6F_5 was not observed. **^{19}F NMR (CD_3CN, 282 MHz):** δ −135.15 (br. d, 6F, $^{3}J_{FF}$ = 21

Hz, *ortho*-C_6F_5), −163.53 (t, 3F, $^3J_{FF}$ = 20 Hz, *para*- C_6F_5), −167.78 (m, 6F, *meta*- C_6F_5). **HRMS (ESI$^-$, *m/z*):** for **[**$H_3COBC_{18}F_{15}]^-$ **Calcd:** 543.0043. **Found:** 543.0055. **IR (cm^{-1}):** 2958 (w), 1705 (w), 1643 (s), 1512 (s), 1452 (s), 1281 (w), 1193 (w), 1056 (m), 964 (m), 916 (s), 810 (s), 763 (s), 692 (s), 667 (s). **Anal. Calcd.** for $C_{25}H_{16}BF_{15}N_2O_2$: C 45.76; H 2.46; N 4.27. **Found:** C 45.68; H 2.52; N 4.22.

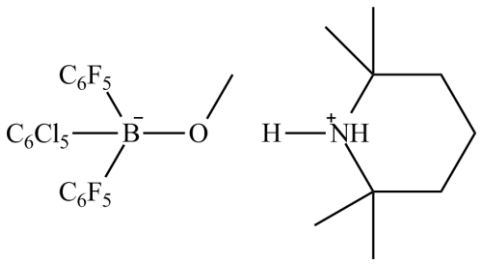
5.5.4.2 Synthesis of [1-OMe][H-DABCO] (4.13)



A 50 mL Schlenk was charged with a magnetic stirrer bar, **1** ($B(C_6F_5)_2(C_6Cl_5)$) (351 mg, 0.59 mmol), DABCO (66 mg, 0.59 mmol) and toluene (10 mL). Methanol (24 μl, 0.59 mmol) was added. The solution first became orange and then turned colourless. The reaction was stirred at 22 ^oC for 24 h under N_2. The solvent was removed under vacuum to yield a colourless solid, which was washed with pentane (2 x 10 mL). The colourless solid was collected and dried under vacuum to give [**1**-OMe][H-DABCO] (298 mg, 77%, 0.45 mmol). **^{1}H NMR (CD_3CN, 300 MHz):** δ 3.26 (s, 1H, OC*H*$_3$); 3.01 (s, 12H, C*H*$_2$N). N*H* was not observed. **^{11}B{^{1}H} NMR (CD_3CN, 128 MHz):** δ 0.22 (s). **^{13}C{^{1}H} NMR (CD_3CN, 75 MHz):** δ 148.95 (d, $^1J_{CF}$ = 242 Hz, *ortho*-C_6F_5); 139.80 (dm, $^1J_{CF}$ = 237 Hz, *para*-C_6F_5); 138.88 (s, *ipso*-C_6Cl_5); 137.62 (dm, $^1J_{CF}$ = 245 Hz, *meta*- C_6F_5); 131.94 and 131.58 (both s, *meta*-C_6Cl_5 and *ortho*-C_6Cl_5); 53.22 (s, BO*C*H$_3$); 45.98 (s, N*C*H$_2$). *ipso*-C_6F_5 and *ipso*-C_6Cl_5 were not observed. **^{19}F NMR (CD_3CN, 282 MHz):** δ −135.54 (d, 4F, $^3J_{FF}$ = 21 Hz, *ortho*-C_6F_5), −163.95 (t, 2F, $^3J_{FF}$ = 20 Hz, *para*-C_6F_5), −167.84 (m, 4F, *meta*-C_6F_5). **HRMS (ESI$^-$, *m/z*):** for $[(C_6F_5)_2(C_6Cl_5)BOCH_3]^-$ **Calcd:** 622.8565. **Found:** 622.8577. **IR (cm^{-1}):** 1734 (w), 1641 (w), 1521 (s), 1452 (s), 1074 (s), 1055 (s), 966 (m), 912 (m),

831 (s), 771 (m), 671 (s). **Anal. Calcd.** for $C_{25}H_{16}BF_{10}Cl_5N_2O$: C 40.66; H 2.18; N 3.79. **Found:** C 40.73; H 2.24; N 3.83.

5.5.4.4 Synthesis of [1-OMe][H-TMP] (4.14)



A 50mL Schlenk was charged with a magnetic stirrer bar, **1** ($B(C_6F_5)_2(C_6Cl_5)$) (175 mg, 0.30 mmol), TMP (32 mg, 0.30 mmol) and toluene (5 mL). Methanol (10 μl, 0.30 mmol) was added at 22 ^oC for 24 h under N_2. The solvent was removed under vacuum to yield a colourless solid, which was washed with pentane (2 x 10 mL), filtered and dried under vacuum to afford [**1**-OMe][H-TMP] as a colourless solid (45 mg, 20 %, 0.06 mmol). **^{1}H NMR (CD_3CN, 300 MHz):** δ 3.12 (s, 3H, OC*H*$_3$); 1.72 (m, 2H, NC(CH_3)CH_2C*H*$_2$); 1.62 (m, 4H, NC(CH_3)C*H*$_2$$CH_2$); 1.34 (s, 12H, C*H*$_3$). **^{11}B NMR ($CD_3CN$, 128 MHz):** δ 0.22 (br. s). **^{13}C{^{1}H} NMR (CD_3CN, 75 MHz):** δ 149.11 (dm, $^1J_{CF}$ = 235 Hz, *ortho*-C_6F_5); 139.14 (dm, $^1J_{CF}$ = 250 Hz, *para*-C_6F_5); 138.50 (s, *ipso*-C_6Cl_5); 137.89 (dm, $^1J_{CF}$ = 250 Hz, *meta*-C_6F_5); 137.80 (s, *para*-C_6Cl_5); 130.33 and 130.13 (both s, *meta*-C_6Cl_5 and *ortho*-C_6Cl_5); 59.12 (s, N*C*(CH_3)$_2$$CH_2$); 51.72 (s, BO*C*$H_3$); 35.61 (s, NC($CH_3$)$_2$*C*$H_2$); 27.64 (s, NC(*C*$H_3$)$CH_2$); 16.89 (s, NC($CH_3$)$_2$$CH_2$*C*$H_2$). *ipso*-$C_6F_5$ was not observed. **^{19}F NMR (CD_3CN, 282.2 MHz):** δ –133.30 (br. d, 4F, *ortho*-C_6F_5, $^3J_{FF}$ = 22 Hz); δ –164.60 (t, 2F, $^3J_{FF}$ = 20 Hz, *para*-C_6F_5); δ –168.25 (m, 4F, *meta*-C_6F_5). **HRMS (ESI, *m*/*z*):** for **[**$H_3OCBC_{18}C_{l5}F_{10}]^-$ **Calcd:** 622.8565. **Found:** 622.88584. **IR (cm^{-1}):** 2941 (w), 1728 (s), 1641 (s), 1597 (s), 1510 (s), 1450 (s), 1384 (w), 1205 (w), 1056 (s), 975 (s), 910 (m), 831 (w), 771 (m), 671 (s). **Anal. Calcd.** for $C_{28}H_{23}BF_{10}Cl_5NO$: C 43.81; H 1.82; N 3.02. **Found:** C 43.88; H 1.90; N 3.08.

5.6 References

(1) Errington, R. J. *Advanced Practical Inorganic and Metalorganic Chemistry*; Blackie A + P: London, 1997.
(2) Cosier, J.; Glazer, A. M. *J. Appl. Crystallogr.* **1986**, *19*, 105-107.
(3) CrysAlisPro, A. T., Version 1.171.35.8.
(4) Betteridge, P. W.; Carruthers, J. R.; Cooper, R. I.; Prout, K.; Watkin, D. J. *J. Appl. Crystallogr.* **2003**, *36*, 1487.
(5) Thompson, A. L.; Watkin, D. J. *J. Appl. Crystallogr.* **2011**, *44*, 1017-1022.
(6) Keen, D. A.; Gutmann, M. J.; Wilson, C. C. *J. Appl. Crystallogr.* **2006**, *39*, 714-722.
(7) Sheldrick, G. *Acta Crystallographica Section A* **2008**, *64*, 112-122.
(8) Beckett, M. A.; Strickland, G. C.; Holland, J. R.; Varma, K. S. *Polymer* **1996**, *37*, 4629-4631.
(9) Welch, G. C.; Cabrera, L.; Chase, P. A.; Hollink, E.; Masuda, J. D.; Wei, P. R.; Stephan, D. W. *Dalton Trans.* **2007**, 3407-3414.
(10) Childs, R. F.; Mulholland, D. L.; Nixon, A. *Can. J. Chem.* **1982**, *60*, 801-808.
(11) Becke, A. D. *J. Chem. Phys.* **1993**, *98*, 5648-5652.
(12) Lee, C.; Yang, W.; Parr, R. G. *Phys. Rev. B* **1988**, *37*, 785-789.
(13) Vosko, S. H.; Wilk, L.; Nusair, M. *Can. J. Phys.* **1980**, *58*, 1200-1211.
(14) Stephens, P. J.; Devlin, F. J.; Chabalowski, C. F.; Frisch, M. J. *J. Phys. Chem.* **1994**, *98*, 11623-11627.
(15) Schafer, A.; Huber, C.; Ahlrichs, R. *J. Chem. Phys.* **1994**, *100*, 5829-5835.
(16) Frisch, M. J. In *Gaussian 03, Revision E.01*; Gaussian, Inc.: Wallingford CT.
(17) Ditchfield, R. *Mol. Phys.* **1974**, *27*, 789-807.
(18) Wolinski, K.; Hinton, J. F.; Pulay, P. *J. Am. Chem. Soc.* **1990**, *112*, 8251-8260.
(19) Tomasi, J.; Mennucci, B.; Cammi, R. *Chem. Rev.* **2005**, *105*, 2999-3094.
(20) Jensen, F. *J. Chem. Theory Comput.* **2008**, *4*, 719-727.
(21) Cairncross, A.; Sheppard, W. A.; Wonchoba, E. *Org. Synth.* **1988**, *50-9*, 875-882.
(22) Duchateau, R.; Lancaster, S. J.; Thornton-Pett, M.; Bochmann, M. *Organometallics* **1997**, *16*, 4995-5005.
(23) Harada, K.; Hart, H.; Frank Du, C. J. *J. Org. Chem.* **1985**, *50*, 5524-5528.
(24) Rausch, M. D. T., F.E.; Gordon,H.B. *J. Organomet. Chem.* **1966**, *5*, 493-500.
(25) Ashley, A. E.; Thompson, A. L.; O'Hare, D. *Angew. Chem., Int. Ed.* **2009**, *48*, 9839-9843.